THE UNIVERSITY OF QUEENSLAND

AUSTRALIA

Interface and Composite Behaviour of Geosynthetic-Reinforced Soils

Youwei Xu

A thesis submitted for the degree of Doctor of Philosophy at

The University of Queensland in 2018

School of Civil Engineering

Geotechnical Engineering Centre

Abstract

Reinforcing soils with geosynthetics can significantly improve their engineering behaviour and performance, mainly by increasing their bearing capacity, providing additional confinement, reducing vertical settlement and lateral deformation, and increasing overall stiffness. Reinforcement is achieved by the tensile forces that the geosynthetics develop under load, which contributes to the overall stability of the reinforced soil composite. Geotextiles and geogrids are the two geosynthetic products commonly used as reinforcement elements in a soil mass. In particular, the apertures within geogrids provide additional interlock embedded soil particles. Due to the increasing use of geosynthetics in geotechnical engineering for soil reinforcement, stabilisation and ground improvement, a deeper understanding of the interface and composite behaviour of geosynthetic-reinforced soils is required.

The interface parameters, such as interface friction angle, adhesion and pull-out resistance, are essential for the design and stability analysis of geosynthetic-reinforced soil structures. The two commonly used experimental techniques to determine these interface parameters are large-scale direct/interface shear tests, and pull-out tests. However, the interaction mechanisms between soils and geosynthetics in these two testing modes remain poorly understood, as does the theory used to describe them. In particular, geogrids have complex and varying aperture shapes, sizes and thicknesses. The contribution of each shear strength component at the soil-geogrid interface has not been well established in the literature. To investigate the interface behaviour of geosynthetic-reinforced soils, laboratory large-scale direct/interface shear and pull-out tests were carried out on different types of materials, including roadbase, crusher run aggregate, sand, and four types of geosynthetics. The applications of geosynthetics in base reinforcement and subgrade stabilisation were experimentally modelled in the large-scale interface shear tests. Theoretical frameworks were then proposed to interpret the experimental results by quantifying the contribution of different shear strength components mobilised along the interface between the soil and geogrid. Furthermore, the effects of scalping on the direct and interface shear strengths of aggregate were investigated. The particle breakage caused by loading and shearing in the direct and interface shear tests on aggregate with different degrees of scalping was assessed and discussed, based on sieving analyses and inferred particle breakage indices.

In terms of testing techniques, the conventional single-stage testing method was found to be very labour intensive and time consuming for large-scale direct/interface shear and pull-out tests. This is because single-stage tests require at least three specimens tested under three different normal stresses, so a large amount of soil is needed, with sample preparation required for each test. This makes single-stage large-scale direct shear and pull-out testing very expensive in commercial laboratories. Based on the limited references to multi-stage direct shear tests in the literature, a multi-stage testing method was attempted for the large-scale direct/interface shear and pull-out tests. The feasibility, reliability and applicability of the multi-stage testing method were evaluated, including its advantages and disadvantages, and an optimum multi-stage testing procedure is recommended.

Anchored geosynthetics are able to withstand higher tension and provide higher anchorage capacity. The influence of anchorage angles on the pull-out resistance of geotextile wrap around anchorage was investigated both experimentally and theoretically. The three-stage mobilisation of the pull-out resistance of a geotextile wrap around anchorage was investigated, and theoretical equations were derived to predict the pull-out resistance of the geotextile wrap around anchorage for varying anchorage angles.

Finally, the composite behaviour of clay reinforced with ordinary sand column (OSC) and geotextile encased sand column (GESC) was experimentally investigated using direct shear, triaxial and oedometer tests. The effects of OSC and GESC on the shear strength, consolidation characteristics, pore water pressure, Mohr circle, failure envelope and stress path, are discussed and analysed, in terms of both total and effective stresses.

Declaration by author

This thesis is composed of my original work, and contains no material previously published or written by another person except where due reference has been made in the text. I have clearly stated the contribution by others to jointly-authored works that I have included in my thesis.

I have clearly stated the contribution of others to my thesis as a whole, including statistical assistance, survey design, data analysis, significant technical procedures, professional editorial advice, financial support and any other original research work used or reported in my thesis. The content of my thesis is the result of work I have carried out since the commencement of my higher degree by research candidature and does not include a substantial part of work that has been submitted to qualify for the award of any other degree or diploma in any university or other tertiary institution. I have clearly stated which parts of my thesis, if any, have been submitted to qualify for another award.

I acknowledge that an electronic copy of my thesis must be lodged with the University Library and, subject to the policy and procedures of The University of Queensland, the thesis be made available for research and study in accordance with the Copyright Act 1968 unless a period of embargo has been approved by the Dean of the Graduate School.

I acknowledge that copyright of all material contained in my thesis resides with the copyright holder(s) of that material. Where appropriate I have obtained copyright permission from the copyright holder to reproduce material in this thesis and have sought permission from co-authors for any jointly authored works included in the thesis.

Publications included in this thesis

Xu, Y., Williams, D. J., Serati, M., 2018. Investigation of shear strength of interface between roadbase and geosynthetics using large-scale single-stage and multi-stage direct shear test. Road Materials and Pavement Design. https://doi.org/10.1080/14680629.2018.1561378 – incorporated as **Paper I**.

Contributor	Statement of contribution
Xu. Y. (Candidate)	Conception and design (85%) Analysis and interpretation (85%) Drafting and production (85%)
Williams, D.J.	Conception and design (10%) Analysis and interpretation (10%) Drafting and production (10%)
Serati, M.	Conception and design (5%) Analysis and interpretation (5%) Drafting and production (5%)

Xu, Y., Williams, D. J., Serati, M., Vangsness, T., 2018. Effects of scalping on direct shear strength of crusher run and crusher run/geogrid interface. Journal of Materials in Civil Engineering. 30 (9) 04018206. https://doi.org/10.1061/(ASCE)MT.1943-5533.0002411 – incorporated as **Paper II**.

Contributor	Statement of contribution
Xu. Y. (Candidate)	Conception and design (80%) Analysis and interpretation (80%) Drafting and production (80%)
Williams, D.J.	Conception and design (10%) Analysis and interpretation (10%) Drafting and production (10%)
Serati, M.	Conception and design (5%) Analysis and interpretation (5%) Drafting and production (5%)
Vangsness, T.	Conception and design (5%) Analysis and interpretation (5%) Drafting and production (5%)

Xu, Y., Williams, D. J., Serati, M., 2018. Measurement of shear strength and interface parameters by multi-stage large-scale direct/interface shear and pull-out tests. Measurement Science and Technology. 29 (8) 085601. https://doi.org/10.1088/1361-6501/aacb8a – incorporated as **Paper III**.

Contributor	Statement of contribution
Xu. Y. (Candidate)	Conception and design (85%) Analysis and interpretation (85%) Drafting and production (85%)
Williams, D.J.	Conception and design (10%) Analysis and interpretation (10%) Drafting and production (10%)
Serati, M.	Conception and design (5%) Analysis and interpretation (5%) Drafting and production (5%)

Xu, Y., Williams, D. J., Serati, M., 2018. Influence of anchorage angles on pull-out resistance of geotextile wrap around anchorage. Geosynthetics International. 25 (4), 378-391. https://doi.org/10.1680/jgein.18.00022 – incorporated as **Paper IV**.

Contributor	Statement of contribution
Xu. Y. (Candidate)	Conception and design (85%) Analysis and interpretation (85%) Drafting and production (85%)
Williams, D.J.	Conception and design (10%) Analysis and interpretation (10%) Drafting and production (10%)
Serati, M.	Conception and design (5%) Analysis and interpretation (5%) Drafting and production (5%)

Xu, Y., Methiwala, J., Williams, D. J., Serati, M., 2018. Strength and consolidation characteristics of clay with geotextile-encased sand column. Proceedings of the Institution of Civil Engineers - Ground Improvement. 171 (3) 125-134. https://doi.org/10.1680/jgrim.17.00070 – incorporated as **Paper VI**.

Contributor	Statement of contribution
Xu. Y. (Candidate)	Conception and design (80%) Analysis and interpretation (80%) Drafting and production (80%)
Methiwala, J.	Conception and design (10%) Analysis and interpretation (10%) Drafting and production (10%)
Williams, D.J.	Conception and design (5%) Analysis and interpretation (5%) Drafting and production (5%)
Serati, M.	Conception and design (5%) Analysis and interpretation (5%) Drafting and production (5%)

Submitted manuscripts included in this thesis

Xu, Y., Wu, S., Williams, D. J., Serati, M., 2018. Triaxial testing of clay with geotextile encased sand column. – incorporated as **Paper V**.

Contributor	Statement of contribution
Xu. Y. (Candidate)	Conception and design (80%) Analysis and interpretation (80%) Drafting and production (80%)
Wu, S.	Conception and design (10%) Analysis and interpretation (10%) Drafting and production (10%)
Williams, D.J.	Conception and design (5%) Analysis and interpretation (5%) Drafting and production (5%)
Serati, M.	Conception and design (5%) Analysis and interpretation (5%) Drafting and production (5%)

Publications during candidature

Peer-reviewed journal papers:

Xu, Y., Wu, S., Williams, D. J., Serati, M., 2018. Determination of peak and ultimate shear strength parameters of compacted clay. Engineering Geology. 243, 160-167. https://doi.org/10.1016/j.enggeo.2018.07.001

Xu, Y., Williams, D. J., Serati, M., 2018. Influence of anchorage angles on pull-out resistance of geotextile wrap around anchorage. Geosynthetics International. 25 (4), 378-391. https://doi.org/10.1680/jgein.18.00022

Xu, Y., Williams, D. J., Serati, M., Vangsness, T., 2018. Effects of scalping on direct shear strength of crusher run and crusher run/geogrid interface. Journal of Materials in Civil Engineering. 30 (9) 04018206. https://doi.org/10.1061/(ASCE)MT.1943-5533.0002411

Xu, Y., Williams, D. J., Serati, M., 2018. Measurement of shear strength and interface parameters by multi-stage large-scale direct/interface shear and pull-out tests. Measurement Science and Technology. 29 (8) 085601. https://doi.org/10.1088/1361-6501/aacb8a

Xu, Y., Methiwala, J., Williams, D. J., Serati, M., 2018. Strength and consolidation characteristics of clay with geotextile encased sand column. Proceedings of the Institution of Civil Engineers - Ground Improvement. 171 (3) 125-134. https://doi.org/10.1680/jgrim.17.00070

Xu, Y., Williams, D. J., Serati, M., 2018. Investigation of shear strength of interface between roadbase and geosynthetics using large-scale single-stage and multi-stage direct shear test. Road Materials and Pavement Design. https://doi.org/10.1080/14680629.2018.1561378

Xu, Y., Yan, G., Williams, D. J., Serati, M., Scheuermann, A., Vangsness, T., 2018. Experimental and numerical studies of a strip footing on geosynthetic-reinforced sand. Journal of Physical Modelling in Geotechnics. (Accepted)

Peer-reviewed conference papers:

Xu, Y., Williams, D. J., Serati, M., 2017. Effect of scalping on shear strength of aggregate. 51st U.S. Rock Mechanics/Geomechanics Symposium, 25-28 June, San Francisco, California, USA.

Xu, Y., Williams, D. J., Serati, M., 2017. Investigation of shear strength and breakdown of mine waste rock. 51st U.S. Rock Mechanics/Geomechanics Symposium, 25-28 June, San Francisco, California, USA.

Xu. Y., Williams, D. J., Hacker, J., 2018. Shear strength of compacted clay liner at McArthur River Mine. Mine Waste and Tailings 2018, 23-24 July, Brisbane, Australia.

Yan G., **Xu Y.,** Murgana V., Scheuermanna A. (2018) Application of Image Analysis on Two-Dimensional Experiment of Ground Displacement Under Strip Footing. Proceedings of GeoShanghai 2018 International Conference: Ground Improvement and Geosynthetics. GSIC 2018. Springer, Singapore, https://doi.org/10.1007/978-981-13-0122-3_2

Contributions by others to the thesis

Principle advisor (Prof David J. Williams) and associate advisor (Dr Mehdi Serati) advised on all aspects of designing the experiments, analysing and interpreting the test results obtained. They also reviewed all the journal and conference papers and this PhD thesis.

Statement of parts of the thesis submitted to qualify for the award of another degree

Some research outcomes in incorporated Paper VI formed part of an undergraduate engineering thesis submitted by Ms. Jayamini Methiwala, who was supervised by this PhD candidate and Prof David J. Williams.

Research Involving Human or Animal Subjects

No animal or human subjects were involved in this research.

Acknowledgements

First of all, I would like to express my greatest gratitude to my principle advisor Prof David J. Williams for his kind guidance and advice throughout my PhD candidature at UQ. Without his encouragement and continued support, I would have quit my PhD multiple times, and then this PhD thesis that you are reading now would not have been possible. I've got so much to acknowledge David, and the most important thing that I've learned from him and also valued the most is about the attitude towards research and life. For research, David taught me not to just simply accept what other people had written, published or believed, but to keep questioning whether they are right, wrong and why. For life, life is not always smooth sailing. Just like soil, starting with the letter "S", with a lot of soil characteristics showing "S"-shaped behaviours. Based on his over sixty years' life experiences, he told me that everything is a game, and think outside the box. That's another prosperity mindset that I've developed at UQ. David also provides me with the valuable consulting experience in working on several commercial industry projects.

I would also like to thank my associate advisor Dr Mehdi Serati, who advised me about research methods, result analysis and interpretation, academic writing, publication skills, etc. I appreciate that he has spent a huge amount of time from his busy schedule on editing and reviewing my papers. His insightful opinions and suggestions greatly increase the chances of getting my papers published. His advice, support, and encouragement have also largely promoted my research progress. In addition, I am very grateful to the research advice, assistance, help and encouragement from Dr Alexander Scheuermann, Dr Robert Day, Dr Chenming Zhang, Dr jurij Karlovsek, Dr Marcelo Llano Serna, Dr Ali Shokouhi, Dr Yunpeng Zhang, Dr Pei Zhang, Dr Chengji Shen, Dr Shengshen Wu (RMIT).

I would also thank our laboratory technical staffs, Sebastian Quintero Olaya, Jennifer Speer and Stewart Matthews for their kind assistance and help with my extensive experimental work. I would also thank Jayamini Methiwala, Vignesh Murgan, Stuart Kinsella, Keshini Preeyadarshanan, Cameron Fitzgerald, Tim Vangsness, Farzin Hamidi, Shriful Islam, Habibullah Bhuyan, Guanxi Yan, Scott Lines for their assistance to my laboratory experiments and research work, for sharing ideas and knowledge, and for wonderful time spent together at UQ.

Last but not the least, not like most of other PhDs' acknowledgement, I would like to write a short paragraph to acknowledge myself, who has experienced the pain that a lot of PhDs have experienced, who has been to the "place" where a lot of PhDs have been to, and who has finally survived the PhD. The knowledge, skills and experience that I've gained at UQ will help me excel and thrive, and my future success will be the best reward for all the people that I've acknowledged herein.

Financial support

I would like to acknowledge the UQ International (UQI) scholarship provided by the University of Queensland. Furthermore, I would like to acknowledge some extra commercial consulting revenue, which was paid by several industry clients, under the supervision of Prof David J. Williams at Geotechnical Engineering Centre (GEC) of UQ.

Keywords

composite behaviour, consolidation, direct shear, geosynthetics, interface behaviour, pull-out, reinforced soil, shear strength, triaxial

Australian and New Zealand Standard Research Classifications (ANZSRC)

ANZSRC code: 090501, Civil Geotechnical Engineering, 100%

Fields of Research (FoR) Classification

FoR code: 0905, Civil Engineering, 100%

TABLE OF CONTENTS

LIST OF FIGURES

LIST OF TABLES

LIST OF NOTATIONS

τ_s	direct shear strength of soil alone
$\tau_{s\text{-}s}$	stress strength between the soil and the soil in the aperture
$\tau_{s\text{-}g}$	stress strength between the soil and the geogrid ribs
τ_{ds}	interface shear strength between the geosynthetic and the soil
τ_f	shear strength at failure
τ_i	interface shear strength at failure
τ_p	pull-out shear strength between the geosynthetic and the soil
$\tau^{max}_{S/GG}$	interface shear strength between soil and geogrid
$\tau^{max}_{S/GSY}$	shear resistance between soil and geosynthetic surface
$\tau^{max}_{S/S}$	maximum shear strength of soil
$\tau^{max}_{bearing}$	maximum shear strength provided by transverse bearing members
η	shear strength contribution ratio caused by the shear resistance between the soil and the geogrid ribs
f_{ds}	direct shear interface coefficient
f_b	pull-out interface coefficient
C_i	interface coefficient
α	top angle
β	bottom angle
ϕ	internal friction angle
ϕ_{sec}	secant friction angle
δ_0	friction angle between soil and geogrid ribs
δ	interface friction angle
α_{ds}	the proportion of the surface area of the geogrid ribs in contact with soil
σ_n	normal stress
σ_b	bearing stress against the geogrid bearing members
σ_h	horizontal stress
c	apparent cohesion of soil
c_a	apparent adhesion between the geogrid and the soil
F_p	pull-out force
F^*	pull-out resistance factor
P_R	pull-out resistance per unit width
P_{Rmax}	maximum pull-out resistance

P_{RS}	frictional component of pull-out resistance
P_{RB}	bearing component of pull-out resistance
L_R	reinforcement length in the anchorage zone
S	spacing between geogrid bearing members
L_R/S	the number of geogrid bearing members
α_B	the fraction of total frontal area of geogrid available for bearing resistance
L	length of the bottom layer of the geotextile anchorage
D	the height of the anchor
B	length of the top layer of the geotextile anchorage
H	the height of the sand on top layer of the geotextile
T_1, T_2, T_3	tensile stress after a change of angle
T_1', T_2', T_3'	initial tensile stress before a change of angle
K_1, K_2, K_3	weighting coefficient (dimensionless)
K_0	coefficient of lateral earth pressure at rest (dimensionless)
Ψ	an angle in trigonometric function
W_g	width of the geotextile
D_{10}	the diameter in the particle size distribution curve corresponding to 10% finer
D_{30}	the diameter in the particle size distribution curve corresponding to 30% finer
D_{50}	the diameter in the particle size distribution curve corresponding to 50% finer (average particle size)
D_{60}	the diameter in the particle size distribution curve corresponding to 60% finer
F_{200}	Percentage passing through the No. 200 sieve
B_{10}	particle breakage index ($1-D_{10f}/D_{10i}$)
B_{15}	particle breakage index (D_{15i}/D_{15f})
B_{60}	particle breakage index ($D_{60i}-D_{60f}$)
C_u	uniformity coefficient
C_z	coefficient of gradation
G_s	specific gravity
ρ_{dmax}	maximum dry density
ρ_{dmin}	minimum dry density
w	moisture content
c'	intercept of the effective stress failure envelope
ϕ'	slope of the effective stress failure envelope

a'	intercept of the K_f line on the p-q diagram
ψ'	slope of the K_f line on the p-q diagram
Δu_f	induced pore water pressure at failure
u_0	initial pore pressure (back pressure)
σ_{3c}'	effective confining pressure
σ_{3f}'	effective minor principal stress at failure
σ_{3f}	total minor principal stress at failure
σ_{1f}'	effective major principal stress at failure
σ_{1f}	total major principal stress at failure
$\Delta\sigma_{df}'$	effective maximum deviator stress at failure
$\Delta\sigma_{df}$	total maximum deviator stress at failure
τ	shear stress
σ	total normal stress
σ'	effective normal stress
A_f	Skempton's pore water pressure parameters
p	$(\sigma_1 + \sigma_3)/2$
p'	$(\sigma_1' + \sigma_3')/2$
q	$(\sigma_1 - \sigma_3)/2$
p_f	$(\sigma_{1f} + \sigma_{3f})/2$
p_f'	$(\sigma_{1f}' + \sigma_{3f}')/2$
q_f	$(\sigma_{1f} - \sigma_{3f})/2$
e	void ratio
e_0	initial void ratio
σ_{vc}'	effective consolidation stress
F	shear resistance
D_f	shear displacement at failure
σ_{nf}	applied normal stress at failure
A_t	total contact area during shearing
A_c	plane area of the clay
A_s	plane area of the sand
τ_c	shear strength of the clay
$\tau_{f,\,exp}$	experimental obtained shear strength
$\tau_{f,\,pred}$	predicted shear strength

α_c	proportions of the surface area of the clay
α_s	proportions of the surface area of the sand
m_c	dry mass of the clay
m_s	dry mass of the sand
m_t	total mass of the composite specimen
$G_{s,c}$	specific gravity of the clay
$G_{s,s}$	specific gravity of the sand
$G_{s,comp}$	specific gravity of the composite specimen
C_c	compression index
C_s	swell index
C_r	recompression index
C_α	secondary compression index
c_v	coefficient of consolidation
a_v	coefficient of compressibility
m_v	coefficient of volume compressibility
E_s	modulus of compressibility
k	hydraulic conductivity
H	length of drainage path
t	time

LIST OF ABBREVIATIONS

GCL	Geosynthetics Clay Liner
OSC	Ordinary Sand Column
GESC	Geotextile Encase Sand Column
UU	Unconsolidated Undrained
CU	Consolidated Undrained
OCR	Over Consolidation Ratio
PWP	Pore Water Pressure
TS	Total Stress
ES	Effective Stress
TSP	Total Stress Path
ESP	Effective Stress Path
$(T-u_0)SP$	(Total stress-Initial pore pressure)Stress Path
LL	Liquid Limit
PL	Plastic Limit
PI	Plasticity Index
USCS	Unified Soil Classification System
SP	Poorly Graded Sand
SW	Well Graded Sand
GW	Poorly Graded Gravel
LDS	Large-scale Direct Shear
MDS	Medium-scale Direct Shear
SDS	Small-scale Direct Shear
PSD	Particle Size Distribution
MRM	McArthur River Mine
HDPE	High-density Polyethylene
PVC	Polyvinyl Chloride
EPDM	Ethylene Propylene Diene Terpolymer

1 INTRODUCTION

1.1 Background

The use of inclusions to improve the mechanical properties of soils dates back to ancient times. Over two thousand years ago, people had already found that putting some additional inclusions into soils will significantly improve their engineering behaviour and performance. This is because the tensile strength of a soil is much weaker than its compression strength and shear strength. The additional included materials that are stronger in tensile resistance complement the tensile weakness of the soils when they work together. Back to the old times, natural materials, such as branches, straws, bamboos or other wooden plants were typically chosen as the inclusions. However, the uses of these natural materials had been restricted to their limited tensile resistance, poor durability and uncontrollable variability. Over the past three decades, artificial geosynthetic materials have become widely used in engineering practices due to the excellent strength and high durability, which was regarded as a revolution in geotechnical engineering (Giroud 1986). Geosynthetic-reinforced soils structures, such as building foundations, slopes, retaining walls, embankments, pavements, etc., have become increasingly popular in the field of geotechnical engineering. In particular for ground improvement purpose, a soil mass can be embedded with horizontally placed layers of geosynthetics, or vertically replaced with ordinary sand column (OSC) and geosynthetic-encased sand columns (GESC). When subjected to a vertical load (compression) or horizontal load (shear), a reinforced soil composite typically exhibits better mechanical performance than an unreinforced soil mass, with higher load carrying capacity, strength and stiffness.

1.2 Statement of research questions

Geotechnical instability and potential failure of geosynthetic-reinforced soil masses are the major concerns for geotechnical engineers. The behaviour and performance of a geosynthetic-reinforced soil composite involves complex interaction mechanisms between the soil and geosynthetic reinforcing elements. Due to this complexity, the behaviour and performance of geosynthetic-reinforced soil composites are not fully understood and cannot be reliably predicted. The main focus of the research is to give more insight into the

understanding of the interface and composite behaviour of geosynthetic-reinforced soils, as summarised in the following questions.

Interface behaviour:

(1) What are the interaction mechanisms between the soil particles and geogrids with different aperture shapes, sizes and thicknesses?

(2) How can the contribution of each shear strength component mobilised along the interface between the soil and geogrid, such as the soil-soil friction and the soil-geogrid rib friction, be quantified?

(3) Interface shear and pull-out tests are most commonly used to determine soil-geosynthetic interface parameters.

   a. What are the interactions and relationships between the interface shear stress and pull-out shear stress mobilised along the soil-geosynthetic interface in these two testing methods?

   b. Can the interface shear strength and pull-out shear strength be predicted from each other for the same soil and geosynthetic materials, or be directly predicted from the internal shear strength of the soil using some interface coefficients?

(4) Can the multi-stage testing method be successfully applied in large-scale direct/interface shear and pull-out tests, and provide reasonable and acceptable results in order to save time and money, and under what circumstances?

(5) How does the anchorage angle influence the pull-out performance of a wrap around anchorage, and what are the mobilisation processes of the pull-out resistance for a geosynthetic wrap around anchorage and the theoretical pull-out mechanism at the soil-geosynthetic interface?

Composite behaviour:

(1) How does the composite clay reinforced with OSC and GESC respond when subjected to lateral and vertical loading?

(2) What is the strength and consolidation behaviour of the composite clay with OSC and GESC?

(3) How does the OSC and GESC influence the shear strength parameters, consolidation parameters, pore water pressure, Mohr circle, failure envelope and stress path?

1.3 Research objectives and methodologies

As the statement of research questions mentioned above, this research was motivated by the need for an improved understanding of the interface and composite behaviour of geosynthetic-reinforced soils to contribute towards the safe and economical design for a wide range of geotechnical applications adopting geosynthetic-reinforced soil techniques. Therefore, laboratory experimental tests, theoretical derivation and mathematical regression analyses are the three main methodologies adopted in this research in order to investigate the interaction mechanism and the composite performance of soils reinforced with geosynthetics at different configurations. Overall, laboratory testing is the main methodology adopted throughout the PhD candidature, and the extensive laboratory tests have been carried out regarding each aspect of the research to seek for the answers to the proposed research questions. Mathematical and theoretical methods are basically used to further explain and interpret the experimental results and findings. Table 1.1 shows a summary of the research objectives for each topic and the corresponding methodologies used. The detailed methodologies for each sub-topic, such as experimental set-up, theoretical interpretation, and step-by-step formula derivation can be found in the relevant papers in Appendix A.

Table 1.1 Summary of research objectives and methodologies

Behaviour	Objectives	Methodologies
Interface	To further investigate the interaction mechanism between soils and geosynthetics, especially for soil-geogrid interface involved with apertures	1. Single-stage and multi-stage large-scale a) direct shear tests; b) interface shear tests; c) pull-out tests 2. Sieving analyses 3. Characterisation Tests 4. Theoretical derivation 5. Mathematical regression analyses
	To study the effect of scalping on direct and interface shear strength of aggregate, and the particle breakage caused by large shear testing	
	To investigate the relationships between direct shear strengths of soils, interface shear strengths and pull-out shear strengths of soil-geogrid interfaces	
	To investigate the feasibility, reliability and applicability of multi-stage testing in large-scale direct/interface shear and pull-out tests	
	To study the influence of anchorage angles on the pull-out resistance of geotextile wrap around anchorage both experimentally and theoretically	
Composite	To investigate the effects of OSC and GESC on triaxial shear strength, consolidation parameters, pore water pressure, Mohr circle, failure envelope, strength parameters, and stress path	1. Small-scale direct shear tests 2. Oedometer tests 3. Slurry consolidation tests 4. CU triaxial tests
	To study the direct shear strength and consolidation characteristics of reinforced clay composites, including clay, clay with OSC, and clay with GESC	

1.4 Thesis structure

This PhD thesis is constructed in a paper-based format by incorporating publications during the PhD candidature. It consists of four chapters and two appendices, comprising six journal papers covering the core of the thesis. The papers in Appendix A are attached in a logical sequence in order to support the main PhD topic. Appendix B shows the practical implications for industry based on the research skills, knowledge and experience gained during the PhD candidature.

The first chapter mainly introduces the background, statement of research questions, research objectives and methodologies, and thesis structure. At the end of this chapter, the links between the included papers are highlighted to ensure the entire thesis has a logical flow.

The second chapter introduces a review of literature relevant to each sub-topic, including reinforced soil, geosynthetics, soil-geosynthetic interface theory, standard testing method and previous soil-geosynthetic interface study, and composite behaviour relevant to strength and consolidation for soils reinforced with geosynthetic-encased granular columns. More specific literature reviews for each relevant topic could also be found in the included papers in Appendix A.

The third chapter provides a summary of six journal papers produced during the PhD candidature. It aims to summarise and highlight the research gaps, questions and objectives, the research methodologies, and the main contributions to the current literature.

The last chapter presents a summary of the most significant findings and conclusions obtained from this PhD research, and the proposed future study to further explore and extend some research topics.

1.5 Links between included papers

The six journal papers are included in a logical and cogent sequence and are linked together, supporting the main research topic of this PhD thesis, i.e., interface and composite behaviour of geosynthetic-reinforced soils. Figure 1.1 shows a logical flowchart of this PhD thesis, breaking down the main topic into four sub-topics, including direct and

interface shear behaviour, pull-out behaviour, strength behaviour, and consolidation behaviour. For each sub-topic, studies were carried out to achieve different research objectives and answer several research questions, as summarised in Figure 1.1. The suitable methodologies adopted for each topic can also be referred to Table 1.1.

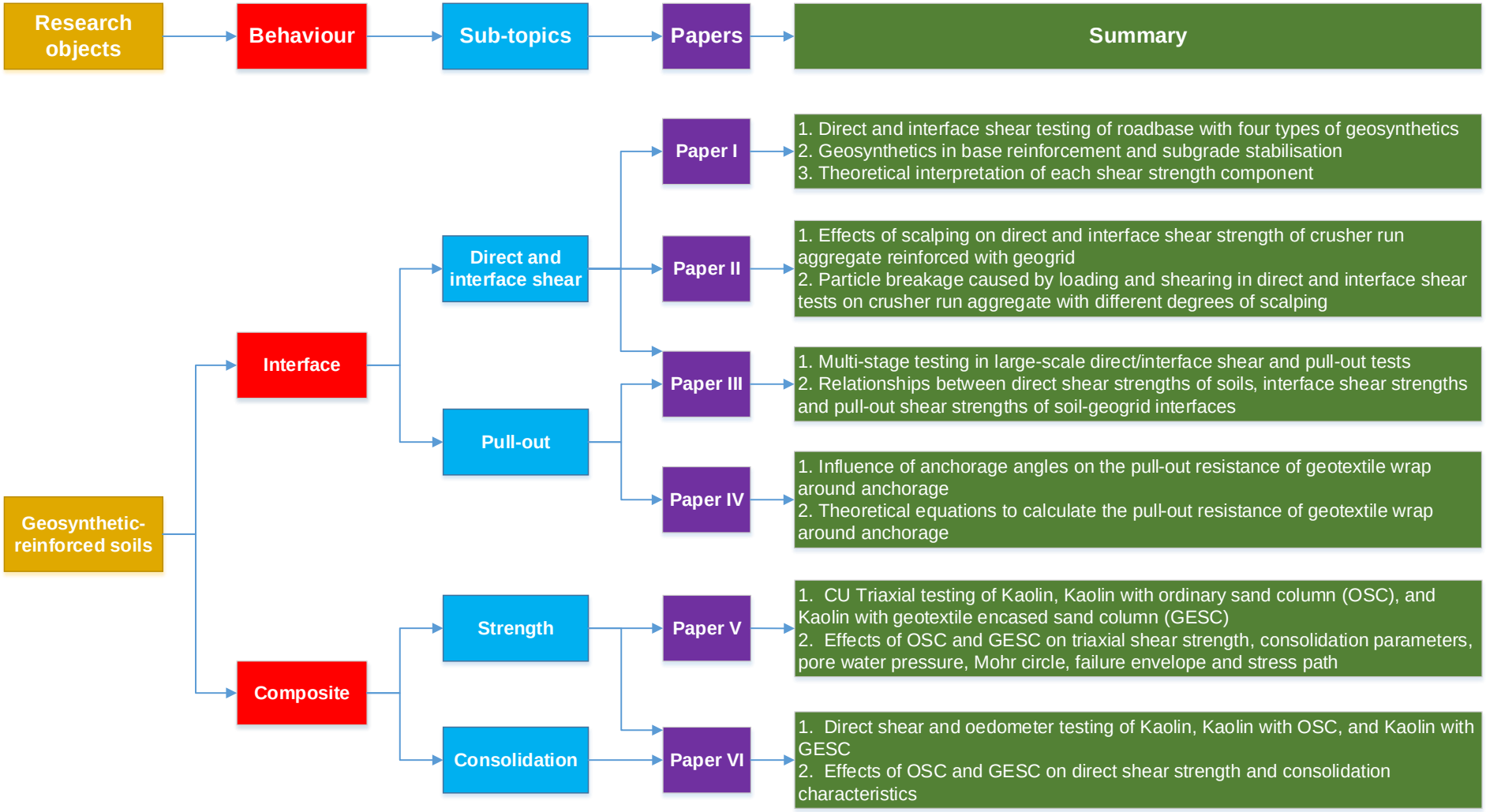

Figure 1.1 Links between thesis topics and incorporated papers

2 LITERATURE REVIEW

2.1 Introduction

This chapter first introduces the concept of reinforced soils and geosynthetics, having a general understanding of what a geosynthetic-reinforced soil is comprised of. Then, it reviews the fundamental interface theories between soils and geosynthetics in direct shear and pull-out tests, including the direct shear resistance, pull-out resistance, interface parameters, and interaction mechanism. Standard ASTM single-stage direct shear and pull-out tests are then introduced, together with the limited references that are related to multi-stage testing available in the literature. Moreover, the previous studies on geosynthetics-soil interface are critically reviewed, in particularly for summarising the contribution and useful information for this PhD research. Finally, the composite behaviour related to the strength of consolidation of the composite soils reinforced with OSC and GESC is reviewed, and the remained research gaps are highlighted.

2.2 Reinforced soils

The use of reinforced soils is much earlier than the use of reinforced concrete in the timelines of world history (Jones 1996). The earliest remaining reinforced soil structure is Babylon ziggurat, which was constructed of clay bricks with inclusions of woven reed mats. The Romans are also known to have mastered the earth reinforcing techniques since 2000 years ago, such as the famous Roman Army project of a wharf for the Port of Londinium where the timber reinforcing elements were embedded in the backfill. Some parts of Great Wall of China, one of the eight wonders of the world, were also constructed using clay and gravel reinforced with tamarisk branches and straws about 2000 years ago. There are also a lot more intelligent applications of reinforced soils in the history. Our smart ancestors have already found that a significant reduction could be made in the lateral pressure acting on the retaining wall if the backfill was reinforced by horizontal layers of brushwood, wooden plants, bamboos, canvas, etc (Jones 1996). This has helped to safely construct higher and steeper soil retaining walls. Furthermore, from an economic point of view, using reinforced soil technique is able to save construction budget by reducing the purchase of expensive high-quality backfill materials.

2.3 Geosynthetics

2.3.1 Types of geosynthetics

Geosynthetic is a planar product manufactured from polymeric materials, which is used with soil, rock, earth, or other geotechnical engineering related materials as an integral part of a man-made project, structure, or system (ASTM D4439). Geosynthetics include a wide range of types, such as Geotextile, Geogrid, Geomembrane, Geonet, Geoweb, Geopipe, Geotube, Geofoam, Geocomposite, Geosynthetics Clay Liner (GCL), etc. Different geosynthetic products have different functions for a wide range of applications, such as drainage, filtration, separation, protection, planar drain, fluid/gas barrier and reinforcement (Shukla 2002).

(1) Geotextile: Geotextile is mainly manufactured from polyester or polypropylene, which has excellent strength and high durability. There are two basic types, i.e., woven and nonwoven. Nonwoven geotextiles are typically used for subsurface drainage and erosion control applications, as well as road stabilisation over soft soils. Woven geotextiles are made from weaving monofilament, multifilament, or slit film yarns. High strength woven geotextiles are primarily used as reinforcement applications.

(2) Geogrid: Geogrid is commonly made from extruding and stretching high-density polyethylene or polypropylene, or by weaving or knitting and coating high tenacity polyester yarns. The geogrids have openings (also called apertures), which can provide confinement to soil particles. The excellent tensile strength and stiffness of geogrids make them function as effective reinforcement elements in soils.

(3) Geomembrane: Geomembrane is a synthetic membrane liner (or barrier) to separate different materials in a human-made project, structure or system, such as nuclear waste, tailings, coarse and fine, etc. The raw materials used for manufacturing geomembranes are basically processed into sheets of various widths and thickness by extrusion, calendaring and spread coating. The geomembranes available in the markets typically include high-density polyethylene (HDPE), polyvinyl chloride (PVC), and ethylene propylene diene terpolymer (EPDM).

(4) Geotube: Geotube is manufactured from high strength woven geotextiles, sewn together to form a tube, which is a dewatering container used for treatment of mining tailings, coal sludge, and other waste.

(5) Geosynthetics Clay Liner (GCL): GCL is manufactured by including a bentonite clay layer within two layers of geotextiles and/or geomembranes. The intermediate clay layer works as an effective hydraulic barrier.

(6) Geofoam: Geofoam is a type of artificial lightweight construction material. The primary function of geofoam is to provide a lightweight fill for slope, retaining wall, embankment, pavement, highway, and parking lot.

(7) Geocell: Geocell is a 3D cellular confinement system, infilled with compacted soils, which can increase confinement and decrease lateral movement of soils.

(8) Geocomposites: Geocomposite means a combination of geotextiles, geogrids, geonets and/or geomembranes, etc, utilising the multiple functions for different specific applications.

2.3.2 Application of geosynthetics

When dealing with weak soils in the field, the conventional methods are normally replacing them, or passing them with expensive deep foundations (Shukla 2002). However, the application of geosynthetic reinforcement has provided much easier and more effective solutions in geotechnical engineering, due to its economic, practical and environmental superiorities. The main distinguished advantages of applying geosynthetics in reinforced soil construction include the high tensile strength, durability, reliability, flexibility, aesthetics, easier to design and construct, fantastic seismic performance, more economical, and the excellent ability to adapt and tolerate large deformation or differential deformation (Shukla 2002). Therefore, geosynthetics have been increasingly used in different geotechnical applications in the past three decades, such as slopes, retaining walls, bridge abutments, embankments, foundations, railways, pavements, etc. With the inclusion of geosynthetics, slopes and retaining walls are able to be constructed much higher and steeper, without inducing geotechnical instability. This has effectively solved the intractable problems where design is controlled by space constraints. For foundation, railway or embankment, a significant increase in bearing capacity could be achieved after

the soil materials are reinforced with geosynthetics. In pavement engineering, geosynthetics are typically embedded as a reinforcing layer at the interface between the soft subgrade and granular base layer for subgrade stabilisation. Further, geosynthetics are also designed to be installed within the base or subbase layer for base reinforcement. The satisfactory performances of geosynthetics have been well discovered and recognised, such as increasing lateral confinement of soils, improving bearing capacity and overall rigidity, reducing vertical and lateral deformations. Moreover, from an economic perspective, it has been found the inclusion of geosynthetics can decrease the required thickness of the base layer, reduce road maintenance costs, and increase road life-time (Zornberg 2011).

2.4 Interface theory between soils and geosynthetics

The geosynthetic reinforcement increases bearing capacity and reduces deformation of soils due to soil-geosynthetic interaction (Lopes 2002). Therefore, the interface behaviour between soils and geosynthetics plays a very important role in the stability of geosynthetic-reinforced soil structures. It is the soil-geosynthetic interface where the geosynthetic reinforcement and the soil interact and communicate with each other. At a soil-geosynthetic interface, the geosynthetic reinforcement restrains the lateral deformation of the surrounding soil by increasing the confinement (internal restraint) of soil particles. This consequently increases the stiffness and strength of the soil composite. Many studies have been conducted on geosynthetic-reinforced soils in the past 30 years, however, the interaction mechanism between soil and geosynthetic reinforcement in a composite soil mass has not yet been fully elucidated, especially for geogrid with complex apertures.

2.4.1 Direct shear resistance

The direct shear resistance between soil and geotextile is only attributed to the friction between the soil and geotextile surface. However, the direct shear resistance between soil and geogrid is made up of two components: one is the friction between the soil and geogrid ribs, and the other one is the friction between the soil and soil in the apertures, as shown in Figure 2.1.

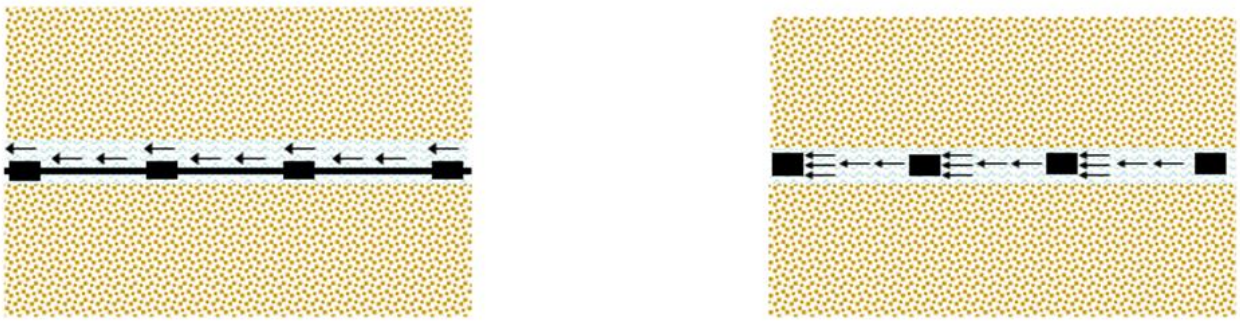

(a) (b)

Figure 2.1 Interaction mechanisms between soil and geogrid in direct shear tests: (a) friction between soil and ribs; (b) friction between soil and soil in apertures

Jewell et al. (1984) conducted the first theoretical study on soil-geogrid interaction under the direct shear condition, which can be described by the following equation:

$$\tau_{ds} = f_{ds}\sigma_n \tan\phi = \sigma_n \left[\alpha_{ds} \tan\delta + (1-\alpha_{ds}) \tan\phi\right] \quad (1)$$

where ϕ is the soil internal friction angle, δ is the theoretical interface friction angle between the soil and reinforcement shear surface, which is a material parameter, f_{ds} is the interface coefficient, α_{ds} is the fraction of geogrid surface area in contact with soil, i.e., the area of ribs (longitudinal and transverse) to total geogrid plane area, σ_n is the normal stress, τ_{ds} is the interface direct shear strength between soil and geosynthetics.

From Eq. (1), it is possible to obtain the theoretical interface coefficient as follows:

$$f_{ds} = 1-\alpha_{ds}(1-\frac{\tan\delta}{\tan\phi_{ds}}) \quad (2)$$

Based on the experimental direct and interface shear test results, the interface coefficient can also be obtained by the following equation:

$$f_{ds} = \frac{\tau_{ds}}{\tau_s} \quad (3)$$

where τ_{ds} is the experimentally determined interface shear strength between soil and geogrid, τ_s is the direct shear strength of soil.

$$\tau_{ds} = c_a + \sigma_n \tan\delta \quad (4)$$

where c_a is the overall adhesion between soil and geogrid, δ is the overall interface friction angle. Herein, c_a and δ are obtained from a best-fit straight line from the experimental results.

This fundamental theory of direct shear resistance (Jewell et al. 1984) lays a foundation for explaining the interaction mechanism between soils and geogrids in the literature. However, Equation (1) is just a theoretical equation, and the interface friction angle δ in Eq. (1) is a theoretical material interface parameter. It is impossible to only measure the shear resistance between the soil and geogrid ribs from the experiments. On the other hand, an overall interface friction angle could be calculated from the experimentally obtained interface shear test results using a best-fit straight line, as shown in Eq. (4). It is worth mentioning that a lot of references in the literature confuse the theoretical interface friction angle with the experimental obtained one. This ambiguity has been discussed in Paper I (see Appendix A), and an in-depth insight into the interaction mechanism between soil and geogrid under direct shear conditions is presented by proposing an equation to quantify the shear resistance between the soil and geogrid ribs based on back calculation.

2.4.2 Pull-out resistance

(a) (b)

Figure 2.2 Interaction mechanisms between soil and geogrid in pull-out tests: (a) friction component; (b) bearing component

For geotextiles with continuous surfaces, the pull-out resistance is only attributed to the friction between the soil and geotextile surfaces. For geogrids with apertures, the pull-out resistance is contributed by the friction on the surfaces of the geogrid ribs (frictional

resistance) and the passive resistance mobilised against the transverse ribs (bearing resistance). The interaction mechanism in pull-out tests is depicted in Figure 2.2.

Jewell et al. (1984) proposed the first theoretical equation to quantify the pull-out resistance per unit width of reinforcement (P_R):

$$P_R = 2 f_b L_R \sigma_n \tan\phi \tag{5}$$

where ϕ is the internal friction angle of soil, L_R is the reinforcement length in contact with soil, σ_n is the normal stress, f_b is the pull-out interface coefficient, P_R is the pull-out resistance per unit width. The frictional component, for a geogrid of length L_R and a unit of width, can be calculated by the following expression:

$$P_{RS} = 2\alpha_{ds} L_R \tau = 2\alpha_{ds} L_R \sigma_n \tan\delta \tag{6}$$

The bearing component can be calculated by the following equation:

$$P_{RB} = \left(\frac{L_R}{S}\right)\alpha_B \sigma_b B \tag{7}$$

where S is the spacing between geogrid bearing members, L_R/S is the number of geogrid bearing members, α_B is the fraction of the total frontal area of geogrid available for bearing resistance, B is the bearing member thickness, and σ_b is the bearing stress against the geogrid bearing members. Therefore, assuming that the shear stress along the reinforcement is uniform during pulling, Jewell (1990) proposed a theoretical expression to evaluate the overall pull-out resistance of a geogrid:

$$P_R = P_{RS} + P_{RB} = 2\alpha_{ds} L_R \sigma_n \tan\delta + \left(\frac{L_R}{S}\right)\alpha_B \sigma_b B = 2 f_b L_R \sigma_n \tan\phi \tag{8}$$

The interface coefficient f_b under a pull-out testing condition can be expressed as a function of reinforcement geometrical parameters (α_{ds}, α_B, B, and S), soil friction angle ϕ, soil-geosynthetic friction angle δ, and effective stresses acting at the interfaces (σ_n and σ_b), as shown below:

$$f_b = \alpha_{ds}\left(\frac{\tan\delta}{\tan\phi}\right) + \left(\frac{\alpha_B B}{S}\right)\left(\frac{\sigma_b}{\sigma_n}\right)\frac{1}{2\tan\phi} \tag{9}$$

Based on the experimental pull-out test results, the pull-out interface coefficient can be obtained by the following equation:

$$f_b = \frac{P_R}{2L_R\sigma_n \tan\phi} = \frac{\tau_p}{\tau_s} \tag{10}$$

where τ_p is the maximum pull-out shear stress obtained from pull-out tests, τ_s is the direct shear strength of soil obtained from direct shear tests.

$$\tau_p = \frac{P_R}{2L_R} \tag{11}$$

For granular soils, bearing stress σ_b on geogrid bearing members is related to the internal friction angle of soil, the initial stress state, the interface roughness, and the reinforcement depth in relation to the sizes of the bearing members (Moraci and Gioffre 2006). Bearing stress can be evaluated by the following bearing capacity theories based on different failure mechanisms.

For the general shear failure mechanism, the ratio σ_b/σ_n can be defined as follows (Peterson and Anderson 1980):

$$\frac{\sigma_b}{\sigma_n} = e^{\pi\tan\phi}\tan^2(\frac{\pi}{4}+\frac{\phi}{2}) \tag{12}$$

For the punch failure mechanism, Jewell et al. (1984) proposed the following equations:

$$\frac{\sigma_b}{\sigma_n} = e^{(\frac{\pi}{2}+\phi)\tan\phi}\tan(\frac{\pi}{4}+\frac{\phi}{2}) \tag{13}$$

Bergado et al. (1993) proposed a solution to calculate bearing stress based on a modified punching mechanism:

$$\frac{\sigma_b}{\sigma_n} = e^{\pi\tan\phi}\tan(\frac{\pi}{4}+\frac{\phi}{2})\frac{1}{\cos\phi} \tag{14}$$

Matsui et al. (1996) proposed an equation based on a Prandtl's mechanism:

$$\frac{\sigma_b}{\sigma_n} = e^{\pi \tan\phi} \tan(\frac{\pi}{4} + \frac{\phi}{2}) \times \left[\cos(\frac{\pi}{4} - \frac{\phi}{2}) + (1 - \sin\phi) \sin(\frac{\pi}{4} - \frac{\phi}{2}) \right] \quad (15)$$

The pull-out resistance per unit width of a reinforcement may be expressed as a function of interface apparent coefficient of friction, $\mu_{S/GSY}$ (Moraci and Recalcati, 2006):

$$P_R = 2L_R \sigma_n \mu_{S/GSY} \quad (16)$$

According to the Federal Highway Administration (FHWA) documents (Berg et al. 2009; Christopher et al. 1990), the pull-out resistance can also be calculated using the following equation:

$$P_R = 2L_R \sigma_n F^* \alpha \quad (17)$$

where F^* is the pull-out resistance, and α is a scale effect correction. The parameter α is related to the strain softening of the compacted soil, and the extensibility and length of the reinforcement (Berg et al. 2009), which are assumed to be 0.8 for geogrids, and 0.6 for geotextiles. For geotextiles, F^* can be simply calculated based on the soil friction angle:

$$F^* = \frac{2}{3} \tan\phi \quad (18)$$

Alternatively, F^* can also be determined from the soil-geotextile interface friction angle.

$$F^* = \tan\delta \quad (19)$$

As shown in Eq. (17), α can be back-calculated as below:

$$\alpha = \frac{P_R}{2L_R \sigma_n \tan\delta} \quad (20)$$

Therefore, the following correlation can be found:

$$f_b \tan\phi = \mu_{S/GSY} = F^* \alpha \quad (21)$$

This review brings up a very important research question about the relationships between the direct shear strengths of soils, interface shear strengths and pull-out shear strengths of soil-geogrid interfaces. Equations (4, 10, 16-21) have shown that they may have some

empirical correlations related to the interface parameters and coefficients. This question is also significantly meaningful to understand the different interface mechanisms in direct/interface shear and pull-out tests. More information could be found in Paper III in Appendix A.

2.5 Interface testing methods

2.5.1 Conventional single-stage testing standard

There are mainly two experimental methods to determine the interface parameters in laboratory characterised by direct shear and pull-out tests, corresponding to the following two testing standards respectively.

(1) Standard test method for determining the coefficient of soil and geosynthetic or geosynthetic and geosynthetic friction by the direct shear method (ASTM D5321-14)

The conventional direct shear apparatus with the size of (60 mm by 60 mm or 100 mm by 100 mm) has serious limitations for testing the soil specimens with large particles and geogrid with large apertures due to the scale effect and boundary conditions. It has been proved that the size of the shear box can influence the direct shear test results. Ingold (1982) concluded that the friction angle obtained from a small shear box (60 mm by 60 mm) was 2-3° higher than that obtained from a large shear box (300 mm by 300 mm). The minimum dimension of a shear box recommended by ASTM D5321 for testing the soil-geosynthetic interface should be the greater of 300 mm, 15 times the D_{85} of coarser soil or a minimum of 5 times the maximum opening size of the geosynthetic. The depth of each container that contains soil must be a minimum of 50 mm or 6 times the maximum particle size, whichever is greater. Therefore, it is not suitable to use a conventional small shear box for testing the geosynthetics with large aperture size and coarse-grained soils with large particles. Instead, large-scale shear box tests are recommended to be selected in order to test enough representative specimens.

The conventional single-stage direct/interface shear testing method is summarised herein. A geosynthetic specimen is fixed on the top of the lower shear box or the bottom of the upper shear box, which is embedded within the soil. A constant normal force is applied to the top of the specimen, and then a tangential (shear) force is applied to the apparatus so

that one section of the box moves in relation to the other. The interface shear stress is therefore mobilised along the soil-geosynthetic interface during the shearing process. The measured shear force is recorded as a function of shear displacement during the shearing process. The single-stage tests are normally carried out on at least three specimens under three different normal stresses, which are representative of the field conditions. The interface shear test results can be interpreted by Mohr-Coulomb shear strength criteria, referring to the interface friction angle and adhesion. That is, the obtained maximum shear stresses are plotted against the applied normal stresses, which are represented by a best-fit straight line (failure envelope). The inferred slope of the failure envelope is the interface friction angle between the soil and geosynthetic, and the y-intercept is the adhesion.

(2) Standard test method for measuring geosynthetic pull-out resistance in soil (ASTM D6706-13)

According to the specification of ASTM D6706, the standard pull-out box should be square or rectangular with minimum dimensions 610 mm long by 460 mm wide by 305 mm deep if the sidewall friction is minimised; otherwise, the minimum width should be 760 mm. The dimensions of the pull-out box need to be increased if necessary in order to satisfy the testing standard. The minimum width should be the greater of 20 times D_{85} of the soil or 6 times the maximum particle size of the soil. The minimum length should be greater than 5 times the maximum geogrid aperture size. The box shall allow for a minimum depth of 150 mm above and below the geosynthetic. The depth of the soil in the box above or below the geosynthetic should be a minimum of 6 times D_{85} of the soil or 3 times the maximum particle size of the soil, whichever is greater. The box must allow for at least 610 mm embedment length beyond the load transfer sleeve and a minimum specimen length to width ratio of 2.0. When testing the geosynthetic specimens with larger apertures, the pull-out box may have to be larger than the stated minimum dimensions. A typical pull-out box is shown in Figure 2.3.

The conventional single-stage pull-out testing method is also summarised herein. A geosynthetic specimen is embedded within the soil in a pull-out box. A normal force is applied to the top of the soil, and a horizontal force is then applied to the geosynthetic to pull it out of the soil specimen. The measured pull-out force is recorded as a function of pull-out displacement during the pulling process. At least three individual pull-out tests need to be carried out under three normal stresses for single-stage tests. The pull-out

resistance is calculated by dividing the pull-out force by the width of the geosynthetic specimen. Finally, a plot of maximum pull-out resistance versus applied normal stress is obtained. The pull-out shear strength can be obtained using Eq. (11) and plotted against applied normal stress. The plot of pull-out shear strength versus normal stress can also be represented by a best-fit straight line from which the interface parameters could be inferred.

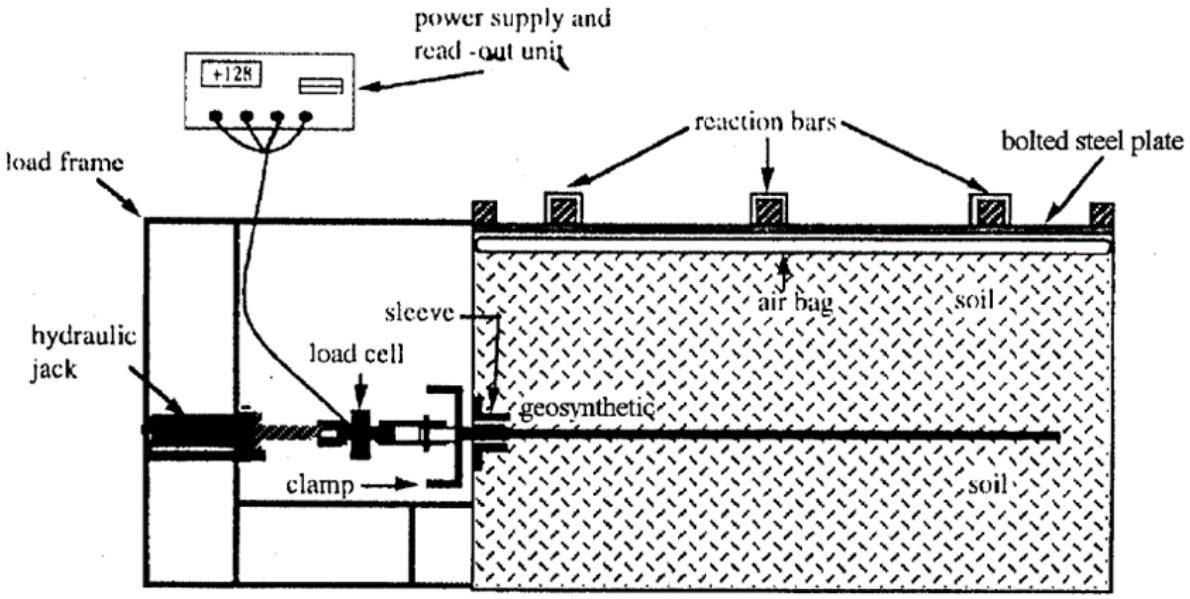

Figure 2.3 Experimental set-up for geosynthetic pull-out testing (ASTM D6706-13)

2.5.2 Multi-stage testing method

(1) Direct shear tests

The earliest literature of multi-stage testing method that could be found is a master thesis written by Gullic (1970) in the University of Missouri-Rolla, USA. Gullic (1970) ran a series of multi-stage direct shear and triaxial tests on a cohesionless soil. In terms of the direct shear tests, Gullic used a small shear box with a diameter of 62.0 mm and a specimen height of 25.8 mm. It was found that the first stage of a multi-stage test was the same as that of a conventional single-stage test. The specimen was first placed in a shear box and compressed under the first-stage normal load. The specimen was then sheared at a constant shearing rate until failure. Failure was defined as a point at which no increase in shear stress takes place with further shear displacement. After completing the first stage,

five different multi-stage procedures were proposed by Gullic (1970) to complete the multi-stage tests, which are summarised as follows:

Procedure “A”: After reaching failure, the shearing is stopped, and the normal load is increased to the next level. In a multi-stage test, failure is defined as the same as in a conventional single-stage test. Under the new normal stress, the specimen is then sheared to failure at the same shearing rate. This multi-stage testing process is then repeated for more stages.

Procedure “B”: After reaching failure, the normal load is maintained, while the shearing force is reversed. The shear box is then pushed back to its original position, i.e., zero shear displacement. Then, the normal load is increased to the next level. Finally, the shearing force is applied again at the same shearing rate until the specimen is taken to a second failure. This procedure is repeated for more stages under increasing normal stresses.

Procedure “C”: This procedure is the same as Procedure “B”, except that the normal load is completely released after each stage. The shear box is then pushed back to its original position. After that, the next stage normal load is applied. Finally, the shearing is repeated until failure.

Procedure “D”: After reaching failure, the normal load remains on the specimen while the shearing force is reversed. When the shear box is pushed back to the point where there is no shear force on the specimen (the reading of the load cell reduces to zero), the normal load is then increased to the next level. Finally, the shearing starts again until reaching the failure.

Procedure “E”: This procedure is the same as Procedure “D” except that the normal load is decreased instead of increased for each stage. That is, the first stage is run at the highest normal load, and then the normal load is decreased for the following stages.

From Gullic’s test results, it was found that Procedure “A” tended to give the best agreement with the conventional test results. The test results using Procedure “A” resulted in slightly lower shear strengths, and slightly lower failure envelope in comparsion with the conventional single-stage test results. In order to choose the best multi-stage procedure for the large-scale direct/interface shear and pull-out tests carried out in this PhD research,

Gullic's procedures used for the small-scale direct shear tests are carefully analysed and discussed below.

It is found that Procedures "B", "D" and "E" choose to remain the normal stress when pushing the shear box back. This would cause difficulty in bringing the specimen back to its original position, which would also possibly cause particle breakage and too much specimen titling. Moreover, in terms of reversing the shear force, it may be not an appropriate procedure because the original failure plane will be destroyed, and a residual failure plane may be sheared multiple times in the later stages. This cannot represent the original properties of the soil. Procedure "C" brings the specimen back, with the normal stress removed, which is believed to be a better approach than Procedures "B" and "D". However, the disadvantage of bringing the specimen back would probably generate a residual failure plane, leading to no peak achieved in the later stages. Thus, the obtained maximum shear strength tends to be lower than that of an original specimen. Finally, Procedure "E" adopts a reverse loading sequence, which is also believed to be inapplicable and irrational because the first failure under the highest normal stress would have a significant impact on the later stages under lower normal stresses. Moreover, the density after compression under the highest normal stress would not be representative of the density of the specimen tested under a lower normal stress. Therefore, Procedures "B", "C" "D" "E" are not recommended, so Procedure "A" was adopted and attempted in the large-scale direct/interface shear and pull-out tests in this research.

Furthermore, Gan and Fredlund (1988) proposed a multi-stage direct shear testing method for unsaturated soils, in order to save the waiting time for suction equilibrium. In Gan and Fredlund's research, the multi-stage procedure was performed by reversing the direction of shearing to remove the shear force after a peak strength was achieved. Then, the matric suction was increased to the next stage. This multi-stage testing method was designed for unsaturated shear strength testing, and the multiple stages referred to increasing the matric suction values for each stage.

Hausmann and Clarke (1994) proposed a concept of stage testing, which involves the shearing testing of the same specimen at four different overburden stresses. This proposal is believed to be the same as Gullic's multi-stage shear testing Procedure "A" after analysing their plots. However, they only attempted the multi-stage procedure to the interface shear tests on fly ash and a geogrid.

Goodhue et al. (2001) carried out small-scale direct shear tests, large-scale multi-stage interface shear tests, and pull-out tests on foundry sands with different fine contents and three geosynthetics (geotextile, geogrid and geomembrane). They found that the interface shear strength obtained from multi-stage testing was essentially the same as the results of single-stage tests at a shear displacement of 5 mm. However, there are no detailed multi-stage testing procedure methods described in this paper. It might be that Procedure “C” was adopted in their experiments based on analysing the shear stress-displacement curves obtained.

Althoff (2010) carried out multi-stage large-scale shear tests on geosynthetic-cohesive soil interfaces using an Interaction Testing Device (ITD) in the Geotechnical Institute at the Freiberg University of Mining and Technology, Germeny. This ITD can be used to carry out both direct shear and pull-out test, with a large shear box having a dimension of 500 mm by 500 mm by 200 mm. It is found that Althoff (2010)’s multi-stage direct shear procedures are similar to the Procedure “A” of Gullic (1970). That is, each stage of a multi-stage test is stopped after maximum shear stress is reached. However, due to the multi-satge tests were carried out on compacted specimens, which are quite stiff, relatively low shear displacements were needed to reach the maximum shear strength. Moreover, there is a sharp decrease in shear stress noticed after the peak before the next stage loading and shearing. As reported by Althoff (2010), their multi-stage test results have a high scatter and do not always reach a peak. Therefore, Althoff (2010) concluded that the multi-stage method is only applicable if the soil specimen will not have an abrupt collapse. This reference has provided relatively detailed information on multi-stage large-scale direct shear and pull-out tests.

Hormdee et al. (2012) performed the multi-stage direct shear tests on a compacted loess soil under a drained condition using a conventional small-scale direct shear apparatus (60 mm by 60 mm). It is found that the testing methodology of their multi-stage tests is in line with Gullic’s Procedure “A”. The multi-stage shear test results matched closely with the single-stage test results. Their results demonstrate that it is possible to carry out multi-stage direct shear tests on compacted soils.

More recently, there is a latest reference to multi-stage tests emerging in the literature. Petro et al. (2017) carried out the standard and limited displacement multi-stage direct shear (LDMDS) tests on rough rock joints. The specimen was returned to its original

position prior to commencing the next stage test for their multi-stage standard direct shear tests, indicating that Procedure “C” was adopted. For the limited displacement multi-stage direct shear (LDMDS) test, the test was quickly paused when a peak strength was reached. Minimising the shear displacement was intended to control the potential asperity damage and remain the specimen less damaged. Therefore, Procedure “A” was used in the LDMDS tests. In general, a good agreement was noticed based on their obtained plots of shear stress versus shear displacement. However, it is believed that it would be very difficult to control when to pause the shearing or when a peak will be achieved, especially for brittle rock specimens.

(2) Pull-out tests

A search of literature revealed that few studies have been conducted on multi-stage pull-out tests. There has been no detailed investigation of the application of the multi-stage testing method in pull-out tests, and it is still not known whether different multi-stage pull-out testing procedures could provide reliable results, compared to multi-stage direct/interface shear tests.

A good example of an attempt of the multi-stage pull-out tests was found in a master thesis (Pradhan 2003) in The University of Hong Kong, China. Pradhan (2003) performed multi-stage pull-out tests on a soil nail, which was installed in the middle of a completely decomposed granite soil in a large-scale pull-out box. The soil nail was then pulled out under different overburden pressures for each stage. It was found that the peak pull-out resistance obtained from the multi-stage pull-out tests was slightly lower than that of the single-stage pull-out results, which is consistent with the general finding of multi-stage direct/interface shear tests. The multi-stage loading procedure adopted by Pradhan (2003) was found to be the same as Procedure “A”. Pradhan’s work has provided useful information and guidance for this research on the multi-stage pull-out testing of geogrid embedded in compacted soils in Paper III in Appendix A.

Moraci and Cardile (2009) developed a new testing procedure to study the factors that affect the cyclic and post-cyclic pull-out behaviour of different geogrids embedded in a granular soil, which was also called multi-stage pull-out test. However, this multi-stage pull-out test is actually a type of cyclic pull-out tests, which is different from the multi-stage loading procedure used in this research. Their cyclic pull-out tests were performed by

applying a constant effective vertical stress, an initial pull-out load, and then adding cyclic tensile pull-out loads, for 20 cycles. The amplitude of the cyclic tensile pull-out loads was increased until the geogrid failed. This study provides insight into the response of the soil-geosynthetic system in cyclic pull-out conditions.

(3) Summary

All the available references to multi-stage testing in the literature are summarised in Table 2.1. Apart from these pioneering multi-stage testing research, there is little data that could be found. As shown in Table 2.1, very little attention has been paid to the role of multi-stage testing in large-scale interface shear and pull-out tests. Furthermore, so far, there is no testing standard for multi-stage direct shear/interface and pull-out tests, and the previous attempts of using multi-stage testing have not been well established and documented. For example, sample preparation, testing procedure, and results interpretation for multi-stage tests are not detailed in the current literature. Overall, all of the studies reviewed indicate that there is a need for systematic research into the application of the multi-stage testing in large-scale direct/interface shear and pull-out tests. The relevant research conducted related to this topic could be found in Paper III in Appendix A.

Table 2.1 Summary of multi-stage testing in the literature

Multi-stage testing	Reference	Material	Maximum particle size (mm)	Normal stress (kPa)	Shearing rate (mm/min)	Equipment size (mm)
Direct shear tests	Gullic (1970)	Fine sand	1	186, 386, 772	0.254	Small circular shear box: 62.0 in diameter, 25.8 in height
	Gan and Fredlund (1988)	Glacial till	2	33.9, 78.1, 126.2, 204.5	0.01	Small square shear box: 51 by 51
	Hausmann and Clarke (1994)	Fly ash, geogrid	Not Given (predominately silt size)	25, 50, 80, 130	1	Large square shear box: 300 by 300 by 180
	Goodhue et al. (2001)	Foundry sand, geosynthetics	4.75	10, 30, 50	0.01-0.03	Large square shear box: 300 by 300 by 152
	Hormdee et al. (2012)	Loess soil	Not Given	100, 200, 300, 400	0.0012	Small square shear box: 60 by 60 by 20
	Petro et al. (2017)	Rock joints	N/A	90, 180, 270	0.2	Large square shear box: 100 by 100 by 180
Pull-out tests	Pradhan (2003)	Soil nail, completely decomposed granite	4.75	16.3, 44.4, 64.3, 84.1	1, 6	Large pull-out box: 690 by 560 by 605
	Moraci and Cardile (2009)	Geogrid, medium sand	Not Given, D50=0.22 (average particle size)	10, 25, 50	1	Large pull-out box: 1700 by 600 by 680

2.6 Soil-geosynthetic interface study

2.6.1 Direct/interface shear behaviour

A large and growing body of literature has investigated the geosynthetic-soil interface behaviour using different direct shear apparatus since the 1980s (Jewell et al. 1984; Palmeira and Milligan 1989; Bergado et al. 1993; Alfaro et al. 1995; Lee and Manjunath 2000; Lopes 2002; Bergado et al. 2006). In recent decades, Abu-Farsakh et al. (2007) carried out large direct shear tests to investigate the effect of moisture content and dry density on the interactions between the geosynthetics and cohesive soils, as shown in Figure 2.4. This paper has provided useful information on the large-scale single-stage testing procedures and the interpretations of direct/interface shear test results. Moreover, the overall interface friction angles were found to be calculated based on the back calculation of the experimentally obtained interface shear strengths using Eq. (4). However, the difference between the theoretical interface frictional angle between the soil and geogrid ribs and the experimentally obtained overall interface frictional angle was found to be still confusing in this paper. Another piece of useful information obtained from this paper was about the concept of applying area correction in stress calculation for the direct and interface shear tests. However, it was found that only the measured shear stresses were corrected by the authors, while the applied normal stresses remained uncorrected in the failure envelopes in their paper. It is believed that both applied normal stress and measured shear stress should be corrected due to the decreasing contact area during the shearing process.

In terms of area correction methods, it is found that there are two methods to select the maximum shear strength. The first method is to directly find the maximum shear stress from the raw data prior to applying area correction. Then, correct the selected maximum shear stress based on the corresponding shear displacement. Finally, correct the normal stress at the same shear displacement where the maximum shear stress is selected. The second method is to correct all the raw data of the obtained shear stress first based on the corresponding shear displacement. Then, find the maximum shear stress from the corrected values. Finally, correct the normal stress at the same shear displacement where the maximum shear stress is selected. The two area correction methods summarised above may result in slightly different corrected maximum shear stress and normal stress (at different shear displacements), leading to slightly different shear strength parameters.

This situation would normally happen when there is an obvious peak occurring during shearing, and then with some drop-off to a residual state. If the shear stress continues increasing with shear displacement throughout the shearing process, the two area correction methods would result in the same result. This is because the failure position is taken as the same, i.e., at the maximum final displacement.

Figure 2.4 Large-scale direct shear machine (Abu-Farsakh et al. 2007)

Liu et al. (2009a, b) made further contributions to the current literature on the soil-geosynthetic interface behaviour. They developed a modified interaction mechanism, which evaluates an additional component caused by the contribution of transverse ribs. Liu et al (2009a) proposed an equation to evaluate the overall shear resistance of the soil-geogrid interface under the direct shear testing mode:

$$\tau_{S/GG}^{\max} = \alpha_{ds} \times \tau_{S/GSY}^{\max} + (1-\alpha_{ds}) \times \tau_{S/S}^{\max} + \tau_{bearing}^{\max} \quad (22)$$

where $\tau_{S/GG}^{\max}$ is the interface shear strength between soil and geogrid, $\tau_{S/GSY}^{\max}$ is the shear resistance between soil and geosynthetic surface, $\tau_{S/S}^{\max}$ is the maximum shear strength of soil obtained from direct shear tests, $\tau_{bearing}^{\max}$ is the maximum shear strength provided by the transverse bearing members.

Therefore, apart from the two components theory proposed by Jewell et al. (1984), as shown in Eq. (1), which includes the soil-soil friction in apertures of the geogrid, and sand–geogrid friction, an additional contribution to the overall shear strength of the soil-geogrid interface was proposed in this modified interaction mechanism, as shown in Eq. (22). This

additional contribution is defined as the passive resistance provided by the transverse ribs of geogrid.

In addition, a new parameter β was proposed to quantify the passive resistance contribution, as shown below.

$$\beta = \frac{\tau_{bearing}^{max}}{\tau_{S/GG}^{max}} = \frac{\tau_{S/GG}^{max} - \alpha_{ds} \times \tau_{S/GSY}^{max} - (1-\alpha_{ds}) \times \tau_{S/S}^{max}}{\tau_{S/GG}^{max}} \quad (23)$$

where β is the passive resistance contribution ratio.

A large-scale direct shear machine was used in their study to verify the modified interaction mechanism, as shown in Figure 2.5. Based on their experimental results, the authors concluded that the bearing resistance contributed by transverse ribs was about 10% of the overall interface shear strength. This modified interaction mechanism was particularly analysed and discussed in this research, which helps with the development of the theoretical framework of Paper I.

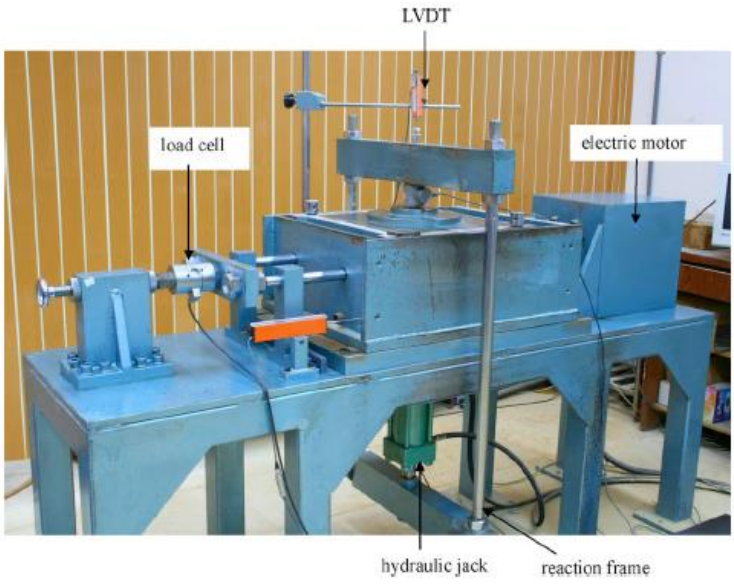

Figure 2.5 Large-scale direct shear machine (Liu et al. 2009a, b)

Another useful information from Liu et al. (2009b) is the selection of the most suitable set-ups for the interface shear tests, as shown in Figure 2.6. Liu et al. (2009b) compared the different set-ups of the lower shear box and concluded that a lower box of the same size

as the upper box filled up with the soil is the most suitable set-up for the soil-geogrid interface shear testing. Therefore, this set-up was also adopted in this research.

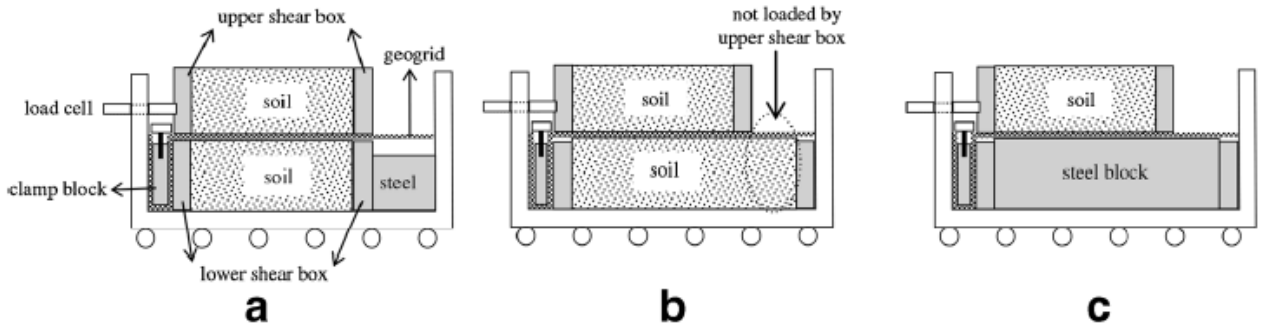

Figure 2.6 Different set-ups of lower shear box (Liu et al. 2009b)

Anubhav and Basudhar (2010) used a small shear box (60 mm by 60 mm) to investigate the soil-geotextile interface behaviour, as shown in Figure 2.7, which may have some scale and boundary effects. A non-linear model was proposed to predict both the pre-peak and the post-peak interface behaviour. The used methodologies in their research were found to be the mathematical back calculation and curve fitting. These skills were learned and adopted in this research.

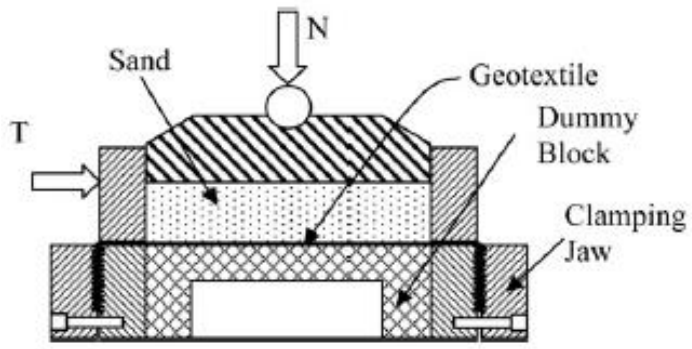

Figure 2.7 Modified shear box assembly (Anubhav and Basudhar 2010)

Arulrajah et al. (2013) investigated the interface shear strength parameters between the geogrid and construction and demolition aggregates using a modified large-scale direct shear apparatus, as shown in Figure 2.8. The tests were undertaken on each representative specimen with and without geogrid reinforcement. The interpretation and key plots of the paper provide useful information for the study presented in Paper I and II.

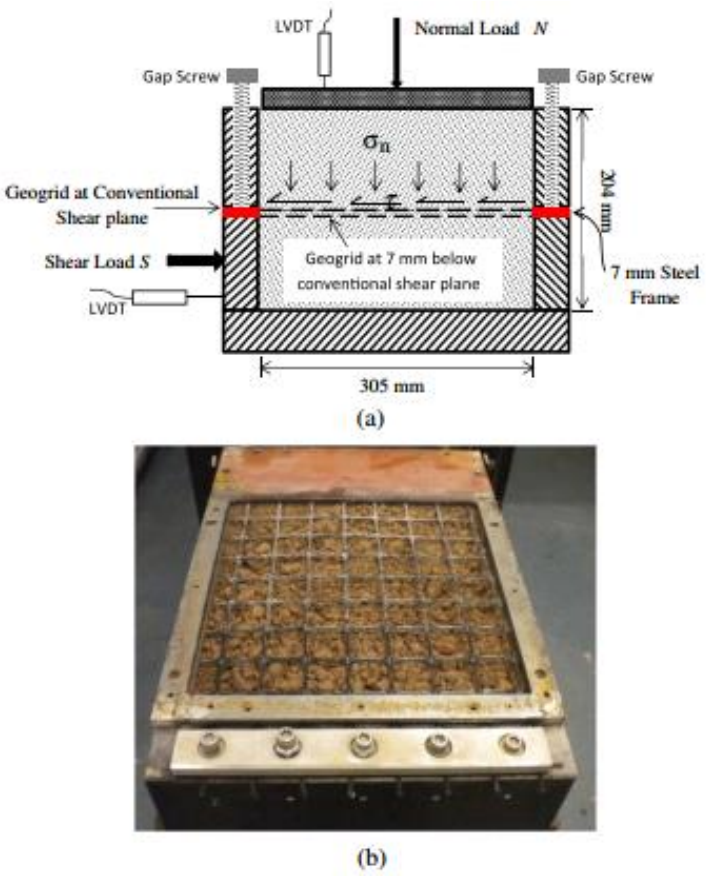

Figure 2.8 Modified large-scale direct shear apparatus: (a) interface shear testing; (b) modified lower shear box with steel frame (Arulrajah et al. 2013)

In addition, a large-scale direct shear apparatus can allow the testing of coarse-grained materials; however, it is not always available and accessible for all the commercial soil testing laboratories or research institutions. It is found the small-scale shear box testing of scalped material (scalping size is normally 4.75 mm or 2.36 mm) is widely adopted by engineers, and the obtained shear strength parameters of the scalped specimens may be directly used to represent the coarse-grained materials. This is believed to be too conservative in practice. This is because the shear strength of a soil is related to its particle size, and scalping has significantly changed the particle size distribution of the soil. Therefore, scalping is expected to have an influence on shear strength. Based on this hypothesis, another extended research presented in Paper II sets out to investigate the effect of scalping on the direct shear strength of crusher run and interface shear strength between crusher run and geogrid.

2.6.2 Pull-out behaviour

Several pioneering researchers have carried out pull-out tests on geosynthetics embedded in soils using different pull-out equipment since 1980s (Ingold 1983; Rowe et al. 1985; Juran and Chen 1988; Fannin and Raju 1993; Farrag et al. 1993; Ochiai et al. 1996; Mallick et al. 1996).

In recent decades, Moraci and Recalcati (2006) carried out more than 40 pull-out tests to study several factors that may affect the pull-out behaviour of extruded geogrids embedded in a compacted granular soil, including reinforcement length, applied vertical stress, and the extensibility of reinforcement. The results of long and short geogrid specimens suggest that the pull-out interaction mechanism develops progressively along the geogrid specimen.

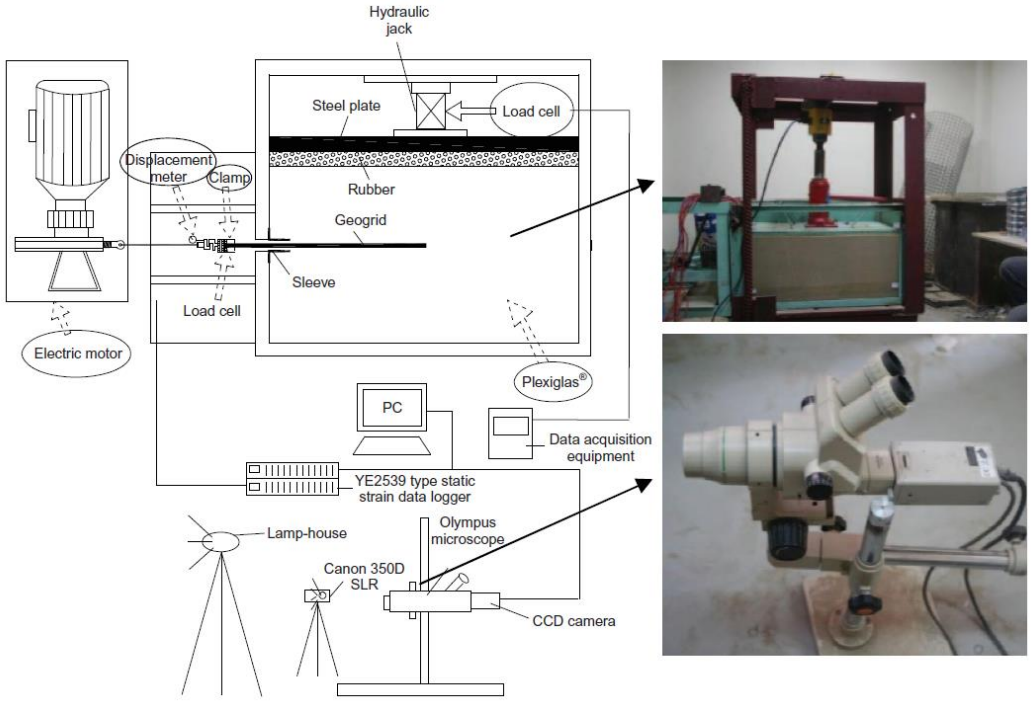

Figure 2.9 Pull-out test set-up with a camera installed (Zhou et al. 2012)

Zhou et al. (2012) conducted a research on the micro-mechanism of the interaction between sand and geogrid transverse ribs through pull-out testing of a geogrid embedded in sand, with a high-resolution camera to capture the sand motion around the ribs during pulling, as shown in Figure 2.9. Therefore, this research provides an interesting insight into

the micro-view of the pull-out behaviour, such as the shear band thickness, particle movement, etc.

Gupta et al. (2014) introduced a new pull-out test equipment for the soil-geosynthetic interface testing in a reinforced flexible pavement. This equipment allows the testing of geosynthetics at low displacement magnitudes in reinforced pavement application, as shown in Figure 2.10. This research has brought the effect of orientation of geosynthetic to attention when carrying out the pull-out tests, which had prevented making geosynthetic installation mistakes in the experimental work presented in Paper III and IV.

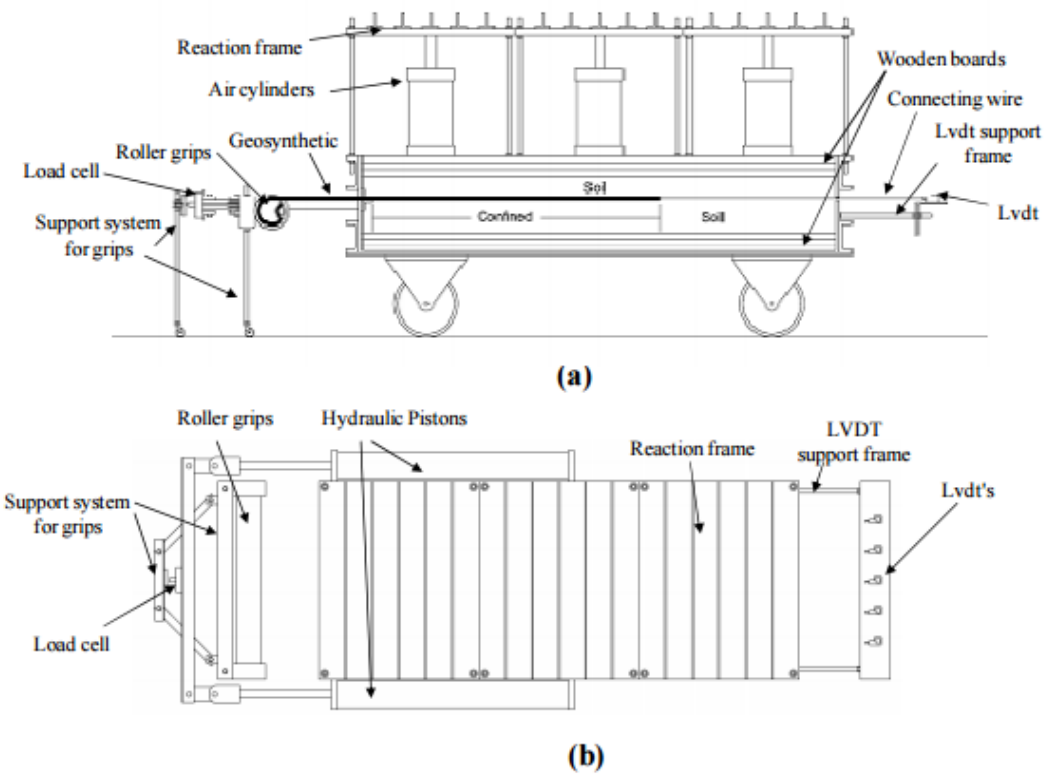

Figure 2.10 Large-scale pull-out testing equipment: (a) side view; (b) top view (Gupta et al. 2014)

A novel pull-out test apparatus with a transparent glass bottom and side window was introduced by Ezzein and Bathurst (2014) and Bathurst and Ezzein (2015), as shown in Figure 2.11. This new equipment facilitates the application of the Digital Image Correlation (DIC) technique to study the displacement of geogrid embedded in a transparent granular soil. It allows to analyse the relative horizontal displacement between the geogrid and the surrounding soil particles throughout the pulling process, which is believed to be responsible for the load transfer mechanism. Some useful inrofmation and guildence on

the pull-out test set-up, sample preparation, test mehtodolgy and result interpretations were obtained from the two papers. This research also provided a useful database for an extended research on analysing and interpreting the load-strain results under different testing conditions, such as different length of geosynthetic specimens and displacement rates, and geogrid specimens with or without the transverse ribs removed (Bathurst and Ezzein 2016).

In addition, recently, Bathurst and Ezzein (2017) further provided insights into geogrid-soil intraction using this experimental set-up to measure the geogrid deformations and interpret load transfer mechanism using a rate-dependent load-strain model. Their recent results show that load transfer is largely due to shear between the soil particles trapped in the plane of the geogrid between transverse members and the surrounding soil. This information helps to understand and interpret the interface shear strength components in the large-scale interface shear and pull-out tests.

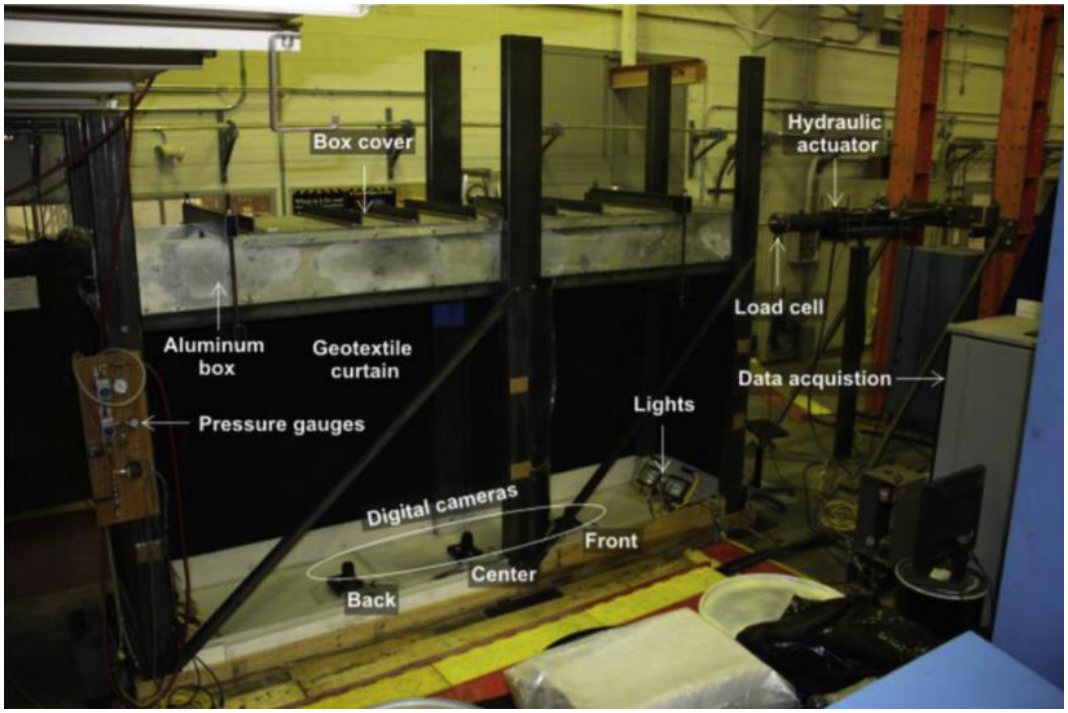

Figure 2.11 Pull-out test apparatus (Ezzein and Bathurst 2014)

Ferreira et al. (2015) conducted the pull-out tests on the four types of geosynthetics embedded in a granite residual soil, compacted to different relative densities, as shown in Figure 2.12. The results obtained from their study suggest that the soil-geosynthetic interaction under pull-out loading conditions is greatly affected by the geosynthetic

properties and soil density. Another useful information obtained from this research is the nodal displacements along the geogrid specimens were found to be non-uniform, which could be measured using inextensible wires and linear potentiometers. The displacement behaviour of different types of geosynthetics in pull-out tests is closely related to the extensibility and stiffness of the geosynthetics tested.

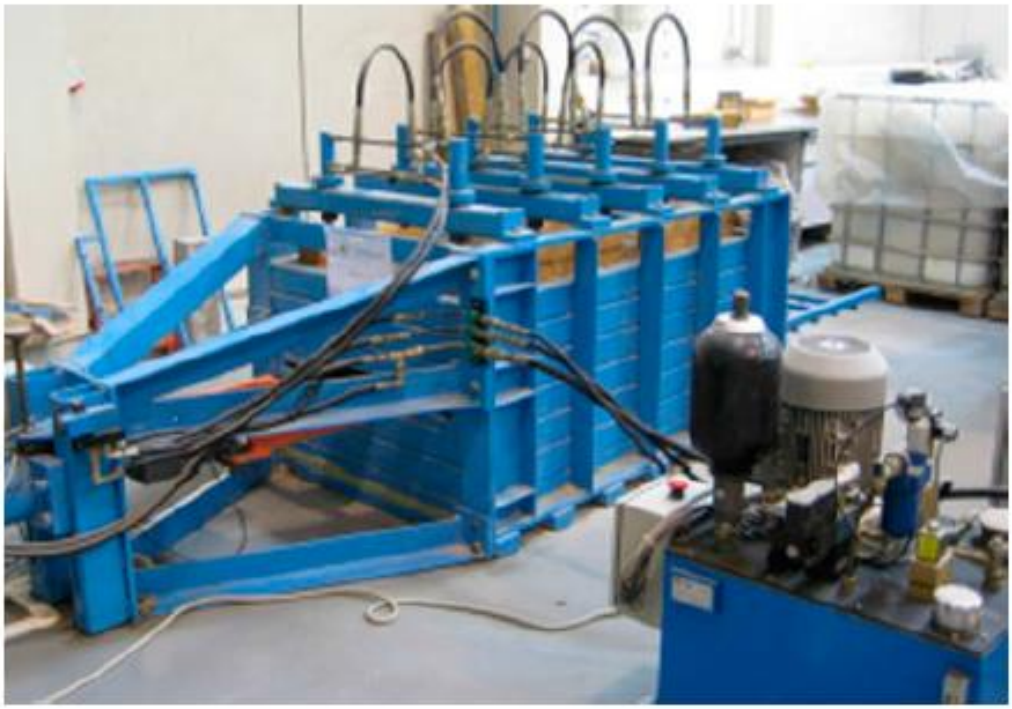

Figure 2.12 Pull-out test apparatus (Ferreira et al. 2015)

Apart from the ASTM testing standard, all of these references reviewed herein have provided useful information on different aspects of gepsynthetics pull-out research, such as the experimental set-up, geosynthetic clamping, sample preparation, testing procedures, result interpretations and interaction mechanisms. Comparing with the direct/interface shear tests, it has been widely accepted that both direct/interface shear and pull-out tests can be adopted to determine the interface parameters between soils and geosynthetics. However, the relationship between the interface shear stress and pull-out shear stress mobilised along the soil-geosynthetic interface in the two testing modes is still a very controversial topic, which may produce significantly different interface parameters (Bergado et al.1993; Alfaro et al. 1995; Mallick et al. 1996; Lopes and Silvano 2010; Hsieh et al. 2011). These controversial findings and discussion have been critically reviewed and analysed in the Introduction of Paper III in Appendix A. In order to avoid repetition, these

content is not mentioned herein again. Overall, although extensive research has been carried out on direct/interface shear and pull-out testing of geosynthetics embedded in soils, there is a lack of comparsion and discussion on the realationship between the interface shear strength, pull-out shear strength, and shear strength of the soil, which is one of the main research aims of Paper III.

In addition, in order to increase the pull-out resistance of geosynthetics in a soil mass to prevent pull-out failure, anchored geosynthetics are designed, typically for anchor trenches. However, different anchorage configurations may have different pull-out performances. Chareyre et al. (2002) conducted the research on the anchorage capacity of geotextiles in trenches, in order to optimise the geometry of the anchorage and to reduce the area taken up by the anchorage at the top of the slope. Therefore, full-scale pull-out tests were carried out on anchored geotextile sheets in anchor trenches with different configurations, including simple run-out anchorage, vertical embedding and L-shaped anchorage geometries, as shown in Figure 2.13 and Figure 2.14.

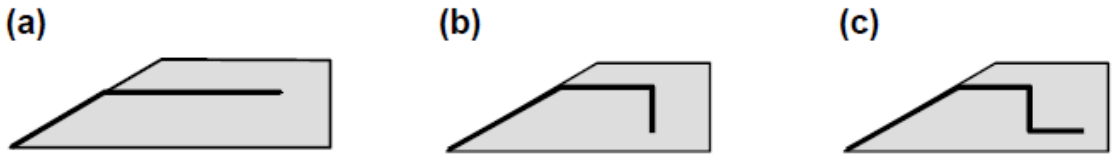

Figure 2.13 Types of anchors studied: (a) run-out anchorage; (b) vertical embedding; (c) L-shaped anchor (Chareyre et al. 2002)

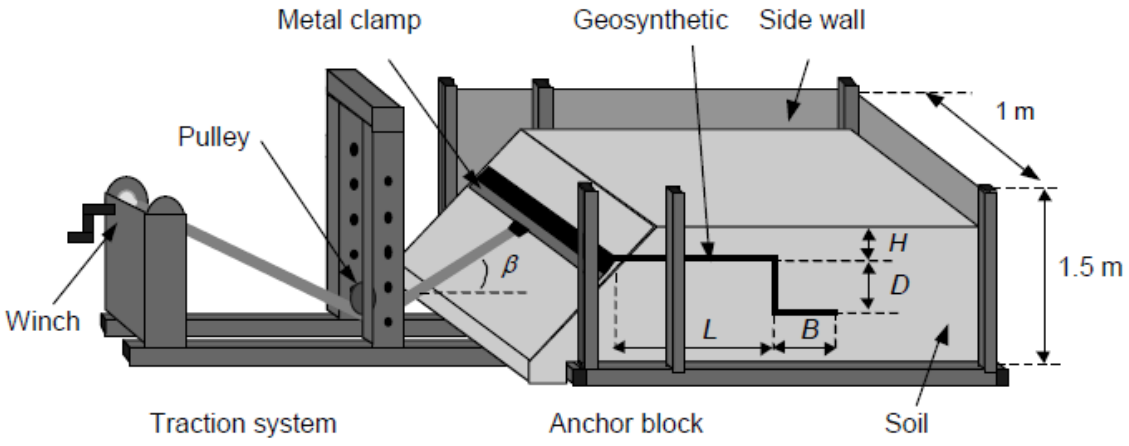

Figure 2.14 Experimental apparatus (Chareyre et al. 2002)

Villard and Chareyre (2004) proposed analytical models for analysing the pull-out failure mechanisms of the geosynthetic anchors, including simple run-out and L- or V-shaped anchor trenches, as shown in Figure 2.15. Two failure hypotheses associated with different types of soils were proposed. For cohesive soils (rigid soil mass assumption), it is relative slippage between the soil and geotextile that happens during the pulling process. For cohesionless soils (soil mass failure assumption), the pull-out process would cause severe deformation of the anchoring soil mass, resulting in failure. This reference provides analytical methodologies and knowledge to conduct the theoretical frameworks for the influence of anchorage angles on the pull-out resistance in Paper IV in Appendix A.

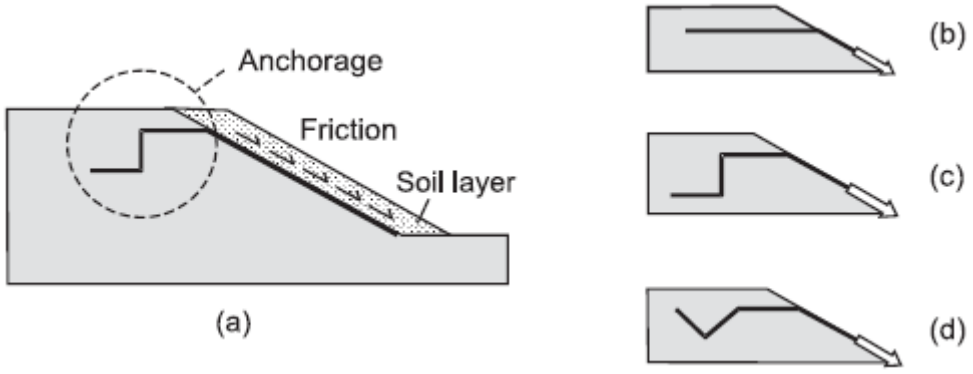

Figure 2.15 Types of system studied: (a) typical geometry, (b) run-out anchor, (c) L-shaped anchor, (d) V-shaped anchor. (Villard and Chareyre 2004)

Girard et al. (2006) carried out the in-situ full-scale pull-out tests on anchored geotextile to determine the best anchorage configuration with a fixed length of geotextile. Anchorage configurations carried out included the simple run-out, L-shaped, V-shaped and trapezoidal trench, as shown in Figure 2.16a. A full-scale pull-out experiment was set-up in the field. The pull-out was generated using a power shovel, and the pull-out resistance was measured using a sensor, as shown in Figure 2.16b. The field tests suggest that the anchorage capacity not only depends on the interface friction between the soil and the geotextile, but is also greatly influenced by the anchorage configurations and the angle of slope. Therefore, the geometric parameters of geosynthetic anchorages should be taken into account in the design.

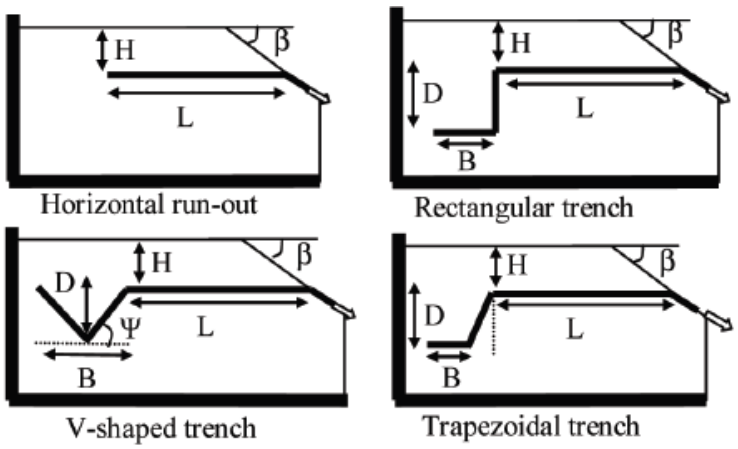

(a)

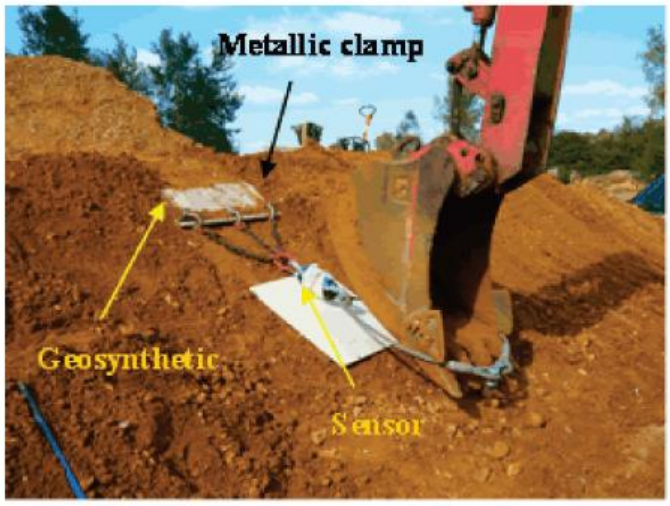

(b)

Figure 2.16 Full-scale in-situ pull-out tests: (a) anchorage configurations; (b) in-situ test set-up (Girard et al. 2006)

Recently, some researchers (Lajevardi et al. 2014, 2015a, b) have further studied two types of anchorage configurations, i.e., simple run-out and wrap around anchorages, as shown in Figure 2.17. Three types of geosynthetic (two geotextiles and one geogrid) embedded in two types of soil (gravel and sand) were investigated. The results show that there is an optimum length for the upper part of the geosynthetic wrap around anchorage. However, it was found that only the vertically (90°) wrap around anchorages have been studied in their study. The influence of the anchorage angles on the pull-out resistance of the wrap around anchorages has not been fully explored. This research gap initiated the

research work conducted in Paper IV. The experimental set-up and results interpretation of these references provide useful insight into the pull-out behaviour of geotextile anchorage with different anchorage angles.

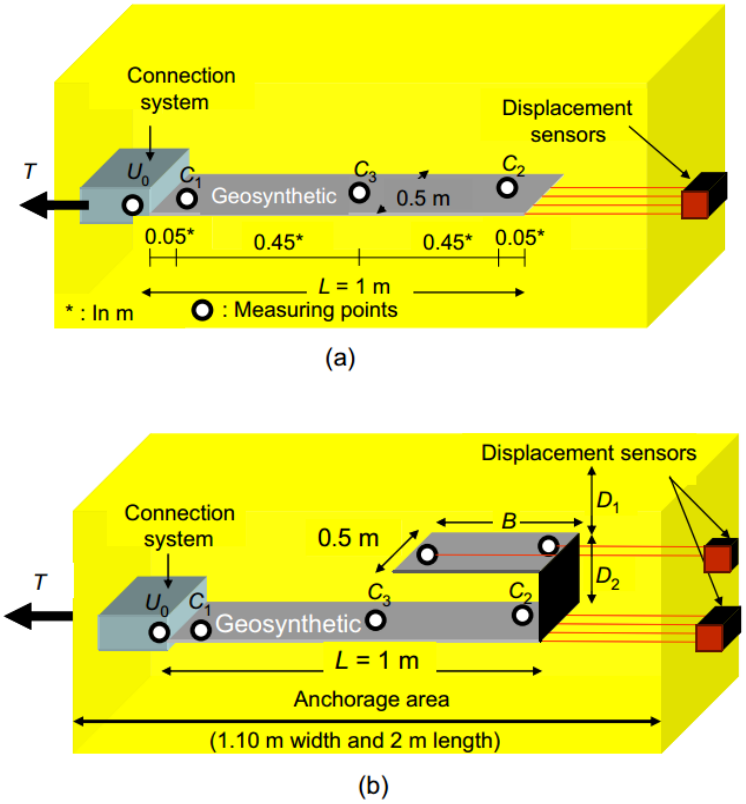

Figure 2.17 Anchorage configurations: (a) simple run out; (b) wrap around (Lajevardi et al. 2014, 2015a, b)

2.7 Composite behaviour

2.7.1 Soil composite with OSC and GESC

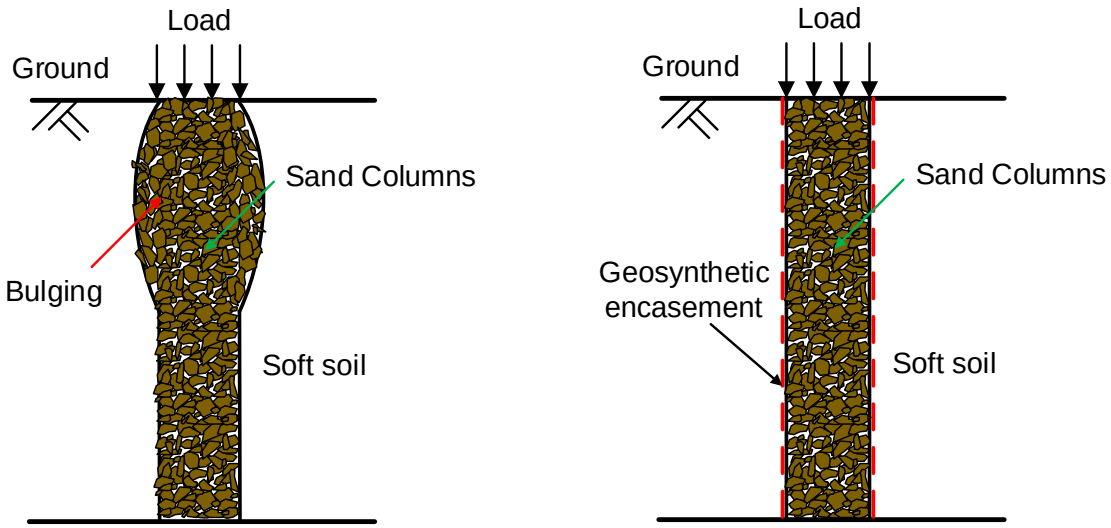

Figure 2.18 Ordinary sand column versus geosynthetic-encased sand column

Replacing soft soils with granular columns is a cost-effective ground improvement technique across the world. However, weak soft soils tend to provide insufficient confinement to granular columns, leading to dissatisfactory reinforcing effects, such as the bulging phenomenon of granular columns (Ayadat and Hanna 2005; Murugesan and Rajagopal 2007; Andreou et al. 2008; Ali et al. 2012, 2014). Bulging phenomenon behaves as a radial deflection of sand column under load, which typically occurs at the top portion of the column, with a depth of about four times the diameter (Murugesan and Rajagopal 2010). Thus, bulging would result in excessive settlements of the foundation and the surrounding soft soil (Sivakumar et al. 2011). However, with the inclusion of geosynthetic to encase the granular columns, the reinforcing performances will be improved significantly. The comparison of OSC and GESC under load is shown in Figure 2.18.

Murugesan and Rajagopal (2006) carried out the finite element analysis to investigate the bulging behaviour and the improvement in load carrying capacity for the sand columns with and without geosynthetic encasement. The results showed that the GESC underwent less bulging and compression, compared to the OSC. It was observed that bulging predominantly occurred at the top portion of the column, which could reach up to a depth of twice the diameter of the OSC. After including a geotextile encasement, bulging at the

top of the sand column was found to be considerably reduced, while slightly obvious bulging was observed at a deeper depth. It was hypothesised that this phenomenon was accounted for the transfer of the upper load to a deeper depth after including the encasement (Murugesan and Rajagopal 2006). This indicates that the top portion of the sand column needs extra lateral confinement in order to further improve its reinforcing performance. Another relevant study conducted by Gu et al. (2015) suggested that the effective length of encasement was three to four times the diameter of the sand column, and any further increase in the length of the encasement will not provide an additional contribution.

Furthermore, the soft clay may also enter the voids of the sand column, contaminating the sand and reducing the drainage of the sand column (Murugesan and Rajagopal 2009; Castro and Sagaseta 2011; Kadhim 2016). Therefore, apart from the reinforcement function, the geosynthetic encasement also works as a filter and separation layer and prevents clogging of the granular materials to guarantee that the drainage path is unblocked. In summary, using GESCs in ground improvement has several advantages over OSCs, including:

(1) Providing the additional confinement to sand columns.

(2) Increasing the stiffness and strength of clay composite, resulting in improved cohesion and friction angle.

(3) Preventing the loss of aggregates and the clogging of sand columns, to ensure a good drainage condition.

(4) Improving a high degree of compaction for sand columns.

Overall, the composite behaviour of clay reinforced with geosynthetic-encased granular column is very complex because three different materials are involved, which attracts a lot of researchers devoting to it. This research sets out to carry out laboratory model tests to investigate the shear strength and consolidation characteristics of the clay with OSC and GESC, including direct shear tests, triaxial tests and consolidation tests. Therefore, more literature reviews of these aspects are focused in the following sections.

2.7.2 Strength behaviour

The tensile stiffness of geotextile encasement plays a vital role in the strength behaviour of reinforced soil composites. Hong et al. (2016) conducted model tests on soft clay reinforced with geotextile encased granular columns, and the tested geotextiles have different tensile stiffness. Their investigation found that a geotextile with higher tensile stiffness is able to transfer the upper load to a deeper depth so that the sand column will deform uniformly along the height, with reduced bulging and less potential for the rupture failure of the geotextile encasement. The load carrying capacity of the clay composite reinforced with GESC increased with the tensile stiffness of the geotextile (Hong et al. 2016).

The shear strength of soils can be determined by laboratory direct shear or triaxial compression tests, and the inferred shear strength parameters will be used for geotechnical design or anlaysis. However, for direct shear and triaxial testing of a composite specimen, such as clay with OSC or GESC, the directions of loading subjected to the specimen are different. A lateral loading condtion can be applied by direct shear tests, which are more suitable to model the granular columns subjected to a shear movement under the toe of an embankment (Murugesan and Rajagopal 2009; Mohapatra et al. 2016, 2017). By constrast, a vertical load condtion can be applied by triaxial tests, which are more suitable to determine the loading carry capacity of the composite materials (Juran and Guermazi 1988; Sivakumar et al. 2004, 2011; Black et al. 2006; Black et al. 2007; Black et al. 2011; Kim et al. 2007; Andreou et al. 2008; Najjar et al. 2010; Frikha et al. 2015).

A number of studies have investigated the composite behaviour of geosynthetic-reinforced soils by carrying out triaxial tests. This is because triaxial testing has advantages over many other laboratory model tests in controlling the stress state, drainage condition, loading rate and lateral pressure, and also in accurately measuring the induced pore pressure and volume change. Some researchers had carried out triaxial tests on the reinforced soil composites, such as the geosynthetic-encased or non-encased granular columns (Rajagopal et al. 1999; Wu and Hong 2009; Miranda and Da Costa 2016; Kadhim 2016), and clay with geosynthetic-encased or non-encased granular columns (Juran and Guermazi 1988; Sivakumar et al. 2004, 2011; Black et al. 2006; Black et al. 2007; Black et al. 2011; Kim et al. 2007; Andreou et al. 2008; Najjar et al. 2010; Frikha et al. 2015). Najjar

and Skeini (2015) reviewed and analysed 114 triaxial test results of clays with encased or non-encased granular columns from 11 previously-published papers, focusing on the effects of loading rate and drainage condition on the bearing capacity of the reinforced soil composites.

Kadhim (2016) found the increase of strength after including geotextile encased was very significant. There were peaks on shear stress curves at a strain of 2-3% for OSC during triaxial testing, resulting in a peak friction angle of 38.6°. However, the deviator stress continued increasing with axial strain linearly until the tests stopped at its maximum axial strain (20%) for GESC. The angles of internal friction for GESC had increased from 39.2° to 53.5° for an axial strain of 2% and 10%, and the corresponding apparent cohesions had dramatically increased from 20 kPa to 120 kPa, respectively.

Wu and Hong (2009) believed that the increase in strength for GESC was caused by hoop stiffness of the geotextile. The geotextile develops an increasing circumferential tensile force per unit length, the value of which depends on the stiffness of the geotextile. Moreover, the increase in the circumferential tensile force of the geotextile results in an extra confining pressure provided by the geotextile encasement, which is equivalent to increasing cell pressure.

These references provide useful information on the experimental design and result interpretation of the research presented in Paper V, such as the OSC and GESC installation methods, clay specimen preparation methods, suitable area replacement ratios, shearing rate, etc, as summarised in Table 2.2. However, most of the literature on triaxial testing of composite materials only paid attention to the load carrying capacity of the clay composites with different reinforcing configurations. There was a lack of analyses and discussion about the effects of the granular column or geosynthetic encasement on the pore water pressure dissipation during the consolidation stage, induced pore water pressure change during the shearing stage, total and effective stress Mohr circles, and total and effective stress paths. These gaps mentioned above were filled by the research and analyses presented in Paper V in Appendix A.

Comparing to the vertical loading conditions, there are relatively few previous studies in the area of clay with OSC and GESC under lateral loading conditions. As introduced previously, OSC or GESC under the toe of the embankment is typically subjected to lateral

loading. It was found that the lateral loading conditions could be experimentally modelled through direct shear box tests (Murugesan and Rajagopal 2009; Mohapatra et al. 2016).

Murugesan and Rajagopal (2009) carried out the first study on the direct shear testing of clay reinforced with stone columns to study the composite performance under the lateral loading condition. However, they only tested and interpreted the clay with OSCs scenarios. In their experimental study, the clay was reinforced with single 100 mm stone column installed in the middle of the shear box, or reinforced with four grouped stone columns at a spacing of 150 mm in the shear box, as shown in Figure 2.19. Obviously, there is a research gap remaining in testing the clay with GESC scenarios to further study the effect of geosynthetic encasement on the direct shear strength behaviour of reinforced soil composites.

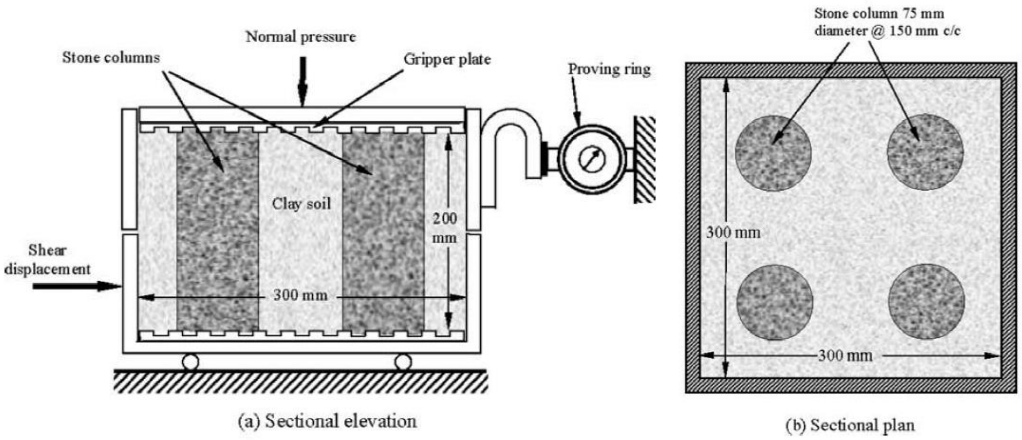

Figure 2.19 Large-scale shear box testing of clay reinforced with ordinary sand columns (Murugesan and Rajagopal 2009)

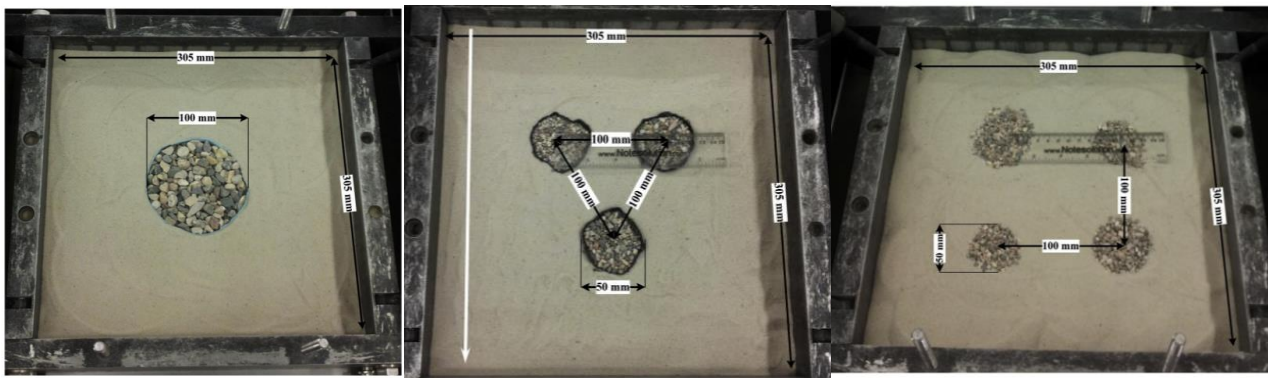

Figure 2.20 Large-scale shear box testing of sand reinforced with geotextile encased stone columns (Mohapatra et al. 2016)

Additionally, Mohapatra et al. (2016) carried out large-scale direct shear box tests on fine sand with single and grouped stone columns, with and without geotextile encasement. However, the main limitation of Mohapatra et al. (2016)'s research was that they used a gravel to reinforce a fine sand, which is not realistic and representative of the field condition, as shown in Figure 2.20. Clay should be used as a surrounding soil in the shear box. With these gaps and motivations in mind, direct shear tests on Kaolin, Kaolin with OSC, and Kaolin with GESC were carried out in this research. The corresponding results and interpretation are presented in Paper VI.

2.7.3 Consolidation behaviour

Most of the existing literature on the composite behaviour of clay with OSC or GESC particularly focuses on loading carrying capacity. For example, an increasing amount of literature has been published on the laboratory model tests on clay with OSC or GESC under vertical loading conditions (Alexiew et al, 2005; Malarvizhi and Ilamparuthi 2007; Murugesan and Rajagopal 2007; Gniel and Bouazza 2009, 2010; Ali et al. 2012, 2014; Dash and Bora 2013; Almeida et al. 2015; Hong et al. 2016). These references all suggest some similar conclusions on the impact of OSC or GESC on the load carrying capacity and settlement. That is, with the inclusion of OSC or GESC, the settlement of clay has been reduced significantly due to the reinforcing effect of the sand column, leading to improved load carrying capacity. Furthermore, apart from the reinforcement function, geotextile materials also have excellent drainage function, which will speed up the drainage and excess pore water pressure dissipation process, so that the time required for consolidation will be shortened.

However, it has not been well established about the effects of OSC and GESC on the consolidation characteristics of the clay composite. To date, there is few research and data available in the literature on quantifying the impacts of OSC and GESC on the consolidation characteristics under vertical loading, such as the compression index C_c, swell index C_s, recompression index C_r, secondary compression index C_α, coefficient of consolidation c_v, coefficient of compressibility a_v, coefficient of volume compressibility m_v, modulus of compressibility E_s, and hydraulic conductivity k. These questions have been addressed and quantified in the research presented in Paper VI.

Table 2.2 Summary of triaxial testing of clay with OSC and GESC in literature

Reference	Specimen diameter / height (mm)	Column installation method	Area replacement ratio (%)	Confining stress (kPa)	Shearing rate (mm/min)
Juran and Guermazi (1988)	100/NG	replacement, compacted inside, single and group	4, 16	200	0.05
Sivakumar et al. (2004)	120/300	replacement, compacted in casing, single	10.24, 64	100	0.01
Kim et al. (2007)	150/300	replacement, compacted in mould, frozen, single	9.6, 23.6, 38.7	98, 196, 294	0.05, 0.2, 1
Black et al. (2007)	100/200	replacement, frozen, single and group	10.24, 12	100	0.56
Andreou et al. (2008)	100/200	special mould, pre-forming, compacted inside, single	4	50, 100, 200	0.003, 0.3
Najjar et al. (2010)	71/142	replacement, frozen, single	7.9, 17.8	100, 150, 200	0.024
Black et al. (2011)	300/400	replacement, compacted, single	17, 28, 40	75	stress control (1 kPa/h)
Sivakumar et al. (2011)	300/400	replacement, compacted, single	44.44, 69.44	50	stress control (1 kPa/h)
Frikha et al. (2015)	70/140	replacement, compacted, single and group	22	100, 200, 300	0.03

3 SUMMARY OF ATTACHED PAPERS

This chapter summarises the six incorporated papers that support the main thesis topic. Figure 1.1 has shown the logical flowchart of each topic and the links between the six papers. In this chapter, under each sub-topic, a summary of each paper is presented, highlighting the research gaps, questions and objectives, the research methodologies used, and the main contributions of each paper.

3.1 Direct/interface shear and pull-out behaviour

3.1.1 Paper I

> ***Xu, Y.,*** *Williams, D. J., Serati, M., 2018. Investigation of shear strength of interface between roadbase and geosynthetics using large-scale single-stage and multi-stage direct shear test. Road Materials and Pavement Design. https://doi.org/10.1080/14680629.2018.1561378 – incorporated as Paper I.*

Roadbase materials and geosynthetics are the integral parts in the construction of geosynthetic-reinforced road projects. The applications of geosynthetics in pavement engineering are mainly base reinforcement and subgrade stabilisation, as shown in Figure 3.1. For base reinforcement, a geosynthetic layer is embedded within the base or subbase layer to reinforce the base course by providing confinement and supporting traffic loads. For subgrade stabilisation, a geosynthetic layer is embedded between the base layer and subgrade layer by separating the roadbase materials and subgrade soils so as to stabilise subgrade layer and distribute traffic loads. Thus, there are two types of soil-geosynthetic interfaces occurring in a geosynthetic-reinforced pavement, and large-scale direct shear tests could be used to investigate the interface parameters between the roadbase materials and geosynthetics (Figure 3.1). However, there is a lack of data in the literature on the interface parameters between roadbase materials and geosynthetics, especially for these two scenarios mentioned above.

Therefore, this research was proposed to investigate the shear strength of Australian commercial roadbase materials and the interface shear strength between the roadbase materials and different types of commercial geosynthetics. Typical Australian commercial Type 2.1 granite roadbase and crusher dust were collected from Pine Mountain Quarry,

Brisbane. Four types of commonly used commercial geosynthetics were supplied by Geofabrics, a local geosynthetic products supplier in Gold Coast. A series of laboratory, large-scale, single-stage and multi-stage direct shear tests were carried out on roadbase materials with and without the inclusion of geosynthetics, under applied normal stresses of 25 kPa, 50 kPa, 75 kPa or 100 kPa, representing the magnitude of the overburden pressure in the pavement. The four normal stresses correspond to the four stages in the multi-stage tests, which is taken as an extended research on multi-stage testing presented in Paper III (three stages only), which has already shown good match between single-stage and multi-stage test results.

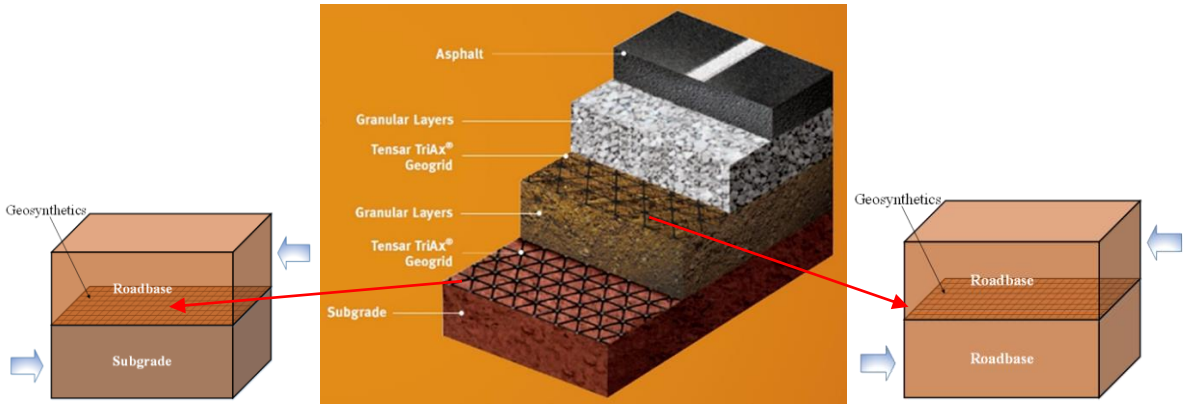

Figure 3.1 Soil-geosynthetic interfaces in a pavement

A key contribution of this research was to provide an insight into the interface behaviour between the roadbase materials and geosynthetics utilising the large-scale shear testing, in particular for the shear strength of the two typical interfaces in base reinforcement and subgrade stabilisation (two scenarios) in a geosynthetic-reinforced pavement. Furthermore, theoretical equations and a new contribution ratio were proposed to quantify the contribution of different shear strength components mobilised along the interface between the roadbase materials and geogrids. Several important factors that might influence the interface shear strength were also discussed and interpreted based on the data collected, including the woven or nonwoven texture of geosynthetics, triangular or square aperture shape of geogrid, opening ratio of apertures, effective contact area between the soil and geogrid ribs, etc. In particular, an important factor, the effective contact area between the soil and geogrid ribs, was brought to attention to extend the soil-geogrid interaction theory proposed by Liu et al. (2009a). These developed theoretical

interpretations contribute to a more in-depth understanding of direct shear interaction mechanism between soils and geogrids.

3.1.2 Paper II

> ***Xu, Y.,*** *Williams, D. J., Serati, M., Vangsness, T., 2018. Effects of scalping on direct shear strength of crusher run and interface shear strength between crusher run and geogrid. Journal of Materials in Civil Engineering. 30 (9) 04018206. https://doi.org/10.1061/(ASCE)MT.1943-5533.0002411 – incorporated as Paper II.*

Crusher run is a type of construction aggregate produced in a quarry by breaking down the rock to various sizes using a mechanical crusher. Scalping is an essential process for a quarry to produce a series of crusher run products with specific grading specifications for various applications. However, the friction angle of the scalped specimen (<4.75 mm), determined by small-scale shear box testing, is widely adopted by engineers for all the scalped crusher run products, which is expected to be too conservative for the coarse scalpings. Because scalping would change the particle size distribution of aggregate, it is believed that scalping would also influence the shear strength of aggregate. However, very little has been reported about the effect of scalping on shear strength of aggregate. Moreover, the effect of scalping on interface shear strength between aggregate and geogrid is another practical research question because these two materials commonly work together in construction, especially for pavement. There is also a lack of experimental data for the commercial crusher run materials with different degrees of scalping.

The success of large-scale direct shear testing using the Willie Machine has also been introduced in Paper I andPaper III, including detailed sample preparation methods and test procedures. Therefore, to study the effects of scalping on direct shear strength of crusher run and interface shear strength between crusher run and a geogrid, large-scale laboratory direct and interface shear tests were carried out on the crusher run specimens scalped to pass 75 mm, 37.5 mm, 19 mm, 9.5 mm, 4.75 mm and 2.36 mm, with and without a geogrid embedded in the middle. Another research question raised by this study is about the particle breakage of the crusher run specimens with different degrees of scalping during the large-scale direct or interface shear testing. There are not many references and data could be found in the literature regarding this question. Thus, sieving analyses were

proposed and carried out before and after the shear tests to assess the degree of particle breakdown caused by loading and shearing in the direct and interface shear tests.

The main contribution was that the results of this study indicate that scalping would significantly reduce the shear strength and friction angle for both direct and interface shear tests; therefore, engineers adopting the data of the scalped materials with smaller particle size range (<4.75 mm), would result in too conservative design. Furthermore, this research detailed and discussed the effects of scalping on the direct and interface shear stresses, failure envelopes, direct and interface friction angles, apparent cohesions and adhesions, and interface efficiencies. Finally, the results of sieving analyses before and after shear tests and the inferred breakage indices were discussed to assess and quantify the particle breakage caused by loading and shearing in the large-scale direct and interface shear tests.

3.1.3 Paper III

> ***Xu, Y.,*** *Williams, D. J., Serati, M., 2018. Measurement of Shear Strength and Interface Parameters by Multi-Stage Large-scale Direct/Interface Shear and Pull-out Tests. Measurement Science and Technology. 29 (8) 085601. https://doi.org/10.1088/1361-6501/aacb8a – incorporated as Paper III.*

Single-stage testing method has been commonly adopted in direct shear, interface shear, triaxial and pull-out testing. For conventional single-stage testing, at least three individual tests are needed to be carried out on specimens of the same material under three different normal stresses. The normal stress is normally doubled for each individual test. However, for a large-scale test, sample preparation would be very tedious with a large amount of specimens required. Therefore, conducting large-scale single-stage tests is not only very labour intensive but also time consuming and expensive. These difficulties in large-scale direct shear testing has also been proven in Paper I and Paper II. Thus, the first research question was to find an easier and reliable testing procedure to save time, labour and cost for large-scale direct shear, interface shear and pull-out tests. It was found that multi-stage testing method could be carried out on the same specimen by doubling confining stress step by step after each shearing stage. Most studies in the literature have only focused on the application of multi-stage testing method in triaxial tests. Very few references and data could be found for multi-stage direct/interface shear and pull-out tests. Researchers have

not treated the multi-stage testing method in much detail. In particular, few attempts were made to apply the multi-stage testing method in large-scale direct/interface shear tests. Thus, the main objectives of this research were to investigate the feasibility, reliability and applicability of multi-stage testing in large-scale direct/interface shear and pull-out tests, and to construct an empirical relationship between the single-stage and multi-stage test results. A Wille Geotechnik ADS-300 large-frame shear device newly setup at UQ in 2015 was utilised in this study, which is capable of performing both direct/interface shear and pull-out tests, as also mentioned in Paper I and Paper II.

In addition, both direct/interface shear and pull-out tests could be adopted to determine the interface parameters between geosynthetics and soils, such as the interface friction angles, apparent adhesions and interface coefficients. However, the relationship between interface shear stress and pull-out shear stress mobilised along the soil-geosynthetic interface in these two tests is still a very controversial topic. Different testing methods may produce significantly different interface parameters for design, and very little was found in the literature about the difference. Therefore, this research also attempted to compare the shear strength parameters and interface parameters obtained from different testing methods, and to construct the empirical relationships between the direct shear strength of soil, interface shear strength and pull-out shear strength between soil and geosynthetics.

The most obvious finding to emerge from this study was that it indicates that multi-stage testing can be successfully applied to large-scale direct shear, interface shear and pull-out testing of compacted soils, resulting in slightly lower shear strengths and considerably accurate c, ϕ strength parameters. This agrees with the findings in Paper I, which attempted four stages in the multi-stage tests. Another important finding was that the shear stress mobilised in pull-out tests during pulling increases much more slowly than that mobilised in direct and interface shear tests during shearing, so more horizontal displacement is required for pull-out tests to reach pull-out failure. This work contributes to existing knowledge of single-stage and multi-stage testing method in laboratory soil testing by providing more data, analyses and interpretations.

It is worth mentioning that after this research on applying the multi-stage testing method in large-scale direct shear tests, an optimum recommended multi-stage testing procedure was summarised and coded in the software of the Willie machine. The software is now able to control the loading and shearing automatically for each stage, which makes the

multi-stage testing much more efficient and user-friendly on this machine. Moreover, a large number of commercial multi-stage large-scale direct shear tests have been carried out at Geotechnical Engineering Centre (GEC) of University of Queensland (UQ) for different industry partners in the past two years, producing satisfactory results for the clients. So far, at UQ, the multi-stage testing method has been applied to test loosely-placed aggregates, compacted roadbase materials, sand, as-sampled fissured clay, scalped rock fill and wet residue mixture, and lacustrine soils for different industry consulting projects. Based on a large amount of data collected and considerable experience gained from different applications, both advantages (Pros) and disadvantages (Cons) of multi-stage testing are summarised. This research has extended our knowledge of multi-stage testing method in geotechnical soil testing.

3.1.4 Paper IV

> ***Xu, Y.,*** *Williams, D. J., Serati, M., 2018. Influence of anchorage angles on pull-out resistance of geotextile wrap around anchorage. Geosynthetics International.* 25 (4), 378-391. https://doi.org/10.1680/jgein.18.00022 – *incorporated as Paper IV.*

Anchored geosynthetics are able to withstand higher tension and provide higher anchorage capacity. Previous studies show that the simple run-out and wrap-around anchorages are two commonly used configurations in anchored geosynthetics. However, the influence of geometric parameters of different anchorage configurations on the pull-out performance is still problematic. Based on the literature review, it was found that only simple run-out and vertically (90°) wrap around anchorages have been studied in the pull-out tests. The influence of anchorage angles on the pull-out resistance of wrap around anchorages has not been fully explored. In order to bridge this research gap and to better understand the anchorage mechanisms for some complex anchorage geometries, two geometric control variables, namely, the top and bottom anchorage angles, were introduced and investigated experimentally and theoretically through pull-out tests and static equilibrium analysis.

The main contribution of this paper was that it summarised three stages to interpret the mobilisation process of pull-out resistance of a geotextile wrap around anchorage during the pull-out testing. Another contribution was that theoretical equations were derived to predict the pull-out resistance of a geotextile wrap around anchorage with varying

anchorage angles. The theoretical equation has also shown that there is an optimum top angle to provide a better pull-out performance. These findings have practical implications for the configurations of wrap around anchorages in the field, and for a better understanding of the mobilisation of the pull-out resistance.

3.2 Strength and consolidation behaviour

3.2.1 Paper V

> ***Xu, Y.,*** *Wu, S., Williams, D. J., Serati, M., 2018. Triaxial testing of clay with geotextile encased sand column. (submitted). – incorporated as Paper VII.*

Including geosynthetic materials in soils is an effective ground improvement technique. In terms of the installation methods, one or several layers of geosynthetics can be horizontally embedded in soils to increase the bearing capacity and confine the soil mass. Another category of installing geosynthetics for ground improvement purpose is using the geosynthetic encasement. Installing sand columns in clays is one of ground improvement techniques used to treat soft soils, and an additional inclusion of geosynthetic to encase the sand column can further improve the performance of the reinforced clay composite. For example, a further increase in bearing capacity and decrease in deformation of the clay composite could be achieved after encasing the sand columns. The two types of sand columns refer to the ordinary sand columns (OSC) and geotextile encased sand columns (GESC). Typical applications of OSC and GESC could be found in embankments and storage tanks constructed on soft clay soils.

This paper sets out to investigate the composite behaviour of clay with OSC and GESC through triaxial tests. Review of literature has revealed that most of the laboratory model tests on clay with OSC or GESC failed to control the drainage condition in the soil and did not allow for the measurement of pore pressure change during the loading and consolidation processes. Triaxial testing method is able to control the stress state, drainage condition, loading rate and lateral pressure, and is also able to measure the induced pore pressure and volume change. Therefore, isotropically consolidated undrained (CU) triaxial tests with pore pressure measurement were carried out on the clay, clay with OSC and clay with GESC, to further study the shear strength and pore water pressure behaviour of the composite materials.

It was found that some researchers have already carried out triaxial tests on cylindrical composite clay specimens with different granular columns and geosynthetic reinforcing configurations, such as changing the diameter or the length of the column, changing the number or the spacing of the columns, changing the numbers of horizontal geosynthetic reinforcement layer, etc. However, most of these previous studies only focused on comparing the improved load carrying capacity of the composite clay specimens, lacking the discussion on the effects of granular column and geosynthetic encasement on the pore water pressure dissipation during the consolidation stage, induced pore water pressure change during the shearing stage, total and effective stress Mohr circles, and total and effective stress paths.

To close these research gaps, in this investigation, the aim of a series of CU triaxial tests with pore water pressure measurement was to discuss and interpret the effects of OSC and GESC on pore water pressure, shear strength, Mohr circle, failure envelope and stress path, from both total stress and effective stress perspectives. In addition, overconsolidated soils are commonly encountered in excavations in the field as a result of overburden unloading, and thus, the effects of over consolidation ratio (OCR) on undrained shear strength, pore pressure change, Mohr circle and stress path were also investigated and interpreted in this paper. This investigation has provided a deeper insight into the triaxial behaviour of clay with the inclusion of OSC and GESC. Together with the next Paper VI about direct shear and 1-D consolidation testing of clay with OSC and GESC, these experimental studies contribute to the existing knowledge of the composite behaviour of clay with OSC and GESC by providing valuable data, analyses and interpretation.

3.2.2 Paper VI

> ***Xu, Y.,*** *Methiwala, J., Williams, D. J., Serati, M., 2018. Strength and consolidation characteristics of clay with geotextile-encased sand column. Proceedings of the Institution of Civil Engineers - Ground Improvement. 171 (3) 125-134. https://doi.org/10.1680/jgrim.17.00070 – incorporated as Paper VI.*

The background of clay reinforced with OSC and GESC has been introduced in the previous Paper V, this paper continues to deal with the same topic in direct shear and oedometer tests. It was found that most studies on clay reinforced with OSC and GESC

have only focused on vertical loading conditions, such as bearing capacity tests, loading tests, compression tests, and triaxial tests. However, in terms of the lateral loading on the OSC or GESC, very limited references could be found in the literature. It is believed that the sand columns below the toe of the embankment are primarily subjected to lateral loading or shear movement, as shown in Figure 3.2. The performance of clay reinforced with OSC or GESC subjected to lateral loading could be experimentally modelled by direct shear box tests (Murugesan and Rajagopal 2009; Mohapatra et al. 2017), as mentioned in the literature review. In this research, the shear strength and consolidation characteristics of clay, clay with OSC, and clay with GESC were investigated by carrying out laboratory direct shear and oedometer tests. The direct shear tests were used to study the response of the reinforced clay composite under lateral loading condition, including direct shear strength, failure envelope, and inferred strength parameters. The oedometer tests were used to study the response of the reinforced clay composite under vertical loading, unloading and reloading conditions. The impacts of OSC and GESC on the consolidation characteristics were discussed in detail, including the compression index C_c, swell index C_s, recompression index C_r, secondary compression index C_α, coefficient of consolidation c_v, coefficient of compressibility a_v, coefficient of volume compressibility m_v, modulus of compressibility E_s, and hydraulic conductivity k.

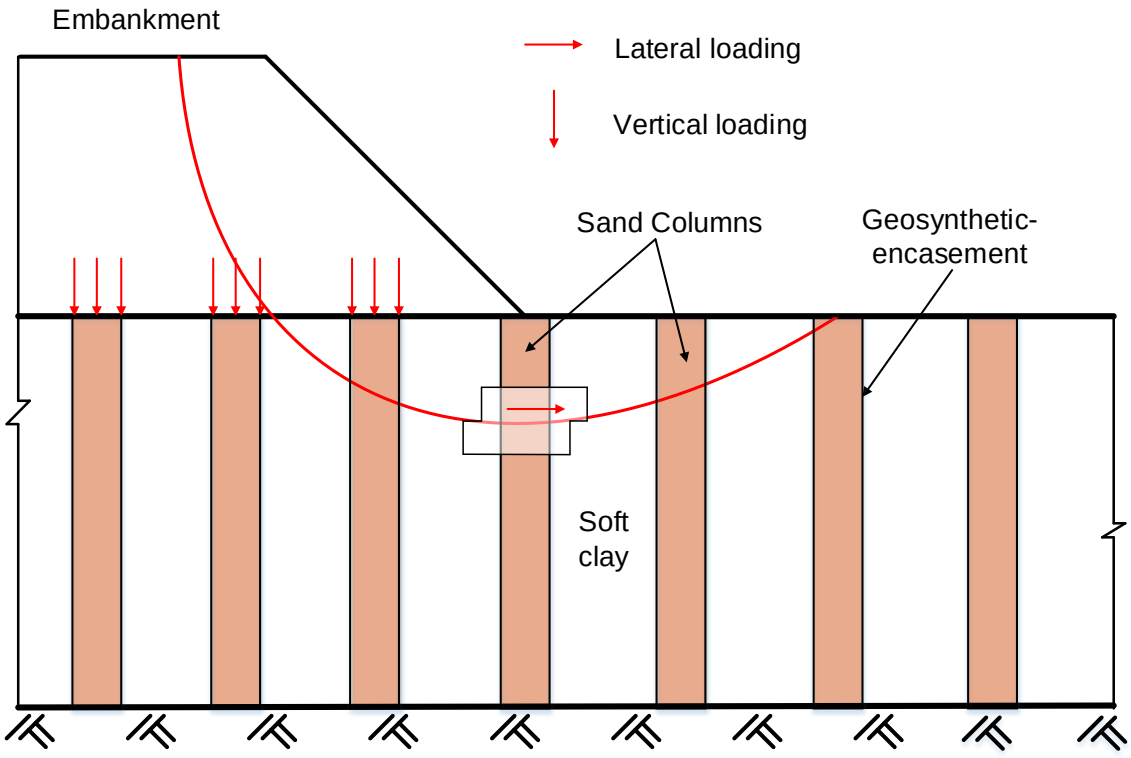

Figure 3.2 Vertical and lateral loading on sand columns under an embankment

These findings enhance a deeper understanding of the shear strength and consolidation characteristics of clay with OSC and GESC under both lateral and vertical loading conditions. A future extended study has been proposed to study the consolidation characteristics of the clay reinforced with OSC and GESC using a special designed large-scale slurry consolidometer (150 mm in diameter and 400 mm in height; Shokouhi et al. 2017) at the University of Queensland. The insights gained from this study will be of assistance to the proposed future study.

4 CONCLUSIONS AND FUTURE RESEARCH

4.1 Conclusions

The aim of this PhD thesis was to investigate the interface and composite behaviour of geosynthetic-reinforced soils, including soil-geosynthetic interface behaviour in direct/interface shear and pull-out tests, and the strength and consolidation behaviour of clay composite reinforced with OSC or GESC. A series of studies was carried out using different experimental and theoretical approaches to answer the research questions and achieve the research objectives, as summarised in Table 1.1. The main outcomes and findings of each study have been included in previous chapters, and in the conclusions of each attached paper in Appendix A. In this chapter, the most significant findings and conclusions are highlighted and summarised.

(1) Based on the experimental results obtained from the large-scale direct and interface shear testing of roadbase materials and the four types of geosynthetics, theoretical equations and a new contribution ratio are proposed to quantify the contribution of different shear strength components mobilised along the interface between the roadbase materials and geogrids. These experimental and theoretical studies extend the current soil-geogrid interaction theory.

(2) Scalping could cause a pronounced reduction in direct and interface shear strength, and the failure envelopes obtained gradually decrease and flatten out with an increasing degree of scalping, resulting in a significant decrease in direct and interface shear strength parameters. The results also imply that small-scale laboratory testing, necessitating highly scalped specimens, would generate conservative shear strength design parameters.

(3) Multi-stage testing can be successfully applied to large-scale direct/interface shear and pull-out testing of compacted soils, resulting in only slightly reduced shear strength parameters compared with those obtained using single stage testing. Both advantages and disadvantages of the multi-stage testing method have been summarised, which provide an insight into the selection of a suitable testing method for different types of soils for different applications.

(4) The three-stage mobilisation of the pull-out resistance of a geotextile wrap around anchorage was investigated and interpreted. Theoretical expressions were derived to predict the pull-out resistance of the geotextile wrap around anchorage with varying anchorage angles, based on static equilibrium analysis.

(5) A series of laboratory isotropically consolidated undrained (CU) triaxial tests with pore pressure measurement was carried out on clay, clay with OSC, and clay with GESC, to study the shear strength, consolidation and pore water pressure behaviour of the composite materials. This study has identified the effects of OSC and GESC on pore water pressure, shear strength, Mohr circle, failure envelope and stress path, in terms of both total and effective stresses.

(6) Shear strength and consolidation characteristics of clay, clay with OSC, and clay with GESC were also investigated by a series of laboratory direct shear and oedometer tests to study their response under both lateral and vertical loading conditions. The test results have shown that the impacts of OSC and GESC on direct shear strength and consolidation characteristics, including a large number of soil parameters discussed.

4.2 Future Research

The findings presented in Papers V and VI, warrant extension of the study of clay with geosynthetic-encased sand columns to a larger scale. Larger-scale laboratory testing may overcome scale effects and also allow the testing of groups of columns.

Apart from the influence of OSC or GESC, other variables in the response of the composite clay specimen to lateral or vertical loading include:

(1) Area replacement ratio

(2) Length to diameter ratio

(3) Group of columns

The interpretation of large-scale model tests may contain the following key plots in order to compare and analyse different controlled variables:

(1) shear stress versus shear displacement

(2) vertical displacement versus shear displacement

(3) shear strength versus normal stress

(4) pore water pressure versus time

(5) load versus settlement

These large-scale model tests will further enhance the understanding of shear strength and consolidation characteristics of clay with OSC and GESC under both lateral and vertical loading conditions. In addition, further numerical and/or analytical analyses may be required to back up the experimental tests.

REFERENCE

Abu-Farsakh, M., Coronel, J., and Tao, M., (2007). Effect of soil moisture content and dry density on cohesive soil–geosynthetic interactions using large direct shear tests. Journal of Materials in Civil Engineering, 19(7), 540-549.

Alexiew D., Brokemper D., and Lothspeich S., (2005) Geotextile Encased Columns (GEC): Load Capacity, Geotextile Selection and Pre-Design Graphs. Proceedings of GeoFrontiers 2005, Austin, Texas, United States, pp. 497-510.

Alfaro, M. C., Miura, N., Bergado, D. T., (1995). Soil geogrid reinforcement interaction by pullout and direct shear tests. Geotechnical Testing Journal, 18(2), 157–167.

Ali, K., Shahu, J. T., and Sharma, K. G., (2012). Model tests on geosynthetic-reinforced stone columns: a comparative study. Geosynthetics International, 19(4), 292-305. doi: 10.1680/gein.12.00016.

Ali, K., Shahu, J. T., and Sharma, K. G., (2014). Model tests on single and groups of stone columns with different geosynthetic reinforcement arrangement. Geosynthetics International, 21(2), 103-118. doi: 10.1680/gein.14.00002.

Almeida M. S. S., Hosseinpour I., Riccio M., and Alexiew D., (2015) Behavior of Geotextile-Encased Granular Columns Supporting Test Embankment on Soft Deposit. Journal of Geotechnical and Geoenvironmental Engineering, 141(3), 04014116.

Althoff, S., (2010) Contribution to use multi-stage large shear-frametest to investigatethe interactionbehaviour between geosynthetics and cohesive soil, TU-Bergakademie, Freiberg, Germany. https://tu-freiberg.de/sites/default/files/media/professur-fuer-bodenmechanik-6558/2010althoff.pdf

Andreou, P., Frikha, W., Frank, R., Canou, J., Papadopoulos, V., and Dupla, J. C., (2008). Experimental study on sand and gravel columns in clay. Proceedings of the Institution of Civil Engineers - Ground Improvement, 161(4), 189-198. doi: 10.1680/grim.2008.161.4.189.

Anubhav and Basudhar, P. K., (2010). Modeling of soil-woven geotextile interface behavior from direct shear test results. Geotextiles and Geomembranes, 28(4), 403-408.

Arulrajah, A., Rahman, M. A., Piratheepan, J., Bo, M. W., and Imteaz, M. A., (2013). Evaluation of interface shear strength properties of geogrid-reinforced construction and demolition materials using a modified large-scale direct shear testing apparatus. Journal of Materials in Civil Engineering, 25(8), 1077-1088.

ASTM D4439-15. (2015). Standard Terminology for Geosynthetics. ASTM International, West Conshohocken, PA

ASTM D5321-14. (2014). Standard Test Method for Determining the Shear Strength of Soil-Geosynthetic and Geosynthetic-Geosynthetic Interfaces by Direct Shear, ASTM International, West Conshohocken, PA, www.astm.org

ASTM D6706-13. (2013). Standard Test Method for Measuring Geosynthetic Pullout Resistance in Soil, ASTM International, West Conshohocken, PA, www.astm.org

Ayadat, T., and Hanna, A. M., (2005). Encapsulated stone columns as a soil improvement technique for collapsible soil. Proceedings of the Institution of Civil Engineers - Ground Improvement, 9(4), 137-147. doi: 10.1680/grim.2005.9.4.137.

Bathurst, R. J., and Ezzein, F. M. (2015). Geogrid and Soil Displacement Observations During Pullout Using a Transparent Granular Soil. Geotechnical Testing Journal, 38(5), 673–685. doi:10.1520/GTJ20140145.

Bathurst, R. J., and Ezzein, F. M. (2016). Geogrid pullout load–strain behaviour and modelling using a transparent granular soil. Geosynthetics International, 23(4), 271–286. http://dx.doi.org/10.1680/jgein.15.00051.

Bathurst, R. J., and Ezzein, F. M. (2017). Insights into geogrid–soil interaction using a transparent granular soil, Géotechnique Letters, 7(2), 179-183.

Berg, R. R., Christopher, B. R., and Samtani, N. C., (2009). Design and construction of mechanically stabilized earth walls and reinforced soil slopes (FHWA-NHI-10-024), Washington, DC: Federal Highway Administration.

Bergado, D. T., Chai, J. C., Abiera, H. O., Alfaro, M. C., Balasubramaniam, A. S., (1993). Interaction between cohesive-frictional soil and various grid reinforcements. Geotextiles and Geomembranes, 12(4), 327–349.

Bergado, D. T., Ramana, G. V., Sia, H. I., and Varun, (2006). Evaluation of interface shear strength of composite liner system and stability analysis for a landfill lining system in Thailand. Geotextiles and Geomembranes, 24, 371–393.

Black, J. A, Sivakumar, V., Madhav, M. R., and McCabe, B., (2006). An improved experimental test set-up to study the performance of granular columns. Geotechnical Testing Journal, 29(3), 193-199.

Black, J. A., Sivakumar, V., and Bell, A., (2011). The settlement performance of stone column foundations. Géotechnique, 61(11), 909-922. doi: 10.1680/geot.9.P.014.

Black, J. A., Sivakumar, V., Madhav, M. R., and Hamill, G. A., (2007). Reinforced stone columns in weak deposits: laboratory model study. Journal of Geotechnical and Geoenvironmental Engineering, 133(9), 1154-1161. doi: 10.1061/(ASCE)1090-0241(2007)133:9(1154).

Castro J., and Sagaseta C., (2011) Deformation and consolidation around encased stone columns. Geotextiles and Geomembranes, 29(3), 268-276.

Chareyre, B., Briançon, L., and Villard, P., (2002). Theoretical Versus Experimental Modeling of the Anchorage Capacity of Geotextiles in Trenches. Geosynthetics International, 9(2), 97-123.

Christopher, B. R., Gill, S. A., Giroud, J. P., Juran, I., Mitchell, J. K., Schlosser, F., and Dunnicliff, J., (1990). Reinforced soil structures (FHWA-RD-89-043), Washington, DC: Federal Highway Administration.

Dash S. K., and Bora M. C., (2013) Influence of geosynthetic encasement on the performance of stone columns floating in soft clay. Canadian Geotechnical Journal, 50(7), 754-765.

Ezzein, F. M., and Bathurst, R. J., (2014). A new approach to evaluate soil-geosynthetic interaction using a novel pullout test apparatus and transparent granular soil. Geotextiles and Geomembranes, 42(3), 246-255. https://doi.org/10.1016/j.geotexmem.2014.04.003.

Fannin, R. J., and Raju, D. M., (1993). On the pullout resistance of geosynthetics. Canadian Geotechnical Journal, 30(3), 409-417.

Farrag, K., Acar, Y. B., and Juran, I., (1993). Pull-out resistance of geogrid reinforcements. Geotextiles and Geomembranes, 12(2), 133-159.

Ferreira, F. B., Vieira, C. S., Lopes, M. L., and Carlos, D. M., (2015). Experimental investigation on the pullout behaviour of geosynthetics embedded in a granite residual soil. European Journal of Environmental and Civil Engineering, DOI: 10.1080/19648189.2015.1090927.

Frikha, W., Tounekti, F., Kaffel, W., and Bouassida, M., (2015). Experimental study for the mechanical characterization of Tunis soft soil reinforced by a group of sand columns. Soils and Foundations, 55(1), 181-191. doi: https://doi.org/10.1016/j.sandf.2014.12.014.

Gan, J. K., and Fredlund, D. G., (1988). Multistage Direct Shear Testing of Unsaturated Soils. Geotechnical Testing Journal, 11(2), pp. 132–138.

Girard, H., Briançon, L., and Rey, E., (2006). Experimental tests for geosynthetic anchorage trenches. In Proceedings of the Eighth International Conference on Geosynthetics, 8th ICG, Japan, 18–22 September 2006, pp. 211-216.

Giroud, J. P., (1986). From Geotextiles to Geosynthetics: A Revolution in Geotechnical Engineering. Proceedings of the Third International Conference on Geotextiles, Vol. 1, Vienna, Austria, April 1986, pp. 1-18.

Gniel J., and Bouazza A., (2009) Improvement of soft soils using geogrid encased stone columns. Geotextiles and Geomembranes, 27(3), 167-175.

Gniel J., and Bouazza A., (2010) Construction of geogrid encased stone columns: A new proposal based on laboratory testing. Geotextiles and Geomembranes, 28(1), 108-118.

Goodhue, M. (1998). Reuse of foundry sands in reinforced earth structures. Master thesis, University of Wisconsin, Madison, USA.

Gu, M., Zhao, M., and Han, J., (2015). Effects of geogrid encasement on lateral and vertical deformations of stone columns in model tests. Geosynthetics International, 23(2), 100-112.

Gullic, R. C., (1970). Multi-stage shear testing of a cohesionless soil. Master thesis, Univerisity of Missouri-Rolla, USA.

Gupta, R., Swan Jr. R. H., and Zornberg J. G., (2014). Laboratory Pullout Equipment for Testing Soil-Geosynthetic Interface for Reinforced Flexible Pavement Design. Geo-Congress 2014 Technical Papers: Geo-Characterization and Modeling for Sustainability, GSP 234, ASCE.

Hausmann, M. R., and Clarke, J. W., (1994). Fly ash/geogrid direct shear tests. Australian Geomechanics, 4(25), 67-70.

Hong Y., Wu C., and Yu Y., (2016) Model tests on geotextile-encased granular columns under 1-g and undrained conditions. Geotextiles and Geomembranes, 44(1), 13-27.

Hormdee, D., Kaikeerati, N., and Angsuwotai, P., (2012). Evaluation on the results of multistage shear test. International Journal of GEOMATE, 2(1), 140–143.

Hsieh, C. W., Chen, G. H., and Wu, J., (2011). The shear behavior obtained from the direct shear and pullout tests for different poor graded soil-geosynthetic systems. Journal of GeoEngineering, 6(1), 15–26.

Ingold, T. S. (1983). Laboratory Pull-out Testing of Grid Reinforcements in Sand. Geotechnical Testing Journal, 6(3), 101-111.

Ingold, T. S., (1982). Some observations on the laboratory measurement of soil-geotextile bond. Geotechnical Testing Journal, 5, 57-67.

Jewell, R. A., (1990). Reinforcement bond capacity. Géotechnique, 40(3), 513–518.

Jewell, R. A., Milligan, G. W. E., Sarsby, R. W., and Dubois, D., (1984). Interaction between soil and geogrids. In Proceedings of Symposium on Polymer Grid Reinforcement. Thomas Telford Ltd, London, pp. 18–29.

Jones, C. J .F. P., (1996). Earth reinforcement and soil structures. Thomas Telford Publishing.

Juran, I., and Chen, C. L., (1988). Soil-Geotextile Pull-out Interaction Properties, Testing and Interpretation. Transportation Research Record, 67th Annual Meeting.

Juran, I., and Guermazi, A., (1988). Settlement response of soft soils reinforced by compacted sand columns. Journal of Geotechnical Engineering, 114(8), 930-943. doi: 10.1061/(ASCE)0733-9410(1988)114:8(930).

Kadhim, S. T., (2016). Stability analysis of geotextile encased sand columns. PhD dissertation, The University of Kansas, USA.

Kim, S. S., Han, S. J., Jung, S. Y., and Shin, H. Y., (2007). Drained triaxial behavior of scp-reinforced composite ground with low area replacement ratio. International Society of Offshore and Polar Engineers, 17(2), 152-158.

Lajevardi, S. H., Briançon, L., and Dias, D., (2014). Experimental studies of the geosynthetic anchorage – Effect of geometric parameters and efficiency of anchorages. Geotextiles and Geomembranes, 42(5), 505-514.

Lajevardi, S. H., Dias, D., and Briançon, L., (2015a). Experimental studies of the behaviour of geosynthetic wrap around anchorage. Geosynthetics International, 22(3), 249-256.

Lajevardi, S. H., Silvani, C., Dias, D., Briançon, L., and Villard, P., (2015b). Geosynthetics anchorage with wrap around: experimental and numerical studies. Geosynthetics International, 22(4), 273-287.

Lee, K. M., and Manjunath, V. R., (2000). Soil–geotextile interface friction by direct shear test. Canadian Geotechnical Journal, 37(1), 238–252.

Liu, C. -N., Ho, Y. -H., and Huang, J. -W., (2009a). Large scale direct shear tests of soil/PET-yarn geogrid interfaces. Geotextiles and Geomembranes, 27(1), 19-30.

Liu, C. -N., Zornberg, J. G., Chen, T. -C., Ho, Y. -H., and Lin, B. -H., (2009b). Behavior of geogrid-sand interface in direct shear mode. Journal of Geotechnical and Geoenvironmental Engineering, 135(12), 1863-1871.

Lopes, M. L., (2002). Soil-geosynthetic interaction. Geosynthetics and their applications, S. K. Shukla, ed., Thomas Telford, London.

Lopes, M. L., and Silvano, R., (2010). Soil/geotextile interface behaviour in direct shear and pullout movements. Geotech. Geol. Eng., 28(6), 791–804.

Malarvizhi S. N., and Ilamparuthi K., (2007) Comparative study on the behavior of encased stone column and conventional stone column. Soils and Foundations, 47(5), 873-885.

Mallick, S. B., Zhai, H., Adanur, S., and Elton, D. J., (1996). Pullout and direct shear testing of geosynthetic reinforcement: state-of-the-art report. Transportation Research Record, TRB 1534, 80–90.

Matsui, T., San, K. C., Nabesahirna, Y., and Arnii, U. N., (1996). Bearing mechanism of steel reinforcement in pull-out test. In Proceedings of the International Symposium: Earth Reinforcement, Fukuoka, Kyushu, Japan. Balkema Publisher, 101–105.

Miranda, M., and Da Costa, A., (2016). Laboratory analysis of encased stone columns. Geotextiles and Geomembranes, 44(3), 269-277. doi: https://doi.org/10.1016/j.geotexmem.2015.12.001.

Mohapatra S. R., Rajagopal K., and Sharma J., (2016) Direct shear tests on geosynthetic-encased granular columns. Geotextiles and Geomembranes, 44(3), 396-405.

Mohapatra S. R., Rajagopal K., and Sharma J., (2017) 3-Dimensional numerical modeling of geosynthetic-encased granular columns. Geotextiles and Geomembranes, 45(3), 131-141.

Moraci, N., and Cardile, G., (2009). Influence of cyclic tensile loading on pullout resistance of geogrids embedded in a compacted granular soil. Geotextiles and Geomembranes, 27(6), 475–487.

Moraci, N., and Gioffre, D., (2006). A simple method to evaluate the pullout resistance of extruded geogrids embedded in a compacted granular soil. Geotextiles and Geomembranes, 24(2), 116–128.

Moraci, N., and Recalcati, P., (2006). Factors affecting the pullout behaviour of extruded geogrids embedded in a compacted granular soil. Geotextiles and Geomembranes, 24(4), 220–242.

Murugesan S., and Rajagopal K., (2009) Shear load tests on stone columns with and without geosynthetic encasement. Geotechnical Testing Journal, 32(1), 35-44.

Murugesan, S., and Rajagopal, K., (2006). Geosynthetic-encased stone columns: Numerical evaluation. Geotextiles and Geomembranes, 24(6), 349–358.

Murugesan, S., and Rajagopal, K., (2007). Model tests on geosynthetic-encased stone columns. Geosynthetics International, 14(6), 346-354. doi: 10.1680/gein.2007.14.6.346.

Murugesan, S., and Rajagopal, K., (2010). Studies on the behavior of single and group of geosynthetic encased stone columns. Journal of Geotechnical and Geoenvironmental Engineering, 136(1), 129-139. doi: 10.1061/(ASCE)GT.1943-5606.0000187.

Najjar S. S., Sadek, S., and Maakaroun, T., (2010). Effect of sand columns on the undrained load response of soft clays. Journal of Geotechnical and Geoenvironmental Engineering, 136(9), 1263-1277. doi: 10.1061/(ASCE)GT.1943-5606.0000328.

Najjar, S. S., and Skeini, H., (2015). Triaxial response of clays reinforced with granular columns. Proceedings of the Institution of Civil Engineers - Ground Improvement, 168(4), 265-281. doi: 10.1680/grim.13.00049.

Ochiai, H., Otani, J., Hayashic, S., and Hirai T., (1996). The Pull-out Resistance of Geogrids in Reinforced Soil. Geotextiles and Geomembranes, 14(1), pp 19-42.

Palmeira, E. M., and Milligan, G. W. E., (1989). Large scale direct shear tests on reinforced sand. Soils and Foundations, 29(1), 18–30.

Peterson, L. M., and Anderson, L. R., (1980). Pull-out resistance of welded wire mesh embedded in soil. Research report submitted to Hilfiker Pipe Co., Department of Civil Engineering, Utah State University, Logan, UT, USA.

Petro, M. J., Sordo, B., Berry , S. M., and MacLaughlin, M. M., (2017). Characterization of the peak strength of rough rock joints using limited displacement multi-stage direct shear tests. 51st U.S. Rock Mechanics/Geomechanics Symposium, 25-28 June, San Francisco, California, USA.

Pradhan, B., (2003). Study of pullout behavior of soil nails in completely decomposed granite fill. Master thesis, The University of Hong Kong, China.

Rajagopal, K., Krishnaswamy, N. R., and Madhavi Latha, G., (1999). Behaviour of sand confined with single and multiple geocells. Geotextiles and Geomembranes, 17(3), 171-184. doi: https://doi.org/10.1016/S0266-1144(98)00034-X.

Rowe, R. K., Ho, S. K., and Fisher, D. G. (1985). Determination of Soil-Geotextile Interface Strength Properties. Second Canadian Symposium on Geotextiles and Geomembranes, pp 25-34.

Shokouhi A., Zhang C., and Williams D. J., (2017) Settling, consolidation and desiccation behaviour of coal tailings slurry. Mining Technology,1-11.

Shukla, S. K., (2002). Geosynthetics and their applications. Thomas Telford Publishing.

Sivakumar, V., Jeludine, D. K. N. M., Bell, A., Glynn, D. T., and Mackinnon, P., (2011). The pressure distribution along stone columns in soft clay under consolidation and foundation loading. Géotechnique, 61(7), 613-620. doi: 10.1680/geot.9.P.086.

Sivakumar, V., McKelvey, D., Graham, J., and Hughes, D., (2004). Triaxial tests on model sand columns in clay. Canadian Geotechnical Journal, 41(2), 299-312. doi: 10.1139/t03-097.

Villard, P. and Chareyre, B., (2004). Design methods for geosynthetic anchor trenches on the basis of true scale experiments and discrete element modelling. Canadian Geotechnical Journal, 41(6), 1193-1205.

Wu, C. -S., and Hong, Y. -S., (2009). Laboratory tests on geosynthetic-encapsulated sand columns. Geotextiles and Geomembranes, 27(2), 107-120. doi: https://doi.org/10.1016/j.geotexmem.2008.09.003.

Zhou, J., Chen, J. F., Xue, J. F., Wang, J. Q., 2012. Micro-mechanism of the interaction between sand and geogrid transverse ribs. Geosynthetics International, 19(6), 426-437.

Zornberg, J. G. (2011). Advances in the Use of Geosynthetic in Pavement Design. Invited Keynote Paper, Proceedings of the Second National Conference on Geosynthetics, India Institute of Technology Madras, Chennai, India, September 23-24, 3-21.

APPENDIX A - ATTACHED PAPERS

Attached Paper I

Paper I: Investigation of shear strength of interface between roadbase and geosynthetics using large-scale single-stage and multi-stage direct shear test

Xu, Y., Williams, D. J., Serati, M., 2018. Investigation of shear strength of interface between roadbase and geosynthetics using large-scale single-stage and multi-stage direct shear test. Road Materials and Pavement Design. https://doi.org/10.1080/14680629.2018.1561378 – incorporated as **Paper I.**

Investigation of shear strength of interface between roadbase and geosynthetics using large-scale single-stage and multi-stage direct shear test

Youwei Xu[a,], David J. Williams[b], Mehdi Serati[c]*

[a] PhD candidate, School of Civil Engineering, The University of Queensland, Brisbane, QLD 4072, Australia. Email: youwei.xu@uq.edu.au

[b] Professor, School of Civil Engineering, The University of Queensland, Brisbane, QLD 4072, Australia. Email: d.williams@uq.edu.au

[c] Postdoctoral Research Fellow, School of Civil Engineering, The University of Queensland, Brisbane, QLD 4072, Australia. Email: m.serati@uq.edu.au

Abstract

The application of geosynthetics in the road pavement industry as a reinforcement has increased dramatically in recent years. Geosynthetic inclusions can significantly: i) increase the bearing capacity of the pavement, ii) prolong the road service life, iii) reduce maintenance costs, and iv) diminish unfavourable large vertical and lateral pavement deformations. Although considerable research has been carried out on the interfaces between soils and geosynthetics through large-scale direct shear testing, there is a lack of research in the interfaces between roadbase materials and geosynthetics in pavement engineering. The main innovation of this paper is to investigate the shear strength behaviour of the interfaces existing in a geosynthetic-reinforced pavement. One interface is existing between roadbase and geosynthetic reinforcement for base reinforcement; another one is existing between roadbase and subgrade with geosynthetic reinforcement for subgrade stabilisation. Therefore, a series of laboratory, large-scale direct shear tests was carried out on roadbase materials with and without the inclusion of geosynthetics, under applied normal stresses of 25 kPa, 50 kPa, 75 kPa or 100 kPa, representing the magnitude of the overburden pressure in the pavement. In addition, theoretical interpretations are

developed to back up the experimental results, and to quantify the contribution of different shear strength components mobilised along the interface between roadbase materials and geogrids. Finally, the applicability of multi-stage, large-scale direct shear box testing is assessed by comparing the results obtained with those from conventional single-stage tests obtained in the present experimental study.

Keywords: geosynthetics; interface behaviour; large-scale direct shear test; multi-stage; roadbase material; single-stage

1 Introduction

Geosynthetic reinforcements are used in pavement engineering in two major applications: i) base reinforcement (embedded within the base or subbase layers), and ii) subgrade stabilisation (embedded between the subgrade and the granular base course). The inclusion of geosynthetics in road pavements can improve pavement performance through increasing the lateral confinement, bearing capacity, and overall rigidity of the pavement, as well as reducing the vertical and lateral pavement deformations. From an economical point of view, it can also: i) decrease the required thickness of base course, ii) reduce road maintenance costs, and iii) increase road pavement life. Hence, geosynthetic reinforcement is recognised as an easy and effective solution compared to traditional alternatives for improving weak subgrade soils in pavement engineering.

Interface parameters between geosyntheics and roadbase materials are key factors in the design of a geosynthetics reinforced pavement. There are two commonly accepted experimental techniques to determine interface parameters: i) the direct shear test, and ii) the pull-out test. Since the 1980s, numerous experimental studies have been carried out to investigate soil-geosynthetic interface parameters using different modified direct shear apparatus or pull-out equipment (Jewell et al. 1984; Palmeira and Milligan 1989; Bergado et al. 1993; Alfaro et al. 1995; Lee and Manjunath 2000; Lopes 2002; Tang et al. 2008).

Jewell et al. (1984) were among the pioneers in the testing of soil-geosynthetic interfaces, and first proposed the following theoretical equation to understand the soil-geogrid interaction under direct shear conditions:

$$\tau_{ds} = f_{ds}\sigma_n \tan\phi = \sigma_n \left[\alpha_{ds} \tan\delta + (1-\alpha_{ds}) \tan\phi\right] \quad (1)$$

where ϕ is the soil internal friction angle, δ is the friction angle between soil and the reinforcement, f_{ds} is the direct shear interface coefficient, α_{ds} is the proportion of the surface area of the geogrid ribs in contact with soil, i.e., the area of ribs (longitudinal and transverse) relative to the total geogrid area, σ_n is the normal stress, and τ_{ds} is the interface direct shear strength between the geogrid and the soil. Based on the experimental results, the Mohr-Coulomb criteria can then be applied to obtain the best-fit straight line failure envelope, which can be interpreted by the following equation for cohesionless soil:

$$\tau_{ds} = \sigma_n \tan\delta \quad (2)$$

From Eq. (1), it is possible to obtain the theoretical direct shear interface coefficient as:

$$f_{ds} = 1 - \alpha_{ds}(1 - \frac{\tan\delta}{\tan\phi_{ds}}) \quad (3)$$

From the experimental results, the direct shear interface coefficient can then be calculated as:

$$f_{ds} = \frac{\tau_{ds}}{\tau_s} \quad (4)$$

where τ_{ds} is the experimentally determined interface direct shear strength between the geogrid and the soil, and τ_s is the direct shear strength of soil.

It should be noted that unlike the direct shear resistance between soil and a geotextile, which is attributed only to the friction between the soil and the geotextile, the direct shear resistance between soil and a geogrid is made up of two components. One is the friction between the soil and the geogrid ribs, and the other is the friction between the soil above and below the geogrid and the soil in open area of the geogrid (see also Figure 1 and Eq. (1)).

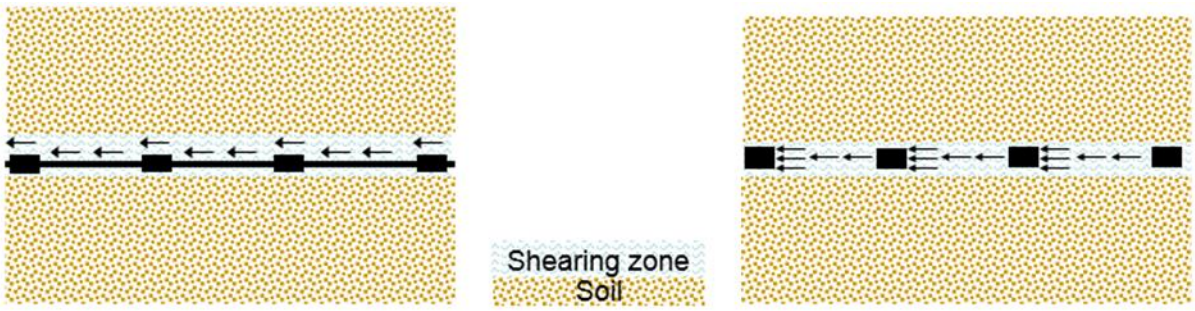

(a) (b)

Figure 1 Interaction mechanisms between soil and geogrid in interface shear test: (a) friction between soil and ribs; (b) friction between soil and soil in open area

Recent studies include the work of Bergado et al. (2006), who conducted over 70 large direct shear tests to evaluate the interface shear strength parameters of a liner system using project-specific materials under site conditions. Abu-Farsakh et al. (2007) studied the effect of moisture content and dry density on cohesive soil-geosynthetic interactions using large direct shear tests. Liu et al. (2009a) evaluated the contribution of transverse ribs to the soil-geogrid interaction under large-scale direct shear testing. Liu et al. (2009b) compared different dimensions of the lower half of the shear box for their soil-geogrid interface testing and concluded that a lower box of the same size as the upper box was most suitable. Palmeira (2009) presented and discussed comprehensive studies on experimental, theoretical and numerical methods for evaluating the interaction between soils and geosynthetics, and outlined the main advantages and limitations of each. Anubhav and Basudhar (2010) carried out an experimental study on soil-geotextile interaction using two differently textured woven geotextiles in the direct shear test. They proposed a non-linear constitutive model to predict both the pre-peak and the post-peak interface behaviour. Arulrajah et al. (2013) investigated the interface shear strength parameters of geogrid-reinforced construction and demolition aggregate interfaces using a modified large-scale direct shear apparatus. Vieira et al. (2013) investigated the sand-geotextile behaviour through monotonic and cyclic direct shear tests under both stress and strain controlled conditions, and the obtained interface shear strengths, stiffness and damping ratio were discussed and interpreted. Other recent

large-scale direct or interface shear testing research could also be found in literature by testing various types of materials (Piratheepan et al. 2013; Arulrajah et al. 2015; Ferreira et al. 2015; Chen et al. 2015; Vieira and Pereira 2015; Liu et al. 2016; Ghaaowd et al. 2017; Sakleshpur et al. 2017; Hazirbaba 2017).

The conventional single-stage direct shear testing method requires a minimum of three individual samples tested under three different applied normal stresses. In order to reduce the time and expense of laboratory testing, and to ensure that sample variability is eliminated, using multi-stage direct shear testing method to determine the shear strength and interface parameters is reported and developed herein. Multi-stage direct shear test is carried out on only one representative specimen by applying multiple loading and shearing stages. The maximum shear strengths obtained at each stage are plotted against different normal stresses applied for each stage to determine the failure envelopes obtained from a multi-stage test. The earliest literature on multi-stage direct shear testing can be found in a Master's thesis written by Gullic, at the University of Missouri-Rolla, USA, in 1970. Gullic (1970) performed a series of multi-stage direct shear tests on a cohesionless soil using a small shear box with the diameter of 62.0 mm and a specimen height of 25.8 mm. Five different multi-stage direct shear testing procedures were studied and compared against conventional single-stage results. It was reported that multi-stage direct shear testing resulted in a lower shear strength, with a failure envelope slightly below that of conventional single-stage tests. The applicability of the multi-stage direct shear test has since been examined with different soils under saturated and unsaturated conditions (Gan and Fredlund 1988; Nam et al. 2011; Hormdee et al. 2012).

Based on the research gaps mentioned above, the interface parameters between roadbase materials and geosynthetics for roadbase reinforcement and subgrade stabilisation require further investigation, and the application of multi-stage large-scale direct shear testing warrants further consideration. In this paper, a series of large-scale direct shear tests was carried out on roadbase materials with and without the inclusion of geosynthetic reinforcement using both single-stage and multi-stage testing. Interface parameters, such as interface adhesion, interface friction angles and interface friction coefficients are derived and analysed from the experimental

results. The contribution of the geogrid ribs to overall interface shear strength is also quantified by defining a new contribution ratio. Finally, the multi-stage test results are compared with those of conventional single-stage test results to evaluate the feasibility, reliability and limitations of multi-stage testing in a large-scale direct shear apparatus.

2 Material studied

2.1 Roadbase materials

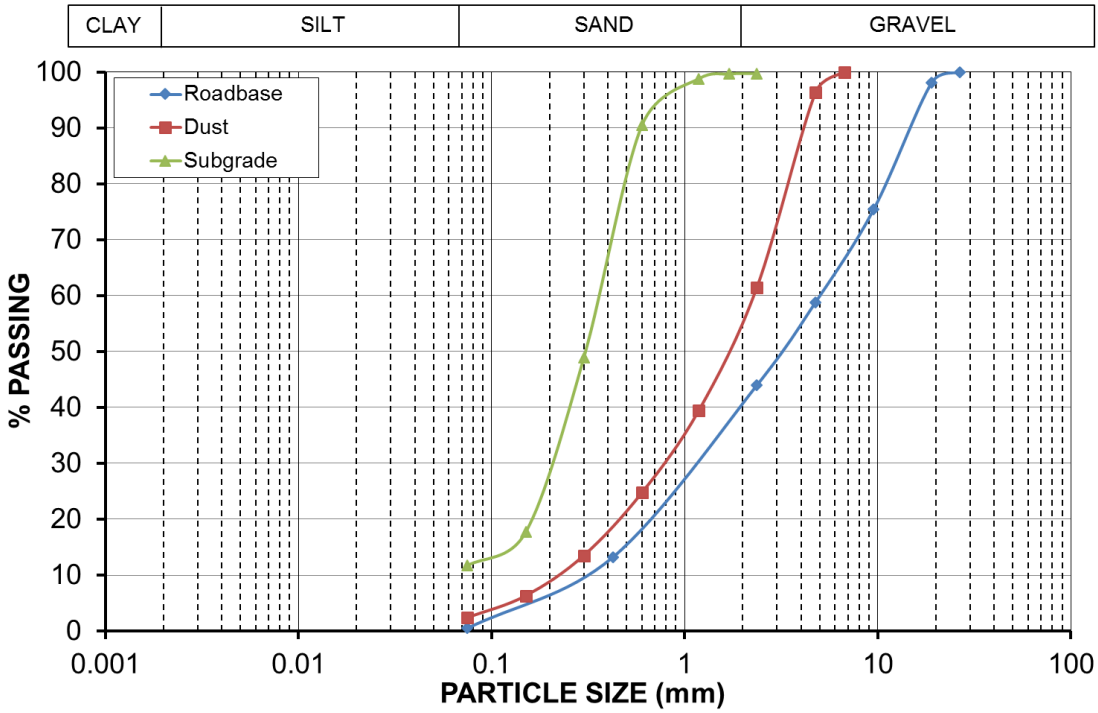

Figure 2 Particle-size distributions of roadbase materials

Typical Australian roadbase materials were studied, including Australian Type 2.1 granite roadbase (designated as roadbase) and greenstone crusher dust (designated as dust). The materials were collected from Pine Mountain Quarry, Brisbane. According to the material specifications of the quarry, Type 2.1 granite roadbase is predominantly granite (85%), with the remainder greenstone dust (15%). The granite is basically made up of quartz (Hardness=7) and feldspars minerals (Hardness=6-6.5). The hardness of the granite particles on the Mohs scale was found to be 6-7. The same roadbase materials had also been studied by Bhuyan et

al. (2017). Natural silty sand obtained from the St Lucia Campus of The University of Queensland was used as a subgrade layer (designated as subgrade). Basic characterisation tests were carried out on the roadbase, dust and subgrade, including sieving analysis, standard compaction testing and specific gravity. The results of the sieving analysis are shown in Figure 2, and the basic parameters of the roadbase, dust and subgrade are summarised in Table 1.

Table 1 Basic parameters of tested samples

Sample	D_{50} (mm)	C_u	C_z	G_s	OMC (%)	ρ_{dmax} (t/m^3)	USCS
Roadbase	3.1	15.45	1.34	2.706	5.9	2.275	GW
Dust	1.8	9.58	1.16	2.725	8.8	2.158	SW
Subgrade	0.3	4.80	1.79	2.483	-	-	SP-SM

2.2 Geosynthetics

Four different types of geosynthetic products, commonly used for base reinforcement and subgrade stabilisation in pavement engineering in Australia, were selected, including Tensar TX160 (Triangular apertures geogrid), Tensar SS40 (Rectangular apertures geogrid), Tencate Miragrid GX40/40 (Rectangular apertures geogrid), and Tencate Mirafi HP340 (woven geotextile).

According to the material specifications provided by the supplier, the detail information on constitutive polymer and method of manufacture for each geosynthetic material is shown below. Tensar TX160 is manufactured from a punched polypropylene sheet, which is then oriented in three substantially equilateral directions. Tensar SS40 is manufactured from a punched polypropylene sheet, which is then oriented in two directions. Tencate Miragrid GX40/40 is manufactured from high modulus polyester yarns. Tencate Mirafi HP340 is manufactured from high-density woven polypropylene (HDPE). The geosynthetics selected were carefully chosen to have a similar tensile strength of about 40 kN/m in both Machine Direction (MD) and Cross Machine Direction (XMD) in order to ensure comparability of the final results (see Table 2).

Table 2 Geometric and mechanical characteristics of tested geosynthetics

Material	Aperture Shape	Tensile Strength (kN/m)	Nominal thickness (mm)	Aperture size (mm)	Nodal thickness (mm)	Area ratio of ribs (%)
TX160	Equilateral triangle	40	2	40	2.8	38.7
SS40	Square	40	3.5	33	5.8	22.6
GX40/40	Square	40	1	25	1.3	23.2
HP340	Woven	40	0.6	-	-	-

3 Equipment and sample preparation

3.1 Test equipment

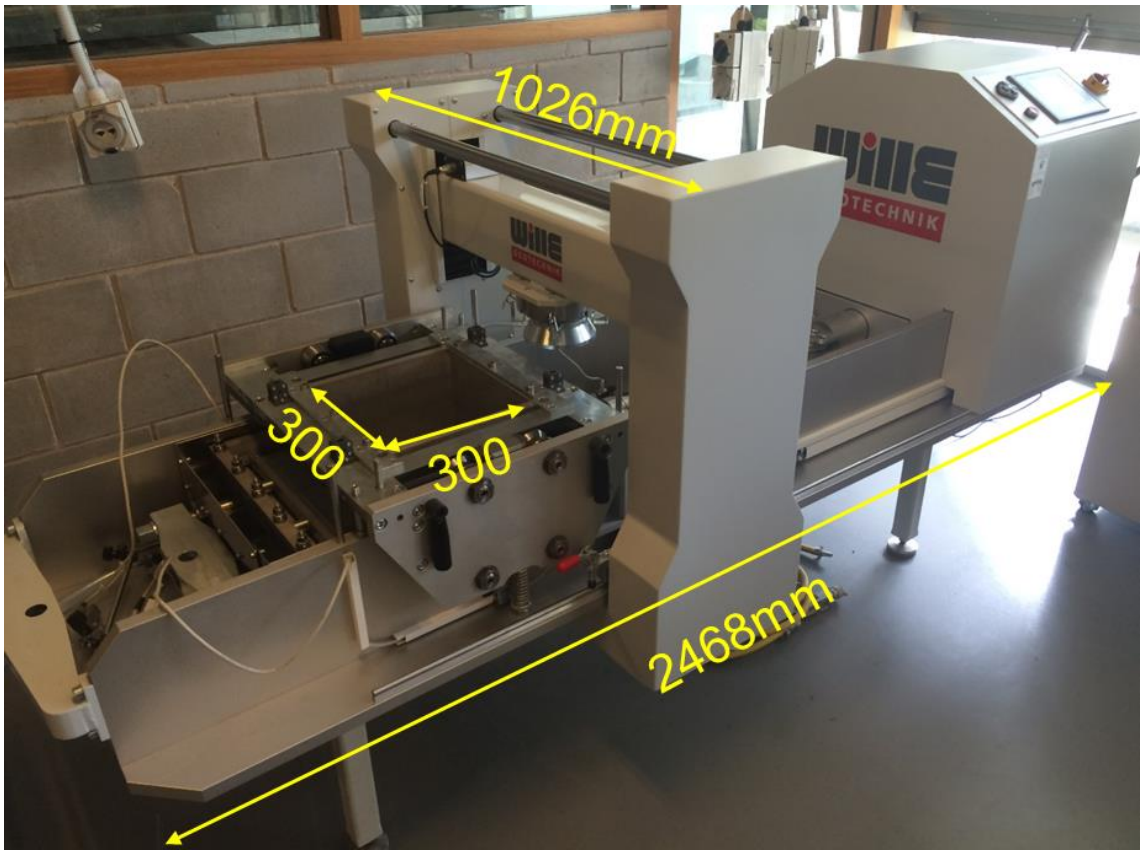

Figure 3 Large-scale direct shear apparatus ADS-300 (manufactured by Wille Geotechnik)

A large-frame direct shear device ADS-300 (manufactured by Wille-Geotechnik of Germany, 2015), with a loading capacity of 100 kN in both horizontal and vertical directions, was used to perform the tests (Figure 3). The shear box has a dimension of 300 mm by 300 mm by 200 mm complying with ASTM 5321 recommendations when testing soils having large particles. During the shearing process, the upper half of the shear box is fixed, and the shear load is transmitted by moving the lower half of the box. This machine has the following features:

(1) High stresses of up to 1000 kPa.

(2) Floating upper box to create a gap between the upper and lower halves of the shear box by means of two compression springs.

(3) Grooved clamping systems to fix the geosynthetics.

(4) Four linear variable displacement transducers (LVDTs) on the four corners of the top loading cap to measure settlement and monitor tilting.

(5) Water tank in which the shear box can be mounted for testing under wet conditions.

3.2 Sample preparation

Previous studies indicate that the set-up of the direct shear box can influence the test results substantially (Richards and Scott 1985; Jewell 1996; Liu et al. 2009b). For instance, Liu et al. (2009b) tried three different set-ups for the lower shear box and concluded that a lower box filled with soil having the same size as the upper box is more favourable for testing a soil-geogrid interface. Therefore, this preferred configuration was adopted for sample preparation in the present study.

Compaction of the soil samples was carried out in the shear box prior to mounting it in the machine, to prevent damage to the sensitive electronic controllers inside the machine. Soil samples were compacted in three layers in the shear box to ensure uniformity. For the interface direct shear tests with the inclusion of geosynthetics, the soil samples were prepared in two layers (i.e., the lower box layer and the upper box layer) and the geosynthetic was clamped on all four sides using the grooved

clamping bars on the top of the lower half of the shear box (see Figure 4). The required mass of wet soil for each layer was calculated and carefully measured, and then compacted uniformly to reach the desired height for the desired dry density. The initial conditions for the three types of soils tested are given in Table 3 The shear box containing the prepared specimens (weighing about 300 kg) was then placed in the machine using a crane, and the LVDT system was installed on top of the loading cap.

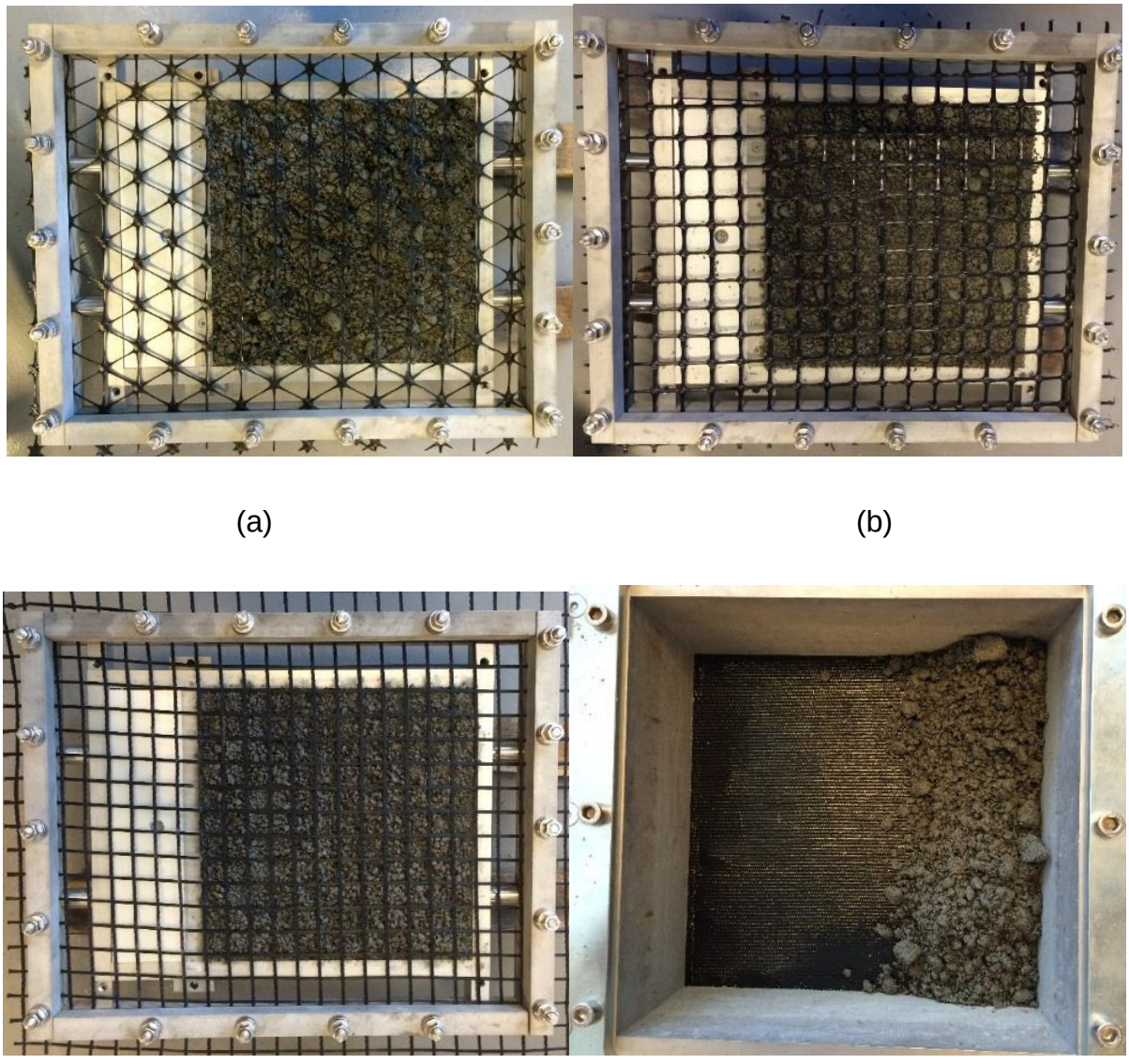

(a) (b)

(c) (d)

Figure 4 Sample preparation in the large shear box: (a) TX160; (b) SS40; (c) GX40/40; (d) HP340

Table 3 Initial conditions controlled for tested specimens

Soil	Moisture content (%)	Dry density (t/m^3)	Void ratio
Roadbase	5.9	1.934	0.40
Dust	8.8	1.834	0.49
Subgrade	22.2	1.592	0.56

The direct shear tests were carried out under applied normal stress of 25 kPa, 50 kPa, 75 kPa, or 100 kPa. After the compression was completed under each normal stress, shearing was commenced at a constant shearing rate of 1 mm/min until the shear displacement reached 30 mm (i.e., 10% shear strain). The shearing rate of 1 mm/min was selected due to testing roadbase materials with large particles where drainage is not a problem. For coarse materials, which are highly permeable, the shearing rate does not need to be very slow to allow for a drained condition. The same shearing rate (1 mm/min) has also been adopted by many other researchers for the direct shear testing of sands or gravels (Alfaro et al. 1995; Liu et al. 2009a, b; Vieira and Pereira 2015). The shear displacement was limited to 30 mm to avoid excessive distortion of the top cap and possible erroneous results. During the shearing process, the shear displacement, vertical displacement and shear load were measured and recorded. Since there is a reduction in contact area during shearing, area correction was applied to both the normal and shear stresses.

4 Testing program

In order to determine the apparent cohesion (c) and friction angle (ϕ) of the compacted roadbase, dust and subgrade, and the apparent adhesion (c_a) and friction angle (δ) of the soil-geosynthetic interface, the following four groups of tests were carried out:

Group 1 – Single-stage direct shear tests on roadbase, dust and subgrade (a total of 12 tests). The purpose of this series of tests was to determine basic shear strength parameters of the test soils and to obtain the stress-displacement relationship as the basis for analysing interface behaviour with the inclusion of geosynthetics.

Group 2 – Single-stage interface direct shear tests to model the different geosynthetic reinforcement (a total of 32 tests). The results of this series of tests were used to investigate the performance of the four types of geosynthetic reinforcement (TX160, SS40, GX40/40, HP340). Due to the particle size difference of the roadbase (gravel) and dust (sand), the results of this series were also used to analyse interface efficiency with regard to soil particle size.

Group 3 – Single-stage interface direct shear tests to model subgrade stabilisation (a total of 20 tests). This series of tests was designed to evaluate the interface parameters between roadbase and subgrade reinforced with geosynthetics, in order to compare the performance of the four types of geosynthetics embedded between the roadbase and subgrade with the unreinforced roadbase-subgrade case, and to analyse the impacts of changing soil type in the lower half of the shear box on the interface shear stress.

Group 4 – Multi-stage direct shear tests (a total of 5 tests). This series of tests was carried out to compare with the single-stage tests, in order to evaluate the feasibility and reliability of multi-stage testing.

5 Results and discussion

5.1 Results of Group 1 Series

The failure envelopes obtained from large-scale direct shear tests on Roadbase, Dust and Subgrade are shown in Figure 5. As shown in Figure 5, apparent cohesion values of 18.8 kPa, 8.9 kPa and 10.6 kPa, and friction angles of 39.6°, 38.7° and 32.7° were obtained for the Roadbase, Dust and Subgrade, respectively. Both Type 2.1 Roadbase and Dust are high quality roadbase materials with high friction angles. It was found that particle breakage for roadbase materials was not significant under a normal stress of 100 kPa.The shear strength parameters derived from Group 1 Series of tests are used as the basis for the analyses and comparisons with the other series of tests.

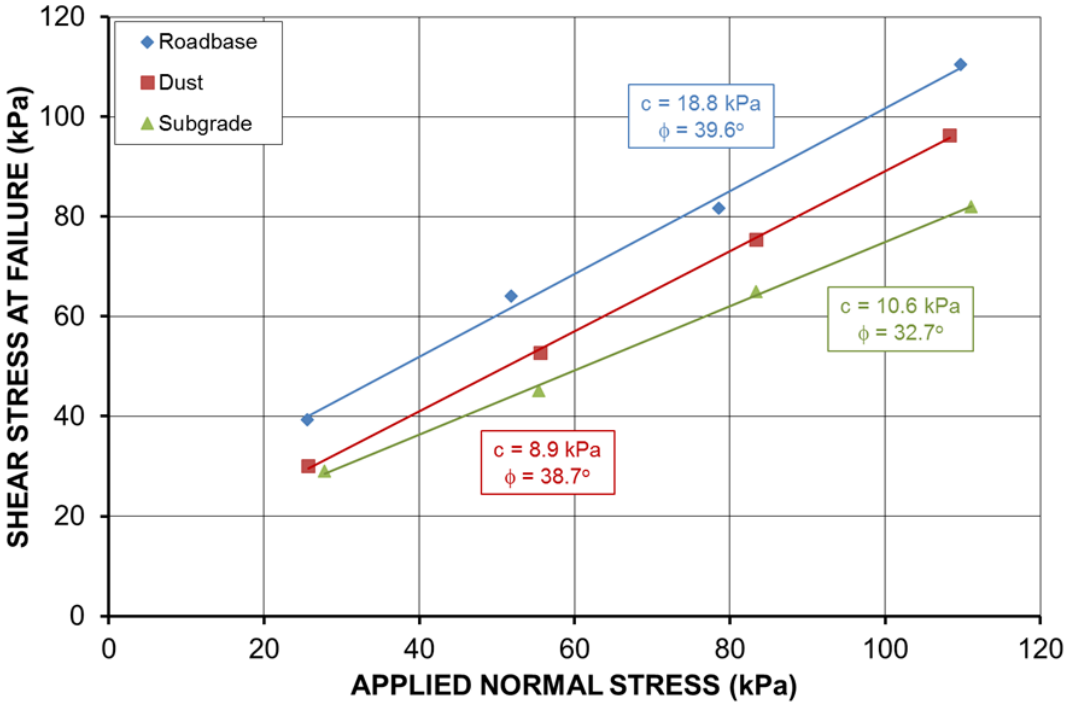

Figure 5 Failure envelopes of roadbase materials

5.2 Results of Group 2 Series

Interface shear stresses with the inclusion of four types of geosynthetics were compared in Figure 6 for Roadbase and Dust, respectively. Due to the limits on numbers of figures, only the test results under applied normal stress of 50 kPa were selected and presented herein. The failure envelopes of the geosynthetic-reinforced Roadbase and Dust obtained from the large-scale interface direct shear tests are also shown in Figure 7. Accordingly, Figure 8 presents the interface coefficient f_{ds} for the different geosynthetic-reinforced Roadbase and Dust calculated using Eq. (4). Due to the high tensile strength (40 kN/m) of the geosynthetic specimens and relatively low applied normal stresses (25 kPa, 50 kPa, 75 kPa and 100 kPa, representing the magnitude of overburden pressures in pavements), the geosynthetic specimens remained intact after the direct shear tests. Very little damage was observed, except some noticeable dents on the geotextile HP340 caused by the coarse particles under loading.

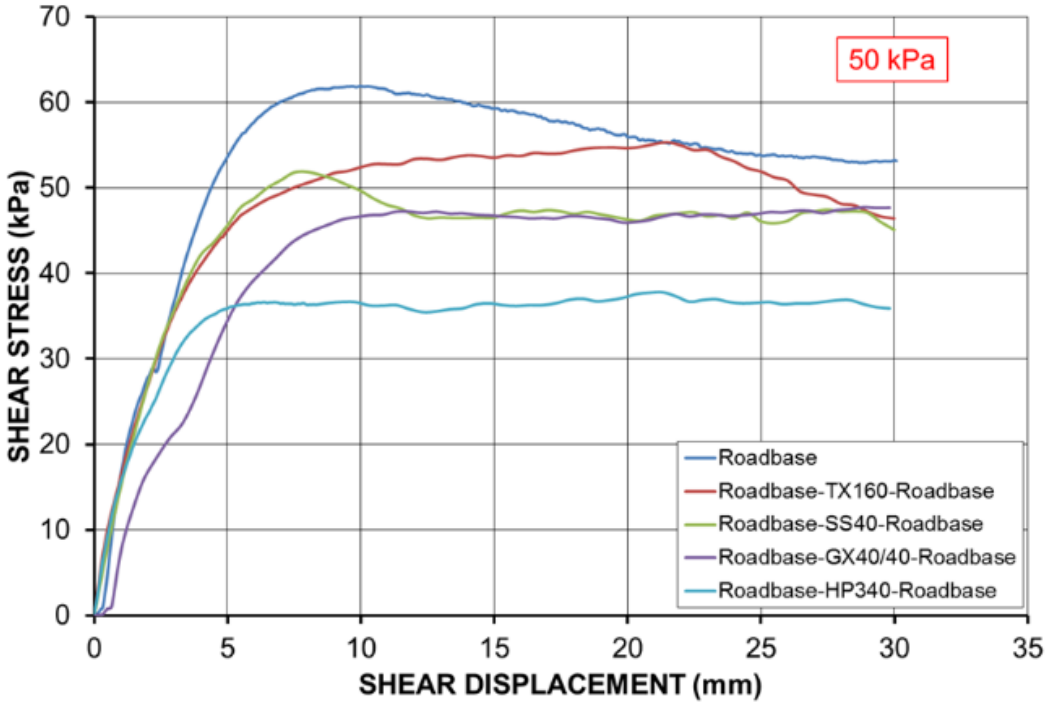

(a)

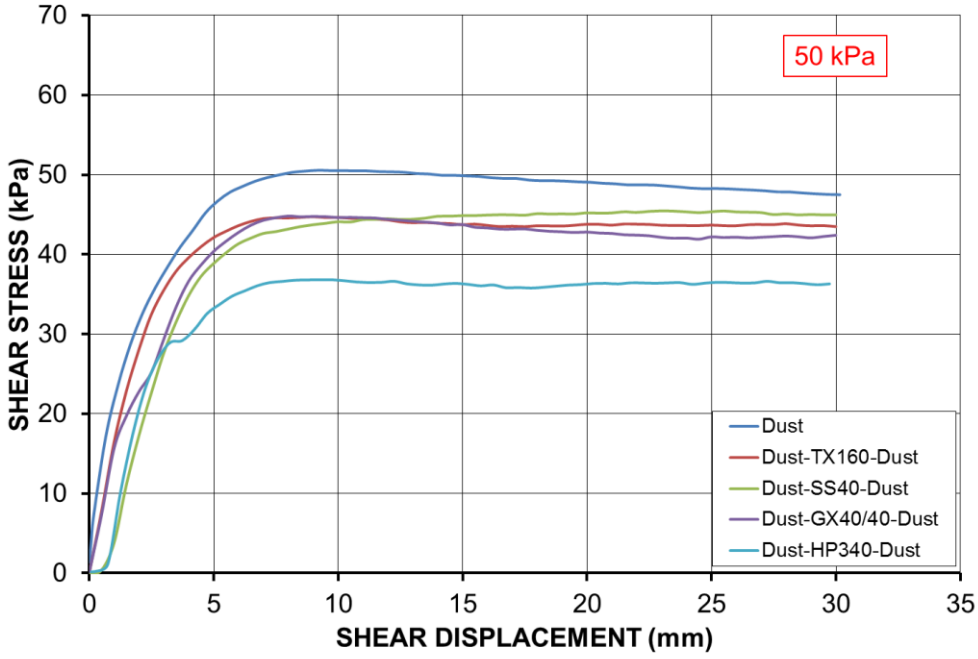

(b)

Figure 6 Shear stress versus shear displacement for different geosynthetic-reinforced roadbase materials under applied normal stress of 50 kPa: (a) Roadbase; (b) Dust

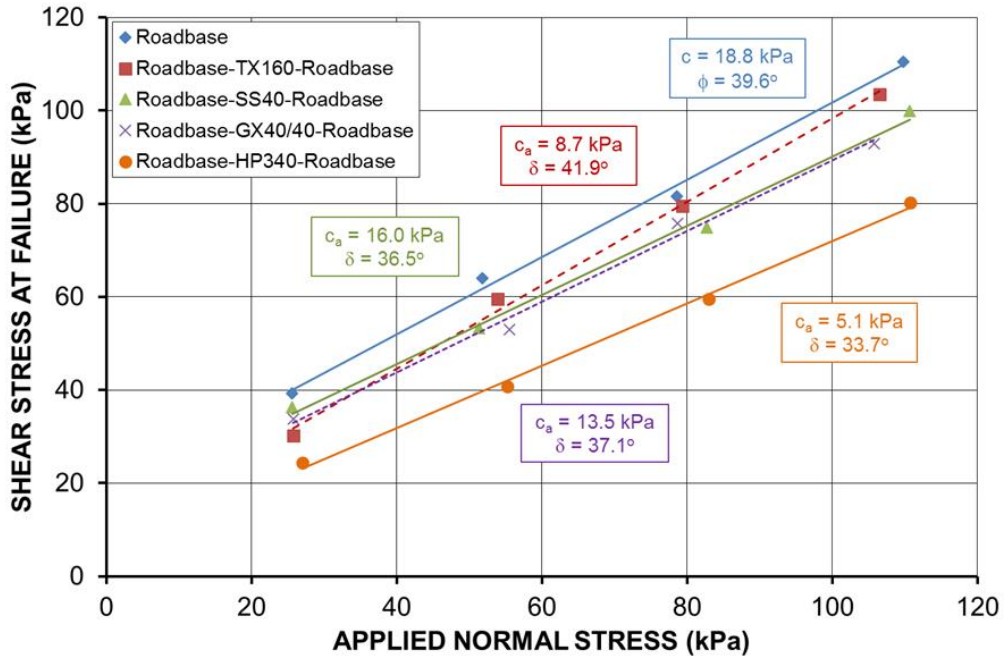

(a)

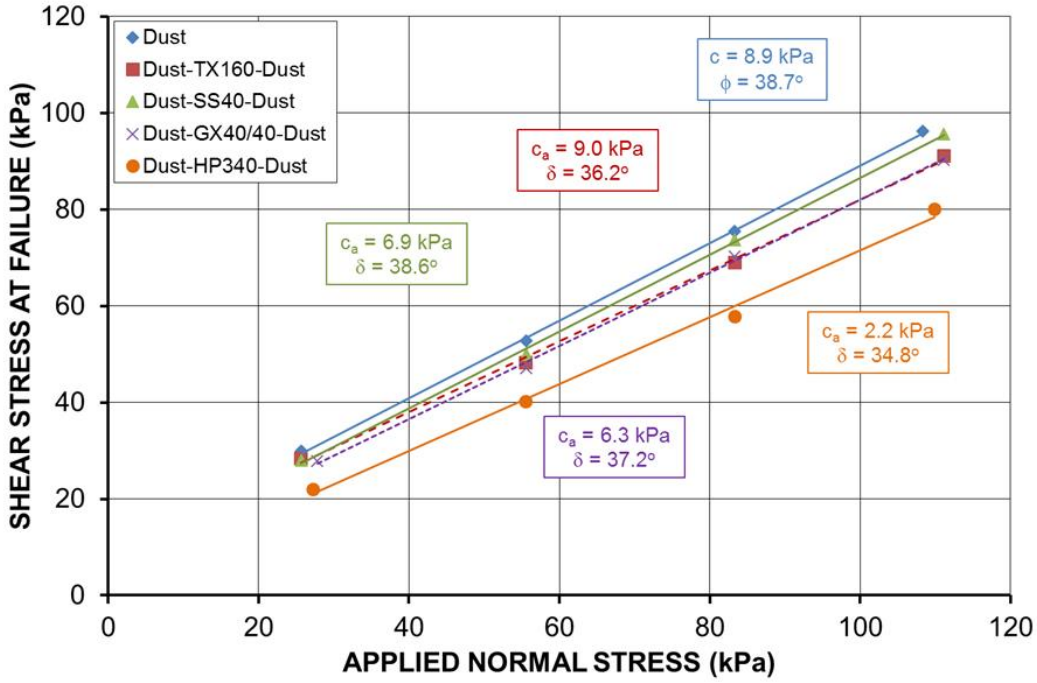

(b)

Figure 7 Failure envelopes of geosynthetic-reinforced roadbase materials: (a) Roadbase; (b) Dust

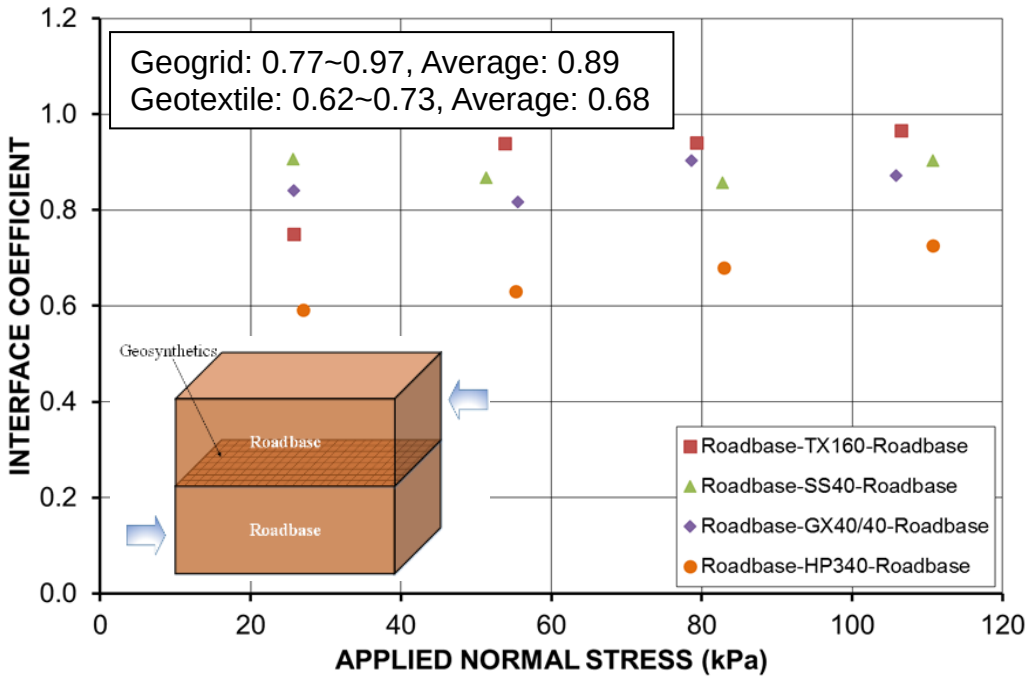

(a)

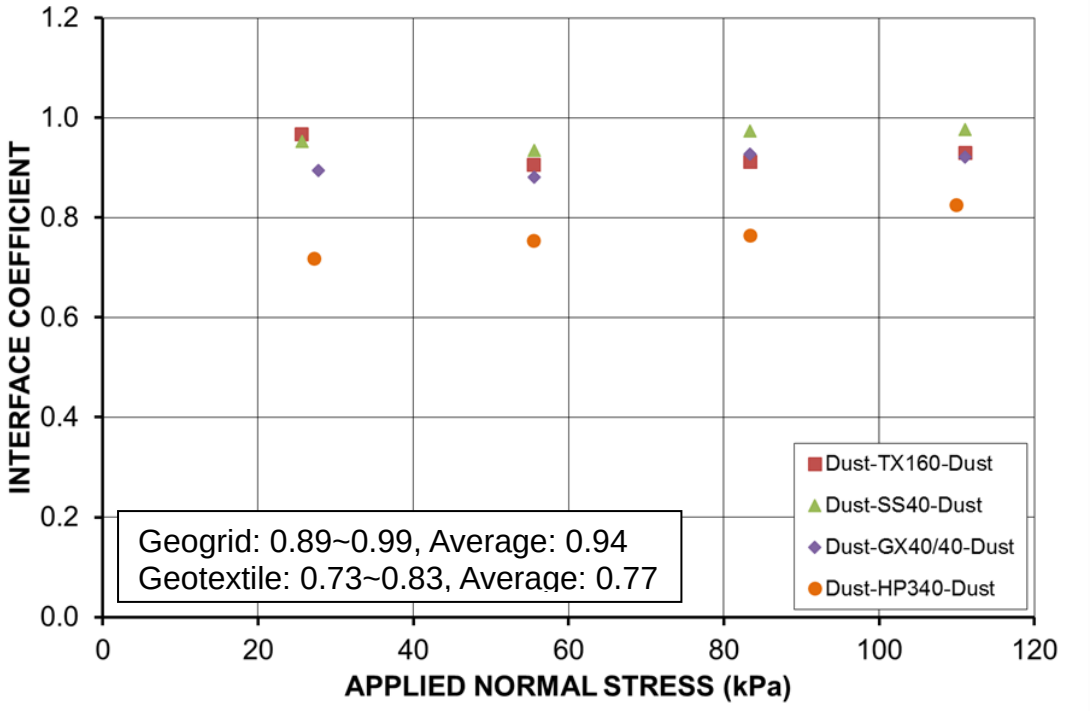

(b)

Figure 8 Interface coefficients for base reinforcement: (a) Roadbase; (b) Dust

The following observations and discussion are made from the experimental results:

(1) Both Roadbase and Dust without the inclusion of a geosynthetic showed slightly higher shear strengths under four different applied normal stresses in the large-scale direct shear tests. The failure envelopes of the Roadbase and Dust without geosynthetic reinforcement are highest, while the interface failure envelopes for reinforcement with geotextile HP340 are lowest, as shown in Figure 7. This indicates that the interface between the soil and geosynthetic reinforcement is a weak plane when subjected to lateral loading. By contrast, it has been proven that the bearing capacity of geosynthetic-reinforced soils would be greatly improved when subjected to vertical loading.

(2) Comparing the effects of the four types of geosynthetics tested on the interface shear strength, geogrids generally result in higher interface shear stress than geotextiles, due to the contribution of interlocking in geogrid apertures. The smooth surface of the geotextiles results in a significant reduction in interface shear stress, making the interface of the soil with the geotextile weaker than that of the soil alone. Therefore, special attention should be paid to the geotextile-reinforced soils when sliding along the interface is more likely to occur. The shear stress curves for both the Roadbase and Dust reinforced with the three types of geogrids (TX160, SS40 and GX40/40) are very close, especially for the Dust, under different normal stresses (Figure 6). This is because the ratios of the opening area for the three geogrids are very close.

(3) For Roadbase with coarser particles (up to 20 mm), the relationship between interface shear stress and shear displacement was not as smooth as that for Dust with relatively finer particles, suggesting that the geogrid-reinforced coarser-grained Roadbase is far less homogeneous. This is most noticeable for the geogrid TX160 with equilateral triangle apertures, which resulted in a better interaction performance compared to the other three geosynthetics, The friction mobilised in the apertures is crucial in analysing the overall interface shear stress. However, the effective contact area between the soil

and soil in the aperture of the geogrid is problematic, which needs to consider the aperture shape, size, and soil particle size.

(4) It can be seen in Figure 8 that geosynthetic-reinforced Dust has higher values of interface coefficient compared to geosynthetic-reinforced Roadbase, especially for the geogrid-reinforced Dust with an average interface coefficient of 0.94. That is, the interface shear strength between the geogrid and the Dust is similar to the shear strength of the Dust alone. By contrast, the average interface coefficients between soil materials and geogrids obtained by other researchers ranged from 0.65 to 1.16, depending on different materials studied (Abu-Farsakh et al. 2007; Liu et al. 2009a, b; Vieira and Pereira 2015). Dust, having finer particles can interact with the geosynthetics more effectively than can Roadbase with coarser particles. This phenomenon is also likely relevant to the effective contact area for the soil in the aperture. The actual effective contact area tends to be larger for fine materials than coarse particles, which is suggested to be equal to the original opening area of the apertures multiplied by an empirical reduction factor (<1). The empirical reduction factor is believed to be closely related to the aperture shape of geogrid, the relative size of the geogrid and the particle size of the soil.

5.3 Results of Group 3 Series

The shear stress curves for the Roadbase, Subgrade, Roadbase-Subgrade, and Roadbase-Subgrade reinforced with four types of geosynthetics at the interface under normal stress of 50 kPa are compared and plotted in Figure 9, and the failure envelopes are shown in Figure 10. It can clearly be seen that the interface shear stress curves of Roadbase-Subgrade are bounded by those of Roadbase being higher and Subgrade being lower (except for the lowest normal stress of 25 kPa). Roadbase-HP340-Subgrade gives the lowest interface shear strength under the different normal stresses due to the smooth surface of the geotextile sheet. The interface shear stress curves of geogrid-reinforced Roadbase-Subgrade is generally quite close to that of Roadbase-Subgrade without reinforcement, and the peak values are a little higher than those of Roadbase-Subgrade without reinforcement.

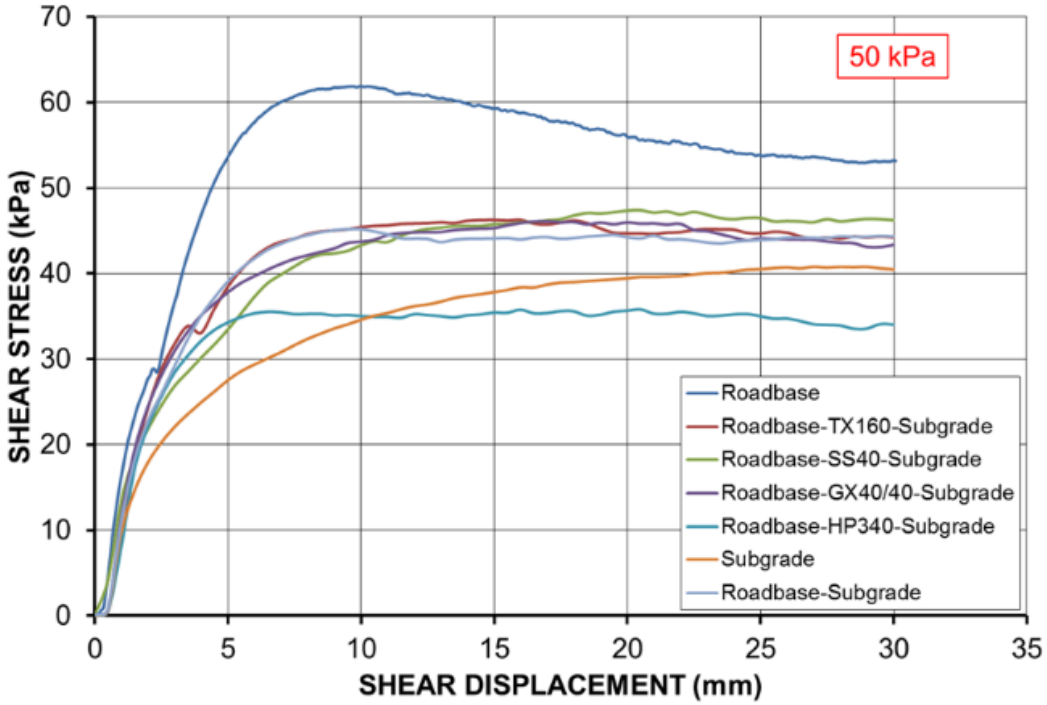

Figure 9 Shear stress versus shear displacement for different geosynthetic-reinforced Roadbase-Subgrade under applied normal stress of 50 kPa

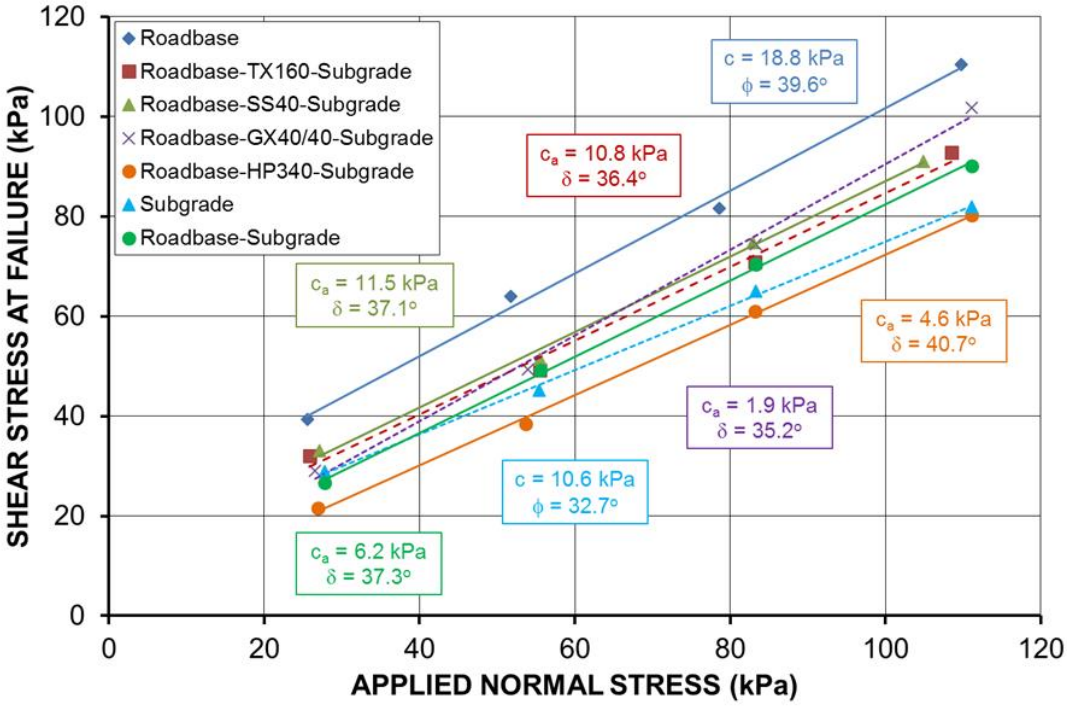

Figure 10 Failure envelopes of geosynthetic-reinforced Roadbase-Subgrade

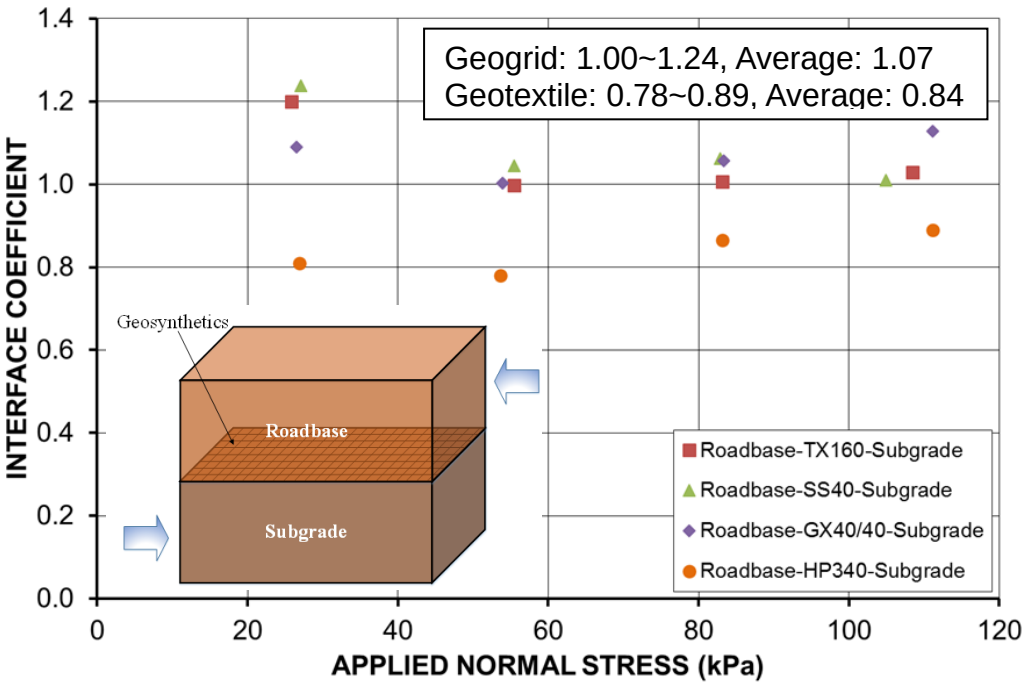

Figure 11 Interface coefficients for stabilised subgrade

A possible explanation for these results might be that the actual effective contact areas for Roadbase in the apertures of the three geogrids are very close. The performances of the different geosynthetic reinforcements of Raodbase-Subgrade are readily observed by the interface coefficients shown in Figure 11. Geogrid reinforcement gives a relatively better interface efficiency (higher than 1) between Roadbase and Subgrade in the application of geosynthetics in subgrade stabilisation. Therefore, the possible sliding surface between the base layer and subgrade layer has been reinforced in the pavement. In contrast, the interface coefficients are less than 1 for the roadbase-geogrid interface (base reinforcement scenario), indicating that this interface is weaker.

Figure 12 compares the influence of changing the Subgrade in the lower half of the shear box on the interface shear stress with geosynthetic reinforcement. Overall, the interface shear stress curves of Roadbase-Geogrid-Roadbase are slightly higher than those of Roadbase-Geogrid-Subgrade. This is most noticeable for the geogrid TX160 with triangular apertures (Figure 12a), indicating that triangular apertures could provide higher effective confinement. However, for geotextile HP340, the soil specimens in the upper and lower shear boxes were completely separated by the

geotextile; therefore, the interfaced shear stress curves between Roadbase-Geotextile-Roadbase are very close to those of Roadbase-Geotextile-Subgrade (Figure 12d). This is because the friction resistance is only attributed to the friction between Roadbase in the upper shear box and the top surface of the geotextile.

5.4 Results of Group 4 Series

In the present study, multi-stage direct shear testing was also conducted, in which a single representative specimen was sheared to failure under a series of applied normal stresses. To allow multi-stage testing, the shear displacement was limited to 10 mm for the first stage and 7 mm for subsequent stages, giving a total shear displacement of about 30 mm to avoid excessive tilting. The single-stage and multi-stage results are compared and presented in Figures 13 and 14. In order to control the numbers of figures, only direct shear testing of the soil (Dust), and interface shear testing of the geogrid-soil (Dust-TX160-Dust) and geotextile-soil (Dust-HP340-Dust) interfaces are typically presented herein.

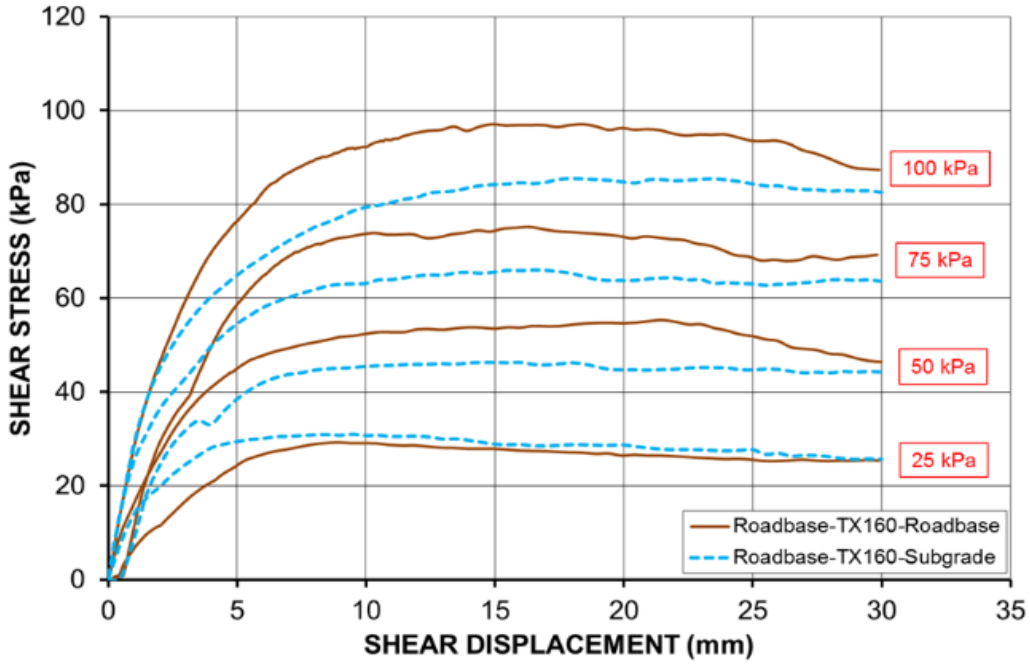

(a)

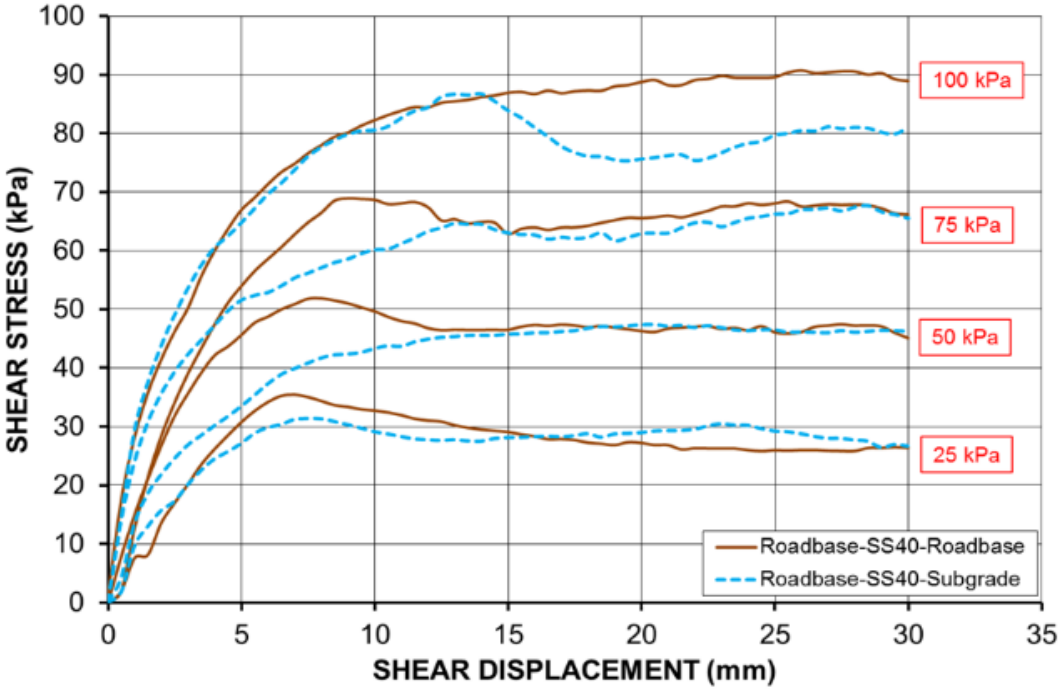
SHEAR STRESS (kPa)
SHEAR DISPLACEMENT (mm)
100 kPa
75 kPa
50 kPa
25 kPa
Roadbase-SS40-Roadbase
Roadbase-SS40-Subgrade

(b)

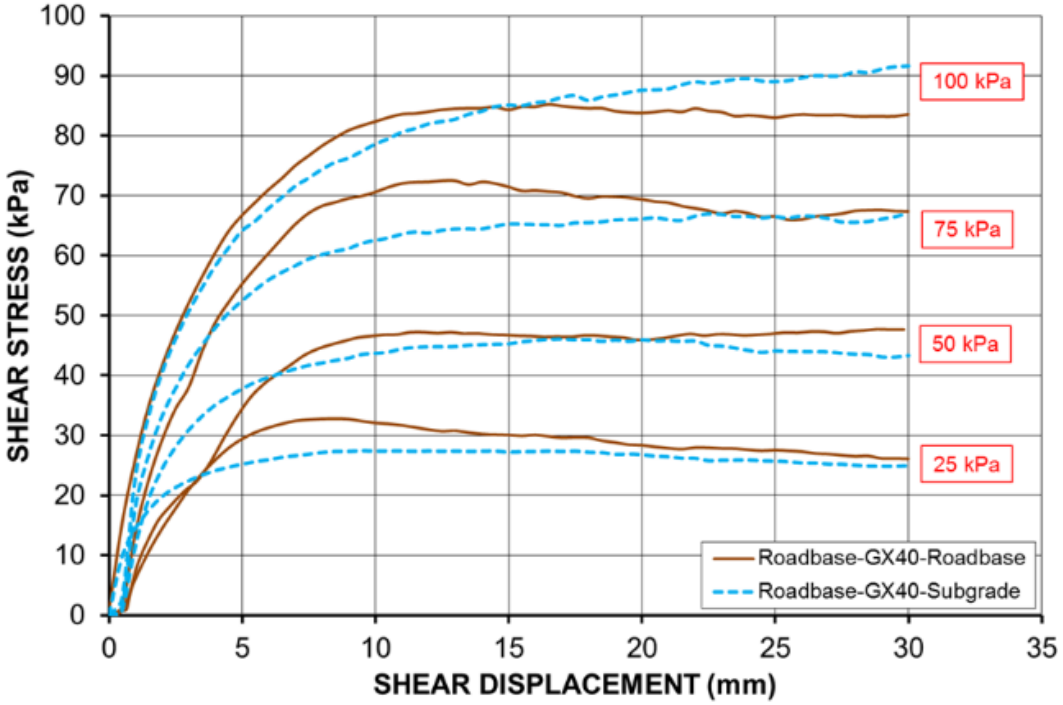
SHEAR STRESS (kPa)
SHEAR DISPLACEMENT (mm)
100 kPa
75 kPa
50 kPa
25 kPa
Roadbase-GX40-Roadbase
Roadbase-GX40-Subgrade

(c)

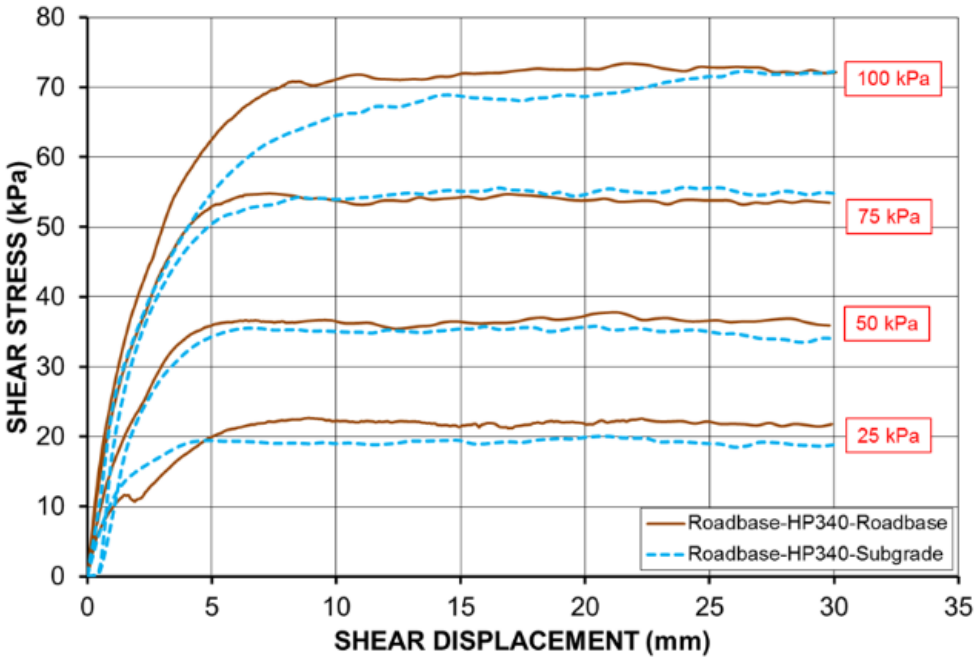

(d)

Figure 12 Comparisons of influence of changing soil in lower half of shear box on interface shear stress: (a) TX160; (b) SS40; (c) GX40/40; (d) HP340

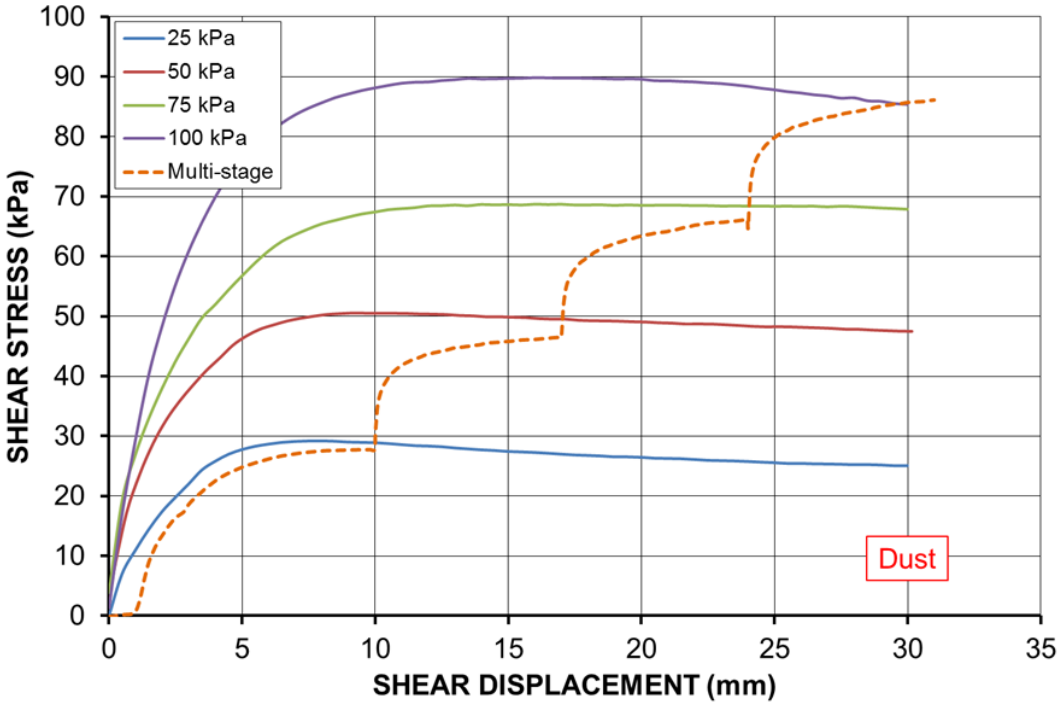

(a)

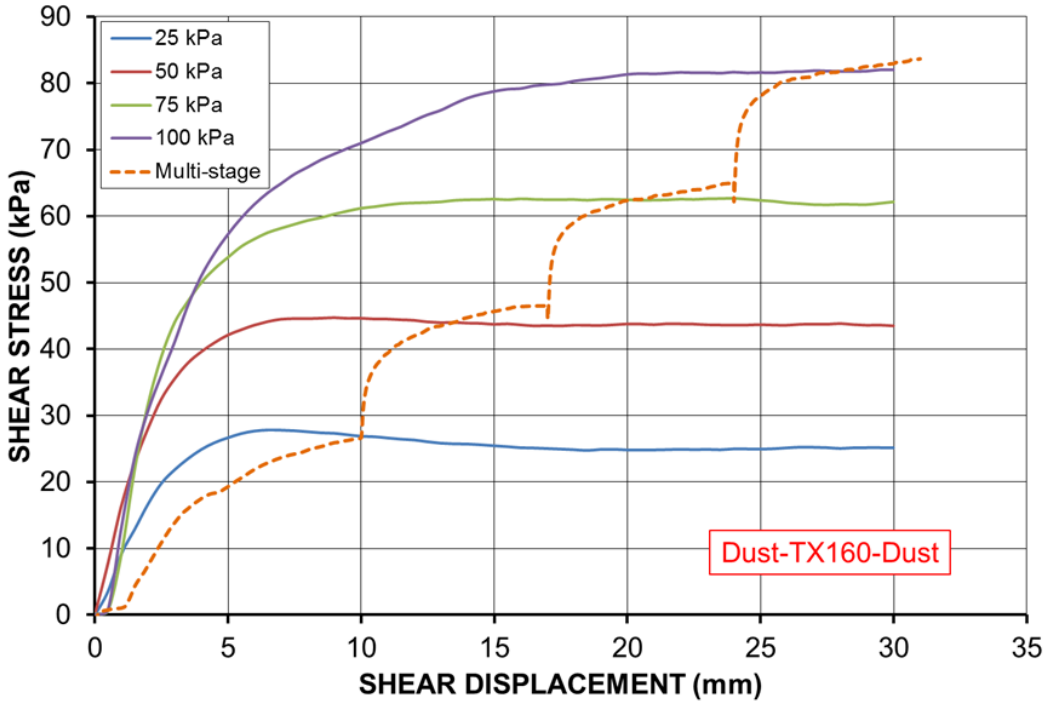

(b)

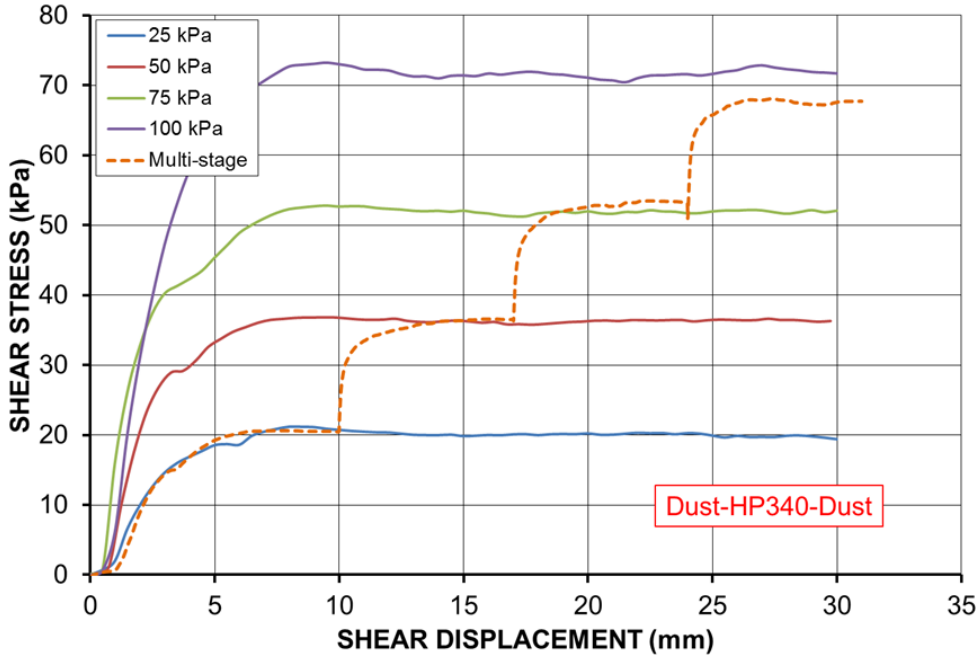

(c)

Figure 13 Comparisons of shear stress curves for single-stage and multi-stage tests: (a) soil; (b) geogrid-soil interface; (c) geotextile-soil interface

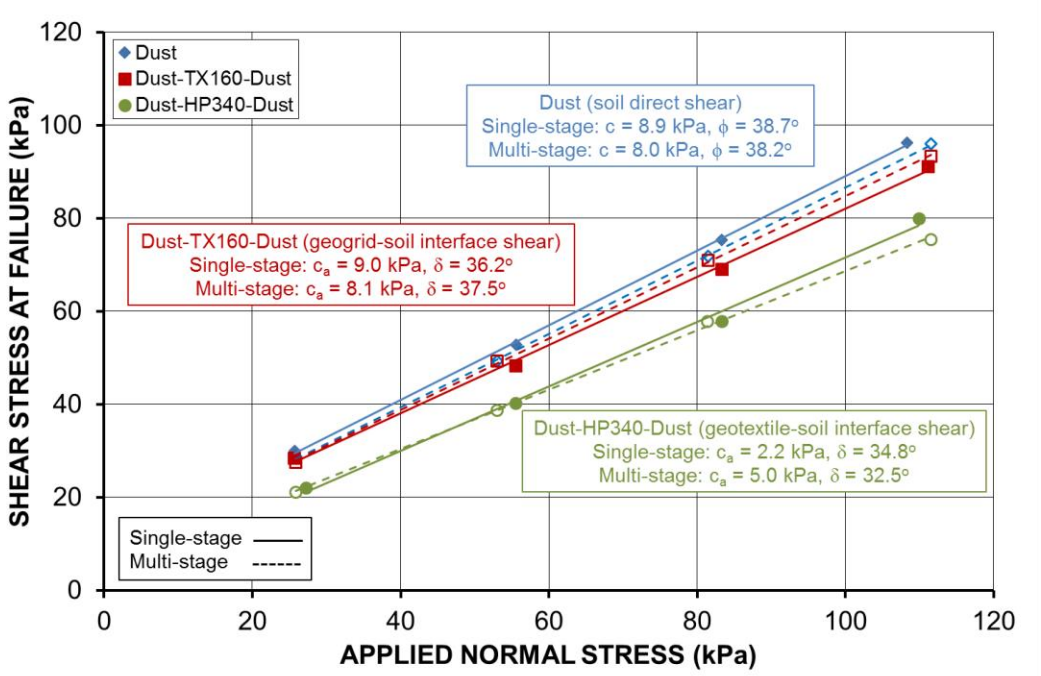

Figure 14 Comparisons of failure envelopes for single-stage and multi-stage tests

Table 4 Interface shear strength results for Roadbase-Geogrid

Roadbase		Roadbase-TX160				Roadbase-SS40				Roadbase-GX40/40			
c (kPa)	φ (°)	c_a (kPa)	δ (°)	δ_0 (°)	α_{ds} (%)	c_a (kPa)	δ (°)	δ_0 (°)	α_{ds} (%)	c_a (kPa)	δ (°)	δ_0 (°)	α_{ds} (%)
18.8	39.6	8.7	41.9	42.3	38.7	16.0	36.5	27.4	22.6	13.5	37.1	25.2	23.2
σ (kPa)	τ (kPa)	σ (kPa)	τ_{ds} (kPa)	$\tau_{s\text{-}s}$ (kPa)	$\tau_{s\text{-}g}$ (kPa)	σ (kPa)	τ_{ds} (kPa)	$\tau_{s\text{-}s}$ (kPa)	$\tau_{s\text{-}g}$ (kPa)	σ (kPa)	τ_{ds} (kPa)	$\tau_{s\text{-}s}$ (kPa)	$\tau_{s\text{-}g}$ (kPa)
26	39	26	30	25	6	26	36	31	5	26	34	31	3
52	64	54	60	39	21	51	53	48	6	56	53	50	3
79	82	79	80	52	28	83	75	68	7	79	76	65	11
110	110	107	103	66	38	111	100	86	14	106	93	82	11

Table 5 Interface shear strength results for Dust-Geogrid

Dust		Dust-TX160				Dust-SS40				Dust-GX40/40			
c (kPa)	φ (°)	c_a (kPa)	δ (°)	δ_0 (°)	α_{ds} (%)	c_a (kPa)	δ (°)	δ_0 (°)	α_{ds} (%)	c_a (kPa)	δ (°)	δ_0 (°)	α_{ds} (%)
8.9	38.7	9.0	36.2	36.0	38.7	6.9	38.6	38.0	22.6	6.3	37.2	30.2	23.2
σ (kPa)	τ (kPa)	σ (kPa)	τ_{ds} (kPa)	$\tau_{s\text{-}s}$ (kPa)	$\tau_{s\text{-}g}$ (kPa)	σ (kPa)	τ_{ds} (kPa)	$\tau_{s\text{-}s}$ (kPa)	$\tau_{s\text{-}g}$ (kPa)	σ (kPa)	τ_{ds} (kPa)	$\tau_{s\text{-}s}$ (kPa)	$\tau_{s\text{-}g}$ (kPa)
26	30	26	28	18	10	26	28	23	5	28	28	24	4
56	53	55	48	33	16	56	50	41	9	56	47	41	6
83	75	83	69	46	23	83	74	59	15	83	70	58	12
108	96	111	91	60	31	111	96	76	20	111	90	75	15

It can be seen that shear stress curves and failure envelopes of the single-stage and multi-stage tests generally match closely. Both the shear strength and interface parameters obtained from the two methods are in fairly good agreement, as shown in Table 4. However, the slopes of the shear stress curves in the later stages of multi-stage tests are much steeper than those of the single-stage tests, indicating that shear failure was achieved at lower shear displacements in the multi-stage test due to the stiffer response. Overall, multi-stage large-scale direct shear testing is both less time consuming and labour intensive than single-stage testing. Based on the multi-stage, large-scale direct testing experience gained, both advantages and disadvantages (applicability) of multi-stage testing method are summarised below:

•Advantages: (1) Multi-stage testing could eliminate the effects of soil variability on the results because only one representative specimen is required. However, single-stage testing requires at least three identical samples. (2) Multi-stage testing could simplify the sample preparation process since the sample preparation is tedious for large-scale testing. (3) Multi-stage testing could save a large amount of soil materials for large-scale tests, and reduce both sampling and testing time and expense. (4) Multi-stage testing could be a very helpful alternative when the test materials are in short supply or the shear strength parameters are needed urgently in the field applications.

• Disadvantages: (1) Multi-stage testing would limit the shear displacement that can be applied to each stage, which may not be sufficient to achieve the peak shear strength. Therefore, the multi-stage testing is not suitable for loose specimens, for example, loose-placed aggregate, clay spoil, etc. In addition, an optimum shear displacement applied to each stage is hard to select, especially for the very first stage. (2) For very brittle intact sample, for example as-sampled fissure clay, peak would normally achieve at a very small shear displacement, with a sudden drop-off because a crack would quickly develop along the failure surface. Consequently, for the later stages, the shear stress is generated along an existing failure surface (ultimate shear stress), which has been found to be lower than the result of single-stage testing of a new specimen. (3) The shear strength obtained in later stages is built upon the easier stage, so the earlier stages may significantly affect the maximum shear strength achieved in the later stages.

5.5 Theoretical interpretation

It should be noted that δ in Eq. (1) is the friction angle between the soil and the geogrid ribs, which is a theoretical material interface parameter between soil and geogrid ribs. However, δ in Eq. (2) is the overall interface friction angle, which is a shear strength parameter determined experimentally from the failure envelope. In order to avoid confusion, δ_0 is used to denote the theoretical friction angle between the soil and the geogrid ribs. It is believed that transverse members of geogrids are more effective in developing shear resistance than longitudinal members. This is because transverse members are perpendicular to the shear direction. Under an applied normal stress, soil particles are forced to roll over the transverse ribs during shearing, further contributing to the overall shear resistance. Liu et al. (2009a) determined the component of shear resistance between Ottawa sand and geogrid ribs from the interface shear strength of the sand-geotextile multiplied by the geogrid rib surface area ratio α_{ds}, as the geogrid and geotextile used in their study were manufactured from the same polymeric material. However, they found that the shear strength calculated by using Eq. (1) is generally lower than the experimental results obtained. Passive resistance induced by the transverse ribs was therefore back-calculated from the experimental results to achieve a better match between experiment and theory. This approach raises some questions. Firstly, although the geotextile and geogrid may be manufactured from the same material, the interface shear strength of the soil-geotextile interface cannot be applied directly to the soil-geogrid ribs, due to the geometry and texture differences of the geogrid ribs and geotextile. Secondly, the actual contact area between soil and geogrid ribs cannot simply be represented by α_{ds}, because the effective contact area is also related to the soil particle size, aperture shape and size of geogrid, and the dimension of the geogrid ribs, as mentioned previously. Thirdly, when the soil particles are larger than the thickness of the geogrid ribs, the passive resistance provided by transverse ribs is actually the friction between the soil and geogrid ribs.

In the present study, it is assumed that there is no adhesion between the soil and geogrid ribs, only friction. The relationship between the shear and normal stresses is assumed to be represented approximately by a straight line. Therefore, for roadbase materials under near-OMC conditions (with an apparent cohesion obtained from experimental results), the interface direct shear resistance can theoretically be expressed by:

$$\tau_{ds} = (1-\alpha_{ds})c + \sigma_n \left[\alpha_{ds} \tan\delta_0 + (1-\alpha_{ds}) \tan\phi\right] \quad (5)$$

The contributing components can theoretically be evaluated using:

$$\tau_{s-s} = (1-\alpha_{ds})(c + \sigma_n \tan\phi) \quad (6)$$

$$\tau_{s-g} = \alpha_{ds}\sigma_n \tan\delta_0 \quad (7)$$

where $\tau_{s\text{-}s}$ is the shear strength between the continuous soil and the soil in the open area of the geogrid, $\tau_{s\text{-}g}$ is the shear strength between the soil and the geogrid ribs, and δ_0 is the theoretical friction angle between the soil and the geogrid ribs.

For geogrid-reinforced roadbase materials, the interface shear strength can be interpreted from the experimental results using:

$$\tau_{ds} = c_a + \sigma_n \tan\delta \quad (8)$$

where c_a is the adhesion between the soil and the geogrid, δ is interface friction angle. c_a and δ are obtained from the best-fit straight line to the experimental results.

Substituting the experimental relationship given by Eq. (8) into the theoretical relationship Eq. (5), to quantify the contribution to the shear strength by the friction between soil and the geogrid ribs, the following equation can be obtained:

$$\tau_{s-g} = \tau_{ds} - \tau_{s-s} = \alpha_{ds}\sigma_n \tan\delta_0 \quad (9)$$

Therefore, δ_0 can be calculated using the linear relationship:

$$\frac{\tau_{s-g}}{\alpha_{ds}} = \sigma_n \tan\delta_0 \quad (10)$$

It should be noted Eq. (7) is a theoretical equation, and it is impossible to only measure the shear resistance between the soil and geogrid ribs through experiment. The only way to quantify it is based on back calculation. The overall interface shear strength between soil and geogrid could be measured through interface shear tests (Eq. 8), and the internal shear strength of soil could also be measured through direct shear tests. Therefore, the contribution of the frictional resistance between the soil and geogrid ribs could be back

calculated using Eq. (9) based on the interaction mechanism (two components; Eq. (5)). Then, Equation (10) was derived to calculate the δ_0. It is worth mentioning that a lot of references in the literature confuse δ_0 with δ. Therefore, this ambiguity is clarified in this paper herein. δ_0 is a theoretical material interface parameter between soil and geogrid ribs; δ is an experimental obtained overall interface friction angles between soil and geogrid.

A new ratio η gives the contribution to shear strength made by the shear resistance between the soil and the geogrid ribs:

$$\eta = \frac{\tau_{s-g}}{\tau_{ds}} \tag{11}$$

Based on the theoretical interpretation, the shear strength results are summarised in Table 4 and Table 5. The calculated contribution ratios are given in Table 6. The interface shear stress versus normal stress between the roadbase materials and the geogrid ribs are shown in Figure 15, which show a reasonably good linear relationship for the Dust and geogrid ribs, since the Dust has more fines and is more uniform than the Roadbase. By contrast, the Roadbase does not show good linearity because the actual contact area between the large particles and the geogrid ribs cannot simply be calculated by α_{ds}, as discussed previously. The effective contact area between the soil particles and the geogrid ribs or the effective contact area between the soil and soil in the apertures deserve further study, considering the particle size of soil, the shape and size of geogrid's apertures, and the dimension of the geogrid ribs.

This section attempts to quantify the two components that are contributing to the overall interface shear strength between the soils and geogrids in direct shear tests. The contribution made by the friction between the soil and the geogrid ribs is highest for the geogrid with triangular apertures TX160 ($\eta \approx 30\%$), while the average η is only less than 15% for the geogrid with rectangular apertures SS40 and GX40/40 (see Table 6). Therefore, the interface shear resistance between the soil and geogrid is mainly attributed to the shear resistance between the soil and soil in open area of the geogrid. This can be used to explain why the interface shear strength between roadbase materials and the three types of geogrids tends to be quite close, as also shown in Figures 6 and 9.

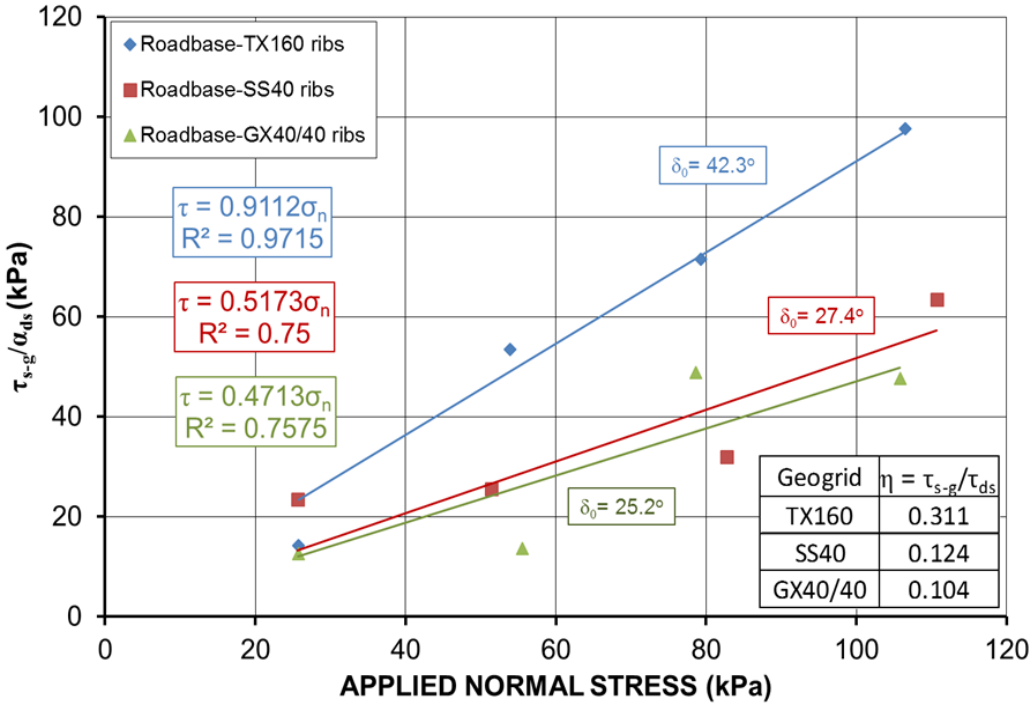

(a)

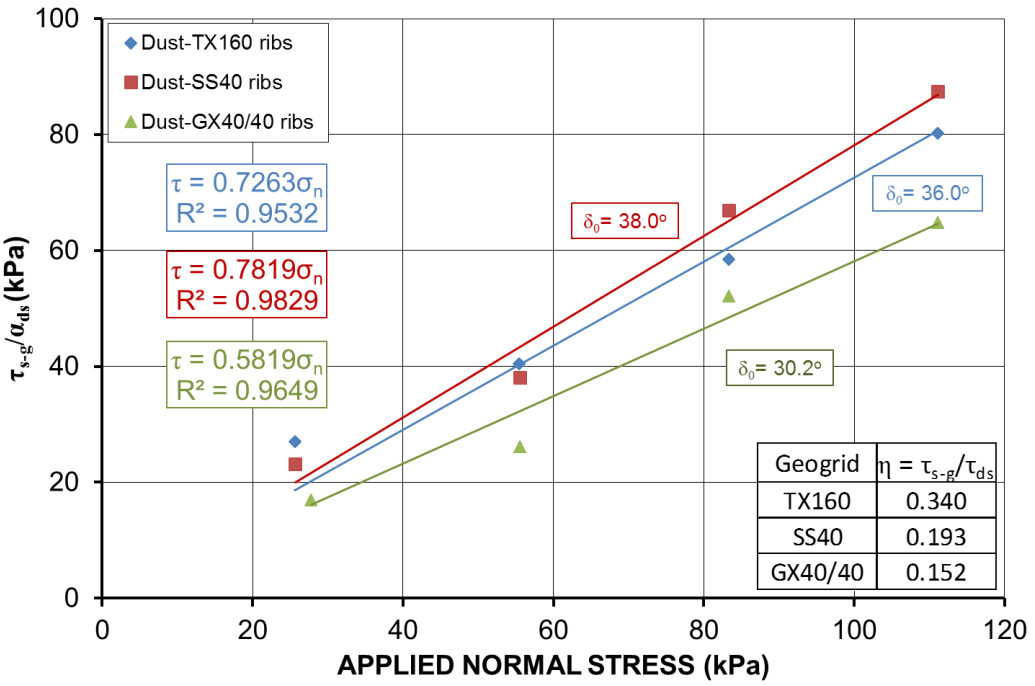

(b)

Figure 15 Component of overall shear strength contributed by friction between roadbase materials and geogrid ribs: (a) Roadbase; (b) Dust

Table 6 Calculated value of ratio η

σ_n (kPa)	Roadbase-TX160 ribs	Roadbase-SS40 ribs	Roadbase-GX40/40 ribs	Dust-TX160 ribs	Dust-SS40 ribs	Dust-GX40/40 ribs
25	0.183	0.146	0.086	0.367	0.187	0.142
50	0.347	0.108	0.060	0.324	0.172	0.129
75	0.348	0.097	0.149	0.328	0.205	0.172
100	0.365	0.144	0.119	0.341	0.207	0.167
Average $\eta=\tau_{s\text{-}g}/\tau_{ds}$	0.311	0.124	0.104	0.340	0.193	0.152

6 Conclusions

A comprehensive laboratory testing program was carried out to investigate the interface characteristics between geosynthetics and roadbase materials, including the application of geosynthetics in base reinforcement and subgrade stabilisation, using a large-scale, laboratory, direct shear apparatus. The multi-stage method was also tested and compared with the single-stage method in large-scale direct shear testing. The experimental results were analysed and the results for the different series of tests compared. The shear strength parameters of the roadbase materials and the interface parameters between geosynthetics and roadbase materials were derived from the test results. The following main conclusions can be drawn from this study:

(1) In terms of the performances of the four types of geosynthetics embedded in roadbase materials, it was found that geogrids (TX160, SS40 and GX40/40) have relatively good interaction efficiency in roadbase materials, with interface coefficients ranging from 0.77 to 0.97 for Roadbase, and 0.89 to 0.99 for Dust. However, the interface between geotextile (HP340) and roadbase materials acts as a weak plane in the interface direct shear test, which results in lower shear strength and interface coefficients (average of 0.68 for Roadbase and 0.77 for Dust). The interface shear strength between roadbase materials and geosynthetics is weaker than the shear strength of the roadbase alone.

(2) Comparing the influence of soil particle size on the interface coefficient, the results show that Dust, with finer soil particles, have relatively higher values of interface

coefficient than Roadbase with coarser soil particles, indicating that finer particles interact and interlock more efficiently with geosynthetics. Further, the geosynthetic-reinforced Roadbase, with coarser particles, are more non-homogeneous and non-uniform.

(3) In subgrade stabilisation, the interface shear strength of Roadbase-geogrid-Subgrade is higher than that of Roadbase-Subgrade without geogrid reinforcement and the interface coefficient ranges from 1.00 to 1.24. Further, there is no significant change in the shear stress curves on changing the soil in lower half of the shear box when geotextile is clamped on the top of the lower box. However, in general, the shear stress curves of Roadbase-geogrid-Roadbase are slightly higher than those for Roadbase-geogrid-Subgrade, due to the shear resistance provided by the soil particles in the apertures of geogrid.

(4) The effective contact area between the soil particles and the geogrid ribs or the effective contact area between the soil and soil in the apertures play very important roles in the interaction mechanism between soil and geogrid. The actual effective contact area is likely related to the particle size of soil, the shape and size of geogrid's apertures, and the dimension of the geogrid ribs. It was found that the interface shear resistance between the soil and geogrid is mainly attributed to the shear resistance between the soil and soil in open area of the geogrid.

(5) Multi-stage, large-scale direct shear test results for compacted samples are generally in good agreement with the single-stage results. However, the feasibility, reliability and applicability of multi-stage testing greatly depend on the initial conditions of the specimen tested.

References

Abu-Farsakh, M., Coronel, J., and Tao, M., (2007). Effect of soil moisture content and dry density on cohesive soil–geosynthetic interactions using large direct shear tests. Journal of Materials in Civil Engineering, 19(7), 540-549.

Alfaro, M. C., Miura, N., Bergado, D. T., (1995). Soil geogrid reinforcement interaction by pullout and direct shear tests. Geotechnical Testing Journal, 18(2), 157–167.

Anubhav and Basudhar, P. K., (2010). Modeling of soil-woven geotextile interface behavior from direct shear test results. Geotextiles and Geomembranes, 28(4), 403-408.

Arulrajah, A., Rahman, M. A., Piratheepan, J., Bo, M. W., and Imteaz, M. A., (2013). Evaluation of interface shear strength properties of geogrid-reinforced construction and demolition materials using a modified large-scale direct shear testing apparatus. Journal of Materials in Civil Engineering, 25(8), 1077-1088.

Arulrajah, A., et al., (2015). Evaluation of interface shear strength properties of geogrid reinforced foamed recycled glass using a large-scale direct shear testing apparatus. Advances in Materials Science and Engineering, 1–8. doi:10.1155/2015/235424.

ASTM D5321. (2002). Standard test method for determining the coefficient of soil and geosynthetic or geosynthetic and geosynthetic friction by the direct shear method. ASTM Designation: D5321-02. ASTM, USA.

Bergado, D. T., Chai, J. C., Abiera, H. O., Alfaro, M. C., and Balasubramaniam, A. S., (1993). Interaction between cohesive-frictional soil and various grid reinforcements. Geotextiles and Geomembranes, 12(4), 327–349.

Bergado, D. T., Ramana, G. V., Sia, H. I., and Varun, (2006). Evaluation of interface shear strength of composite liner system and stability analysis for a landfill lining system in Thailand. Geotextiles and Geomembranes, 24, 371–393.

Bhuyan, H., Scheuermann, A., Bodin, D., and Becker, R (2017). Use of Time Domain Reflectometry to estimate Moisture and Density of Unbound Road Materials: Laboratory Calibration and Real Field Investigation. Transportation Research Record (TRR): Journal of Transportation Research Board. No. 2655, pp. 71–81. DOI: 10.3141/2655-10.

Chen, X., Zhang, J., Xiao, Y., and Li, J., (2015). Effect of roughness on shear behavior of red clay-concrete interface in large-scale direct shear tests, Canadian Geotechnical Journal, 52, 1122–1135.

Ferreira, F. B., Vieira, C. S., and Lopes, M. L., (2015). Direct shear behaviour of residual soil–geosynthetic interfaces – influence of soil moisture content, soil density and geosynthetic type. Geosynthetics International, 22(3), 257–272.

Gan, J. K., and Fredlund, D. G., (1988). Multistage direct shear testing of unsaturated soils. Geotechnical Testing Journal, 11(2), pp. 132–138.

Ghaaowd, I., McCartney, J. S., Thielmann, S. S., Sanders, M. J., and Fox, P. J., (2017). Shearing behavior of tire-derived aggregate with large particle size. I: Internal and concrete interface direct shear. Journal of Geotechnical and Geoenvironmental Engineering, 143(10), 04017078.

Gullic, R.C., (1970). Multi-stage shear testing of a cohesionless soil. Master thesis, Univerisity of Missouri-Rolla, USA.

Hazirbaba K., (2017). Large-scale direct shear and CBR performance of geofibre-reinforced sand. Road Materials and Pavement Design, DOI: 10.1080/14680629.2017.1310667

Hormdee, D., Kaikeerati, N., and Angsuwotai, P., (2012). Evaluation on the results of multistage shear test. International Journal of GEOMATE, 2(1), 140–143.

Jewell, R. A., Milligan, G. W. E., Sarsby, R. W., and Dubois, D., (1984). Interaction between soil and geogrids. In: Symposium on Polymer Grid Reinforcement in Civil Engineering, ICE, London, Paper 1.3.

Jewell, R. A., (1996). Soil reinforcement with geotextiles. Thomas Telford, London.

Lee, K. M., and Manjunath, V. R., (2000). Soil–geotextile interface friction by direct shear test. Canadian Geotechnical Journal, 37(1), 238–252.

Liu, C. N., Zornberg, J. G., Chen, T. C., Ho, Y. H., and Lin, B. H., (2009a). Behavior of geogrid-sand interface in direct shear mode. Journal of Geotechnical and Geoenvironmental Engineering, 135(12), 1863-1871.

Liu, C. N., Ho, Y. H., and Huang, J. W., (2009b). Large scale direct shear tests of soil/PET-yarn geogrid interfaces. Geotextiles and Geomembranes, 27(1), 19-30.

Liu, F. -Y., Wang, P., Geng, X., Wang, J., and Lin, X., (2016). Cyclic and post-cyclic behaviour from sand–geogrid interface large-scale direct shear tests. Geosynthetics International, 23(2), 129–139.

Lopes, M. L., (2002). Soil-geosynthetic interaction: Geosynthetics and their applications, Thomas Telford, London.

Nam, S., Gutierrez, M., Diplas, P., and Petrie, J., (2011). Determination of the shear strength of unsaturated soils using the multistage direct shear test. Engineering Geology, 122(3), 272-280.

Palmeira, E. M., and Milligan, G. W. E., (1989). Large scale direct shear tests on reinforced sand. Soils and Foundations, 29(1), 18–30.

Palmeira, E. M., (2009). Soil–geosynthetic interaction: Modelling and analysis. Geotextiles and Geomembranes, 27(5) 368-390.

Piratheepan, J., Arulrajah, A., and Disfani, M. M., (2013). Large-scale direct shear testing of recycled construction and demolition materials. Advances in Civil Engineering Materials, 2(1), 25–36, doi:10.1520/ACEM20120009

Richards, E. A., and Scott, J. D., (1985). Soil geotextile frictional properties. Second Canadian Symposium on Geotextiles and Geomenbranes, Edmonton. 13–24.

Sakleshpur, V. A., Prezzi, M., Salgado, R., Siddiki, N. Z., and Choi, Y. S., (2017). Large-scale direct shear testing of geogrid-reinforced aggregate base over weak subgrade, International Journal of Pavement Engineering, 1–10. DOI: 10.1080/10298436.2017.1321419

Tang X., Chehab G. R., and Palomino A., (2008) Evaluation of geogrids for stabilising weak pavement subgrade, International Journal of Pavement Engineering, 9(6), 413-429, DOI: 10.1080/10298430802279827

Vieira, C. S., Lopes, M. L., and Caldeira, L. M., (2013). Sand–geotextile interface characterisation through monotonic and cyclic direct shear tests. Geosynthetics International, 20(1), 26–38.

Vieira, C. S., and Pereira, P. M., (2016). Interface shear properties of geosynthetics and construction and demolition waste from large-scale direct shear tests. Geosynthetics International, 23(1), 62–70.

Attached Paper II

Paper II: Effects of scalping on direct shear strength of crusher run and crusher run/geogrid interface

Xu, Y., Williams, D. J., Serati, M., Vangsness, T., 2018. Effects of scalping on direct shear strength of crusher run and crusher run/geogrid interface. Journal of Materials in Civil Engineering. 30 (9) 04018206. https://doi.org/10.1061/(ASCE)MT.1943-5533.0002411 – incorporated as **Paper II.**

Effects of Scalping on Direct Shear Strength of Crusher Run and Crusher Run/Geogrid Interface

Youwei Xu[a,*], *David J. Williams*[b], *Mehdi Serati*[c], Timothy Vangsness[d]

[a] PhD candidate, School of Civil Engineering, The University of Queensland, Brisbane, QLD 4072, Australia. Email: youwei.xu@uq.edu.au

[b] Professor, School of Civil Engineering, The University of Queensland, Brisbane, QLD 4072, Australia. Email: d.williams@uq.edu.au

[c] Postdoctoral Research Fellow, School of Civil Engineering, The University of Queensland, Brisbane, QLD 4072, Australia. Email: m.serati@uq.edu.au

[d] PhD candidate, School of Civil Engineering, The University of Queensland, Brisbane, QLD 4072, Australia. Email: timothy.vangsness@uqconnect.edu.au

Abstract

Crusher run is a type of construction aggregate produced in a quarry by breaking down the rock to various sizes using a mechanical crusher. Scalping is an essential process for a quarry to produce a series of crusher run products with specific grading specifications for various applications. To study the effects of scalping on direct shear strength of crusher run, large-scale laboratory direct shear box tests were carried out on the crusher run specimens scalped to pass 75 mm, 37.5 mm, 19 mm, 9.5 mm, 4.75 mm and 2.36 mm. Furthermore, to study the effects of scalping on interface shear strength between crusher run and geogrid, the interface shear tests were also carried out between the crusher run scalpings and a geogrid reinforcement. The direct and interface shear strength results were then analysed to investigate the effects of scalping on the direct and interface shear stresses, failure envelopes, direct and interface friction angles, apparent cohesions and adhesions, and interface efficiencies. Sieving analyses were carried out before and after the shear tests to assess the degree of particle breakdown caused by loading and shearing in the direct and interface shear tests. The experimental shear test results show that scalping can cause a pronounced reduction in the direct and interface shear strengths.

The results of the sieving analyses imply that the overall particle breakage of the crusher run specimens caused by large-scale direct and interface shear testing was not significant within a normal stress level of 1000 kPa, however some large particle crushing on the top surface of the specimens was observed.

Keywords: aggregate; crusher run; geogrid; scalping; shear strength; particle breakage

1 Introduction

Crusher run is a type of construction aggregate produced in a quarry by breaking down the rock to various sizes using a mechanical crusher. The crushed aggregates are blended and graded to achieve a low-void content to ensure significant interlocking and compaction capabilities. As crusher run includes not only crushed rock but also stone dust, it is less susceptible to shifting, scattering, settling and erosion. Therefore, depending on the project needs, scalping is an essential process for a quarry to produce a series of crusher run products with specific grading specifications for a wide range of applications. Examples of its application include being used as a base or subbase material for roads, as a filter in drainage applications, and for quality controlled backfill on construction sites. Crusher run has been used in Australia extensively for the construction of pavements, foundations, dams and retaining walls.

To improve the interaction and confinement of the crushed aggregates, geogrid has been successfully worked together with the crusher run material in construction, for reinforcement and stabilisation purposes (Giroud and Han 2004; Abu-Farsakh et al. 2007; Chen et al. 2009; Kwon and Tutumluer 2009; Tutumluer et al. 2012). Most studies on the shear strength of aggregate and interface shear strength between aggregate and geogrid have been carried out through large-scale direct and interface shear tests (Alfaro et al. 1995; Bakeer et al. 1998; Yu et al. 2006, Abdelrahman et al. 2008; Nakao and Fityus 2008; Liu et al. 2009a, b; Indraratna et al. 2012; Arulrajah et al. 2014; Vieira and Pereira 2015). Larger-scale triaxial compression testing is another approach to investigate the shear strength of coarse-grained materials (Bathurst and Karpurapu 1993; Indraratna et al. 1993; Maqbool and Koseki 2010; Xu et al. 2012; Chen et al. 2014; Lenart et al. 2014; Xiao et al. 2014a, b; Zhang et al. 2013a, b, 2014; Nair and Latha 2015; Qian et al. 2015). However, very few large-scale shear tests have been conducted on the crusher run products and geogrid materials.

Review of the literature reveals that the shear strengths of coarse-grained materials are related to their particle size, shape, hardness, crushability, surface roughness and other aggregate properties (Vallerga et al. 1957; Cerato and Lutenegger 2006; Cho et al. 2006; Wu et al. 2008; Ueda et al. 2011; Wang et al. 2013; Zhao et al. 2013; Kim and Ha 2014; Xiao et al. 2014a; Vangla and Latha Gali 2016). Given that scalping can significantly change the particle size distribution by reducing the maximum particle size, it is expected that scalping would also have an impact on the direct shear strength of the crusher run material and the interface shear strength between the crusher run and geogrid. However, the friction angle of the scalped specimen (<4.75 mm), determined by small shear box testing, is widely adopted by local engineers in design for all the scalped crusher run products. It is believed that it would be too conservative for coarse-grained crusher run materials. Furthermore, very little is known about the interface parameters between different scalped crusher run products and the geogrid.

Therefore, to better understand the effects of scalping on the direct shear strength of crusher run and interface shear strength between crusher run and geogrid reinforcement, large-scale direct and interface shear tests were carried out on crusher run specimens scalped to pass 75 mm, 37.5 mm, 19 mm, 9.5 mm, 4.75 mm and 2.36 mm, with an increasing degree of scalping. In addition, particle breakage of aggregates during loading has also attracted a lot of research interest, such as in one-dimensional compression testing and triaxial laoding (Einav 2007a, b; Zhang and Baudet 2013; Zhang et al. 2013a, b; Indraratna et al. 2014; Xiao et al. 2014b; Xiao et al. 2017; Xiao and Liu 2017), but there is little published data on particle breakage caused by large-scale direct shear testing of aggregates. Moreover, the particle breakage behaviour is still not clear for the crusher run products with different degrees of scalping. Therefore, sieving analyses were carried out before and after the shear tests to assess the degree of particle breakdown as a result of the loading and shearing in the large-scale shear testing.

2 Materials, equipment and scalping

2.1 Crusher Run

Rock is one of the most common and accessible natural resources on earth, and it is also one of the most abundant and basic raw materials. Generally, rock formation is crushed, reduced in size and screened to various specifications in a quarry to manufacture specific

crusher run products that are needed for different construction applications. To achieve the objective of studying the effects of scalping on direct and interface shear strengths, a commercial scalped crusher run product (-75 mm MC-CR) was collected from Mt Coo-Tha Quarry, Brisbane, Australia, with aggregates ranging in size from 75 mm down to fine particles (see Figure 1).

Figure 1 Crusher run (-75 mm MC-CR) from Mt Coo-Tha Quarry, Brisbane

2.2 Geogrid

Geogrids are commonly used for road pavement constructions, working together with crusher run material within Australia. A commercial biaxial geogrid, which is manufactured from a punched polypropylene sheet, was selected to evaluate the effects of scalping on the interface shear strengths and interface parameters between the crush run scalpings and the geogrid. The geogrid has a nominal tensile strength of 40 kN/m (provided by the supplier), and other geometric and mechanical characteristics are provided in Table 1. It should be noted that the geogrid with square apertures has the same properties in both Machine Direction (MD) and Cross Machine Direction (XMD).

Table 1 Geometric and mechanical characteristics of geogrid used

Geogrid	Polymer	Aperture Shape	Tensile Strength (kN/m)	Aperture size (mm)	Nodal thickness (mm)	Rib thickness (mm)	Opening area (%)
Property or value	Polypropylene	Square	40	33×33	5.8	2.5	77.4

2.3 Large-scale direct shear apparatus

A large-scale direct shear apparatus was used in this study to carry out the direct and interface shear tests. The apparatus has a shear box measuring 300 mm by 300 mm, with a height of 200 mm, and complies with ASTM D5321-12. This machine is moderately stiff (20 mm thick wall) to accommodate a load capacity of 100 kN in both the horizontal and vertical directions (up to 1000 kPa, with respect to an area of 0.09 m^2 for the large shear box used). A grooved clamping system is mounted on all four sides of the lower shear box to fix the geosynthetics for interface shear testing. A floating upper box is specially designed to create a gap between the upper and lower halves of the shear box by means of two compression springs to avoid friction between the two halves. Four Linear Variable Differential Transformers (LVDTs), having an effective resolution of 0.001 mm, are installed on the top of the four corners of the loading plate to provide an average settlement value of the specimen. During the shearing process, the upper half is fixed, and the shear load measured by a load cell is transmitted by moving the lower half.

2.4 Crusher run scalping

Scalping is a process of removing particles larger than a nominal size, and it is normally conducted by sieving specimens through a specifically sized screen. The original crusher run obtained from the quarry had been pre-scalped from 75 mm. In order to study the effects of scalping on the direct and interface shear strength parameters, the crusher run specimens were then further scalped in the laboratory to pass 37.5 mm, 19 mm, 9.5 mm, 4.75 mm and 2.36 mm (fines are also known as crusher dust) for large-scale direct and interface shear testing. The particle size distribution curves of the scalped specimens are shown in Figure 2, the particle sizes of interest, the coefficient of uniformity (C_u), the coefficient of curvature (C_z), and the Unified Soil Classification System (USCS) classification are also given in Table 2.

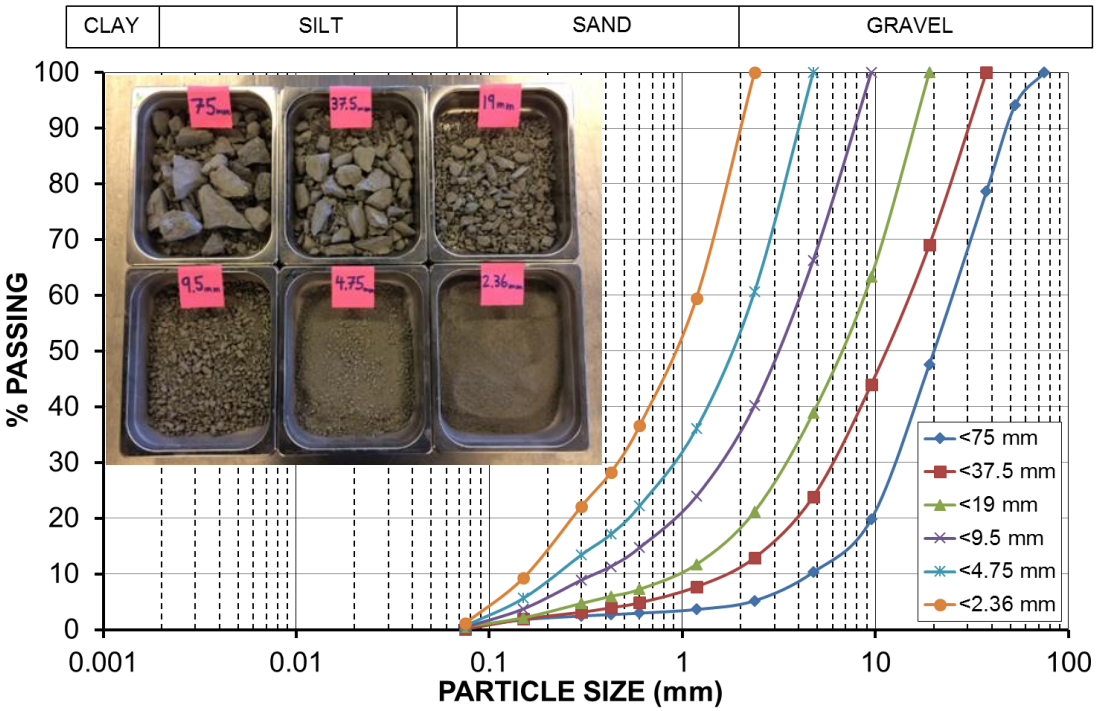

Figure 2 Particle-size distribution curves of scalped crusher run specimens

Table 2 Particle size characteristics of scalped crusher run specimens

Scalped specimens	D_{60} (mm)	D_{50} (mm)	D_{30} (mm)	D_{10} (mm)	C_u	C_z	USCS
<75 mm	23	20	12	4.8	4.79	1.30	GW
<37.5 mm	14	11	6.0	1.8	7.78	1.43	GW
<19 mm	8.8	6.8	3.3	1.0	8.80	1.24	GW
<9.5 mm	4.0	3.1	1.5	0.38	10.53	1.48	GW
<4.75 mm	2.2	1.9	0.9	0.21	10.48	1.75	SW
<2.36 mm	1.2	0.91	0.46	0.14	8.57	1.26	SW

Note: C_u = coefficient of uniformity; C_z = coefficient of curvature

3 Testing program

The air-dried scalped crusher run specimens were loosely-placed into the shear box to represent loose-dumping of dry aggregate in the field, and the specimens were then subjected to single-stage testing under applied normal stresses of 250 kPa, 500 kPa or 1000 kPa to determine the shear strengths and failure envelopes. The initial sample height in the large shear box was carefully controlled to be approximately five times larger than the scalping size using spacers (except for the original crusher run specimens, having a pre-scalping size of 75 mm). The initial loosely-placed density for each specimen was

calculated based on the mass of the specimen dumped. The controlled sample height, mass and initial density are summarised in Table 3. The approximate final density at failure was calculated and obtained based on the average settlement recorded from the four LVDTs.

Table 3 Initial Testing Conditions Controlled for Scalped Crusher Run Specimens

Scalped specimens	<75 mm	<37.5 mm	<19 mm	<9.5 mm	<4.75 mm	<2.36 mm
Sample mass (kg)	25	25	12	6	3.6	2.4
Initial density (t/m^3)	1.462	1.543	1.404	1.333	1.333	1.333

A rapid shearing rate was selected to be 1 mm/min throughout the tests due to the shear testing of coarse aggregates under dry condition (not sitting in a bath), without consolidation or drainage involved. The same shearing rate (1 mm/min) has also been adopted by many other researchers for the shear testing of sand or gravel (Alfaro et al. 1995; Yu et al. 2006; Liu et al. 2009a, b; Kim and Ha 2014; Xiao et al. 2014a; Vieira and Pereira 2015). A shear displacement of 30 mm was controlled for all the direct and interface shear tests (i.e., 10% shear strain), in order to avoid excessive tilting of the top cap. It has been found that the excessive distortion of the top cap would produce possible erroneous results; for example, the shear stress might still keep linearly increasing with the shear displacement at a larger shear strain (10%-20%), without an expected peak occurring. A possible explanation for this might be that excessive tilting would cause the top cap to be stuck and prevent the aggregates from re-orientating or dilating, which results in continuously increasing shear stresses. This is most noticeable for testing the coarse aggregates with large particles under a higher normal stress. Moreover, shearing too much would cause a significant reduction in the contact area, resulting in an increase in actual applied normal stress and shear stress on the shear plane. Thus, both the applied normal stress and the measured shear stress were re-calculated by applying area correction when it comes to the failure envelopes and shear strength parameters in this paper. To compensate for these disadvantages mentioned above, a shear strain of 10% was therefore chosen for all the tests to keep consistency. During the shearing process, shear displacement, vertical displacement and shear force were measured and recorded at time intervals of 30 seconds.

Interface shear tests were also carried out between the geogrid and the six groups of scalped crusher run specimens interfaces (with an increasing degree of scalping), respectively, under the same three normal stress levels applied in the direct shear tests, to investigate the effect of scalping on the interface shear strength characteristics. The geogrid was clamped on the top of the lower shear box and embedded in the scalped crusher run specimens, and the interface between the crusher run specimen and the geogrid was sheared on completion of compression. In addition, in order to further study the particle crushing of the specimens caused by different applied normal stresses and shearing in the large shear box, sieving analyses were carried out on the scalped crusher run specimens before and after the shear tests to measure the change of the particle size distribution curves and quantify the particle breakage indices.

4 Results and discussion

4.1 Direct shear and interface shear test results

Typical raw results (not area-corrected) for the large-scale direct shear testing of the scalped crusher run specimen (<37.5 mm) are shown in Figure 3. Figure 3(a) shows shear stress increases monotonically at a reducing rate with shear strain to an ultimate (maximum) shear strength, with no apparent peak occurring within 10% shear strain. This result may be explained by the fact that the coarse-grained specimen was initially loosely-placed, resulting in a general contraction phenomenon, with a continuous increase in vertical displacement (settlement) observed during shearing, as shown in Figure 3(b). For the lowest applied normal stress of 250 kPa, the shear-induced vertical displacement shows a tendency that it starts decreasing slightly after shearing 20 mm, indicating that a slight dilation behaviour may occur at a larger strain under a lower normal stress. For the highest applied normal stress of 1000 kPa, it seems that the shear stress has not reached to a peak, and the compression is still continuing after shearing 30 mm. This is likely due to a much higher confinement applied to the specimen, which prevents the aggregates from dilating. However, it has been found that applying a larger shear strain might still not be able to reach a peak because the induced excessive tilting of the top cap would produce possible erroneous results, as mentioned before. Hence, a shear displacement of 30 mm was chosen for all the tests to interpret the ultimate (maximum) shear stress that could be mobilised within 10% shear strain.

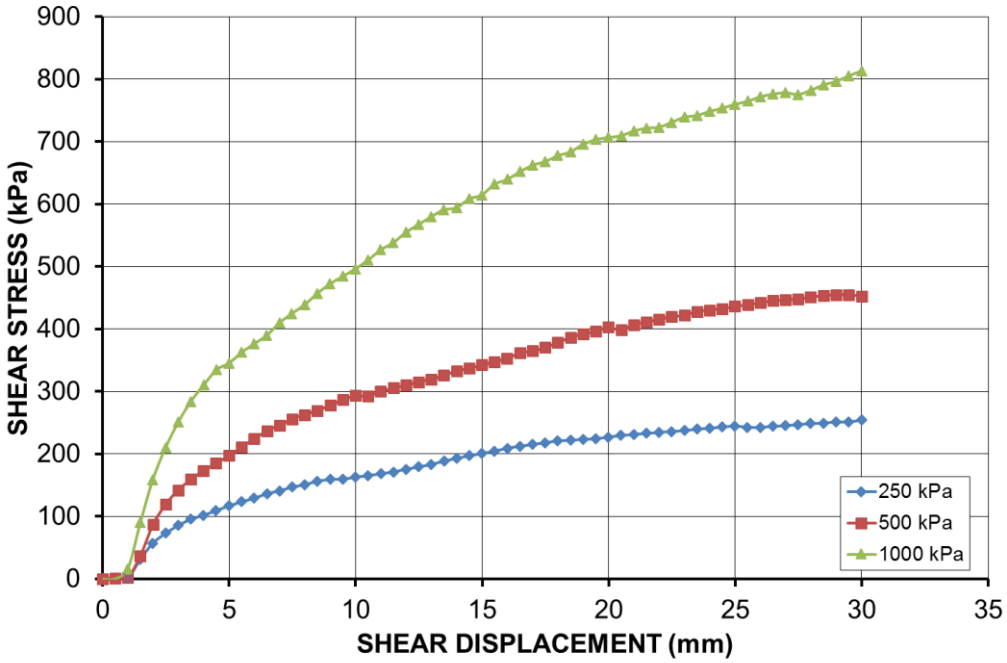

(a)

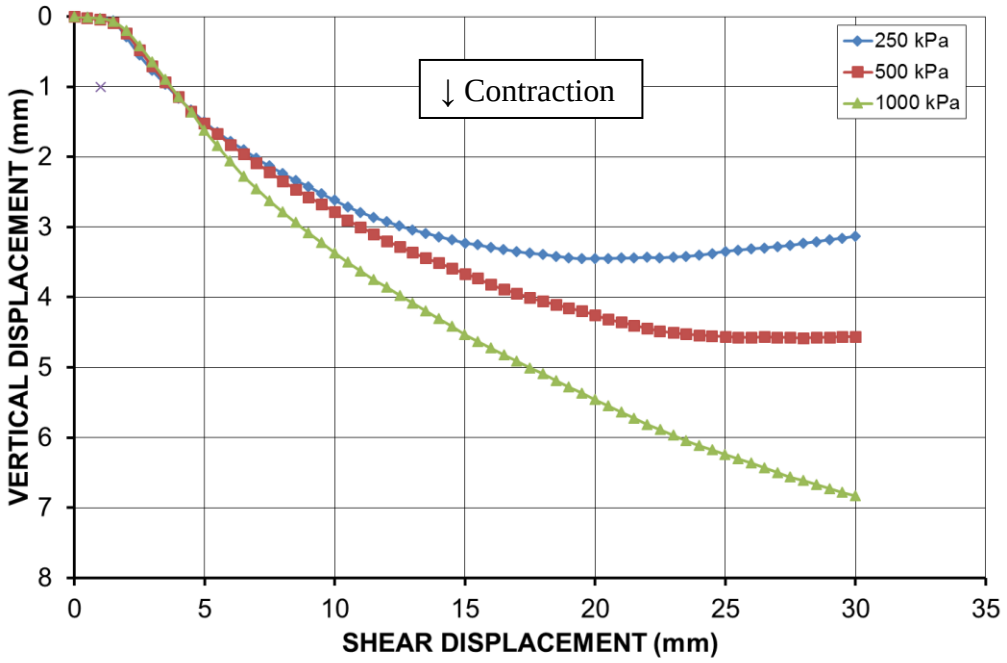

(b)

Figure 3 Typical raw results for large-scale direct shear testing of scalped crusher run specimen (<37.5 mm as an example): (a) shear stress versus shear displacement; (b) vertical displacement versus shear displacement

For interface shear tests, the interface shear resistance between the crusher run specimens and geogrid is generally made up of two components: i) the friction between aggregate particles in the aperture of geogrid, and ii) the friction between aggregates and geogrid ribs. Comparisons of shear stress curves between direct shear and interface shear tests for the six groups of scalped crusher run specimens are shown in Figure 4. It should be noted that all the shear stress curves were plotted using the raw data collected (not area-corrected). It can readily be seen that the interface shear stress curves between the scalped crusher run specimens and the geogrid tend to be slightly lower than the shear stress curves of the scalped crusher run specimens alone when the scalping size is larger than 4.75 mm. Small differences between the direct and interface shear stresses were found when low normal stresses were applied to the specimens (e.g. the curves corresponding to the applied normal stress of 250 kPa or 500 kPa). By contrast, it is evident that a relatively larger difference between the direct and interface shear stresses was observed for the applied normal stress of 1000 kPa. Furthermore, in terms of a smaller scalping size of 4.75 mm or 2.36 mm (i.e., higher degree of scalping), the interface shear stress of the scalped crusher run specimens was decreased drastically, with a clear peak occurring before reaching the maximum shear displacement (peaked at 1-3% strain). This was clearly shown for the highest applied normal stress of 1000 kPa (see for instance Figure 4 e and f)). This finding implies that the fine material tends to reach a peak shear stress earlier than the coarse material in direct and interface shear tests. The higher the applied normal stress, the more shear displacement is needed to reach a peak. The differences with and without geogrid are statistically significant for the samller scalping sizes (4.75 mm or 2.36 mm) under larger normal stresses (500 kPa and 1000 kPa).

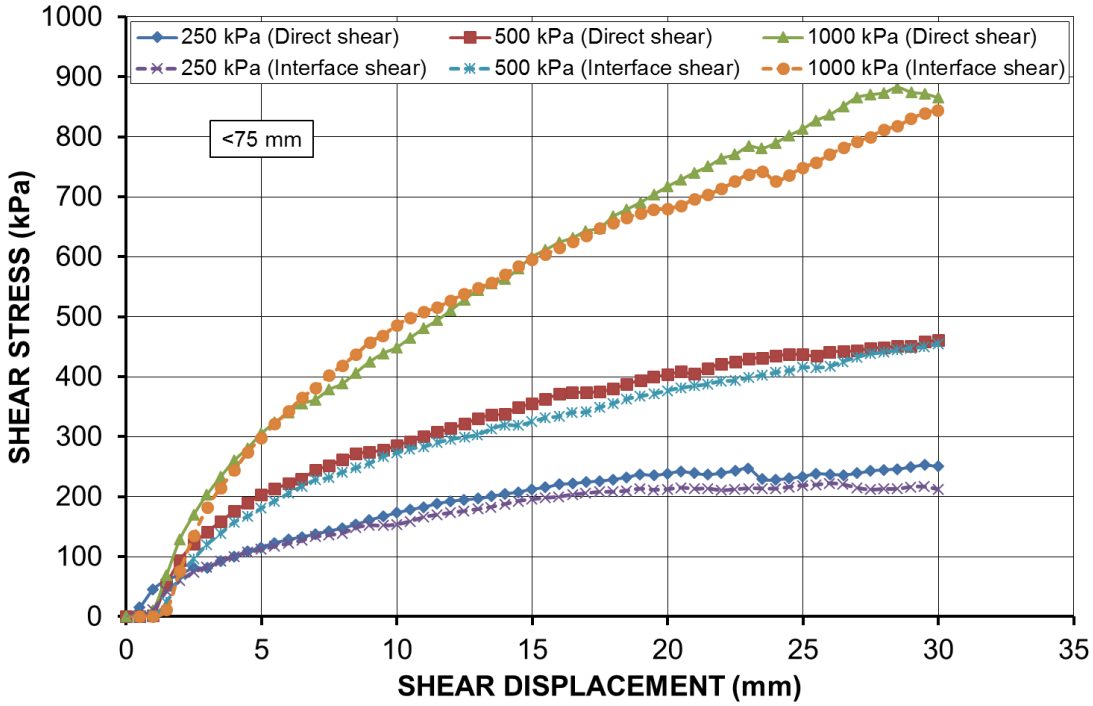
250 kPa (Direct shear)
500 kPa (Direct shear)
1000 kPa (Direct shear)
250 kPa (Interface shear)
500 kPa (Interface shear)
1000 kPa (Interface shear)
<75 mm
SHEAR STRESS (kPa)
SHEAR DISPLACEMENT (mm)
0
100
200
300
400
500
600
700
800
900
1000
0
5
10
15
20
25
30
35

(a)

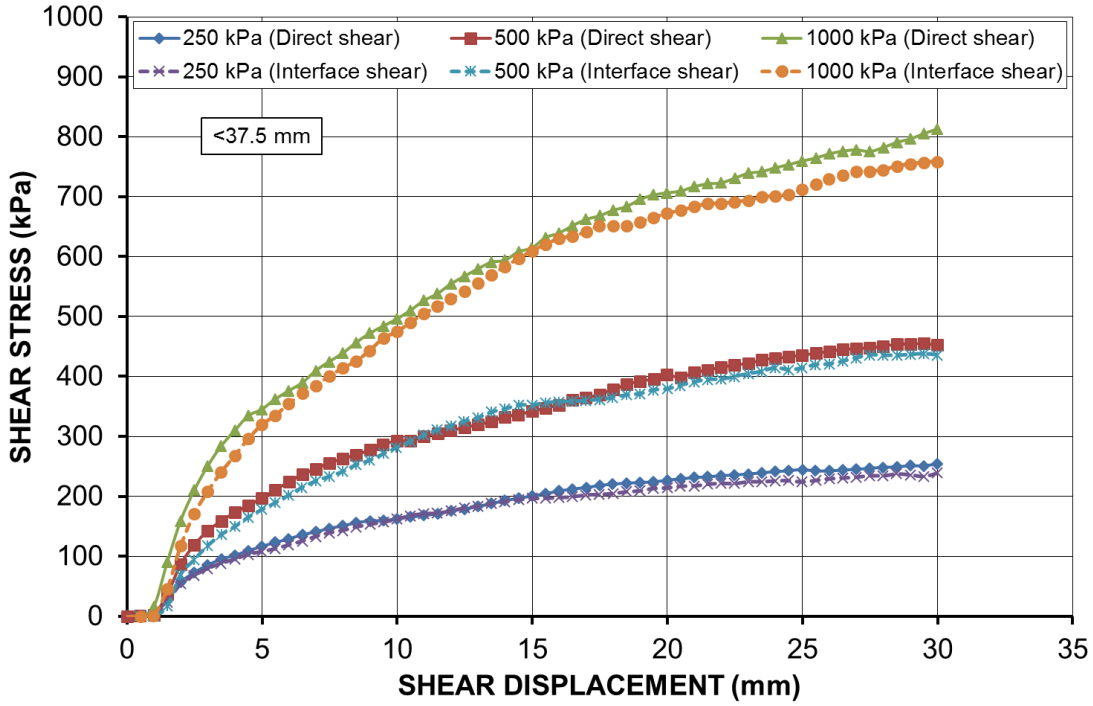
250 kPa (Direct shear)
500 kPa (Direct shear)
1000 kPa (Direct shear)
250 kPa (Interface shear)
500 kPa (Interface shear)
1000 kPa (Interface shear)
<37.5 mm
SHEAR STRESS (kPa)
SHEAR DISPLACEMENT (mm)
0
100
200
300
400
500
600
700
800
900
1000
0
5
10
15
20
25
30
35

(b)

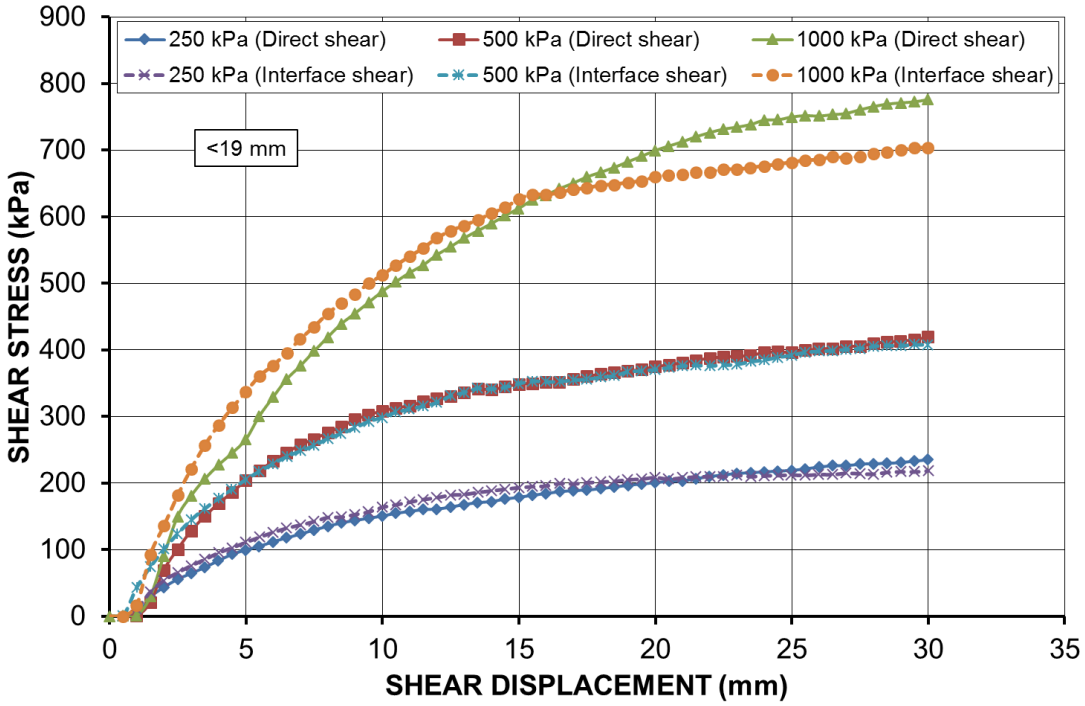
250 kPa (Direct shear)
500 kPa (Direct shear)
1000 kPa (Direct shear)
250 kPa (Interface shear)
500 kPa (Interface shear)
1000 kPa (Interface shear)
<19 mm
SHEAR STRESS (kPa)
SHEAR DISPLACEMENT (mm)
0
100
200
300
400
500
600
700
800
900
0
5
10
15
20
25
30
35

(c)

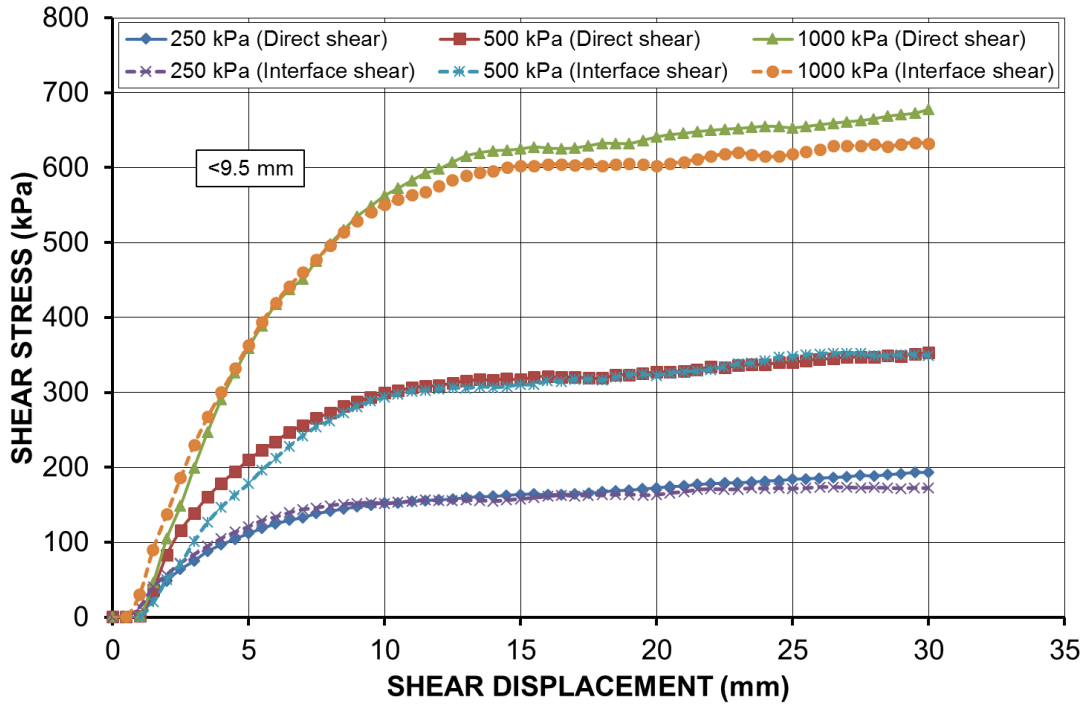
250 kPa (Direct shear)
500 kPa (Direct shear)
1000 kPa (Direct shear)
250 kPa (Interface shear)
500 kPa (Interface shear)
1000 kPa (Interface shear)
<9.5 mm
SHEAR STRESS (kPa)
SHEAR DISPLACEMENT (mm)
0
100
200
300
400
500
600
700
800
0
5
10
15
20
25
30
35

(d)

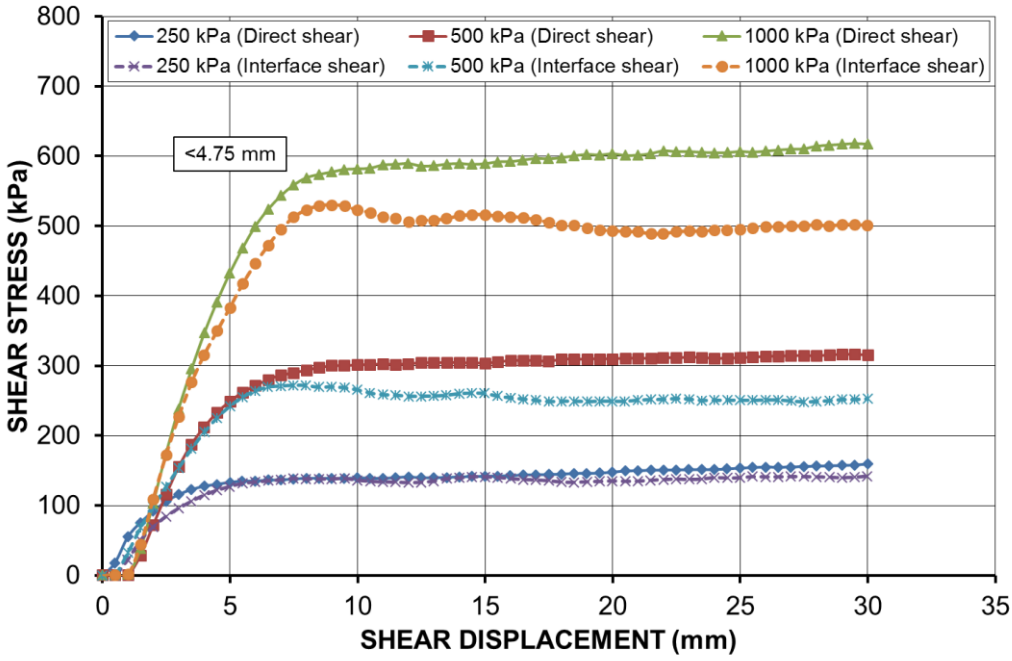

(e)

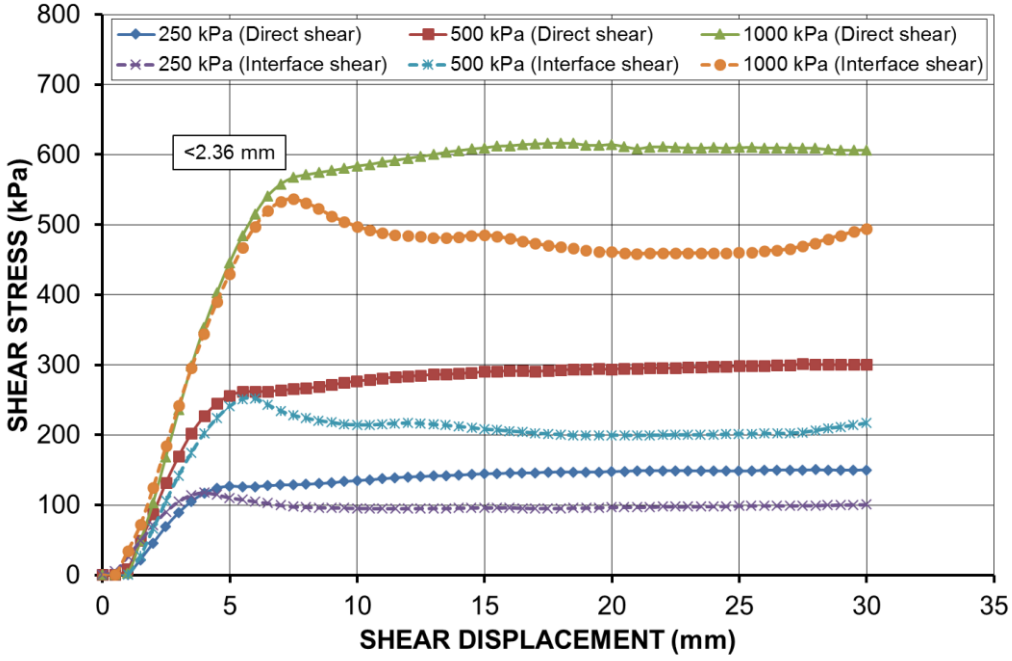

(f)

Figure 4 Comparisons of shear stress curves between direct shear and interface shear tests for scalped crusher run specimens: (a) <75 mm; (b) <37.5 mm; (c) <19 mm; (d) <9.5 mm; (e) <4.75 mm; (f) <2.36 mm

4.2 Relationship between shear stress and final density at failure

The vertical displacement was monitored throughout the tests so that the approximate density at failure could be calculated. It was found that the higher the normal stress applied to a loosely-placed coarse-grained specimen, the larger the settlement monitored after the compression stage, which results in the higher packing density, and the higher shear stress during the shearing stage. For the direct or interface shear testing of the three identical specimens under three applied normal stresses, it is impossible to shear the specimens at the same density under different normal stresses; moreover, the density of a specimen always keeps changing during shearing due to contraction or dilation. Xiao et al. (2014a) also reported the fact that the strength and deformation behaviour of sand are dependent on density and pressure. Therefore, Figure 5 shows the relationship between shear stress and approximate final density at failure for the six groups of scalped crusher run specimens in the direct and interface shear tests. In general, the shear stress at failure increases with the final density due to an increase in applied normal stress. This is similar to what is happening in the field. That is, as more overburden is built up, which is equivalent to higher normal stress, the material will be compressed to a higher density, leading to a higher strength. Furthermore, it was found that the specimen with a smaller scalping size tended to have a higher final density under the same applied normal stress. For example, the final density at failure under the applied normal stress of 1000 kPa increased from 1.462 t/m^3 to 1.677 t/m^3 for the 75 mm scalped specimen, while it increased from 1.333 t/m^3 to 1.810 t/m^3 for the 2.36 mm scalped specimen. This phenomenon could be explained by the fact that the fine material tends to be compressed to a lower void ratio (denser) after particle packing, while for the coarse material, the larger particles would carry most of the load and prevent the smaller particles that are filled in the void spaces from re-orienting and re-packing, leading to a higher void ratio. Lade et al. (1996) had also explained a fact that the void spaces of the final materials will be greatly decreased after the individual particles are packed tightly and supported by enough contact points at higher confining pressures.

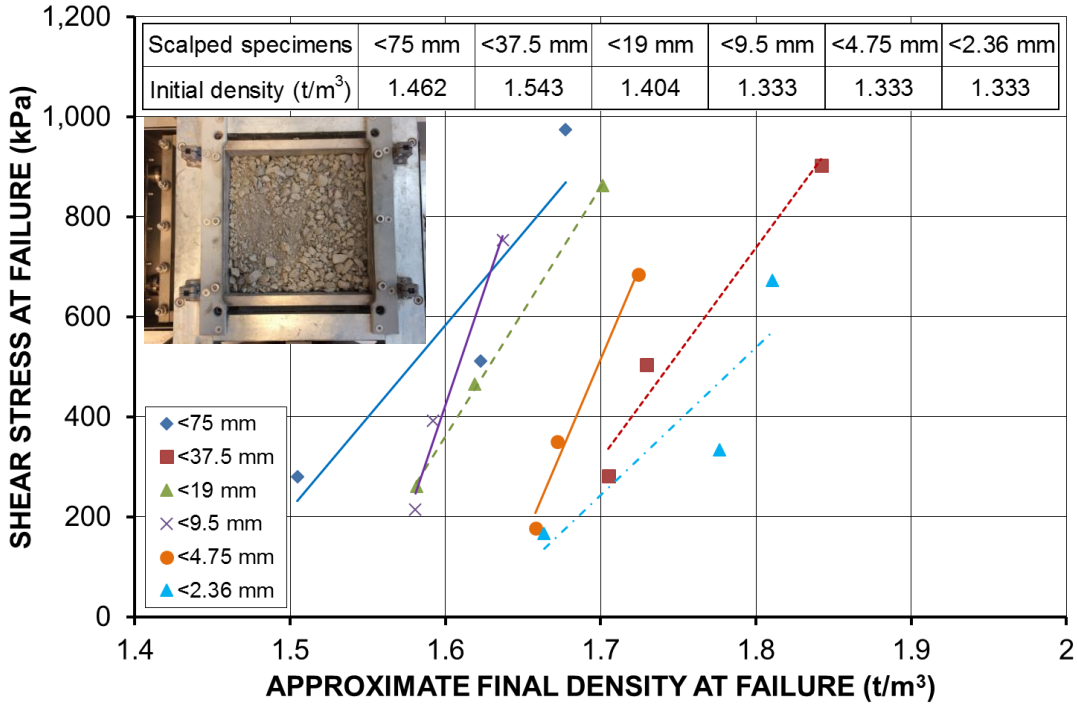

(a)

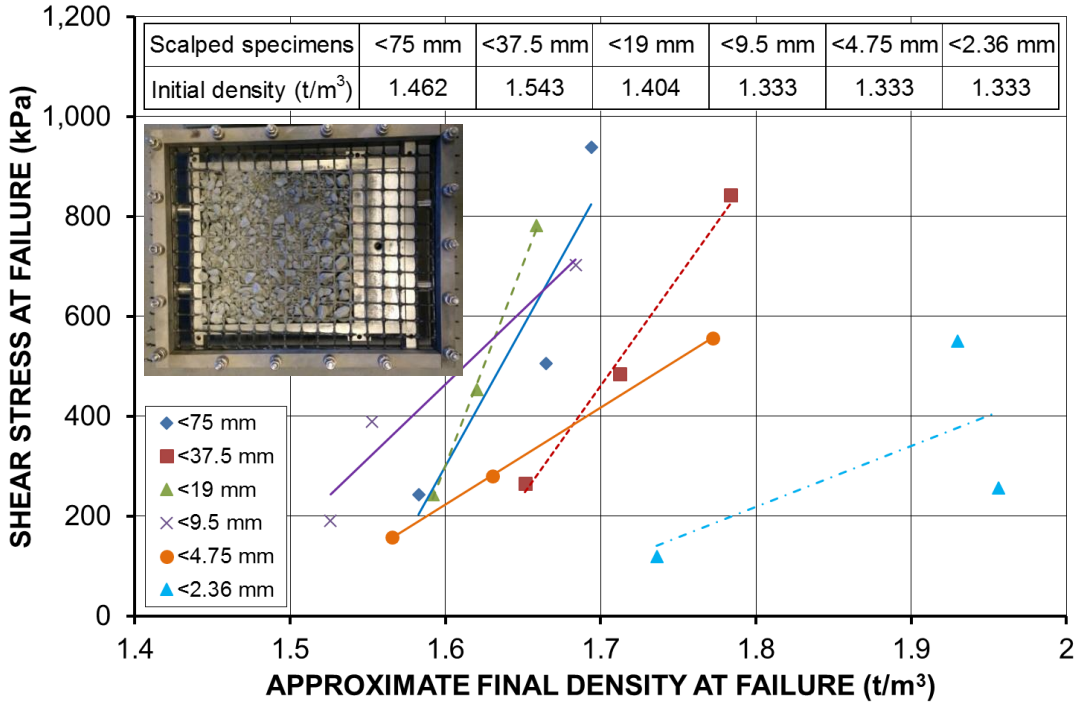

(b)

Figure 5 Relationship between shear stress and final density at failure for scalped crusher run specimens: (a) direct shear test results; (b) interface shear test results

4.3 Effect of scalping on shear stress curves

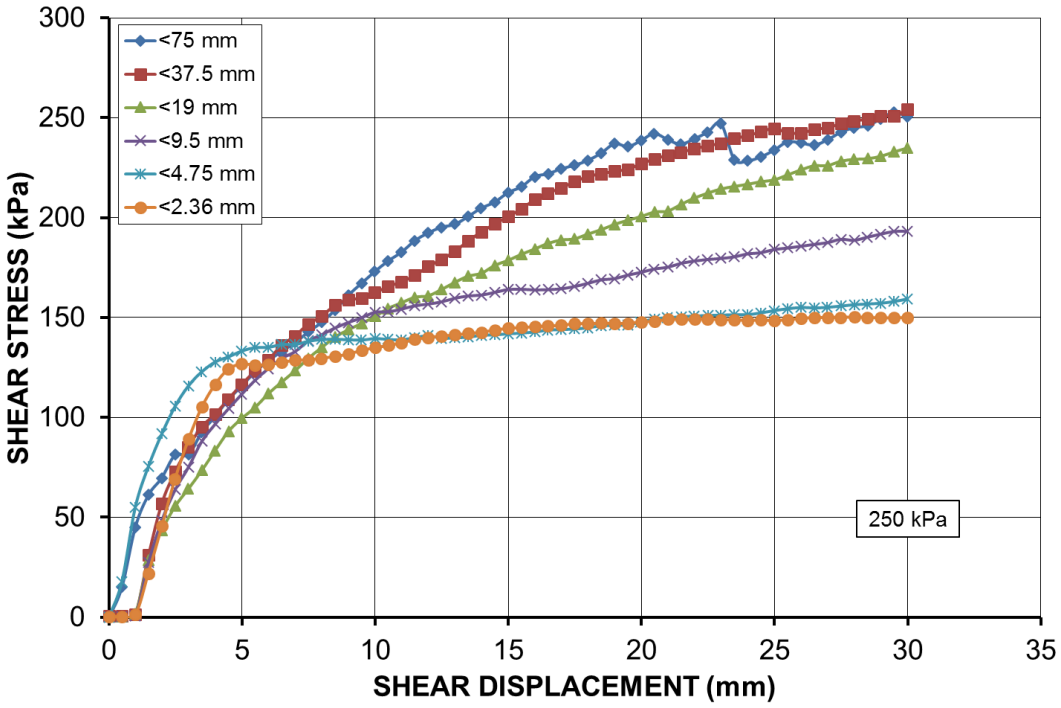

(a)

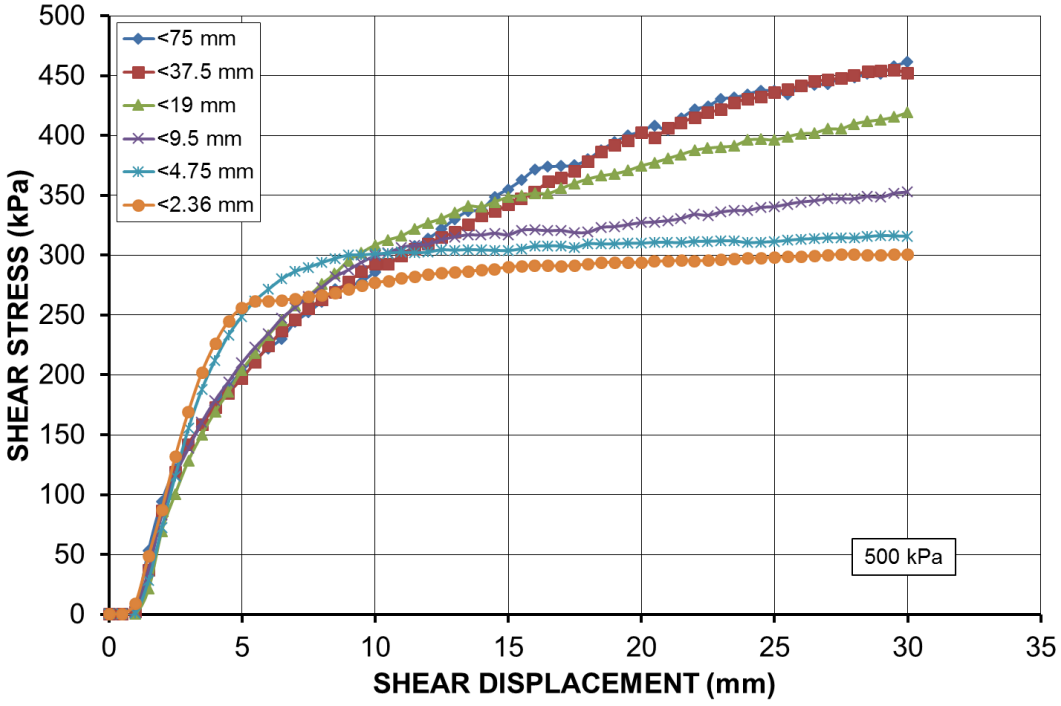

(b)

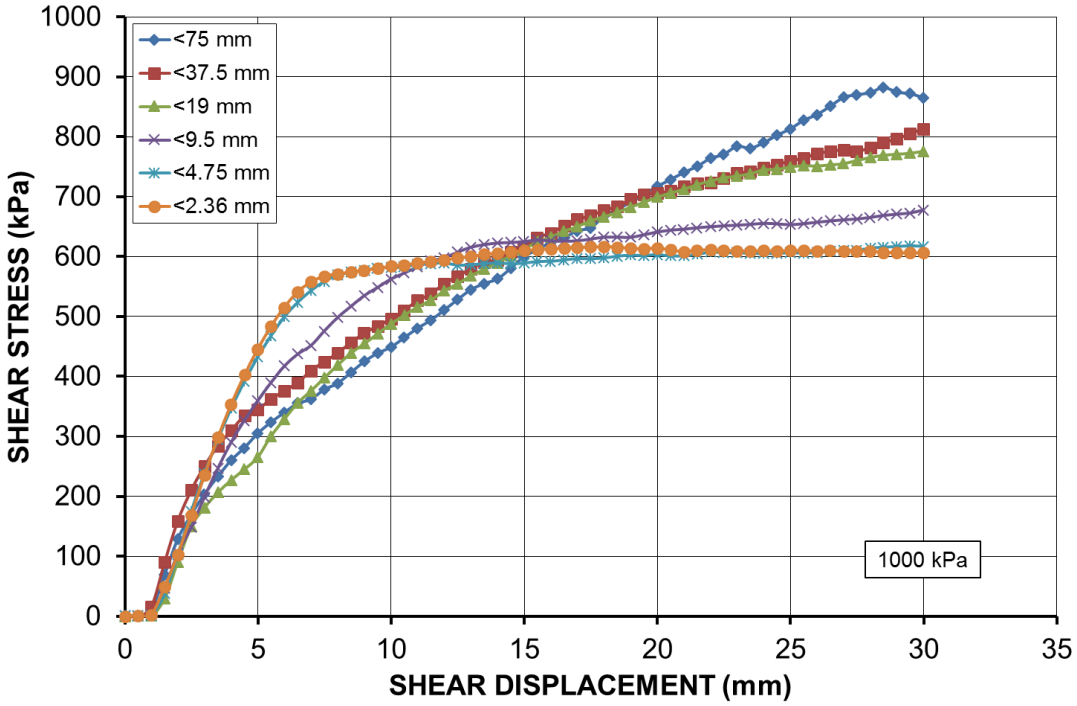

(c)

Figure 6 Effect of scalping on shear stress curves of scalped crusher run specimens under applied normal stress of: (a) 250 kPa; (b) 500 kPa; (c) 1000 kPa

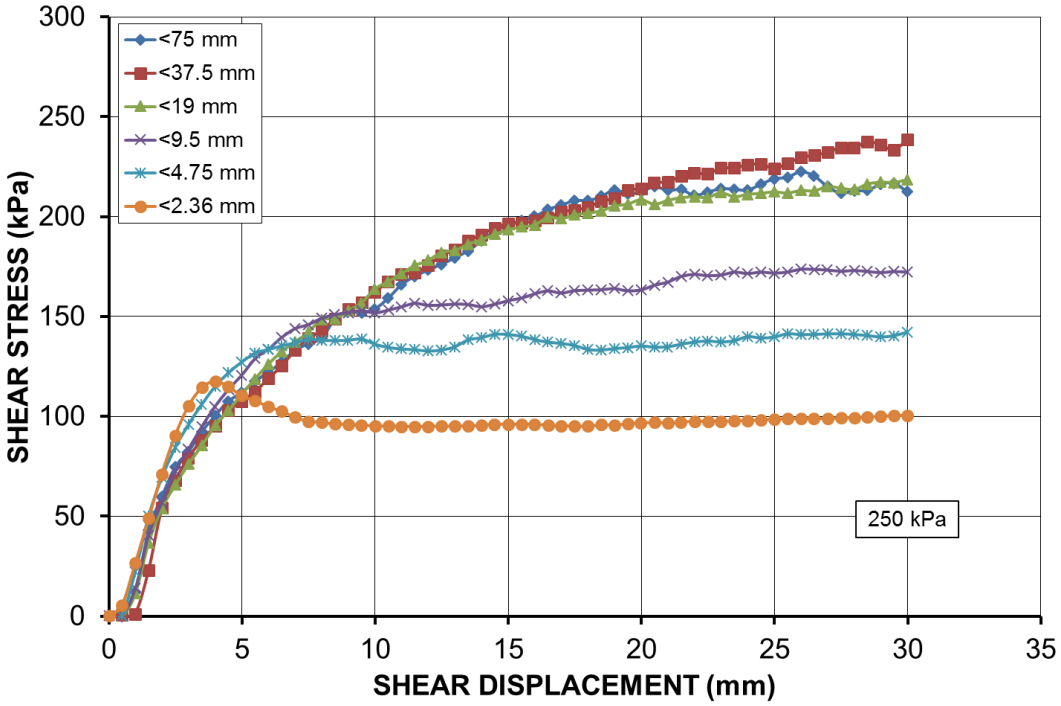

(a)

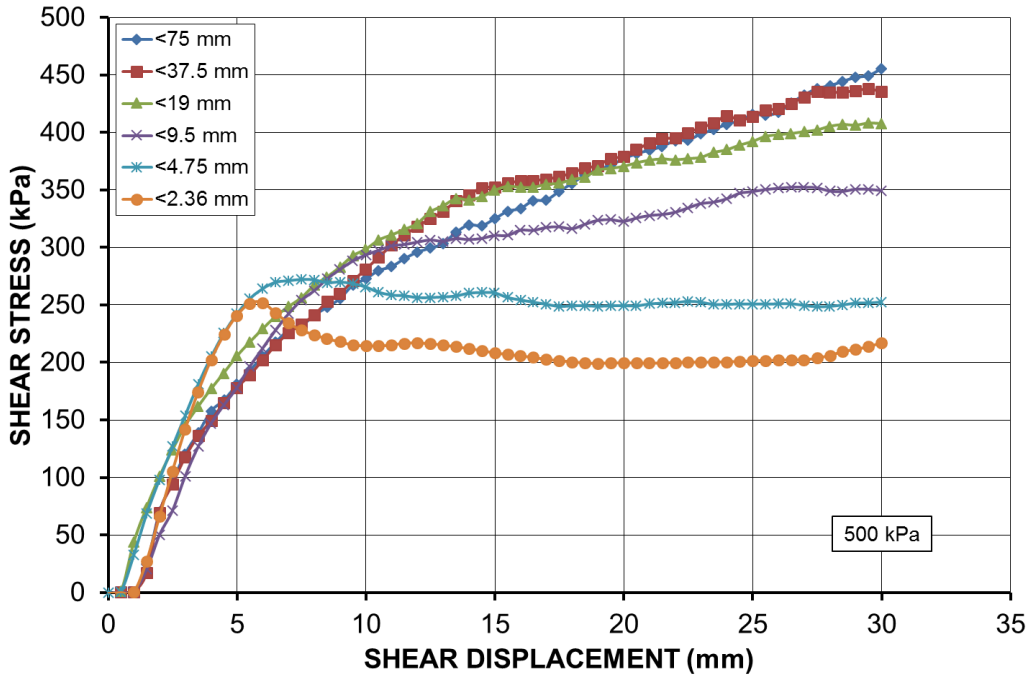

(b)

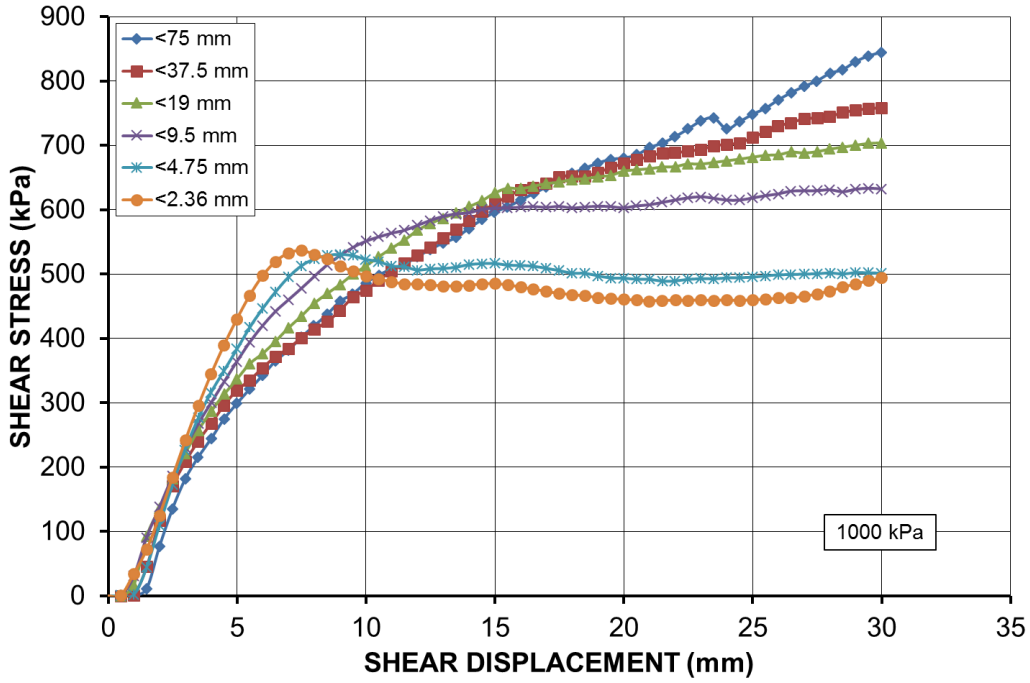

(c)

Figure 7 Effect of scalping on shear stress curves of scalped crusher run specimens-geogrid interface under applied normal stresses of: (a) 250 kPa; (b) 500 kPa; (c) 1000 kPa

The effect of scalping (from 75 mm down to 2.36 mm) on the direct and interface shear stress curves, under applied normal stresses of 250 kPa, 500 kPa or 1000 kPa is shown in Figure 6 and Figure 7. It is clear that the shear stress curves gradually decrease and flatten out as the scalping size decreases, indicating the increased degree of scalping caused an increasingly significant reduction in direct and interface shear stresses. However, the initial slope of the shear stress curves tends to increase with reduced scalping size and increased normal stress. This initial slope refers to the tangent modulus of the specimen (Xiao et al. 2014a). Therefore, it can also be found that the tangent modulus of the specimens tends to increase with an increasing degree of scalping. This finding can be explained by the fact that the packing density of specimens after compression increases with the degree of scalping, as mentioned before, leading to an increase in the initial stiffness at the small shear strain. It should also be noted that a clear peak occurred before a shear displacement of 10 mm for the crusher dust specimens scalped from 4.75 mm and 2.36 mm. This is most noticeable for the interface shear stress curves (see also Figure 7), with an obvious drop-off after the peak, then reaching a critical (residual) state. The drop-off may be caused by the particle rolling over the apertures of the geogrid. Overall, the tendency is that both the direct and interface shear stress curves decreases with an increasing degree of scalping based on the direct and interface shear test results obtained.

4.4 Effect of scalping on failure envelopes

The shear stress at failure is defined as the maximum (peak) shear stress that can be achieved within 10% shear strain. The applied normal and shear stresses at failure are corrected for the area reduction due to a loss in contact area during shearing. The shear strength obtained from laboratory direct shear test can be interpreted by the Mohr-Coulomb straight-line failure criterion (or failure envelope), as given in the following equation:

$$\tau_f = c + \sigma_n \tan\phi \tag{1}$$

where τ_f is the internal shear strength at failure, c is the apparent cohesion, ϕ is the internal friction angle and σ_n is the applied normal stress.

Similarly, the shear strength of the soil-geogrid interface in an interface shear test can be interpreted by:

$$\tau_i = c_a + \sigma_n \tan\delta \tag{2}$$

where τ_i is the interface shear strength at failure, c_a is the apparent adhesion, δ is the interface friction angle and σ_n is the applied normal stress.

The failure envelopes of the six groups of scalped crusher run specimens in the direct and interface shear tests are shown in Figure 8, showing that the failure envelopes gradually move downward and flatten out with increasing degree of scalping for both the direct and interface shear test results. Therefore, scalping process could significantly reduce the shear strength, lowering the magnitude of the failure envelopes.

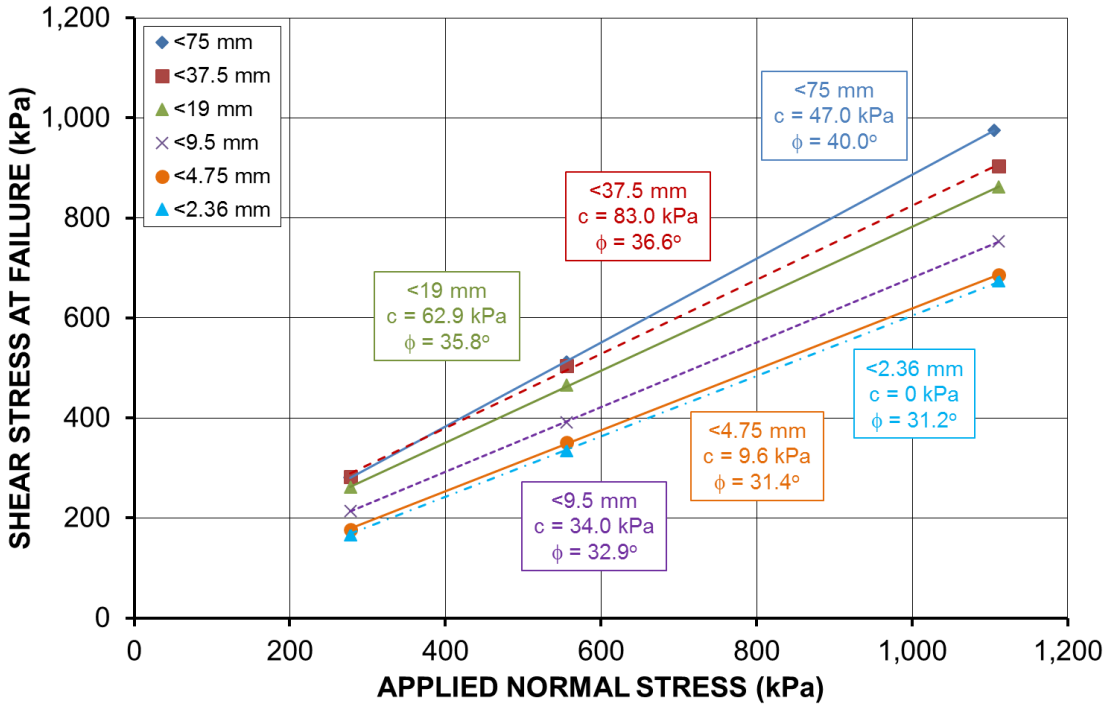

(a)

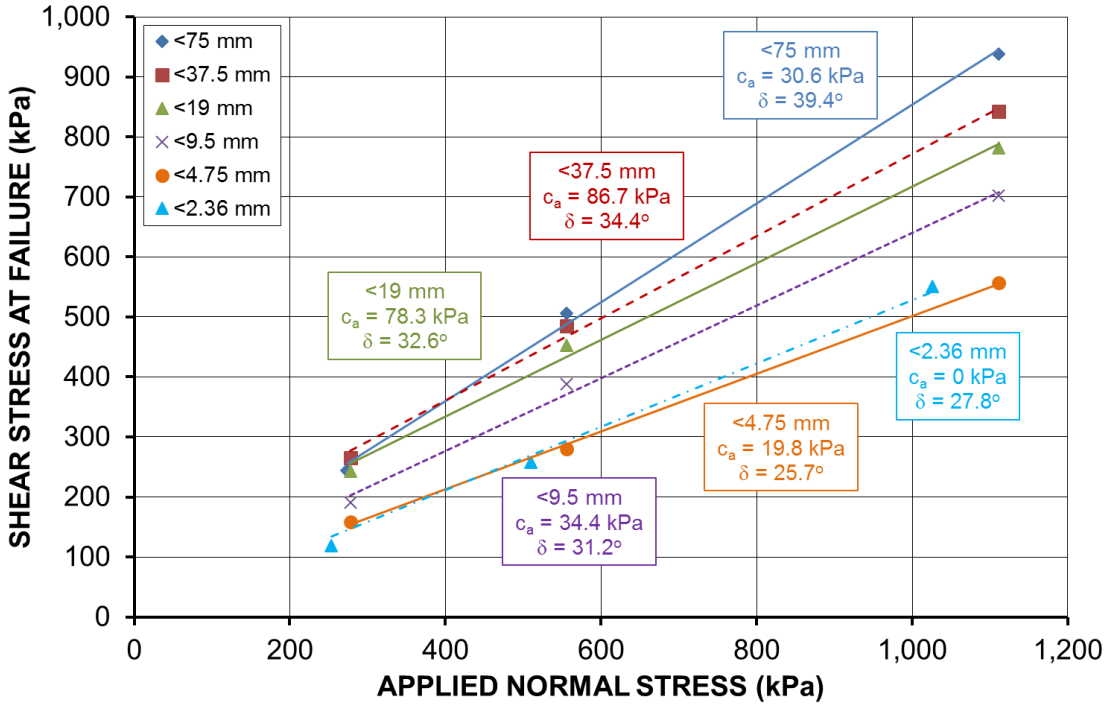

(b)

Figure 8 Effect of scalping on failure envelopes of scalped crusher run specimens: (a) direct shear test results; (b) interface shear test results

4.5 Effect of scalping on direct and interface shear strength parameters

An alternative interpretation of shear strength results is to calculate the secant friction angles at each applied normal stress for each specimen tested, which are the angles of the straight lines from each point drawn back to the origin. The secant friction angle is calculated using the equation below:

$$\tan \phi_{\text{sec}} = \tau / \sigma_n \tag{3}$$

where τ is the shear strength, ϕ_{sec} is the secant friction angle, and σ_n is the applied normal stress. This approach excluding the contribution of apparent cohesion to the shear strength; therefore, the secant friction angles are normally higher than the Mohr-Coulomb friction angles.

The calculated secant friction angle versus applied normal stress is shown in Figure 9. Also shown in Figure 9 are the range of data from poor to good quality rock fill obtained

from 200 mm diameter triaxial testing by Leps (1970), a typical angle of repose for loose-dumped rockfill aggregate of 37°, and an average applied stress of 900 kPa corresponding to about an equivalent depth of 50 m. It can be seen from Figure 9 that scalping also caused a reduction in secant friction angles. Specimens with a scalping size larger than 19 mm have secant friction angles within the range expected for rock fill, while specimens with a scalping size smaller than 9.5 mm have lower secant friction angles than the lower bound for poor quality rock fill.

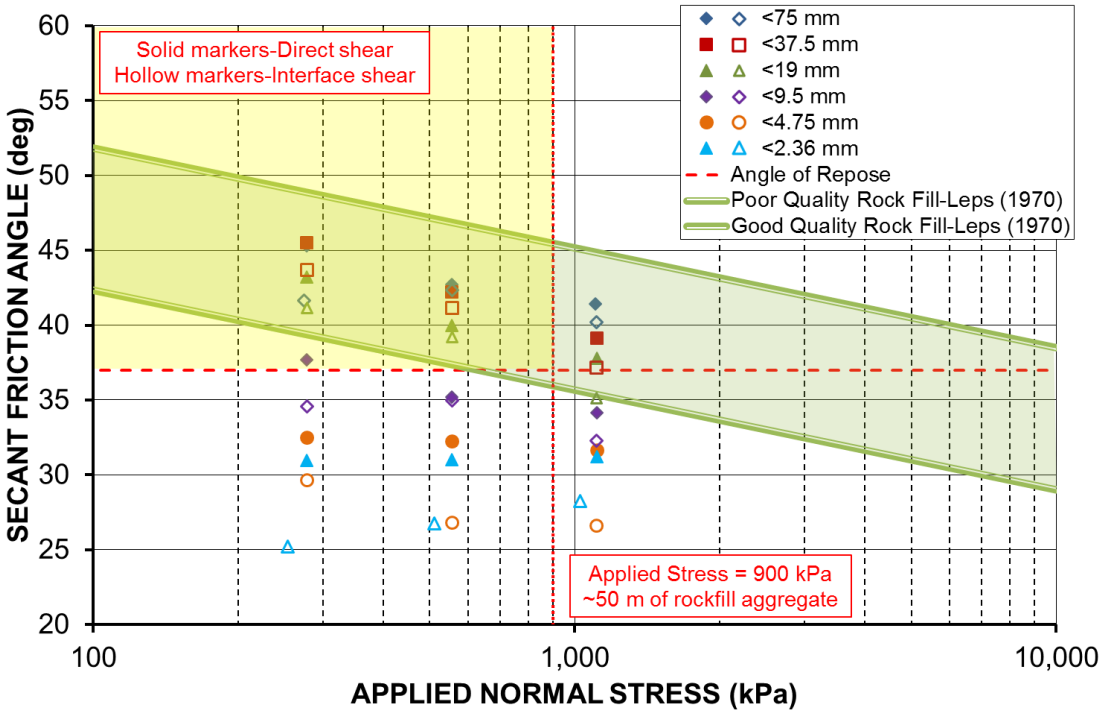

Figure 9 Secant friction angle versus applied normal stress

The direct and interface shear strength parameters obtained by Eq. (1) and Eq. (2), and the secant friction angles calculated by Eq. (3) are plotted in Figure 10 for the six groups of scalped specimens. Figure 10(a) shows that the friction angles decreased by several degrees with an increasing degree of scalping. For example, the friction angle ϕ drops from 40.0° to 31.2°, the interface friction angle δ drops from 39.4° to 27.8°, and the secant friction angle ϕ_{sec} drops from 45.3° to 31° as the scalping size decreases from 75 mm to 2.36 mm. This significant reduction in friction angle caused by scalping indicates that the frictional resistance of a coarse-grained specimen is mainly attributed to the friction among the larger particles. Furthermore, a steep reduction was found for the crusher dust specimens scalped from 4.75 mm, especially for the interface shear tests, as shown in

Figure 10(a). A possible explanation for this might be that as the scalping size decreases to 4.75 mm, the scalped crusher run specimen has changed from a well-graded gravel (GW) to a well-graded sand (SW), as also shown in Table 2 based on the Unified Soil Classification System (USCS). From the particle size distribution point of view (see also Figure 2), the range of particle size decreases with an increasing degree of scalping, which means that scalping makes the crusher run material less well graded, resulting in less effective particle contacts, and hence, the shear strength becomes much lower. Lade et al. (1996) also explained a similar fact that for fine materials, with more particle surrounding each particle, the average contact stress tends to decrease, resulting in lower friction. Therefore, the inferred friction angles for the scalped crusher dust specimens (scalped from 4.75 mm or 2.36 mm) were much lower. In addition, the results also imply that small-scale laboratory testing of aggregates, necessitating scalped specimens, would generate conservative shear strength design parameters. It was also found that the interface friction angles are lower than the friction angles by several degrees for different scalping sizes. However, it was noticed that the inferred interface friction angle of the scalped specimen (<2.36 mm) is higher than that of the scalped specimen (4.75 mm). This inconsistency could be explained by the shear stress curves and failure envelopes obtained (see also Figures 7 and 8(b)). For the scalped specimen (<2.36 mm), the peak shear stress occurred earlier, resulting in a lower normal stress at failure after applying area correction. This leads to a steeper failure envelope (i.e., a higher interface friction angle), compared to the specimen (<4.75 mm), as shown in Figure 8(b).

Figure 10(b) compares the apparent cohesion c and adhesion c_a obtained from the direct and interface shear tests with regard to scalping size. Both the apparent cohesion and adhesion decreased from 80 kPa to zero with an increasing scalping size from 37.5 mm to 2.36 mm. In terms of the originally scalped crusher run specimens with a pre-scalped maximum particle size of 75 mm, the inferred c and c_a are, however, much lower than those of the specimens scalped from 37.5 mm (<37.5 mm), which is probably due to the dimensional limitations of the 300 mm by 300 mm shear box for testing over-sized aggregates. For the crusher run-geogrid interfaces, some aggregates could penetrate through the apertures and abut against the ribs of the geogrid so that the particles could be interlocked more efficiently, resulting in an extra confinement and resistance. The inconsistency of the obtained apparent cohesion and adhesion for the specimen (<75 mm) is probably because too many over-sized particles, which are much larger than the

aperture size (33 mm by 33 mm) of the geogrid, cannot penetrate through the openings of the geogrid, eventually leading to a reduction in the effective confinement.

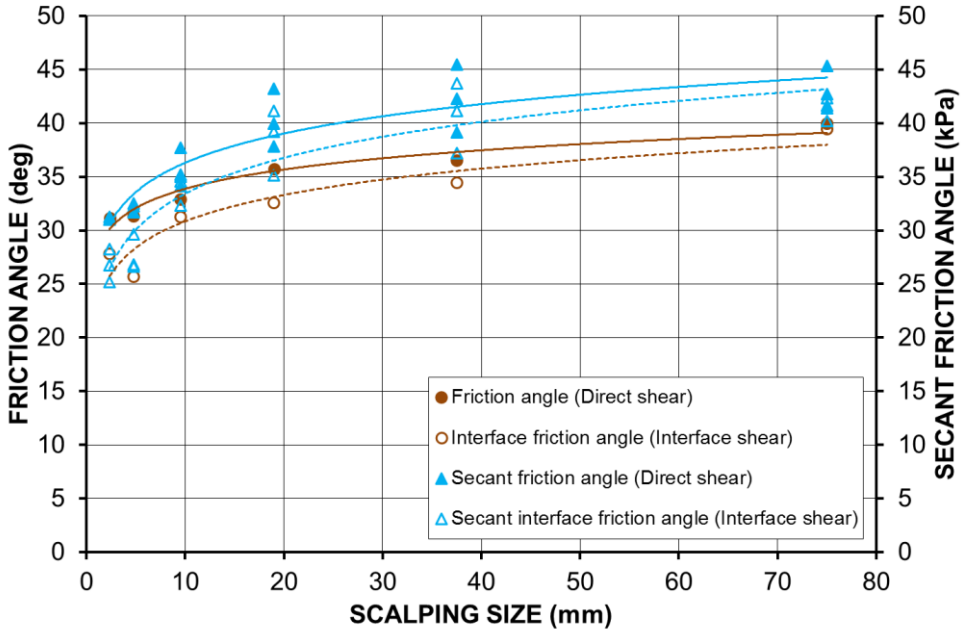

(a)

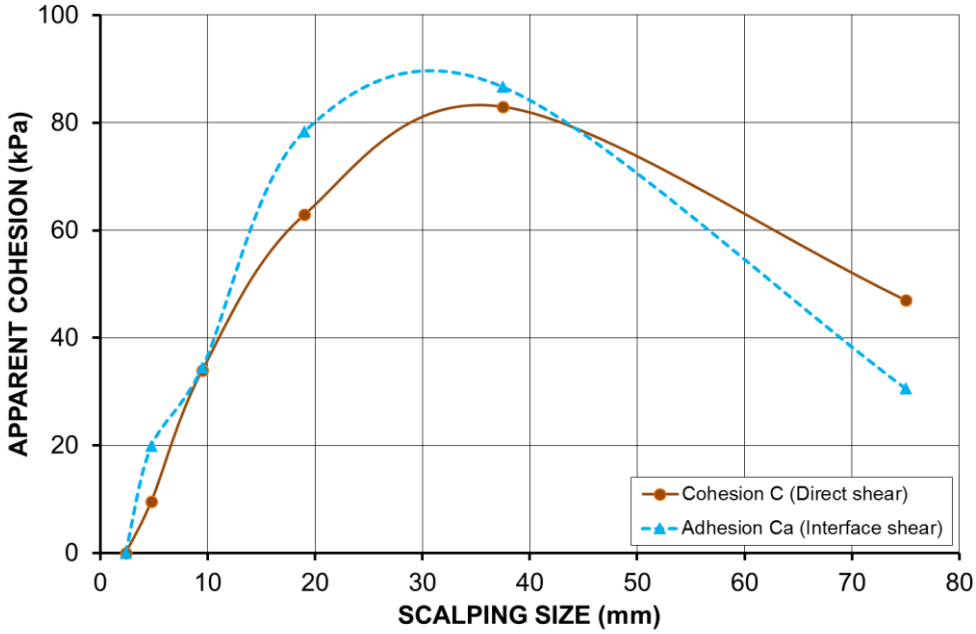

(b)

Figure 10 Effect of scalping on direct and interface shear strength parameters: (a) friction angle and secant friction angle; (b) apparent cohesion

4.6 Effect of scalping on interaction efficiency

Based on the interlocking mechanism mentioned before, the interface friction consists of the friction between aggregate particles and the friction between the aggregates and geogrid ribs. The interface coefficient C_i is defined as the ratio of the interface shear strength between the crusher run specimens and the geogrid to the internal shear strength of the crusher run specimens alone, as shown below.

$$C_i = \frac{\tau_i}{\tau_f} = \frac{c_a + \sigma_n \tan\delta}{c + \sigma_n \tan\phi} \tag{4}$$

where C_i is the interface coefficient.

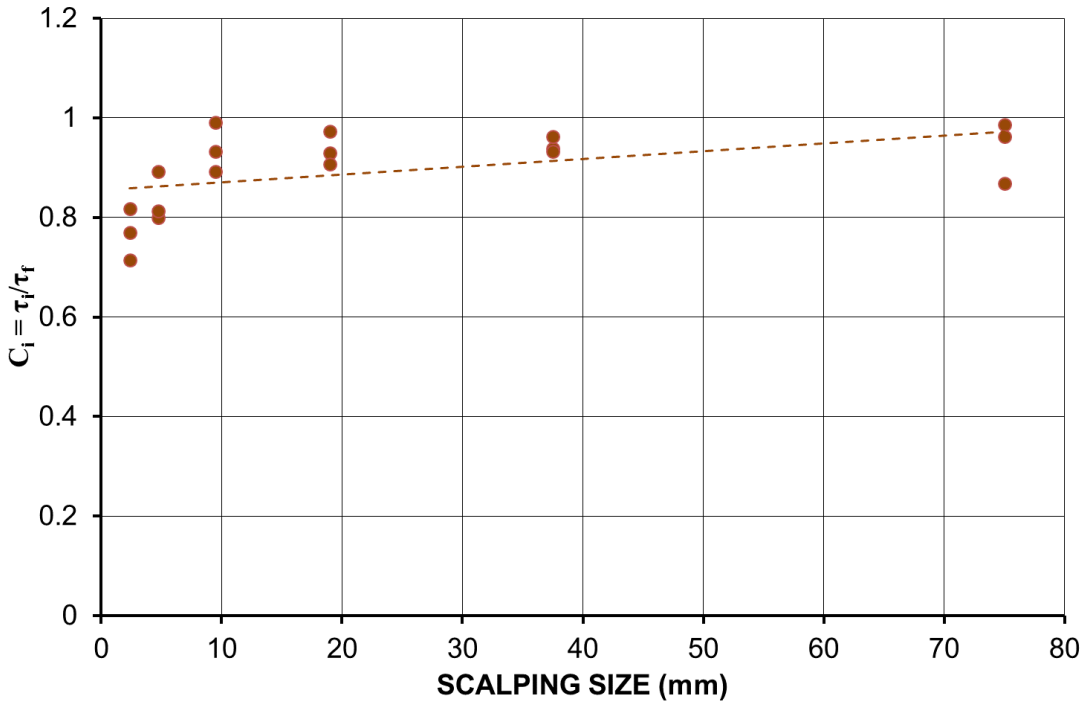

Figure 11 Effect of scalping on interface coefficients of crusher run-geogrid

The calculated interface coefficients using Eq. (4) are compared and plotted against the scalping size in Figure 11. It can be found that the overall interface coefficient C_i ranges from 0.72 to 0.99 (less than 1). A pronounced reduction in C_i was noticed for the more scalped specimens (4.75 mm and 2.36 mm), which decreased from 0.95 to around 0.80. The possible reason has been explained before when discussing the effect of scalping on the shear strength parameters. It is therefore recommended the average interface

coefficients for design purposes herein: an interface coefficient of 0.9 is used for crusher run scalped from 9.5mm or above, and 0.75 or 0.8 for the crusher dust scalped from 2.36mm or 4.75mm. By contrast, the average interface coefficients between granular materials and geogrids obtained by other researchers ranged from 0.65 to 1.16, depending on the different materials studied (Bakeer et al. 1998; Abu-Farsakh et al. 2007; Liu et al. 2009a, b; Indraratna et al. 2012; Vieira and Pereira 2015).

In this study, it was found that the interface shear strengths between the scalped crusher run materials and the geogrid are slightly lower that the direct shear strengths of the scalped crusher run materials alone (see also Figure 4). However, the inferred c_a tends to be slightly higher than c, compensating for a slightly lower δ than ϕ. Therefore, it is believed that the friction component contributes to the overall shear strength more significantly than the cohesion component for the coarse-grained materials.

4.7 Particle size distribution before and after shear test

From the observation of the top surface of the specimens after the large-scale direct shear tests, some large particles below the top cap were found to be crushed to some extent. It was also found that the particle breakage was negligible for the crusher run specimens scalped below 9.5 mm. In general, the larger the scalping size and the higher normal stress applied to a specimen, the greater the observed particle breakage. Lade et al. (1996) also reported that the amount of particle breakage decreases for fine materials because the individual particles are supported by enough contact points, so the average contact stress tends to decrease with more particles surrounding each particle. In order to evaluate the overall particle breakage of specimens, sieving analyses were carried out before and after the shear tests for the selected specimens scalped from 75 mm, 37.5 mm and 19 mm. The whole specimens tested in shear box were sieved (53 mm, 37.5 mm, 19 mm, 9.5 mm screen) until passing through a 9.5 mm screen to obtain an accurate particle size distribution of the whole coarse portion (>9.5 mm). In terms of the finer portion (<9.5 mm), a representative sub-sample (1 kg) was taken and sieved in a shaking machine. It was noticed that the particle size distribution curves for the crusher run specimens before and after direct shear testing are quite close under lower applied normal stresses (250 kPa and 500 kPa). In order to quantify the particle crushing, the following three particle breakage indices (B_{10}, B_{15} and B_{60}) were calculated based on the particle

size distribution curves obtained before and after the shear tests (Lee and Farhoomand 1967; Lade et al. 1996; Zhang et al. 2013a).

$$B_{10} = 1 - \frac{D_{10f}}{D_{10i}} \tag{5}$$

$$B_{15} = \frac{D_{15i}}{D_{15f}} \tag{6}$$

$$B_{60} = D_{60i} - D_{60f} \tag{7}$$

where B_{10}, B_{15} and B_{60} are the particle breakage indices, D_{10i}, D_{15i} and D_{60i} are the particle sizes corresponding to the 10%, 15% and 60% passing before the direct shear test, and D_{10f}, D_{15f} and D_{60f} are the particle sizes corresponding to the 10%, 15% and 60% passing after the direct shear test. Another relative breakage index (an area ratio of particle size distribution curves) defined by Hardin (1985) is also favoured and popularly used in the literature (Einav 2007a, b; Zhang et al. 2013a; Indraratna et al. 2014; Xiao et al. 2014b; Xiao et al. 2017), which is equal to the area between the initial grading and the current grading divided by the area between the initial grading and the ultimate grading. However, the determination of the ultimate grading (maximum breakage) is problematic. Therefore, this study only focuses on the three particle breakage indices (B_{10}, B_{15} and B_{60}) mentioned above. The selected particle size distribution curves before and after direct shear testing under the highest applied normal stress of 1000 kPa are shown in Figure 12. It was found that the calculated breakage indices tend to decrease with an increasing degree of scalping. However, as shown in Figure 12, the overall particle breakage of the specimens within the shear box was not significant although some large particle crushing on the top surface of the specimens was observed mainly due to the normal loading. According to the observations after finishing the tests, damage to the geogird is insignificant for the specimens with smaller scalping sizes, including 19 mm, 9.5 mm, 4.75 mm and 2.36 mm. However, some geogrid ribs (maybe only 1 or 2 ribs) were sometimes found to be damaged or crushed by the sharp coarse aggregates for the tests with larger scalping size, such as 75 mm and 37.5 mm. It mainly happened when the highest normal stress (1000 kPa) was applied.

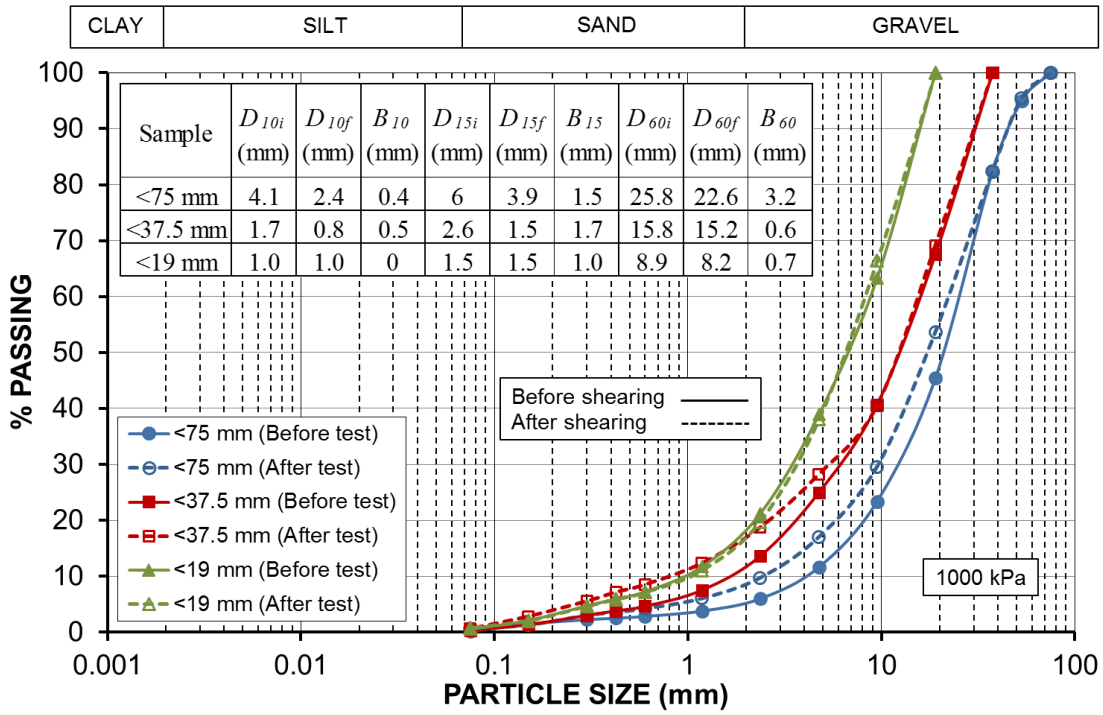

Figure 12 Particle size distribution curves of scalped crusher run specimens before and after shearing under applied normal stress of 1000 kPa

In order to further investigate the particle size distribution characteristics of the shear zone in the middle section of the shear box, the whole specimen after direct shear testing was divided into three layers, namely the top, middle and bottom layers. Sieving analyses were carried out on these three layer specimens after direct shear testing under an applied normal stress of 1000 kPa (see Figure 13 for the crusher run specimens scalped from 19 mm). It was found that the middle layer contained a higher percentage of fines after shearing, resulting in a decrease in effective particle size D_{10} from 1.0 mm to 0.4 mm, whereas the top layer contained a greater percentage of the larger particles. This phenomenon could be explained by the following two reasons. Firstly, during the loading and shearing process, the fines from the top layer sank down and accumulated in the middle layer. This could be proven by a negative breakage index B_{10} obtained for the top layer, indicating a loss in fines. From the experimental observation, it was also noticed that some fine particles that were filled in the voids of the coarse particles on the top surface had disappeared after the shear test. Secondly, some particles in the shear zone within the middle layer were crushed and broken down during the shearing process, resulting in higher breakage indices compared to the top and bottom layers. By contrast, the particle size distribution of the bottom layer is quite close to the results obtained from the sieving

analyses of the whole specimen before shearing, indicating that there was insignificant impact on the specimen in the bottom layer. It should be mentioned that a similar finding of an insignificant particle breakage after interface shear testing was obtained based on the sieving analyses. Furthermore, for the interface shear tests under the highest applied normal stress of 1000 kPa, it was found that the geogrid ribs were not able to crush the aggregates; on the contrary, some geogrid ribs were damaged by the sharp aggregates due to the high confinement and interlocking forces. Therefore, the overall particle breakage of the scalped crusher run specimens was not significant in both the direct shear and interface shear tests within a normal stress level of 1000 kPa in this study.

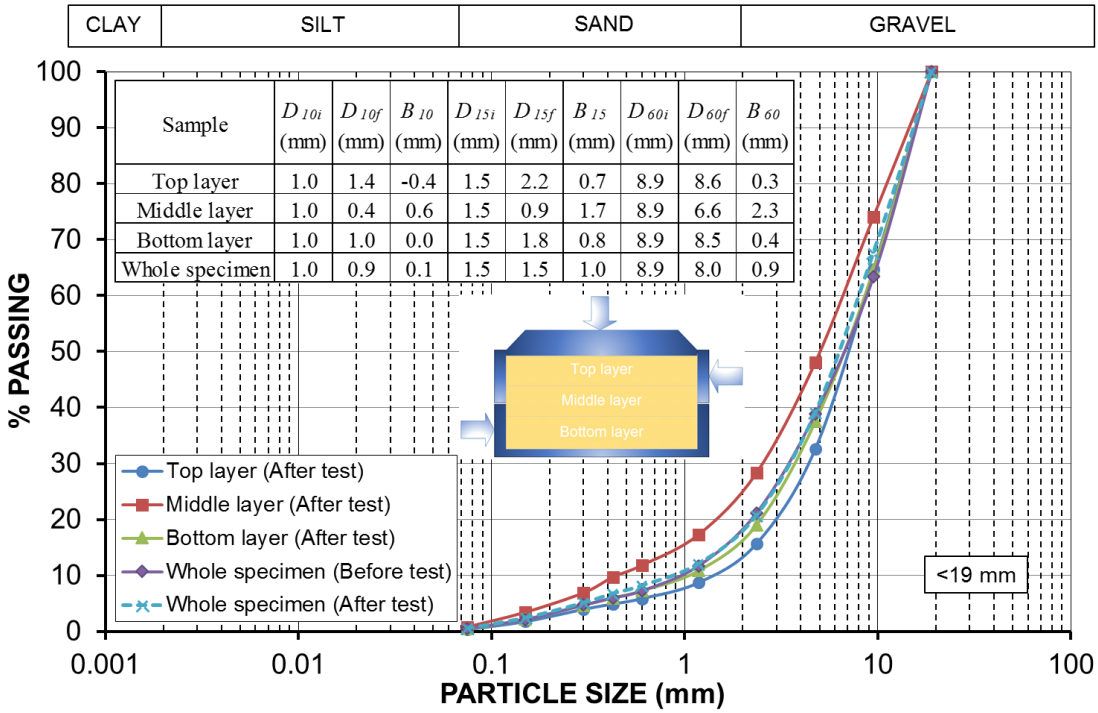

Figure 13 Particle size distribution curves of the three layers of scalped crusher run specimen (<19 mm) along shear box depth after shearing under applied normal stress of 1000 kPa

5 Conclusion

Scalping is an essential process for a quarry to produce a series of crusher run products with specific grading specifications for various applications. In this study, the effects of scalping on direct shear strength of crusher run and interface shear strength between crusher run and geogrid were investigated through large-scale direct and interface shear

testing. Particle breakage of the specimen was assessed through sieving analyses before and after the shear tests. The main findings were summarised as follows:

(1) Scalping can cause a pronounced reduction in direct and interface shear strength, and the failure envelopes obtained gradually decrease and flatten out with an increasing degree of scalping, resulting in a significant decrease in shear strength parameters.

(2) The interface shear strengths between the scalped crusher run specimens and the geogrid were generally lower than the internal shear strengths of the crusher run specimens alone, with average overall interface coefficients ranging from 0.767 to 0.94. The interface friction angle δ was generally lower than the friction angle ϕ, whereas the apparent adhesion ca was slightly higher than the apparent cohesion *c*.

(3) Although some large particle crushing on the top surface was observed, the overall particle breakage caused by large-scale direct and interface shear testing was not significant within a normal stress level of 1000 kPa, based on the results of the sieving analyses.

References

Abdelrahman, A., Ashmawy, A., and Abdelmoniem, M., (2008). An apparatus for direct shear, pullout, and uniaxial testing of geogrids. Geotechnical Testing Journal, 31(6), 470-479.

Abu-Farsakh, M., Coronel, J., and Tao, M., (2007). Effect of soil moisture content and dry density on cohesive soil–geosynthetic interactions using large direct shear tests. Journal of Materials in Civil Engineering, 19(7), 540-549.

Alfaro, M., Miura, N., and Bergado, D., (1995). Soil-geogrid reinforcement interaction by pullout and direct shear tests. Geotechnical Testing Journal, 18(2), 157-167.

Arulrajah, A., Rahman, M. A., Piratheepan, J., Bo, M. W., and Imteaz, M. A., (2014). Evaluation of interface shear strength properties of geogrid-reinforced construction and demolition materials using a modified large-scale direct shear testing apparatus. Journal of Materials in Civil Engineering, 26(5), 974-982.

ASTM. (2012). Standard test method for determining the coefficient of soil and geosynthetic or geosynthetic and geosynthetic friction by the direct shear method. D5321-12, West Conshohocken, PA.

Bakeer, R. M., Sayed, S. M., Cates, P., and Subramanian, R., (1998). Pullout and shear tests on geogrid reinforced lightweight aggregate. Geotextiles and Geomembranes, 16(2), 119-133.

Bathurst, R., and Karpurapu, R., (1993). Large-scale triaxial compression testing of geocell-reinforced granular soils. Geotechnical Testing Journal, 16(3), 296-303.

Cerato, A., and Lutenegger, A., (2006). Specimen size and scale effects of direct shear box tests of sands. Geotechnical Testing Journal, 29(6), 507-516.

Chen, Q., Abu-Farsakh, M., and Tao, M., (2009). Laboratory evaluation of geogrid base reinforcement and corresponding instrumentation program. Geotechnical Testing Journal, 32(6), 516-525.

Chen, X., Zhang, J., and Li, Z., (2014). Shear behaviour of a geogrid-reinforced coarse-grained soil based on large-scale triaxial tests. Geotextiles and Geomembranes, 42(4), 312-328.

Cho, G.-C., Dodds, J., and Santamarina, J. C., (2006). Particle Shape Effects on Packing Density, Stiffness, and Strength: Natural and Crushed Sands. Journal of Geotechnical and Geoenvironmental Engineering, 132(5), 591-602.

Einav, I., (2007a). Breakage mechanics—Part I: Theory. Journal of the Mechanics and Physics of Solids, 55(6), 1274-1297.

Einav, I., (2007b). Breakage mechanics—Part II: Modelling granular materials. Journal of the Mechanics and Physics of Solids, 55(6), 1298-1320.

Giroud, J. P., and Han, J., (2004). Design method for geogrid-reinforced unpaved roads. I. Development of design method. Journal of Geotechnical and Geoenvironmental Engineering, 130(8), 775-786.

Hardin Bobby, O., (1985). Crushing of Soil Particles. Journal of Geotechnical Engineering, 111(10), 1177-1192.

Indraratna, B., Karimullah Hussaini, S., and Vinod, J., (2012). On the shear behavior of ballast-geosynthetic interfaces. Geotechnical Testing Journal, 35(2), 305-312.

Indraratna, B., Sun, Q. D., and Nimbalkar, S., (2014). Observed and predicted behaviour of rail ballast under monotonic loading capturing particle breakage. Canadian Geotechnical Journal, 52(1), 73-86.

Indraratna, B., Wijewardena, L. S. S., and Balasubramaniam, A. S., (1993). Large-scale triaxial testing of grey wacke rockfill. Géotechnique, 43(1), 37-51.

Kim, D., and Ha, S., (2014). Effects of particle size on the shear behavior of coarse grained soils reinforced with geogrid. Materials, 7(2), 963-979.

Kwon, J., and Tutumluer, E., (2009). Geogrid base reinforcement with aggregate interlock and modeling of associated stiffness enhancement in mechanistic pavement analysis. Transportation Research Record: Journal of the Transportation Research Board, 2116, 85-95.

Lade, P. V., Yamamuro, J. A., and Bopp, P. A., (1996). Significance of particle crushing in granular materials. Journal of Geotechnical Engineering, 122(4), 309-316.

Lee, K. L., and Farhoomand, I., (1967). Compressibility And Crushing Of Granular Soil In Anisotropic Triaxial Compression. Canadian Geotechnical Journal, 4(1), 68-86.

Lenart, S., Koseki, J., Miyashita, Y., and Sato, T., (2014). Large-scale triaxial tests of dense gravel material at low confining pressures. Soils and Foundations, 54(1), 45-55.

Leps, T. M., (1970). Review of shearing strength of rockfill. In Proceedings of ASCE, Journal of Soil Mechanics and Foundation Engineering Division, 96(SM4), 1159-1170.

Liu, C. -N., Ho, Y. -H., and Huang, J. -W., (2009a). Large scale direct shear tests of soil/PET-yarn geogrid interfaces. Geotextiles and Geomembranes, 27(1), 19-30.

Liu, C. -N., Zornberg, J. G., Chen, T. -C., Ho, Y. -H., and Lin, B. -H., (2009b). Behavior of geogrid-sand interface in direct shear mode. Journal of Geotechnical and Geoenvironmental Engineering, 135(12), 1863-1871.

Maqbool, S., and Koseki, J., (2010). Large-scale triaxial tests to study effects of compaction energy and large cyclic loading history on shear behavior of gravel. Soils and Foundations, 50(5), 633-644.

Nair Asha, M., and Latha, G. M., (2015). Large diameter triaxial tests on geosynthetic-reinforced granular subbases. Journal of Materials in Civil Engineering, 27(4), 04014148.

Nakao, T., and Fityus, S., (2008). Direct shear testing of a marginal material using a large shear box. Geotechnical Testing Journal, 31(5), 393-403.

Qian, Y., Mishra, D., Tutumluer, E., and Kazmee, H. A., (2015). Characterization of geogrid reinforced ballast behavior at different levels of degradation through triaxial shear strength test and discrete element modeling. Geotextiles and Geomembranes, 43(5), 393-402.

Tutumluer, E., Huang, H., and Bian, X., (2012). Geogrid-aggregate interlock mechanism investigated through aggregate imaging-based discrete element modeling approach. International Journal of Geomechanics, 12(4), 391-398.

Ueda, T., Matsushima, T., and Yamada, Y., (2011). Effect of particle size ratio and volume fraction on shear strength of binary granular mixture. Granular Matter, 13(6), 731-742.

Vallerga, B., Seed, H., Monismith, C., and Cooper, R., (1957). Effect of shape, size, and surface roughness of aggregate particles on the strength of granular materials. ASTM International, Special Technical Publication 212, 63–76, West Conshohocken, PA.

Vangla, P., and Latha Gali, M., (2016). Effect of particle size of sand and surface asperities of reinforcement on their interface shear behaviour. Geotextiles and Geomembranes, 44(3), 254-268.

Vieira, C. S., and Pereira, P. M., (2015). Interface shear properties of geosynthetics and construction and demolition waste from large-scale direct shear tests. Geosynthetics International, 23(1), 62-70.

Wang, J. -J., Zhang, H. -P., Tang, S. -C., and Liang, Y., (2013). Effects of particle size distribution on shear strength of accumulation soil. Journal of Geotechnical and Geoenvironmental Engineering, 139(11), 1994-1997.

Wu, P., Matsushima, K., and Tatsuoka, F., (2008). Effects of specimen size and some other factors on the strength and deformation of granular soil in direct shear tests. Geotechnical Testing Journal, 31(1), 45-64.

Xiao, Y., and Liu, H., (2017). Elastoplastic constitutive model for rockfill materials considering particle breakage. International Journal of Geomechanics, 17(1), 04016041.

Xiao, Y., Liu, H., Chen, Q., Ma, Q., Xiang, Y., and Zheng, Y., (2017). Particle breakage and deformation of carbonate sands with wide range of densities during compression loading process. Acta Geotechnica, 12(5), 1177-1184.

Xiao, Y., Liu, H., Chen, Y., and Jiang, J., (2014a). Strength and deformation of rockfill material based on large-scale triaxial compression tests. I: Influences of density and pressure. Journal of Geotechnical and Geoenvironmental Engineering, 140(12), 04014070.

Xiao, Y., Liu, H., Chen, Y., and Jiang, J., (2014b). Strength and deformation of rockfill material based on large-scale triaxial compression tests. II: Influence of particle breakage. Journal of Geotechnical and Geoenvironmental Engineering, 140(12), 04014071.

Xu, M., Song, E., and Chen, J., (2012). A large triaxial investigation of the stress-path-dependent behavior of compacted rockfill. Acta Geotechnica, 7(3), 167-175.

Yu, X., Ji, S., and Janoyan Kerop, D., (2006). Direct shear testing of rockfill material. GeoShanghai 2006, ASCE, Reston, VA, 149–155.

Zhang, B., Jie, Y., and Kong, D., (2013a). Particle breakage of cement ellipsoid aggregate-Part II: Investigation of particle crushing. Journal of Testing and Evaluation, 41(5), 761-769.

Zhang, B., Jie, Y., and Kong, D., (2013b). Particle size distribution and relative breakage for a cement ellipsoid aggregate. Computers and Geotechnics, 53(Supplement C), 31-39.

Zhang, B., Jie, Y., and Kong, D., (2014). Particle breakage of cement ellipsoid aggregate-Part I: Triaxial compression tests. Journal of Testing and Evaluation, 42(1), 170-180.

Zhang, X., and Baudet, B. A., (2013). Particle breakage in gap-graded soil. Géotechnique Letters, 3(2), 72-77.

Zhao, H. F., Zhang, L. M., and Chang, D. S., (2013). Behavior of coarse widely graded soils under low confining pressures. Journal of Geotechnical and Geoenvironmental Engineering, 139(1), 35-48.

Attached Paper III

Paper III: Measurement of Shear Strength and Interface Parameters by Multi-Stage Large-scale Direct/Interface Shear and Pull-out Tests

Xu, Y., Williams, D. J., Serati, M., 2018. Measurement of Shear Strength and Interface Parameters by Multi-Stage Large-scale Direct/Interface Shear and Pull-out Tests. Measurement Science and Technology. 29 (8) 085601. https://doi.org/10.1088/1361-6501/aacb8a – incorporated as **Paper III**.

Multi-stage Testing in Large-scale Direct/Interface Shear and Pull-out Tests

Youwei Xu[a,], David J. Williams[b], Mehdi Serati[c]*

[a] PhD candidate, School of Civil Engineering, The University of Queensland, Brisbane, QLD 4072, Australia. Email: youwei.xu@uq.edu.au

[b] Professor, School of Civil Engineering, The University of Queensland, Brisbane, QLD 4072, Australia. Email: d.williams@uq.edu.au

[c] Postdoctoral Research Fellow, School of Civil Engineering, The University of Queensland, Brisbane, QLD 4072, Australia. Email: m.serati@uq.edu.au

Abstract

It is essential to measure the shear strength of soils and interface parameters between soils and geosynthetics for the safe design and stability analysis of geosynthetic-reinforced soil structures. These parameters recommended for engineering projects are normally measured by laboratory single-stage direct/interface shear and pull-out tests. The conventional single-stage tests are carried out on at least three representative specimens under three different normal stresses. However, a large quantity of specimens is required for large-scale tests, with tedious sample preparation procedures, so that large-scale single-stage testing becomes very labour intensive, time consuming and expensive. Given that the multi-stage testing method is able to measure the shear strength parameters by testing only one representative specimen, this paper investigates the feasibility, reliability and applicability of the multi-stage testing method in large-scale direct/interface shear and pull-out tests. Two compacted soils and a geogrid were tested using both single-stage and multi-stage tests. It was found that the shear strengths obtained from the multi-stage tests were slightly lower that those obtained from the single-stage tests, and the inferred apparent cohesion and friction angle matched closely. In addition, the limitations of the multi-stage testing method were highlighted. The measured direct shear strength of the

soils, the interface shear strength and pull-out shear strength between the soils and the geogrid are also compared and discussed in this paper.

Keywords: direct shear test; geosynthetics; interface shear test; pull-out test; multi-stage; single-stage

1 Introduction

Direct/interface shear and pull-out tests are commonly used laboratory techniques to measure the shear strength parameters of soils and the interface parameters between soils and geosynthetics. These parameters are necessary for the safe design and stability analysis of geosynthetic-reinforced soil structures. The interface shear test is the most appropriate experimental method for the analysis of soil-geosynthetic interaction when the sliding of the soil mass on the reinforcement surface is likely to occur. However, the pull-out test is more relevant to the study of soil-geosynthetic interaction when the failure surface shears through the geosynthetic in the anchorage zone (Change et al. 2000; Palmeira, 2009; Lopes, 2012; Bathurst and Ezzein 2015; Ferreira et al. 2015; Mosallanezhad et al. 2015; Xu et al. 2018a). Nonetheless, both the two testing methods can be adopted in the laboratory to measure the interface parameters between the soil and the geosynthetic, such as interface friction angles, apparent adhesions and interface coefficients. However, the relationship between the interface shear stress and pull-out shear stress mobilised along the soil-geosynthetic interface in these two testing methods is still a very controversial topic and may produce significantly different interface parameters for design. (Bergado et al.1994; Alfaro et al. 1995; Mallick et al. 1996; Lopes and Silvano 2010; Hsieh et al. 2011).

Mallick et al. (1996) demonstrated that the surface roughness of the geosynthetic and the interlocking between the soil and geosynthetic could influence the frictional resistance in interface shear tests. Apart from the two factors, the geosynthetic extensibility should be taken into account in pull-out tests. The maximum extension of the geosynthetic in an interface shear test is much smaller than that in a pull-out test. This is because the geosynthetic is usually fixed and clamped on the shear box for interface testing, while the geosynthetic is embedded in the soil with its end being pulled for pull-out testing. Lopes and Silvano (2010) have shown that the average pull-out interface coefficients are approximately 55% of the direct shear interface coefficients for a residual granite soil-

geotextile interface in their study, indicating that the pull-out shear strengths obtained from the pull-out tests were much lower than the interface shear strengths obtained from the direct shear tests. By contrast, Hsieh et al. (2011) compared the direct shear and pull-out test results for different types of soil-geosynthetic interfaces and observed that the interface shear stress and pull-out shear stress were close for the crushed stone geotextile interface, while the pull-out shear stress was much higher than the interface shear stress for the crushed stone-geogrid interface. In addition, they also concluded that there existed a linear relationship between the interface shear stress and the applied normal stress for the interface shear tests between crushed stone and geogrid, but the pull-out shear stress appeared to have no consistent relationship with the applied normal stress for the pull-out tests.

The earliest literature concerning multi-stage testing that could be found is a Master's thesis written by Gullic in 1970, at the University of Missouri-Rolla, USA. Gullic (1970) performed a series of multi-stage direct shear tests on a cohesionless soil using a small shear box with a diameter of 62.0 mm and a specimen height of 25.8 mm. Five different multi-stage direct shear testing procedures were studied and compared with conventional single-stage results. Later, Gan and Fredlund (1988) proposed a multi-stage direct shear testing method for unsaturated soils by applying multiple matric suctions on the same specimen. More recently, Hormdee et al. (2012) performed the multi-stage direct shear testing of loess soil under drained conditions using a conventional small direct shear apparatus. Petro et al. (2017) carried out the standard and limited displacement multi-stage direct shear tests on rough rock joints, corresponding to the two multi-stage testing procedures. In general, a good agreement was observed based on their obtained plots of shear stress versus shear displacement. However, it would be very difficult to determine when to cease the shearing or when a peak stress has been achieved, especially for brittle rock samples.

Similar to the multi-stage direct shear testing, there is also very limited multi-stage pull-out testing research work available. For instance, a Master's thesis written by Pradhan, at The University of Hong Kong, China, can be cited. Pradhan (2003) performed both single-stage and multi-stage pull-out tests on soil nails in completely decomposed granite fill and compared the peak pull-out resistances obtained. He concluded that the peak pull-out resistances obtained from the single-stage tests were higher than those from the multi-

stage tests. This is because a continuing reduction in the length of the nail embedded in the soil in the later stages of the multi-stage tests caused a significant reduction in the soil-nail contact surface. Therefore, the peak pull-out resistance obtained was lower than that obtained from the single-stage test under the same normal stress. Another multi-stage pull-out testing method proposed by Moraci and Cardile (2009) was actually a cyclic tensile loading test, which differed from the multi-stage testing method in Pradhan (2003) and that proposed in this paper. Overall, previous studies have not applied the multi-stage testing method in the large-scale interface shear and pull-out tests on the soil-geosynthetic interfaces. Therefore, the application of the multi-stage testing to both large-scale direct/interface shear and pull-out tests deserves further investigation.

In summary, the main aims of this paper are: 1) to investigate the feasibility, reliability and applicability of the multi-stage testing in large-scale direct/interface shear and pull-out tests by testing the compacted soils and a geogrid, 2) to construct an empirical relationship between the single-stage and multi-stage test results based on the collected data; 3) to study the process of shear stress mobilisation during the shearing and pulling in the direct/interface shear and pull-out tests; and 4) to develop empirical relationships between the measured direct shear strength of the soil, the interface shear strength and pull-out shear strength between the soil and geosynthetic so that they could be predicted from one another.

2 Soil-geogrid Interaction Mechanism

The stability of geosynthetic-reinforced soil structures is highly dependent on the soil-geosynthetic interfaces. The interaction mechanism between the soil and geotextile (or other simple sheet types of geosynthetics) is only attributed to the frictional resistance mobilised along the continuous geotextile surface. However, due to the presence of apertures in geogrid products, the interaction mechanism between the soil and geogrid is much more complex than that between the soil and geotextile.

The direct shear resistance between the soil and the geogrid in direct shear tests has two components: (1) frictional resistance between the soil and the geogrid ribs along the single shear surface; and (2) frictional resistance between the soil and the soil in the geogrid apertures. This mechanism can be theoretically interpreted using the following equation (Jewell et al. 1984):

$$\tau_{ds} = f_{ds}\sigma_n \tan\phi = \sigma_n \left[\alpha_{ds} \tan\delta + (1-\alpha_{ds}) \tan\phi\right] \quad (1)$$

where ϕ is the internal friction angle of soil, δ_0 is the friction angle between soil and geogrid ribs, f_{ds} is the direct shear interface coefficient, α_{ds} is the proportion of the surface area of the geogrid ribs in contact with the soil, i.e., the area of ribs (longitudinal and transverse) relative to the total geogrid area, σ_n is the normal stress and τ_{ds} is the interface shear strength between the geogrid and the soil.

From the experimental results of interface shear tests, the interface shear strength τ_{ds} can be interpreted by the Mohr-Coulomb criteria:

$$\tau_{ds} = c_a + \sigma_n \tan\delta \quad (2)$$

where τ_{ds} is the interface shear strength obtained from the interface shear test, c_a is the apparent adhesion between the geogrid and the soil, and δ is the interface friction angle. Thus, the interface coefficient f_{ds} can then be calculated as:

$$f_{ds} = \frac{c_a + \sigma_n \tan\delta}{c + \sigma_n \tan\phi} = \frac{\tau_{ds}}{\tau_s} \quad (3)$$

Additionally, the pull-out resistance also has two components: (1) frictional resistance between the geogrid ribs and the soil above and below the geogrid (double shear surfaces); and (2) passive bearing resistance provided by the transverse ribs in the apertures. This mechanism can be interpreted by the following equation (Jewell 1990):

$$P_R = P_{RS} + P_{RB} = 2 f_b L_R \sigma_n \tan\phi \quad (4)$$

where P_R is the pull-out resistance per unit width, P_{RS} is the frictional component of the pull-out resistance, P_{RB} is the bearing component of the pull-out resistance, L_R is the reinforcement length in the anchorage zone, f_b is the pull-out interface coefficient. The following equations can be used to evaluate the frictional component P_{RS} and bearing component P_{RB} of the pull-out resistance:

$$P_{RS} = 2\alpha_{ds} L_R \sigma_n \tan\delta \quad (5)$$

$$P_{RB} = \left(\frac{L_R}{S}\right) \alpha_B \sigma_b B \quad (6)$$

where S is the spacing between the geogrid bearing members, L_R/S is the number of geogrid bearing members, α_B is the fraction of the total frontal area of the geogrid available for bearing resistance, B is the bearing member thickness, and σ_b is the bearing stress against the geogrid bearing members, which can be calculated using different bearing capacity theories (Peterson and Anderson 1980; Jewell et al. 1985; Matsui et al. 1996).

From the experimental results, the pull-out interface coefficient f_b can be further expressed as a ratio of the maximum shear stress mobilised at the soil-geosynthetic interface in the pull-out test to the shear strength of soil alone obtained from the direct shear test:

$$f_b = \frac{P_R}{2L_R(c + \sigma_n \tan\phi)} = \frac{\tau_p}{\tau_s} \tag{7}$$

where τ_p is the shear strength in the pull-out test, τ_s is the direct shear strength of soil alone. Therefore, the shear stress mobilised at the soil-geogrid interface in the pull-out test can be calculated using the following equation:

$$\tau_p = \frac{P_R}{2L_R} \tag{8}$$

From the experimental results of the pull-out tests, the pull-out shear strength τ_p can also be interpreted by the interface shear strength parameters as in Eq. (9),

$$\tau_p = c_a + \sigma_n \tan\delta \tag{9}$$

where τ_p is the pull-out shear strength obtained from the experimental pull-out results, c_a is the apparent adhesion between soil and geogrid, δ is the interface friction angle. Herein, the interface shear strength parameters c_a and δ are also obtained from a best-fit straight line (that is, the pull-out shear strength failure envelope).

The relationship between the pull-out shear strength τ_p and interface shear strength τ_{ds} mobilised along the soil-geogrid interface can be defined as a parameter α, which is also called scale effect correction factor according to the Federal Highway Administration (FHWA) in USA (Christopher et al. 1990; Elias et al. 2001; Berg et al. 2009).

$$\alpha = \frac{P_R}{2L_R(c_a + \sigma_n \tan\delta)} = \frac{\tau_p}{\tau_{ds}} \tag{10}$$

From Eqs. (3), (7) and (10), the following relationship between the interface coefficients obtained from the interface shear and pull-out tests can be found:

$$\alpha = \frac{f_b}{f_{ds}} \tag{11}$$

In summary, the soil-geogrid interaction mechanisms interpreted above in interface shear and pull-out tests are depicted in Figure 1, to clearly present each component.

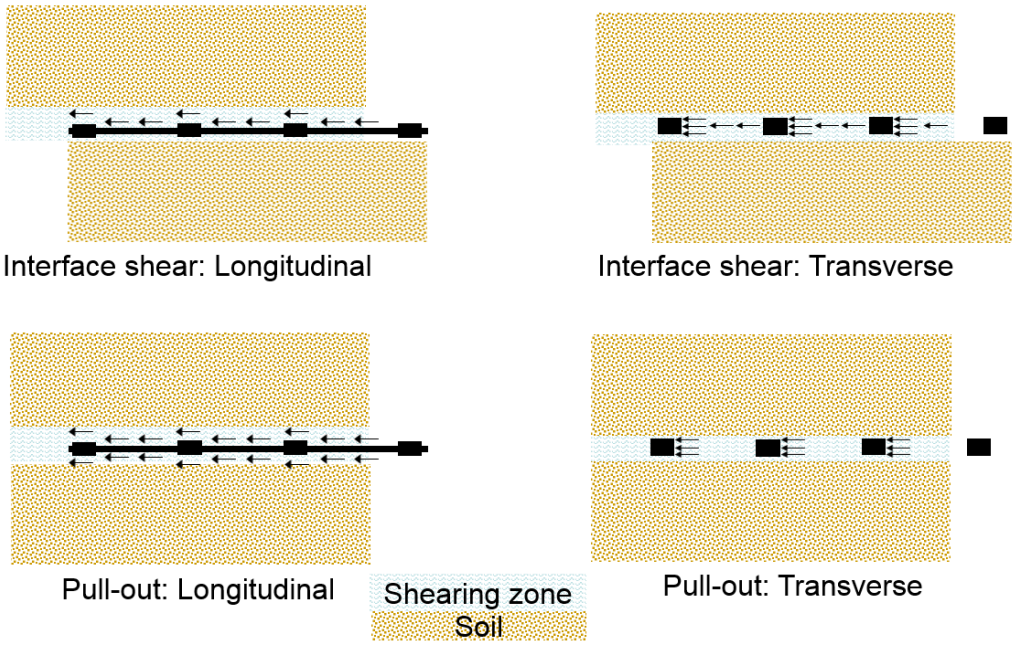

Figure 1 Soil-geogrid interaction mechanisms for interface shear and pull-out testing

3 Multi-stage Testing Methodology

The conventional single-stage test need to be carried out on a minimum of three identical specimens individually under three applied normal stresses, i.e., at least three specimens are required and tested separately. In order to reduce the time and expense of the laboratory testing, it is possible to use only one representative specimen to measure the shear strength, which is defined as the multi-stage testing method (Gullic 1970). The multi-stage testing procedure adopted in this study for direct/interface shear and pull-out tests comprises the following. The specimen is compressed under the first stage normal stress. After the practical completion of compression, the specimen is sheared/pulled out at a constant rate until failure or until a certain predetermined displacement is achieved. When

the failure occurs, the test is stopped, and the normal stress is increased to the next predetermined level. The specimen is again allowed to compress under the new normal stress. After that, the specimen is again sheared/pulled out at the same constant rate until the second failure. This process is repeated for three or more stages (see Figure 2).

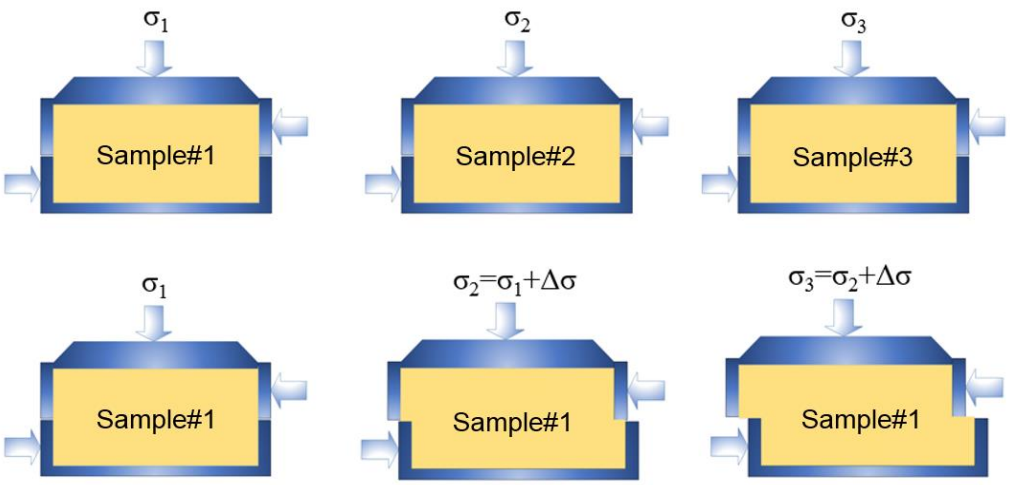

(a)

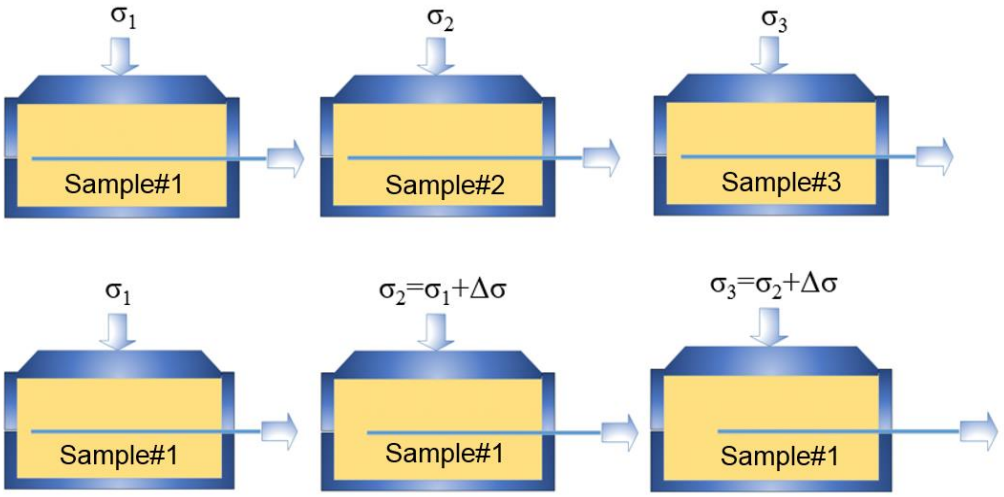

(b)

Figure 2 Single-stage and multi-stage testing in: (a) direct/interface shear test; (b) pull-out test

Comparing the procedures of the single-stage and multi-stage methods, it is found that carrying out single-stage, large-scale tests are both time consuming and labour intensive, resulting in much higher costs. In general, to measure the shear strength parameters for

engineering applications, the total cost of single-stage testing (three tests) will be approximately three times greater than the cost of multi-stage testing (only one test), regardless of more sampling costs that may be involved due to more specimens being required. Therefore, the multi-stage testing method introduced above was attempted in the large-scale direct/interface shear and pull-out tests in this study.

4 Experimental Program

4.1 Test Materials

To pursue the objectives of this study, Australian roadbase materials were collected from Pine Mountain Quarry, Brisbane, and tested at the Geomechanics Laboratory of the Geotechnical Engineering Centre at The University of Queensland (UQ). This included Australian Type 2.1 granite roadbase (designated as roadbase) and greenstone crusher dust (designated as dust). The particle size distributions of the roadbase materials are given in Figure 3. Also, Tensar SS40 geogrid (with a tensile strength of 40 kN/m) was used in this study to carry out the interface shear and pull-out tests, as shown in Figure 4. This type of biaxial geogrid, manufactured from a punched polypropylene sheet, is commonly used to reinforce roadbase materials and to stabilise weak subgrade soils in road pavement construction in Australia. In summary, the basic properties of the test materials are shown in Table 1.

Table 1 Basic properties of tested materials

Soil	D_{50} (mm)	C_u	C_c	G_s	OMC (%)	ρ_{dmax} (t/m^3)	USCS
Roadbase	3.1	15.45	1.34	2.706	6.1	2.275	GW
Dust	1.8	9.58	1.16	2.725	8.8	2.158	SW

Geogrid	Polymer	Aperture Shape	Tensile Strength (kN/m)	Aperture size (mm)	Nodal thickness (mm)	Nominal rib thickness (mm)	Opening area (%)
Tensar SS40	Polypropylene	Square	40	33×33	5.8	2.5	77.4

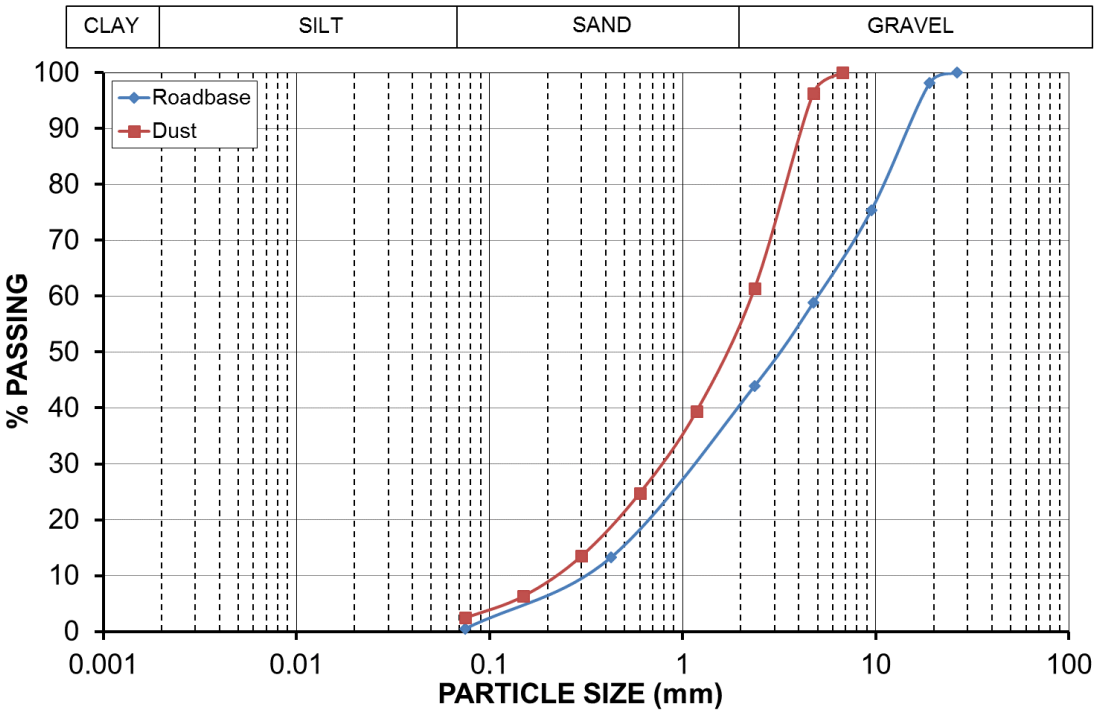

Figure 3 Particle-size distribution curves of tested soils

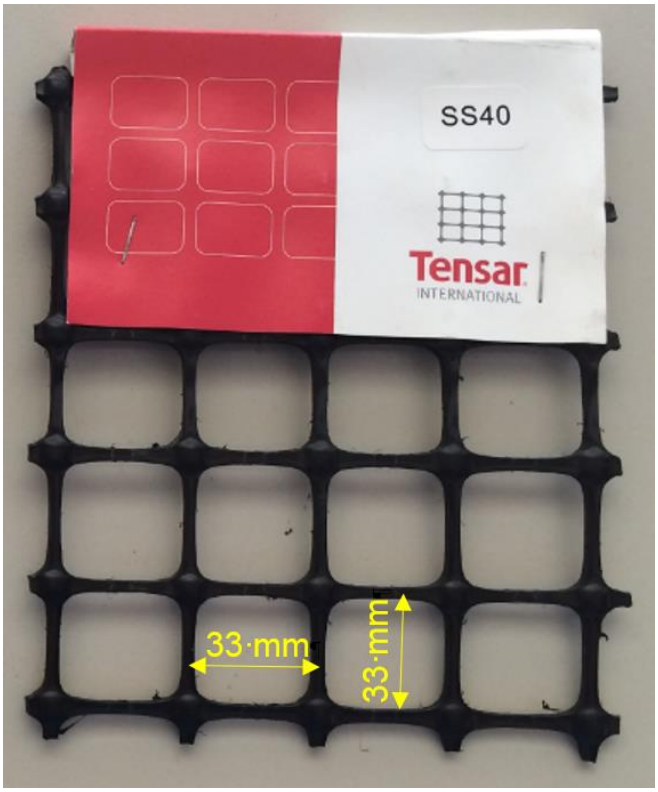

Figure 4 Tensar SS40 geogrid

4.2 Testing Equipment

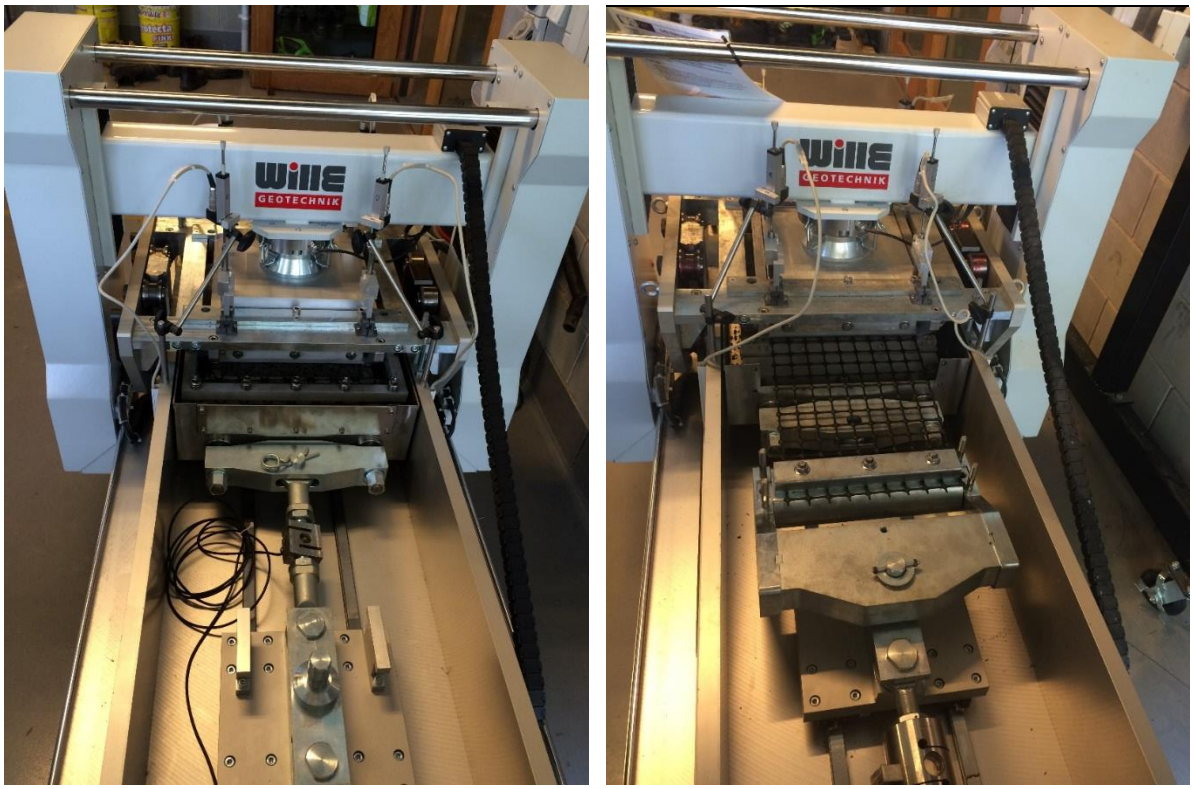

(a) (b)

Figure 5 Testing equipment: (a) direct/interface shear testing mode; (b) pull-out testing

A large-scale direct shear apparatus manufactured by Wille Geotechnik of Germany (capable of performing both direct/interface shear and pull-out tests) was utilised in this study, as shown in Figure 5. The shear box (pull-out box) has dimensions of 300 mm by 300 mm by 200 mm and the sides of the box are 20 mm thick. The machine is moderately stiff to accommodate a load capacity of 100 kN in both horizontal and vertical directions (up to 1000 kPa). The floating upper box is designed to create a gap between the upper and lower halves of the shear box by means of two compression springs. Four linear variable displacement transducers (LVDTs) are installed on the four corners of the top loading cap to measure settlement and tilting. In the direct shear test, the upper half is fixed and the lower half is sheared, and the shear force mobilised during shearing is measured by a load cell. The geosynthetic can be clamped by grooved clamping bars on the top of the lower shear box for interface shear testing. Furthermore, the machine can be changed into pull-out testing mode after reassembling some parts, mainly by fixing the

lower half of the shear box to the front counter-force beam, and reconnecting the pulling rod together with the load cell to a roller clamp used for clamping and pulling the geosynthetic (see Figure 5b). During the shearing or pulling processes, vertical displacement, horizontal displacement and shear force or pull-out force are measured and recorded at desired time intervals. It should be noted that the apparatus dimensions and boundary conditions do not satisfy accepted specifications for standard pull-out tests (e.g. ASTM D6706). Howevever, it is still worthwile carrying out both direct shear and pull-out tests using this apparatus to achieve the research objectives of this paper.

4.3 Testing Program

In order to evaluate the applicability, feasibility and reliability of multi-stage testing in the large-scale direct/interface shear and pull-out tests, both single-stage and multi-stage tests were carried out on the compacted roadbase materials and geogrid, under applied normal stresses of 15 kPa, 25 kPa, or 50 kPa, at the displacement rate of 1 mm/min. The normal stresses applied to the specimens represent the typical stress levels found in road pavements. The initial conditions controlled for the soils tested are summarised in Table 2. The internal shear stress τ_s of soil, interface shear stress τ_{ds} and pull-out shear stress τ_p between the soil and geogrid were obtained and compared in this study. Based on the shear strength results (τ_s, τ_{ds}, and τ_p) obtained, interface coefficients (f_{ds}, f_b and α) were then calculated and analysed.

Table 2 Initial conditions controlled for tested soils

Soils	Moisture content (%)	Specimen mass (kg)	Bulk density ρ (t/m^3)	Dry density ρ_d (t/m^3)	Void ratio
Roadbase	4.80	22	1.95	1.86	0.46
Dust	5.03	21	1.85	1.76	0.55

5 Results and Discussion

5.1 Single-stage and Multi-stage Direct/Interface Shear Testing

Large-scale, single-stage and multi-stage, direct/interface shear tests were carried out on Roadbase, Dust, Roadbase-Geogrid and Dust-Geogrid. Figure 6 compares the results of shear stress versus shear displacement plots under applied normal stresses of 15 kPa,

25 kPa or 50 kPa. In order to avoid excessive tilting of the top cap during the shearing process, a shear displacement of 30 mm (10% of total strain) was selected for the single-stage direct/interface test, while a shear displacement of 10 mm was selected for each stage of the multi-stage test, with the same total shear displacement of 30 mm after three stages. In addition, shear strength failure envelopes and inferred shear strength parameters are shown in Figure 7 (see also Tables 3 and 4). The failure envelopes were plotted using the shear strength (i.e., the shear stress at failure) against the applied normal stress at failure. Failure was taken as the maximum (ultimate) shear stress attained within a shear strain of 10%. It should be noted that both the measured shear stress and applied normal stress were corrected for the area reduction and then plotted to determine the failure envelopes.

Table 3 Direct shear test results for Roadbase and Dust

Roadbase				Dust			
Single-stage		Multi-stage		Single-stage		Multi-stage	
σ_n (kPa)	τ_s (kPa)	σ_n (kPa)	τ_s (kPa)	σ_n (kPa)	τ_s (kPa)	σ_n (kPa)	τ_s (kPa)
16.7	19.8	15.5	15.8	16.4	15.4	15.5	14.7
27.4	27.6	26.7	26.4	27.8	26.4	26.7	24.0
55.6	52.4	55.6	51.3	55.6	46.4	55.6	44.1
c (kPa)	φ (°)	c (kPa)	φ (°)	c (kPa)	φ (°)	c (kPa)	φ (°)
5.2	40.2	2.5	41.4	3.6	37.8	3.9	36.0

Table 4 Interface shear test results for Roadbase-Geogrid and Dust-Geogrid

Roadbase-Geogrid				Dust-Geogrid			
Single-stage		Multi-stage		Single-stage		Multi-stage	
σ_n (kPa)	τ_{ds} (kPa)	σ_n (kPa)	τ_{ds} (kPa)	σ_n (kPa)	τ_{ds} (kPa)	σ_n (kPa)	τ_{ds} (kPa)
16.6	20.3	15.5	17.4	16.2	17.9	15.5	15.1
27.3	29.4	26.7	27.5	27.8	26.3	26.7	24.7
54.0	52.7	55.6	50.4	55.6	48.2	55.6	45.8
c_a (kPa)	δ (°)	c_a (kPa)	δ (°)	c_a (kPa)	δ (°)	c_a (kPa)	δ (°)
5.8	41.0	5.1	39.2	5.2	37.7	3.8	37.2

From Figures 6 and 7, it can clearly be seen that the shear stress curves and failure envelopes match quite closely for the single-stage and multi-stage test results. In particular, for the first stage under the applied normal stress of 15 kPa, the shear stress

curves are almost identical (see Figure 6). However, the multi-stage testing method limits the shear displacement that can be applied to each stage. Especially under a high normal stress, more shear displacement is required to reach a peak. Moreover, the earlier stages may affect the shear strength achieved in the later stages, so the accumulated error of the ultimate shear strength for the last stage is particularly obvious, as shown in Figure 6. Therefore, the failure envelopes of the multi-stage results tend to be slightly lower than those of the single-stage results (see Figure 7). This agrees with the small-scale, multi-stage direct shear test results available in the literature (Gullic 1970; Hormdee et al. 2012). In addition, the slope of the shear stress curve for the later stages obtained from a multi-stage test tends to be steeper than that obtained from a single-stage test under the same applied normal stress. This indicates that shear stress can be mobilised more rapidly in the later stages. The soil specimen in a multi-stage test, with a pre-failure surface associated with particle reorientation, would behave in a more brittle manner than a fresh new specimen in a single-stage test. Furthermore, most of the specimens (Figures 6 a and b) of the large-scale direct shear tests show a strain-hardening behaviour for both single-stage and multi-stage tests; that is, the stress increases with strain without a peak being reached. However, some interface shear tests on the soils and geosynthetic show a slight strain-softening in the post-peak stage if a peak was achieved within 10% of the shear strain, as shown in Figures 6 c and d. A possible explanation for the different behaviour of the direct shear and interface shear tests might be that a peak tends to be achieved in interface shear tests due to the soil particle reorientation along the geogrid ribs and apertures. For all the multi-stage tests, because the maximum strain applied to each stage was limited to 3.3%, the peak shear strength was not obtained. Comparison with the single stage tests without a geogrid, suggests that slight strain-hardening behaviour would be expected, whereas with a geogrid, slight strain-softening behaviour would be expected. Despite this, the multi-stage tests gave similar shear strength parameters to the single stage tests.

As a large shear box can accommodate larger displacements than a small shear box, multi-stage testing using a large shear box can provide more reliable results than those obtained using a small shear box. Also, tedious sample preparation for a large-scale, single-stage direct shear test is both very time consuming and labour intensive because a large quantity of soil specimens is involved.

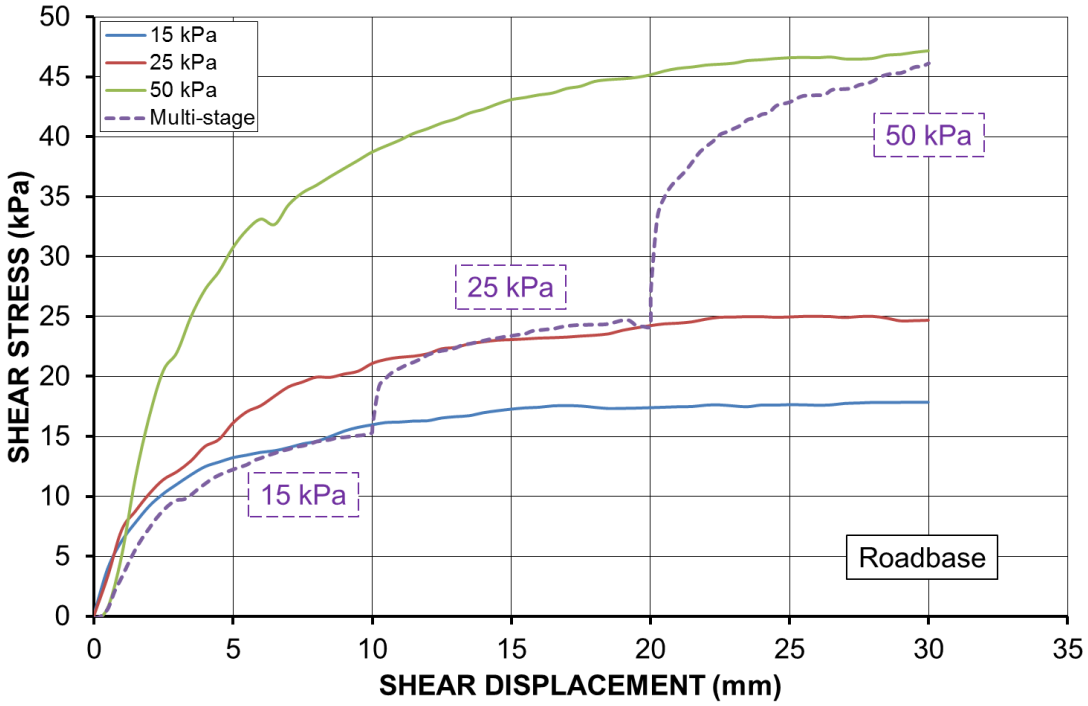
15 kPa
25 kPa
50 kPa
Multi-stage
SHEAR STRESS (kPa)
SHEAR DISPLACEMENT (mm)
50 kPa
25 kPa
15 kPa
Roadbase

(a)

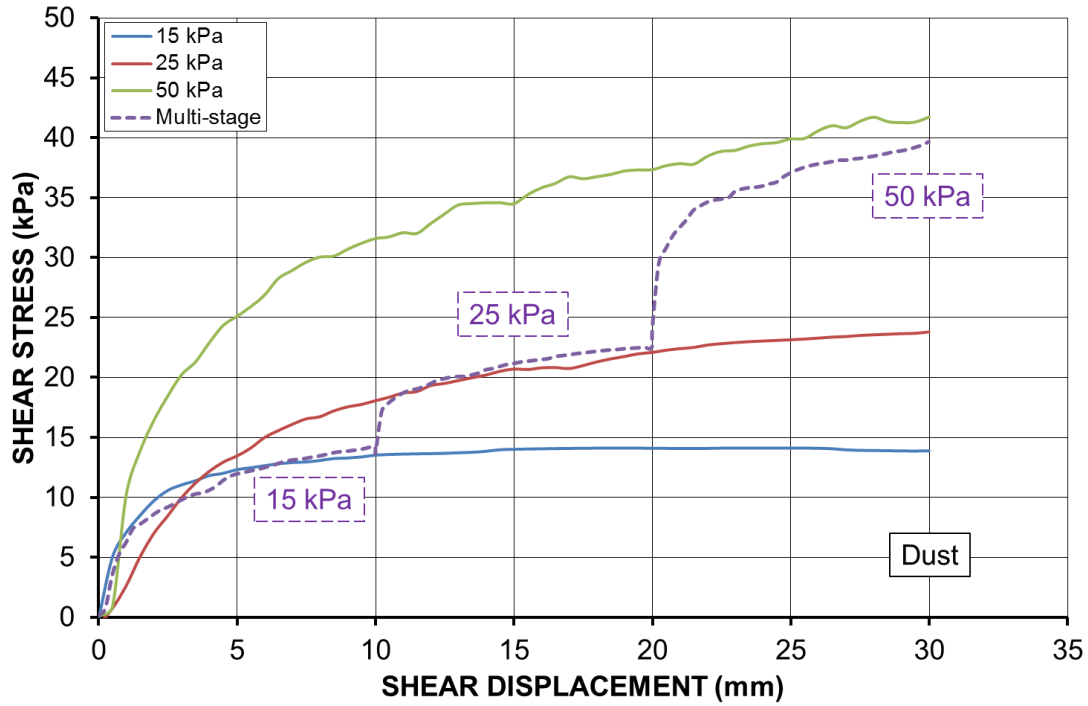
15 kPa
25 kPa
50 kPa
Multi-stage
SHEAR STRESS (kPa)
SHEAR DISPLACEMENT (mm)
50 kPa
25 kPa
15 kPa
Dust

(b)

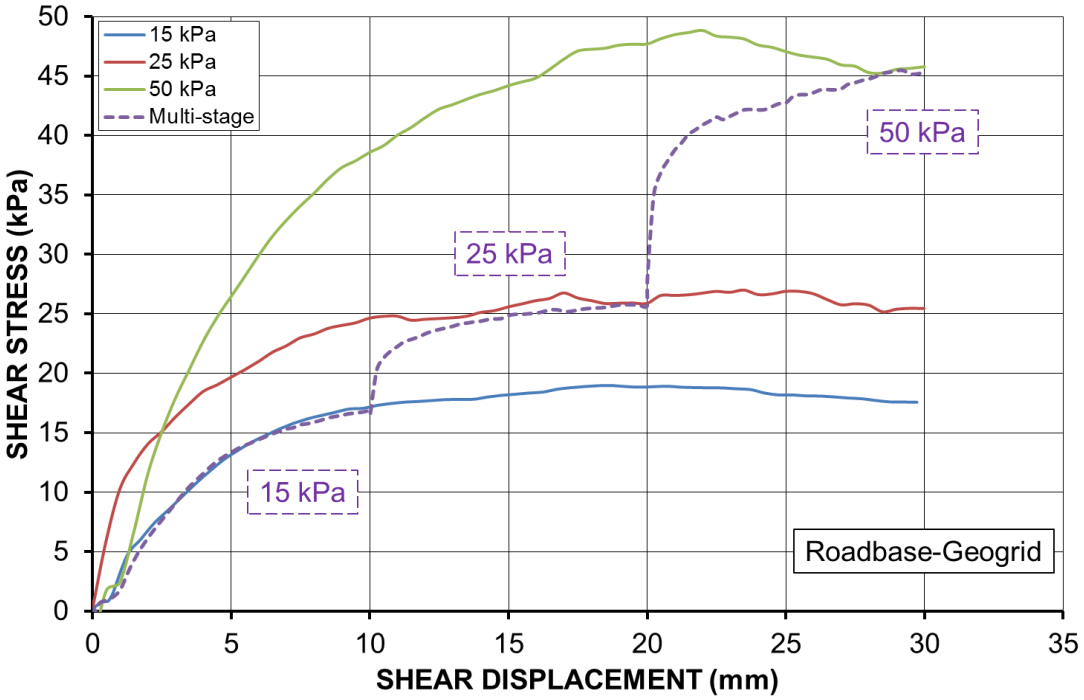

(c)

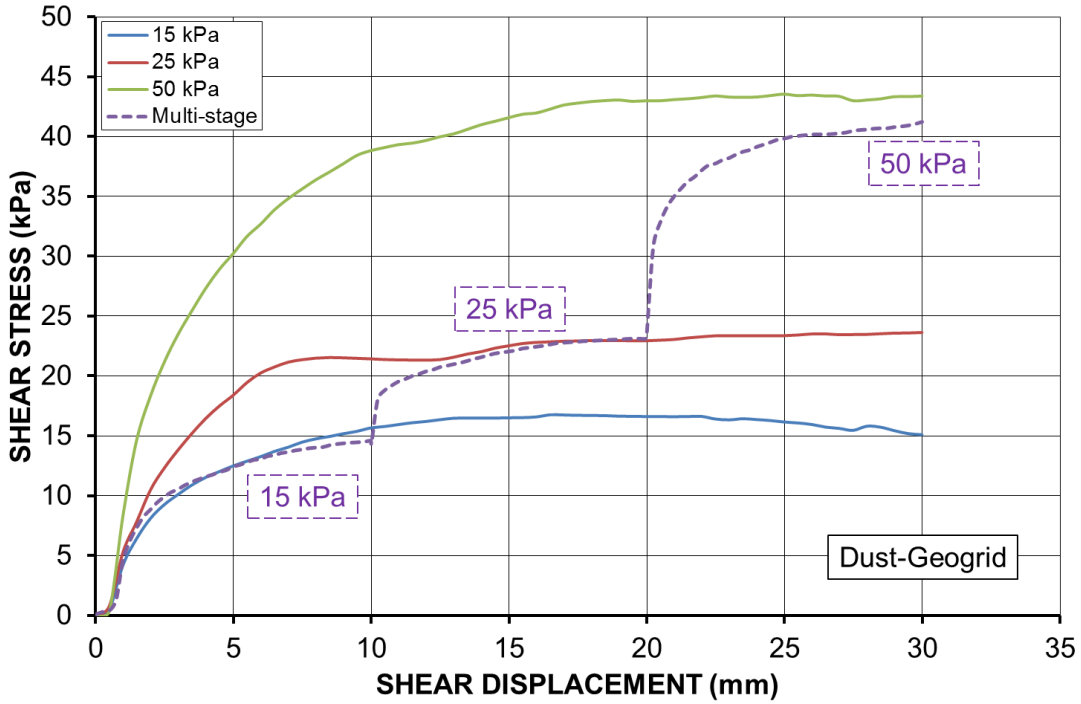

(d)

Figure 6 Single-stage and multi-stage direct/interface shear test results: (a) Roadbase; (b) Dust; (c) Roadbase-Geogrid; (d) Dust-Geogrid

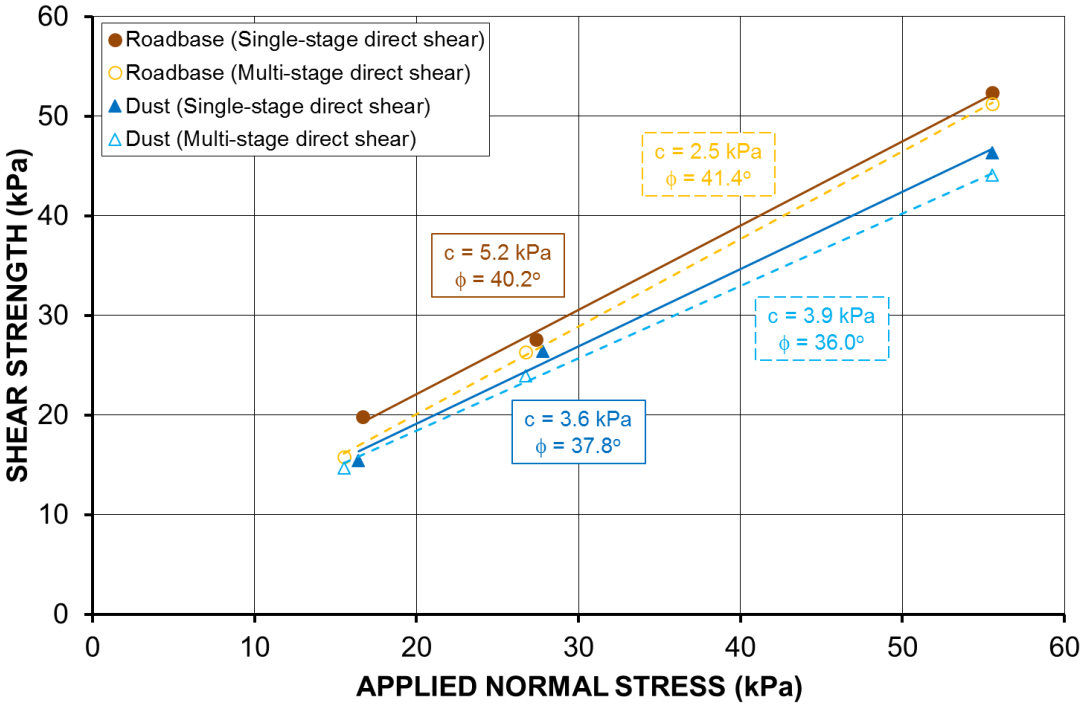

(a)

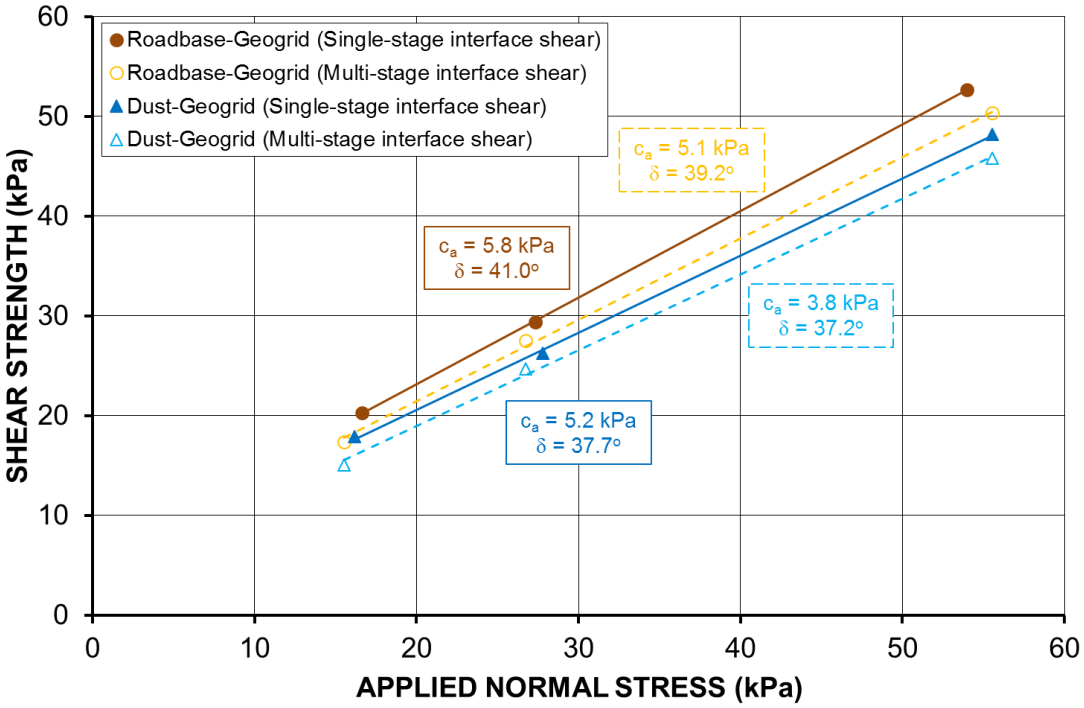

(b)

Figure 7 Comparisons of failure envelopes for single-stage and multi-stage tests: (a) direct shear; (b) interface shear

5.2 Single-stage and Multi-stage Pull-out Testing

A pull-out displacement of 60 mm was selected in the single-stage test, while a pull-out displacement of 20 mm was selected for each stage in the multi-stage test, with the same total pull-out displacement of 60 mm after three stages. Figure 8 shows the pull-out resistance versus pull-out displacement plots under applied normal stresses of 15 kPa, 25 kPa or 50 kPa for the pull-out testing of the geogrid embedded in Roadbase and Dust. The pull-out shear strength failure envelopes obtained by single-stage and multi-stage pull-out testing are compared in Figure 9, showing that the envelopes obtained from the multi-stage tests tend to be slightly lower than those from the single-stage tests, except for one shear strength data point obtained from the multi-stage pull-out testing of Roadbase-Geogrid under the applied normal stress of 50 kPa. The pull-out shear stress τ_p mobilised along the soil-geogrid interface in the pull-out tests was calculated by Eq. 8. As also shown in Figure 8, it is noteworthy that the single-stage pull-out test results tend to show an elastic-plastic behaviour with a yield point, while the multi-stage test results basically show a nonlinear-elastic behaviour. Because the multi-stage pull-out tests were limited to a maximum strain of 3.3% for each stage, it is found that the friction resistance increases with pull-out displacement throughout the pulling process, without a peak being reached.

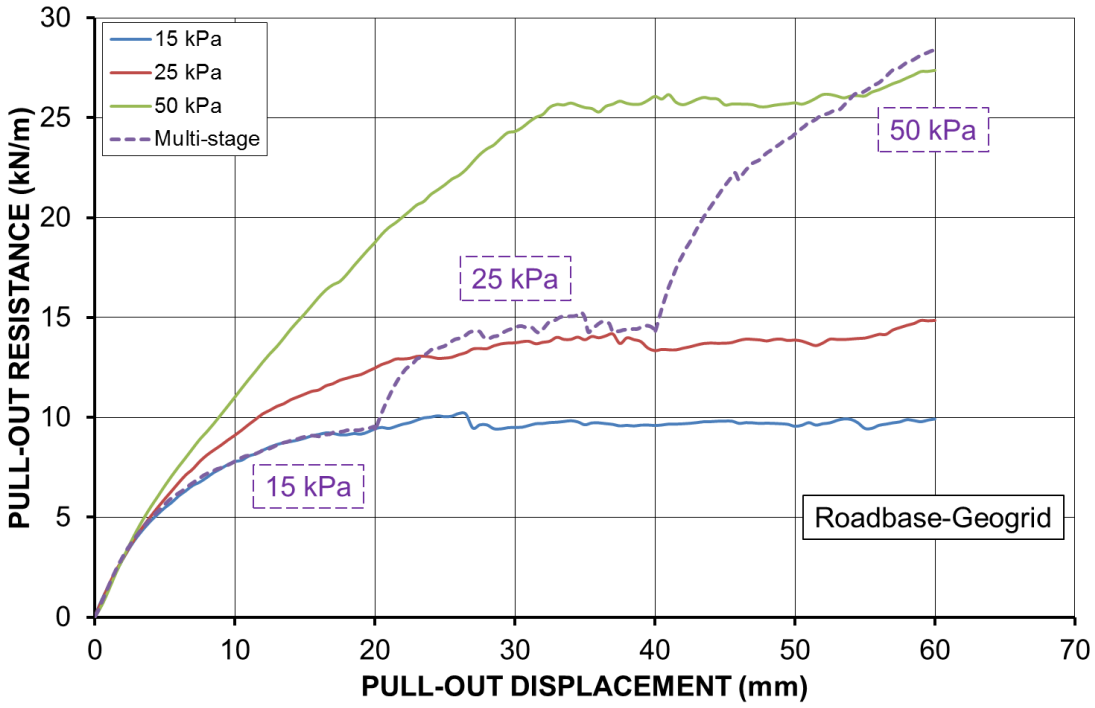

(a)

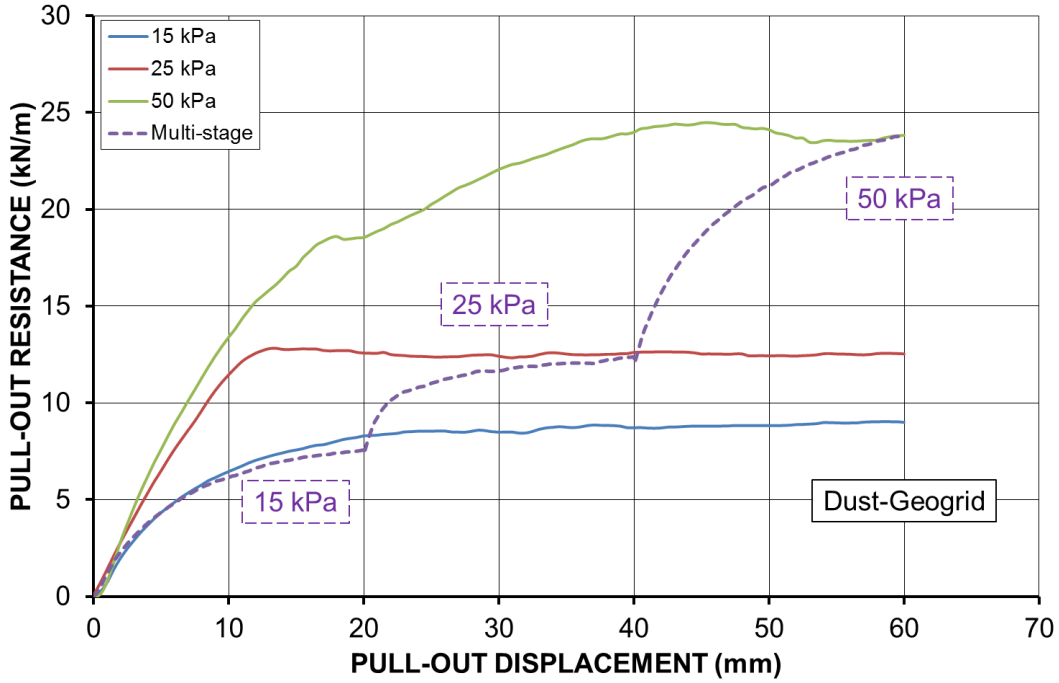

(b)

Figure 8 Single-stage and multi-stage pull-out test results: (a) Roadbase-Geogrid; (b) Dust-Geogrid

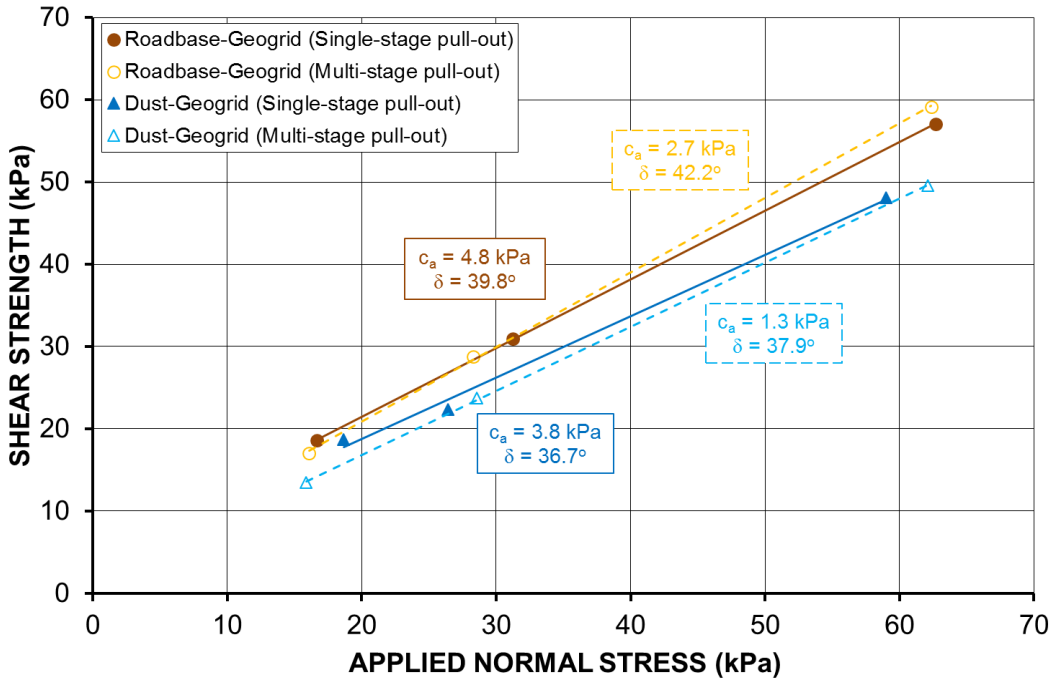

Figure 9 Comparisons of failure envelops for single-stage and multi-stage pull-out tests

Therefore, similar limitations of the multi-stage testing method in pull-out tests can be listed as: 1) multi-stage pull-out test would limit the pull-out displacement that can be applied to each stage, which may not be sufficient to achieve a peak. This is most noticeable for the final stage under the highest normal stress, which tends to require more pull-out displacement, and 2) the earlier stages may affect the maximum (ultimate) pull-out resistance achieved in the later stages. However, the maximum pull-out resistance obtained in this study still matched quite closely despite these limitations, as shown in Figures 8 and 9. All the pull-out results for Roadbase-Geogrid and Dust-Geogrid are further summarised in Table 5 for convenience.

Table 5 Pull-out test results for Roadbase-Geogrid and Dust-Geogrid

Roadbase-Geogrid				Dust-Geogrid			
Single-stage		Multi-stage		Single-stage		Multi-stage	
σ_n (kPa)	τ_p (kPa)	σ_n (kPa)	τ_p (kPa)	σ_n (kPa)	τ_p (kPa)	σ_n (kPa)	τ_p (kPa)
16.6	18.6	16.1	17.0	18.6	18.7	15.9	13.5
31.3	31.0	28.3	28.8	26.4	22.4	28.6	23.7
62.7	57.0	62.3	59.2	59.0	48.1	62.1	49.6
c_a (kPa)	δ (°)	c_a (kPa)	δ (°)	c_a (kPa)	δ (°)	c_a (kPa)	δ (°)
4.8	39.8	2.7	42.2	3.8	36.7	1.3	37.9

It should be noted that the high strength geogrids (such as the Tensar SS series) with strong ribs and thick joints have excellent tensile performance, so the extension of the geogrid embedded in roadbase materials was found to be negligible under the road service load (within 50 kPa) in the pull-out tests. However, higher applied normal stresses of 75 kPa and 100 kPa were also attempted in our study, and sudden rupture failure of the SS40 geogrid at the clamping area was found to occur frequently, instead of the pull-out failure.

(a)

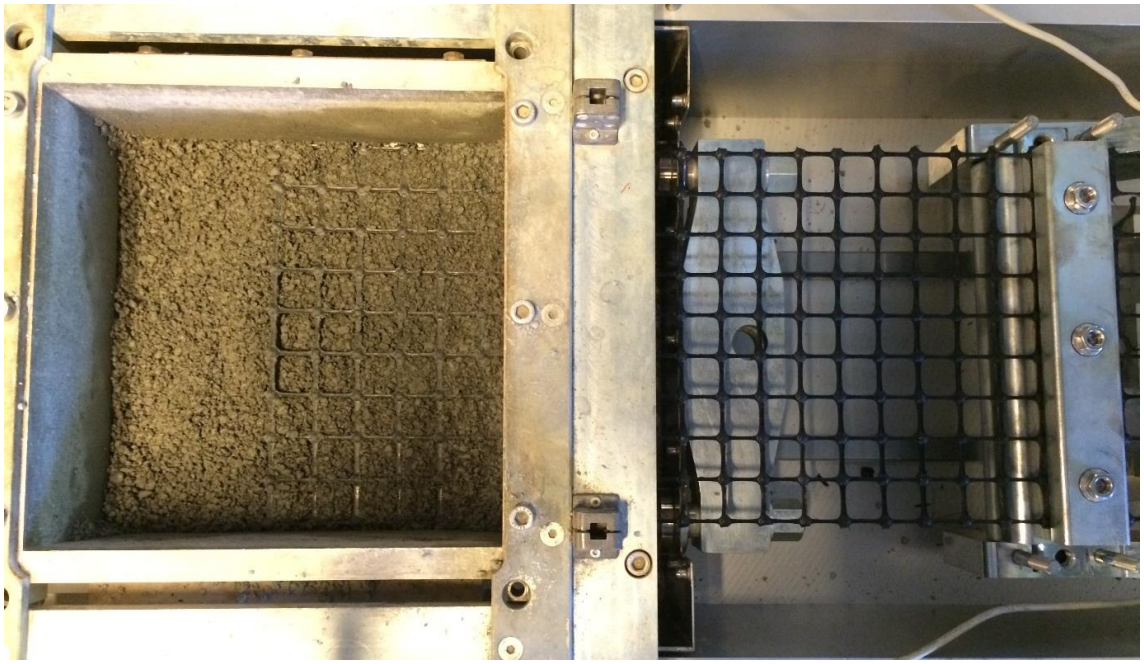

(b)

Figure 10 Two photos of Tensar SS40 geogrid embedded in soils after pull-out testing under applied normal stress of 50 kPa: (a) embedded in Roadbase; (b) embedded in Dust

Figure 10 presents two photos of Tensar SS40 geogrid embedded in Roadbase and Dust following the pull-out testing under the applied normal stress of 50 kPa (after removal of the soil on the top of the geogrid). As shown in Figure 10, the free end of the geogrid moved together with the front clamping bar during the pulling process, and all the nodes of the geogrid had the same horizontal pull-out displacement. Overall, there was no obvious extension or distortion observed for the geogrid. This observation is different from some previously published pull-out studies on different geosynthetics (Alfaro et al. 1995; Alobaidi et al. 1997; Perkins and Cuelho 1999; Moraci and Gioffre; 2006; Moraci and Recalcati 2006; Hsieh et al. 2011; Ferreira et al. 2015). These different findings could be due to three reasons: 1) the poor mechanical properties of geosynthetics tested; 2) relatively higher normal stress applied in their research, which caused significantly non-uniform deformation of geosynthetics during the pulling processes; 3) the occurrence of rupture failures of the geosynthetics rather than the expected pull-out failures.

5.3 Comparisons of Shear Strength Parameters Obtained from Single-stage and Multi-stage Tests

Shear strength parameters (c, ϕ) and interface parameters (c_a, δ) were calculated based on the failure envelopes obtained from the single-stage and multi-stage direct/interface shear and pull-out tests. It was found that the apparent cohesions obtained from the multi-stage tests are slightly lower than those from the single-stage tests (see Figure 11a). However, the friction angles obtained from the multi-stage tests are not always lower, as shown in Figure 11b. In general, they are still very close to the single-stage test results. The errors of the apparent cohesions (either c or c_a) and friction angles (either ϕ or δ) ranged from -2.7 kPa to 0.3 kPa, and -1.8° to 2.4° for all the multi-stage and single-stage tests in this study (see Figure 11c and Table 6). The errors were calculated by the multi-stage test results minus the single-stage test results, as shown in Table 6. Therefore, the multi-stage testing method can produce relatively reliable shear strength parameters for the large-scale direct/interface shear and pull-out tests.

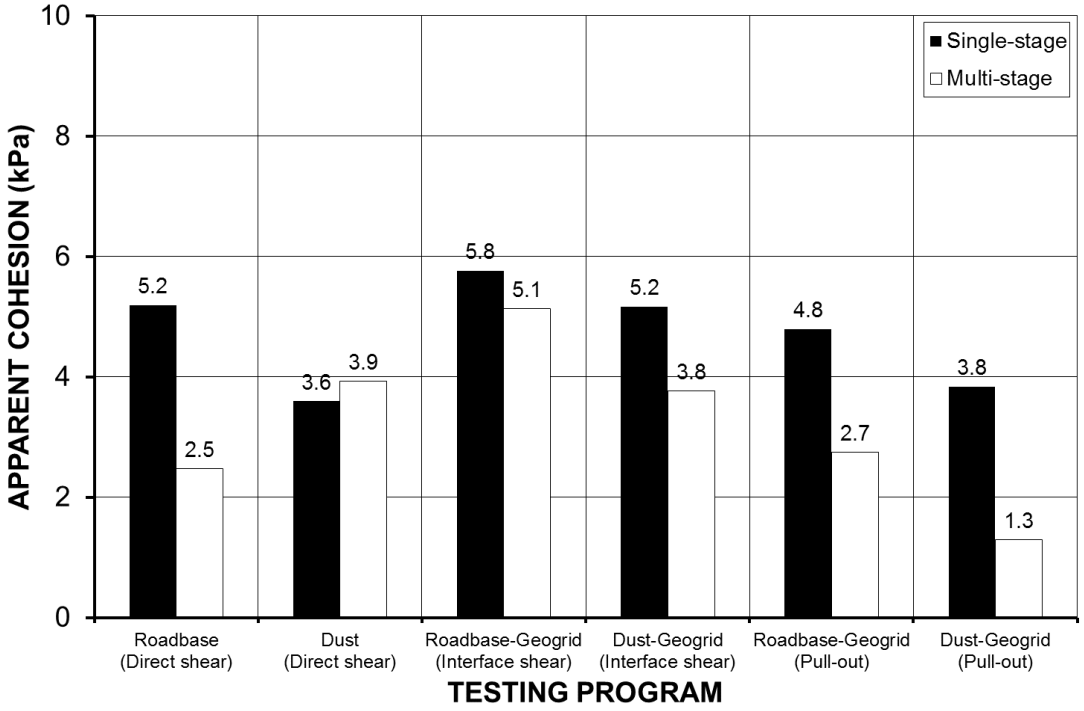
APPARENT COHESION (kPa)
10
8
6
4
2
0
Single-stage
Multi-stage
5.2
2.5
3.6
3.9
5.8
5.1
5.2
3.8
4.8
2.7
3.8
1.3
Roadbase (Direct shear)
Dust (Direct shear)
Roadbase-Geogrid (Interface shear)
Dust-Geogrid (Interface shear)
Roadbase-Geogrid (Pull-out)
Dust-Geogrid (Pull-out)
TESTING PROGRAM

(a)

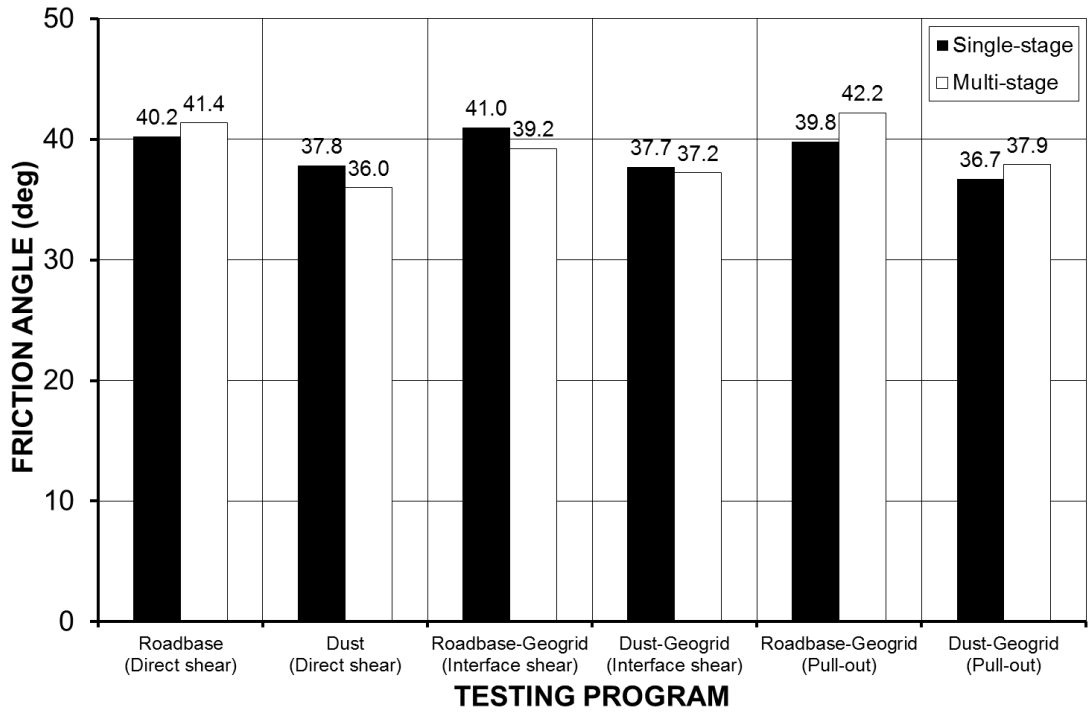
FRICTION ANGLE (deg)
50
40
30
20
10
0
Single-stage
Multi-stage
40.2
41.4
37.8
36.0
41.0
39.2
37.7
37.2
39.8
42.2
36.7
37.9
Roadbase (Direct shear)
Dust (Direct shear)
Roadbase-Geogrid (Interface shear)
Dust-Geogrid (Interface shear)
Roadbase-Geogrid (Pull-out)
Dust-Geogrid (Pull-out)
TESTING PROGRAM

(b)

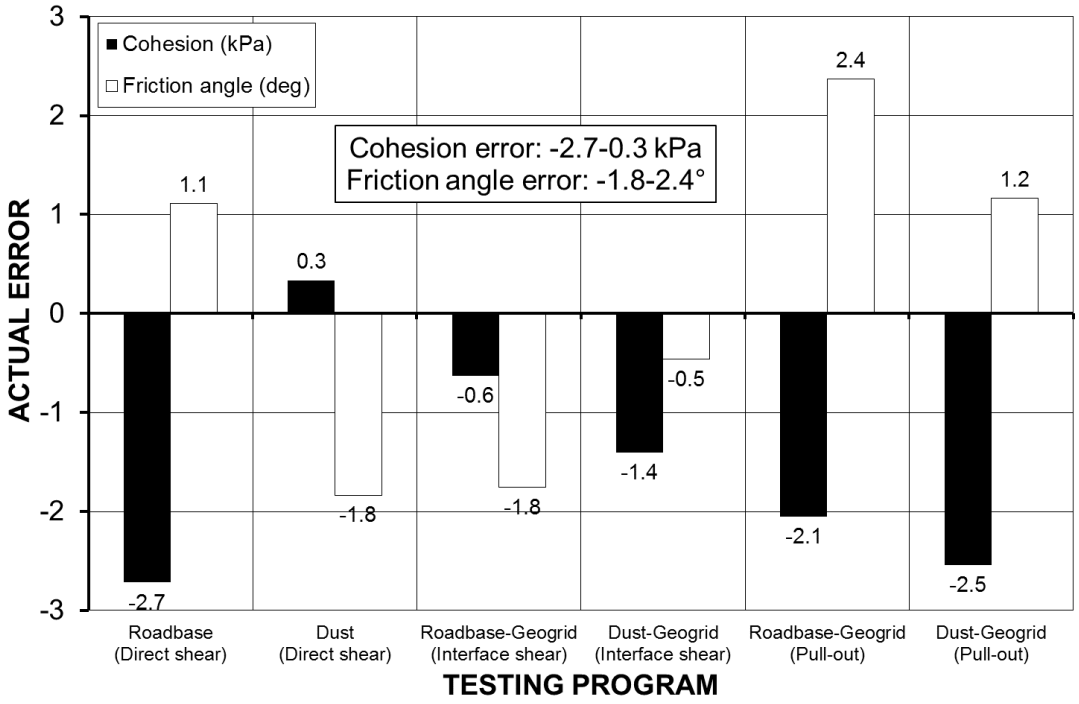

(c)

Figure 11 Comparisons of shear strength parameters obtained from single-stage and multi-stage tests: (a) cohesion; (b) friction angle; (c) error between two testing methods

Table 6 Shear strength parameters obtained from direct/interface shear and pull-out tests

Specimen	Test	Single-stage		Multi-stage		Errors	
		c (kPa)	φ (°)	c (kPa)	φ (°)	c (kPa)	φ (°)
Roadbase	Direct shear	5.2	40.2	2.5	41.4	-2.7	1.1
Dust	Direct shear	3.6	37.8	3.9	36.0	0.3	-1.8
Roadbase-Geogrid	Interface shear	5.8	41.0	5.1	39.2	-0.6	-1.8
Dust-Geogrid	Interface shear	5.2	37.7	3.8	37.2	-1.4	-0.5
Roadbase-Geogrid	Pull-out	4.8	39.8	2.7	42.2	-2.1	2.4
Dust-Geogrid	Pull-out	3.8	36.7	1.3	37.9	-2.5	1.2

Note: For interface shear and pull-out tests, c, φ also stand for the apparent adhesion c_a and interface friction angle δ herein for simplicity.

5.4 Relationship Between Direct Shear Stress, Interface Shear Stress and Pull-out Shear Stress

The relationship between direct shear stress, interface shear stress and pull-out shear stress is still not quite clear due to the different shear mechanisms for a wide range of soils and geosynthetics. It was therefore decided to compare the shear stresses obtained from the direct/interface shear and pull-out tests to seek any potential relationship. Figure 12 shows the shear stress curves obtained from direct/interface shear and pull-out tests using single-stage and multi-stage testing methods, under applied normal stresses of 15 kPa, 25 kPa or 50 kPa. It can be observed that the shear stress curves of the soil-geogrid interface are quite close to those of soils alone for both the single-stage and multi-stage direct/interface shear testing. However, the shear stress curves obtained from the pull-out tests tend to flatten out with more horizontal displacement required to reach the failure, indicating that the mobilisation of shear stress along the soil-geogrid interface is much slower in the pull-out tests than in the interface shear tests. The horizontal displacement required for the pull-out tests was doubled (60 mm for the single-stage tests and 20 mm for each stage of the multi-stage tests) compared to the direct shear tests (30 mm for the single-stage tests and 10 mm for each stage of the multi-stage tests), to ensure that the pull-out resistance could be sufficiently developed.

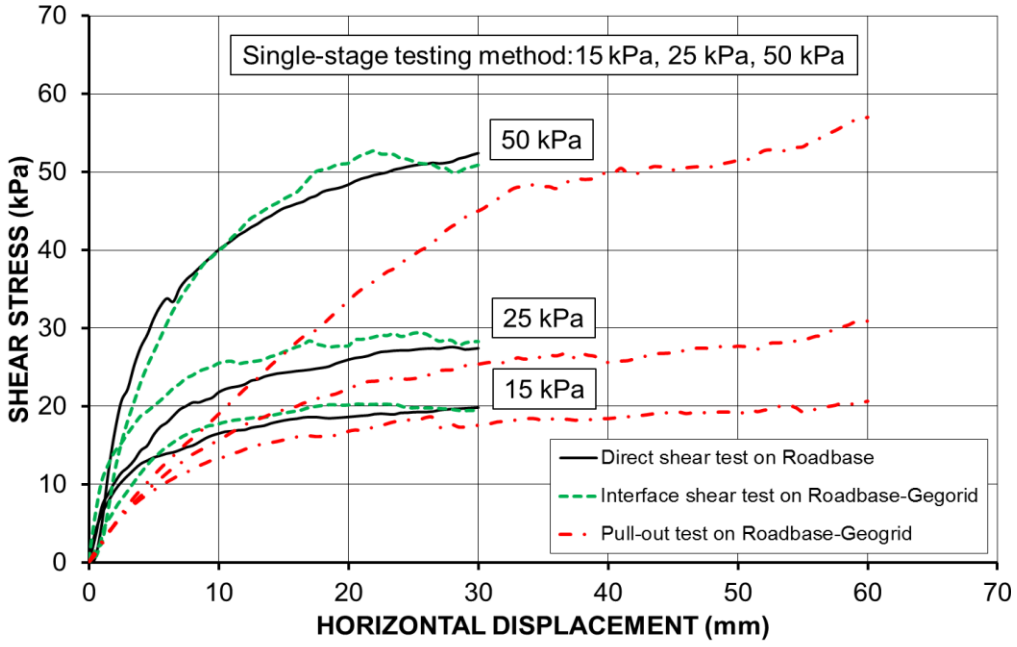

(a)

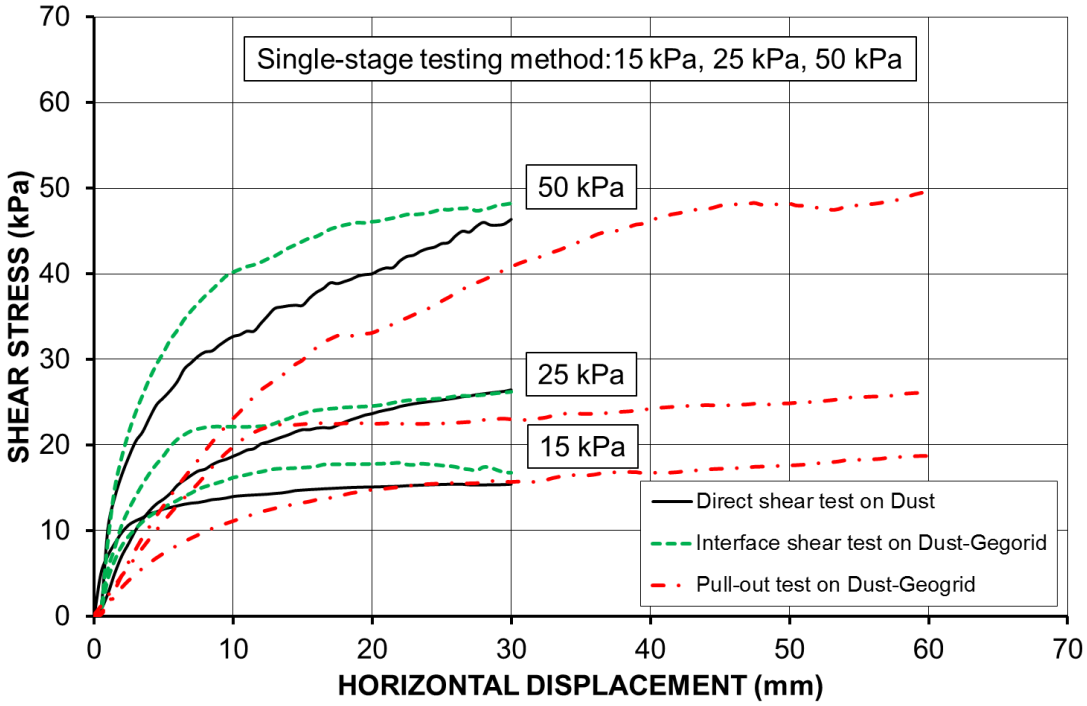
Single-stage testing method:15 kPa, 25 kPa, 50 kPa
50 kPa
25 kPa
15 kPa
Direct shear test on Dust
Interface shear test on Dust-Gegorid
Pull-out test on Dust-Geogrid
SHEAR STRESS (kPa)
HORIZONTAL DISPLACEMENT (mm)
0
10
20
30
40
50
60
70

(b)

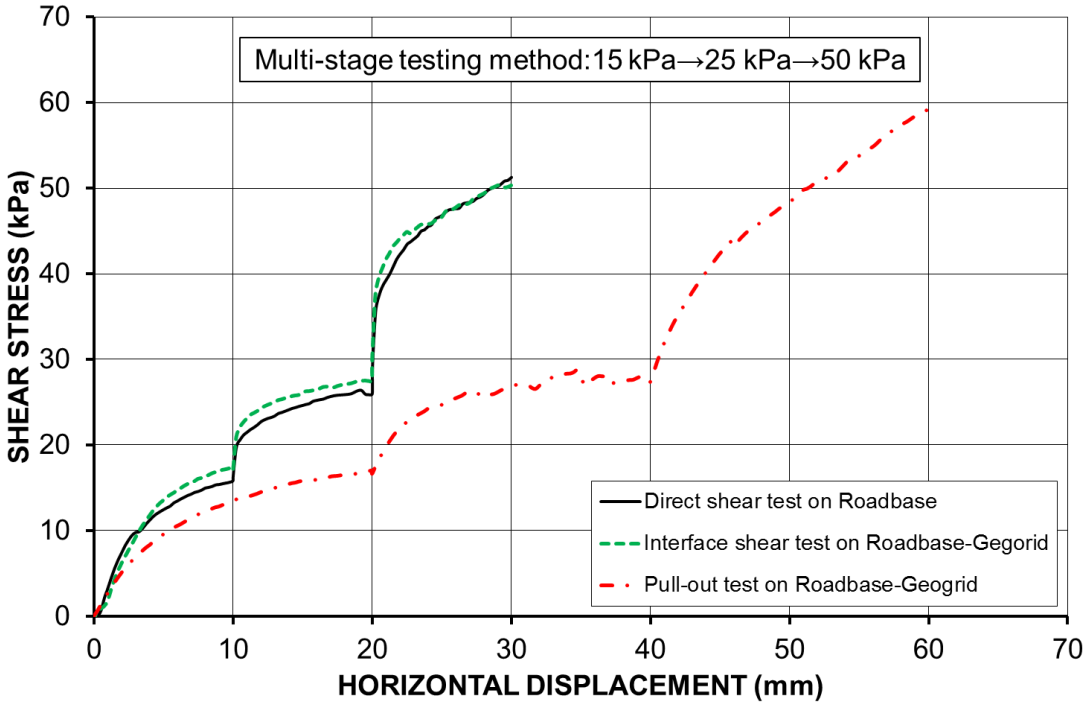
Multi-stage testing method:15 kPa→25 kPa→50 kPa
Direct shear test on Roadbase
Interface shear test on Roadbase-Gegorid
Pull-out test on Roadbase-Geogrid
SHEAR STRESS (kPa)
HORIZONTAL DISPLACEMENT (mm)
0
10
20
30
40
50
60
70

(c)

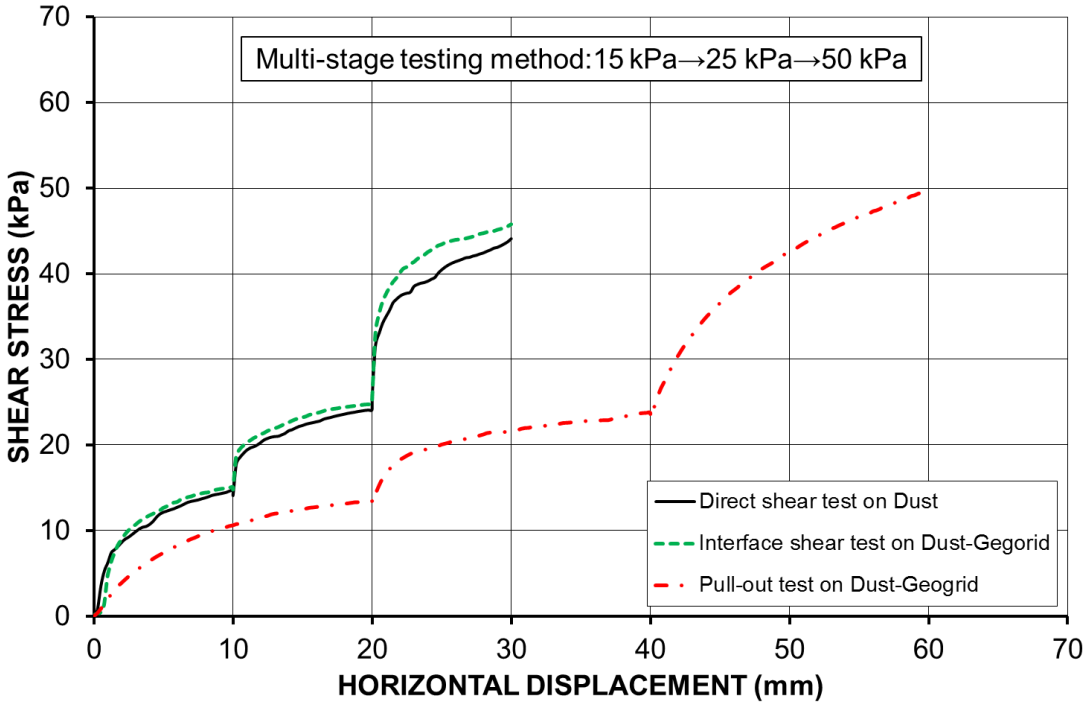

(d)

Figure 12 Comparisons of shear stress curves obtained from direct/interface shear and pull-out tests: (a) single-stage test on Roadbase; (b) single-stage test on Dust, (c) multi-stage test on Roadbase; (d) multi-stage test on Dust

It can be clearly observed that the pull-out shear stress mobilised along the soil-geogrid interface is relatively lower than the corresponding interface shear stress within a horizontal displacement of 30 mm under each normal stress. This is most noticeable for the single-stage tests under the highest normal stress of 50 kPa. However, the maximum interface shear stress mobilised is still comparable when the pull-out displacement reached a horizontal displacement of 60 mm (see Figure 12a-b). Also, from the multi-stage test results (see Figure 12c-d), the same conclusion can readily be drawn. In addition, it is recommended that the required horizontal displacement be increased with increasing applied normal stress (higher confinement) in order to sufficiently develop the shear stress (see also Figure 12).

Figure 13 compares the failure envelopes of the soil-geogrid interface obtained from the interface shear and pull-out tests. In general, the failure envelopes obtained from the pull-out tests are slightly lower than those obtained from the interface shear tests. It should be

noted that area correction for both normal stress and shear stress is necessary since a significant reduction in the contact area would cause an increase in both normal stress and shear stress in large-scale direct/interface shear and pull-out tests. For example, when a normal stress of 50 kPa was subjected to a specimen, the actual applied normal stress at failure was higher than 50 kPa, as shown in Figure 13. Therefore, even though some shear strengths obtained from the pull-out tests were found to be higher than those from the interface shear tests, the failure envelopes were, however, generally slightly lower. This is because the horizontal displacement was doubled (60 mm) for the pull-out tests, so that the actual normal stress at failure increased after applying the area correction. Therefore, the obtained failure envelopes were flattened.

Figure 14 compares the direct shear strength of soils τ_s, interface shear strength τ_{ds} and pull-out shear strength τ_p of soil-geogrid interfaces, and their empirical relationships. In general, quite good linear relationships were found in Figure 14 for both the single-stage and multi-stage results. The interface shear strengths τ_{ds} and pull-out shear strengths τ_p are quite close to the direct shear strengths τ_s of the soil alone.

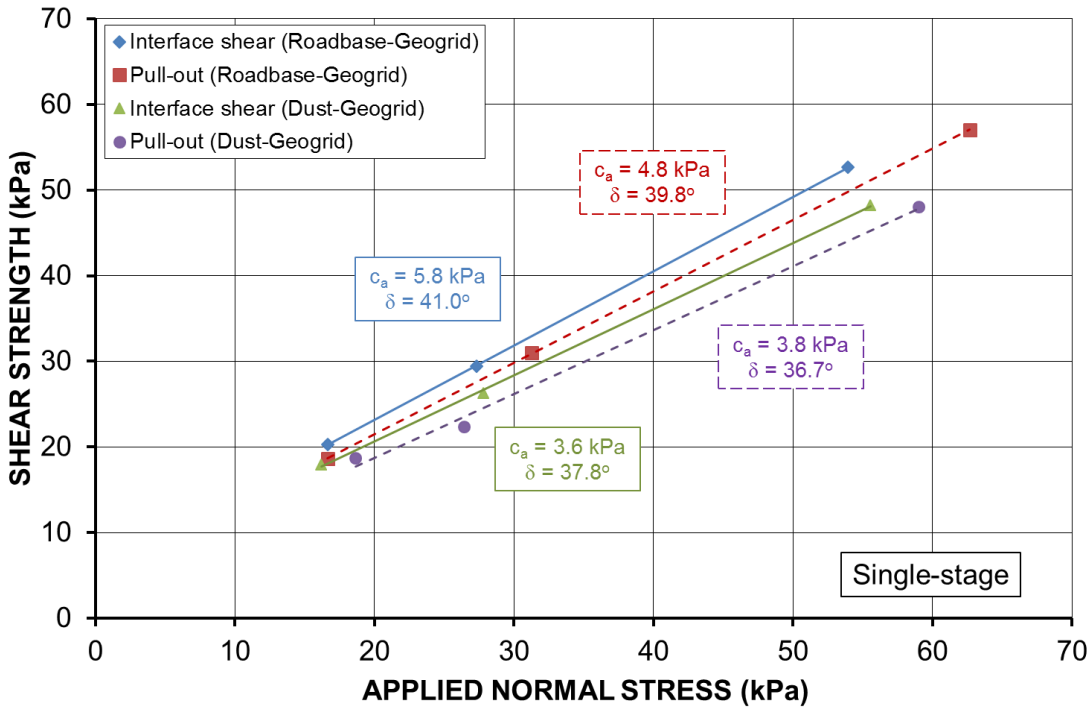

(a)

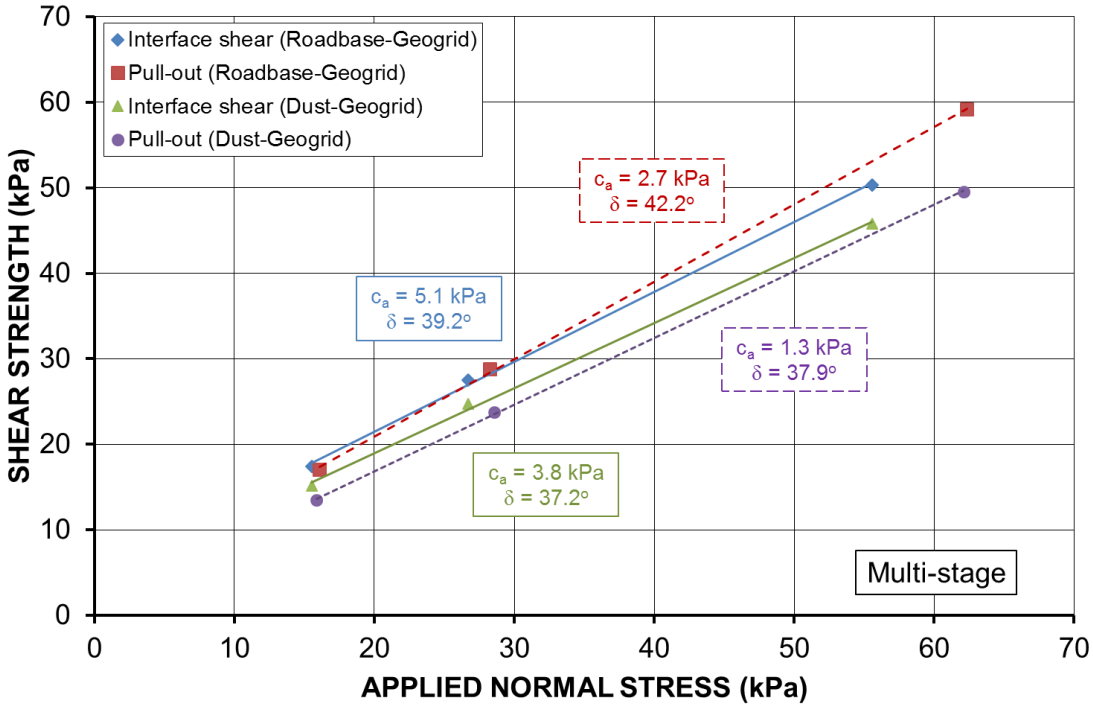

(b)

Figure 13 Comparisons of failure envelops obtained from interface shear and pull-out tests: (a) single-stage; (b) multi-stage

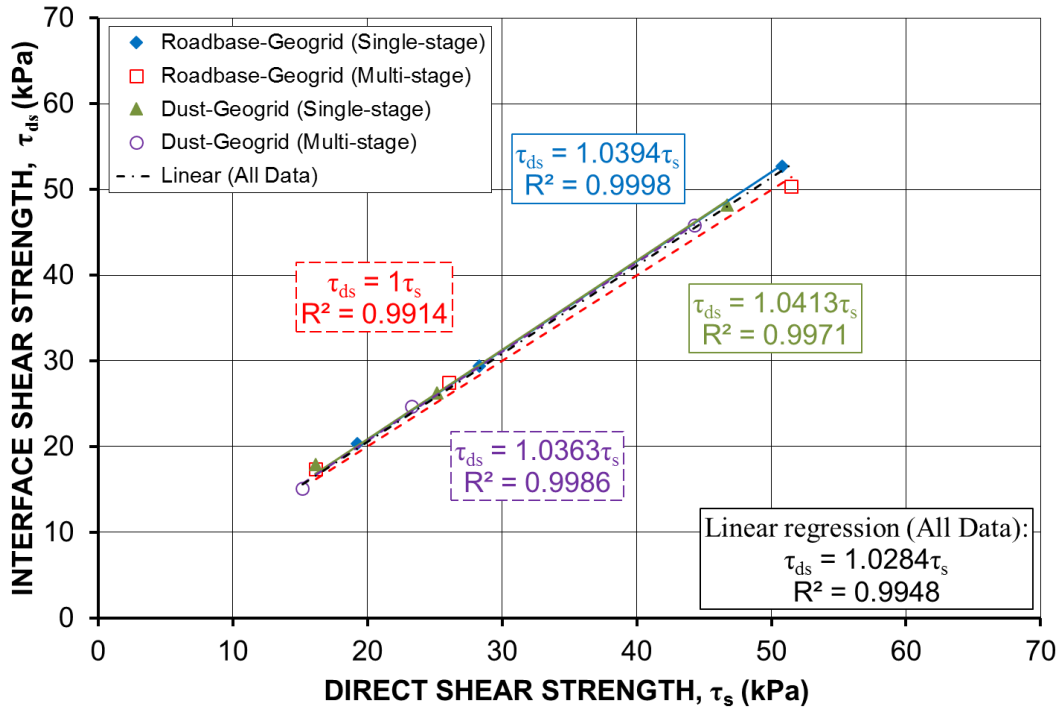

(a)

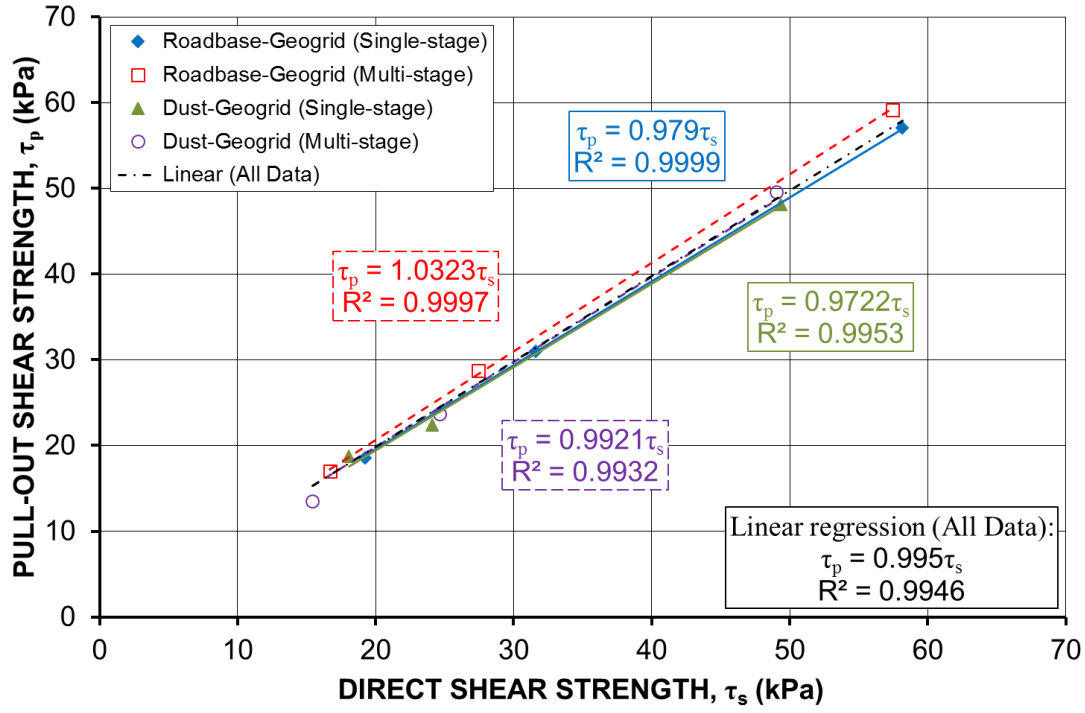

(b)

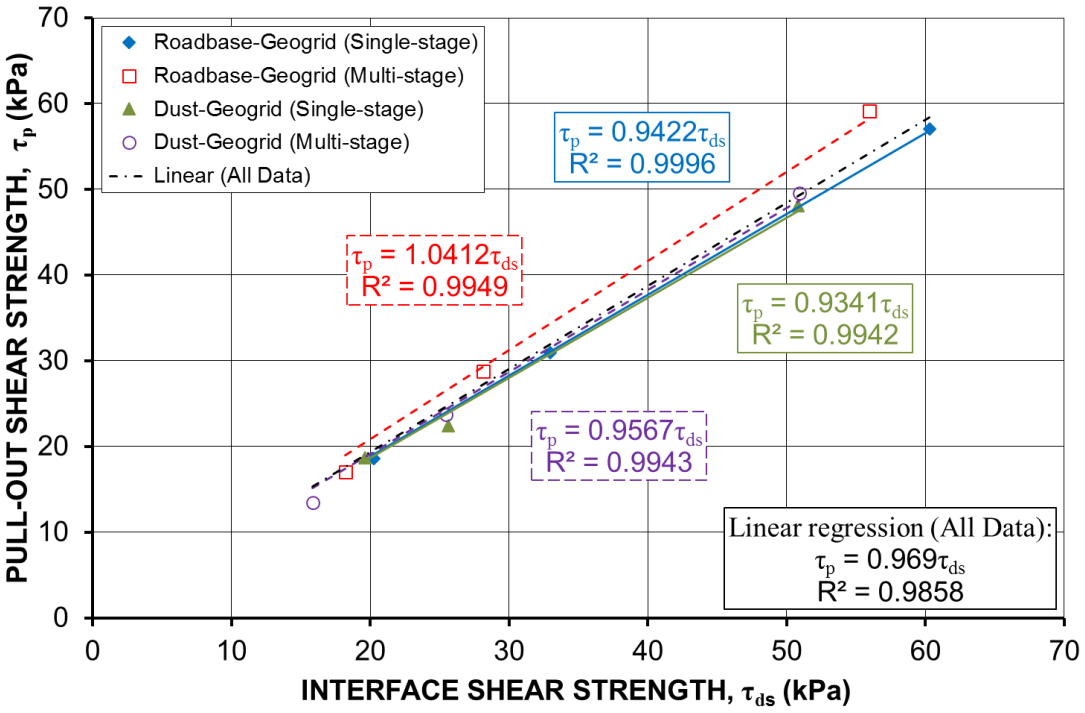

(c)

Figure 14 Comparisons of shear strengths obtained from direct/interface shear and pull-out tests: (a) τ_{ds} versus τ_s; (b) τ_p versus τ_s; (c) τ_p versus τ_{ds}

In addition, interface parameters f_{ds}, f_b, and α calculated by Eqs. (3), (7) and (10) are presented in Figure 15 and Table 7. It can be found that the average values of these three parameters (1.043, 0.984 and 0.946) were similar to the linear regression results of all data (1.028, 0.995 and 0.969), which are all quite close to 1. Therefore, the interface and pull-out shear strengths could be predicted based on the direct shear strength of soil and the interface parameters obtained.

Finally, the relationship between the single-stage and multi-stage test results was constructed through linear regression of all the experimental shear strength data obtained, as shown in Figure 16. It can be found that a good linear relationship exists although the shear strengths obtained from the multi-stage tests were slightly lower. Figure 16 has shown the reliability of the multi-stage testing method applied to both large-scale direct/interface shear and pull-out testing of compacted soils and a geogrid.

Table 7 Interface parameters obtained from interface shear and pull-out tests

Specimen	Test	Direct shear		Pull-out test		
		σ_n (kPa)	f_{ds}	σ_n (kPa)	f_b	α
Roadbase-Geogrid	Single-stage	16.6	1.054	16.6	0.966	0.918
		27.3	1.039	31.3	0.979	0.939
		54.0	1.037	62.7	0.980	0.946
	Multi-stage	15.5	1.076	16.1	1.021	0.935
		26.7	1.056	28.3	1.049	1.022
		55.6	0.978	62.3	1.029	1.057
Dust-Geogrid	Single-stage	16.2	1.110	18.6	1.035	0.953
		27.8	1.044	26.4	0.929	0.873
		55.6	1.032	59.0	0.974	0.947
	Multi-stage	15.5	0.995	15.9	0.874	0.851
		26.7	1.059	28.6	0.963	0.931
		55.6	1.035	62.1	1.011	0.973
Average			1.043		0.984	0.946

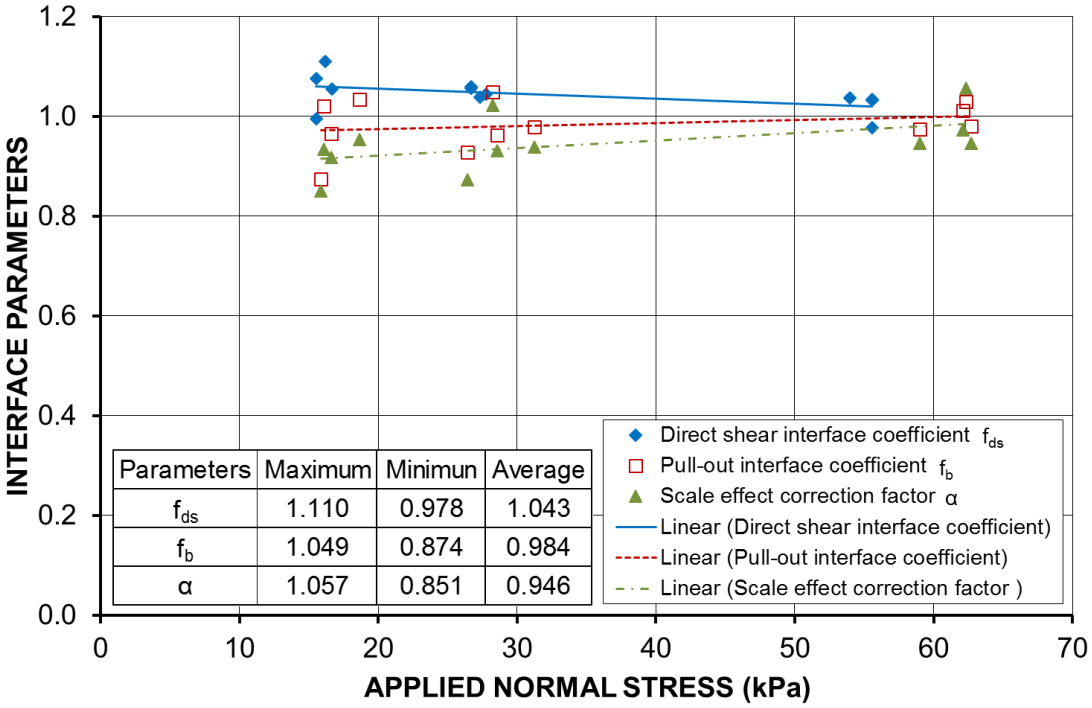

Parameters	Maximum	Minimun	Average
f_{ds}	1.110	0.978	1.043
f_b	1.049	0.874	0.984
α	1.057	0.851	0.946

Figure 15 Calculated value of interface parameters

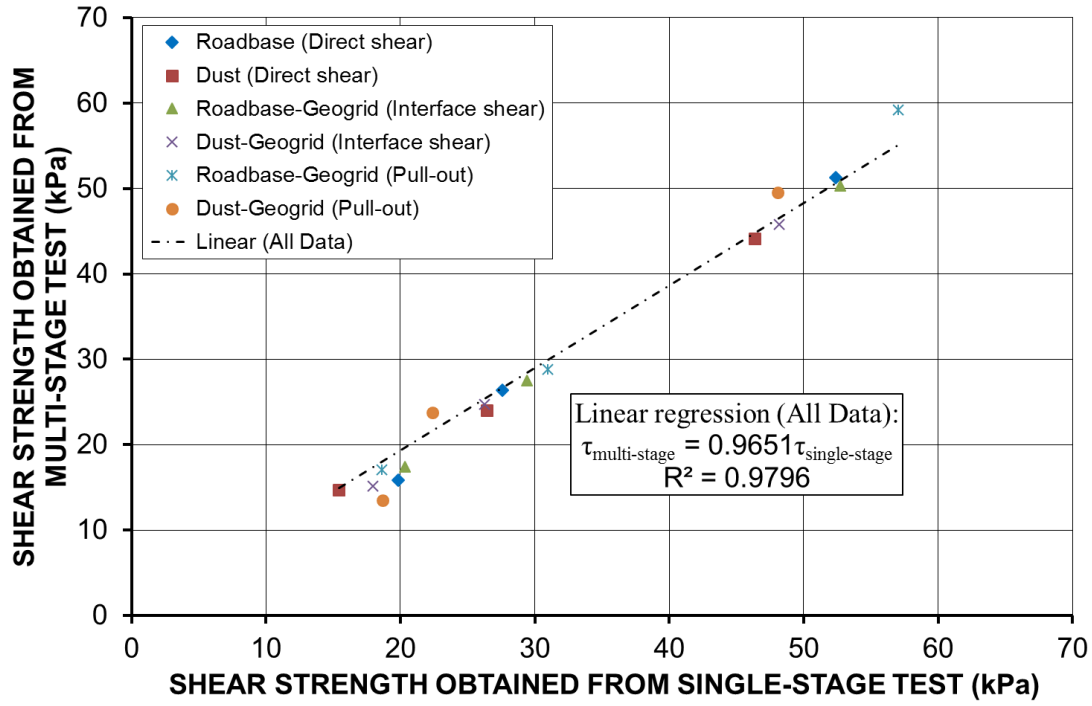

Figure 16 Linear regression of shear strengths for single-stage and multi-stage tests

6 Conclusion

In this paper, multi-stage testing was attempted for both large-scale direct/interface shear and pull-out tests. The obtained multi-stage test results were analysed and compared with the obtained conventional single-stage test results. In summary, the main conclusions of this paper are:

(1) The multi-stage testing method was successfully applied to large-scale direct/interface shear and pull-out testing of compacted soils and a geogrid, resulting in slightly lower shear strengths and reasonably accurate shear strength and interface parameters.

(2) The measured direct shear strengths of soils τ_s, interface shear strengths τ_{ds}, and pull-out shear strengths τ_p of compacted soil-geogrid interfaces are found to be very close in this study, resulting in the interface parameters f_{ds}, f_b, and α close to 1.

(3) The mobilisation of the interface shear stress between the soil and geosynthetic in pull-out tests is much slower than that in the interface shear tests, so that more horizontal displacement is required for pull-out tests.

(4) The main limitation of multi-stage tests is that it limits the shear/pull-out displacement that can be applied to each stage, which may not be sufficient. Therefore, a suitable displacement for each stage should be chosen with particular caution, considering the properties and the initial conditions of the specimen.

Reference

ASTM D6706-13. (2013). Standard Test Method for Measuring Geosynthetic Pullout Resistance in Soil, ASTM International, West Conshohocken, PA, www.astm.org

ASTM D5321-14. (2014). Standard Test Method for Determining the Shear Strength of Soil-Geosynthetic and Geosynthetic-Geosynthetic Interfaces by Direct Shear, ASTM International, West Conshohocken, PA, www.astm.org

Alfaro, M. C., Miura, N., and Bergado, D. T., (1995). Soil-Geogrid Reinforcement Interaction by Pullout and Direct Shear Tests. Geotech. Test. J., 18(2), pp. 157–167.

Alobaidi, I. M., Hoare, D. J., and Ghataora, G.S., (1997). Load Transfer Mechanism in Pullout Tests. Geosynthetics International, 4(5), pp. 509–521.

Bathurst, R. J., and Ezzein, F. M., (2015). Geogrid and Soil Displacement Observations During Pullout Using a Transparent Granular Soil. Geotech. Test. J., 38(5), pp. 1–13.

Bergado, D. T., and Chai, J. C., (1994). Pullout Force-Displacement Relationship of Extensible Grid Reinforcements. Geotextiles and Geomembranes, 13(5), pp. 295–316.

Berg, R. R., Christopher, B. R., and Samtani, N. C., (2009). Design and construction of mechanically stabilized earth walls and reinforced soil slopes (FHWA-NHI-10-024), Washington, DC: Federal Highway Administration.

Chang, D. T. T., Chang, F. C., Yang, G. S., and Yan, C. Y., (2000). The influence factors study for geogrid pullout test, In: Stevenson, P.E. (Ed.), Grips, Clamps, Clamping Techniques, and Strain Measurement for Testing of Geosynthetics, ASTM STP 1379, American Society for Testing and Materials, pp. 129–142.

Christopher, B. R., Gill, S. A., Giroud, J. P., Juran, I., Mitchell, J. K., Schlosser, F., and Dunnicliff, J., (1990). Reinforced soil structures (FHWA-RD-89-043), Washington, DC: Federal Highway Administration.

Elias, V., Christopher, B. R., and Berg, R. R., (2001). Mechanically stabilized earth walls and reinforced soil slopes – Design and construction guidelines (FHWA-NHI-00-043), Washington, DC: Federal Highway Administration.

Ferreira, F. B., Vieira, C. S., Lopes, M. L., and Carlos, D. M., (2015). Experimental investigation on the pullout behaviour of geosynthetics embedded in a granite residual soil. European Journal of Environmental and Civil Engineering, DOI: 10.1080/19648189.2015.1090927.

Gan, J. K., and Fredlund, D. G., (1988). Multistage Direct Shear Testing of Unsaturated Soils. Geotech. Test. J., 11(2), pp. 132–138.

Gullic, R. C., (1970). Multi-stage shear testing of a cohesionless soil. Master thesis, Univerisity of Missouri-Rolla, USA.

Hormdee, D., Kaikeerati, N., and Angsuwotai, P., (2012). Evaluation on the results of multistage shear test. International Journal of GEOMATE, 2(1), 140–143.

Hsieh, C. W., Chen, G. H., and Wu, J., (2011). The shear behavior obtained from the direct shear and pullout tests for different poor graded soil-geosynthetic systems. Journal of GeoEngineering, 6(1), 15–26.

Jewell, R. A., Milligan, G. W. E., Sarsby, R. W., and Dubois, D., (1984). Interaction between soil and geogrids. In Proceedings of Symposium on Polymer Grid Reinforcement. Thomas Telford Ltd, London, pp. 18–29.

Jewell, R. A., (1990). Reinforcement bond capacity. Géotechnique, 40(3), 513–518.

Lopes, M. L., and Silvano, R., (2010). Soil/geotextile interface behaviour in direct shear and pullout movements. Geotech. Geol. Eng., 28(6), 791–804.

Lopes, M. L., (2012). Soil–geosynthetic interaction. In S. K. Shukla (Ed.), Handbook of Geosynthetic Engineering, London: Ice Publishing, Thomas Telford Ltd.

Mallick, S. B., Zhai, H., Adanur, S., and Elton, D. J., (1996). Pullout and direct shear testing of geosynthetic reinforcement: state-of-the-art report. Transportation Research Record, TRB 1534, 80–90.

Matsui, T., San, K. C., Nabesahirna, Y., and Arnii, U. N., (1996). Bearing mechanism of steel reinforcement in pull-out test. In Proceedings of the International Symposium: Earth Reinforcement, Fukuoka, Kyushu, Japan. Balkema Publisher, 101–105.

Moraci, N., and Gioffre, D., (2006). A simple method to evaluate the pullout resistance of extruded geogrids embedded in a compacted granular soil. Geotextiles and Geomembranes, 24(2), 116–128.

Moraci, N., and Recalcati, P., (2006). Factors affecting the pullout behaviour of extruded geogrids embedded in a compacted granular soil. Geotextiles and Geomembranes, 24(4), 220–242.

Moraci, N., and Cardile, G., (2009). Influence of cyclic tensile loading on pullout resistance of geogrids embedded in a compacted granular soil. Geotextiles and Geomembranes, 27(6), 475–487.

Palmeira, E. M., (2009). Soil–geosynthetic interaction: Modelling and analysis. Geotextiles and Geomembranes, 27(5), 368–390.

Perkins, S. W., and Cuelho, E. V., (1999). Soil–geosynthetic interface strength and stiffness relationships from pullout tests. Geosynthetics International, 6(5), 321–346.

Peterson, L. M., and Anderson, L. R., (1980). Pull-out resistance of welded wire mesh embedded in soil. Research report submitted to Hilfiker Pipe Co., Department of Civil Engineering, Utah State University, Logan, UT, USA.

Petro, M. J., Sordo, B., Berry , S. M., and MacLaughlin, M. M., (2017). Characterization of the peak strength of rough rock joints using limited displacement multi-stage direct shear tests. 51st U.S. Rock Mechanics/Geomechanics Symposium, 25-28 June, San Francisco, California, USA.

Pradhan, B., (2003). Study of pullout behavior of soil nails in completely decomposed granite fill. Master thesis, The University of Hong Kong, China.

Attached Paper IV

Paper IV: Influence of anchorage angles on pull-out resistance of geotextile wrap around anchorage

Xu, Y., Williams, D. J., Serati, M., 2018. Influence of anchorage angles on pull-out resistance of geotextile wrap around anchorage. Geosynthetics International. 25 (4), 378-391. https://doi.org/10.1680/jgein.18.00022 – incorporated as **Paper IV**.

Influence of anchorage angles on pull-out resistance of geotextile wrap around anchorage

Youwei Xu[a,], David J. Williams[b], Mehdi Serati[c]*

[a] PhD candidate, School of Civil Engineering, The University of Queensland, Brisbane, QLD 4072, Australia. Email: youwei.xu@uq.edu.au

[b] Professor, School of Civil Engineering, The University of Queensland, Brisbane, QLD 4072, Australia. Email: d.williams@uq.edu.au

[c] Postdoctoral Research Fellow, School of Civil Engineering, The University of Queensland, Brisbane, QLD 4072, Australia. Email: m.serati@uq.edu.au

Abstract

Anchored geosynthetics are able to withstand higher tension and provide higher anchorage capacity. The simple run-out and wrap-around anchorages are two commonly used configurations in anchored geosynthetics. However, the influence of geometric parameters of different anchorage configurations on pull-out performance is still problematic. To study the influence of anchorage angles on pull-out resistance of the geotextile wrap around anchorage, two geometric control variables, namely, the top and bottom anchorage angles, were introduced and investigated experimentally and theoretically. A series of pull-out tests were carried out on the geotextile anchorages with varying configurations embedded in sand, including the simple run-out and wrap around anchorages that were configured at varying top and bottom anchorage angles. Three stages were summarised to interpret the mobilisation of pull-out resistance of the geotextile wrap around anchorage during the pulling process. It was found that the smaller the bottom angle, the higher the initial pull-out resistance achieved at early and middle stages, while the larger the top angle, the higher the final pull-out resistance achieved at final stage. In addition, theoretical studies on pull-out resistance of the geotextile wrap around anchorage with varying anchorage angles were also carried out based on the static equilibrium analysis.

Keywords: geosynthetics; anchorage angles; geotextile; pull-out; simple run-out; wrap around

1 Introduction

Proper configuring anchorage can improve the performance of geosynthetic in landfills, which is able to withstand more tension and provide higher pull-out resistance (Hullings and Sansone 1997; Gurung 2000; Villard and Chareyre 2004; Chareyre and Villard 2005; Gourc et al. 2005; Zornberg 2005; Girard et al. 2006; Yasuhara and Recio-Molina 2007; Ghiassian et al. 2009; Chen et al. 2012; Mosallanezhad et al. 2016; Rajabian and Viswanadham 2016). The pull-out test is a commonly used technique to determine the pull-out resistance of the geosynthetic reinforcement. To investigate the pull-out mechanisms, many researchers have carried out pull-out testing of different geosynthetics embedded in various types of soils using different pull-out equipment (Fannin and Raju 1993; Farrag et al. 1993; Alfaro et al. 1995; Bakeer et al. 1998; Moraci and Recalcati 2006; Sieira et al. 2009; Abdelouhab et al. 2010; Ferreira et al. 2016). The simple run-out and wrap-around anchorages are two commonly used configurations in the anchoring systems, and the geometry of the anchor plays a very important role in design. In recent years, studies on the pull-out behaviour of simple run-out and wrap around anchorages have been of particular interest to some researchers, in order to optimise the required geometric parameters of the anchorage (Chareyre et al. 2002; Chareyre and Villard 2005; De and Vellone 2005; Briançon et al. 2008; Lajevardi et al. 2014; Lajevardi et al. 2015a; Lajevardi et al. 2015b; Raviteja and Munwar Basha 2018). Based on the literature review, it was found that only simple run-out and vertically (90°) wrap around anchorages have been studied in the pull-out tests. The influence of the anchorage angles on the pull-out resistance of the wrap around anchorages has not been fully explored. In order to bridge this research gap and to better understand the anchorage mechanisms for some complex anchorage geometries, two geometric control variables, namely, the top and bottom anchorage angles, were introduced and investigated experimentally and theoretically in this paper.

2 Sand and Geotextile Used

An air-dry fine sand was used in the pull-out tests in this study. Basic characterisation tests were carried out on the sand specimens in the laboratory, including sieving analysis, specific gravity test, maximum and minimum density test and direct shear test. The sand was classified as a poorly graded sand (SP) by the Unified Soil Classification System (USCS), with grain size ranging between 0.3 mm and 0.6 mm. The maximum dry density determined by using a vibratory table was 1734 kg/m^3, and the minimum dry density determined by the funnel method was 1582 kg/m^3. Both large-scale (300 mm by 300 mm) and small-scale (100 mm by 100 mm) direct shear box tests were carried out on loosely-placed sand specimens under applied normal stresses of 25 kPa, 50 kPa, 75 kPa or 100 kPa, giving an average peak friction angle of 31.1°. A woven polypropylene geotextile was used in the pull-out testing program, which has an ultimate tensile strength of 40 kN/m and a nominal thickness of 0.6 mm. All the basic properties of the sand and geotextile are summarised in Table 1.

Table 1 Basic properties of sand and geotextile

Property	Value
Sand	
Average grain size D_{50} (mm)	0.48
Coefficient of uniformity C_u	1.56
Coefficient of gradation C_z	1.16
Peak friction angle (°)	31
Apparent cohesion (kPa)	5.7
Maximum dry density (kg/m^3)	1734
Minimum dry density (kg/m^3)	1582
Specific gravity G_s	2.644
Unified Soil Classification System (USCS)	SP
Geotextile	
Type	Woven
Tensile strength (kN/m)	40
Nominal thickness (mm)	0.6
Strain at maximum load (%)	15
Mass per unit area (g/m^2)	235

3 Testing Equipment

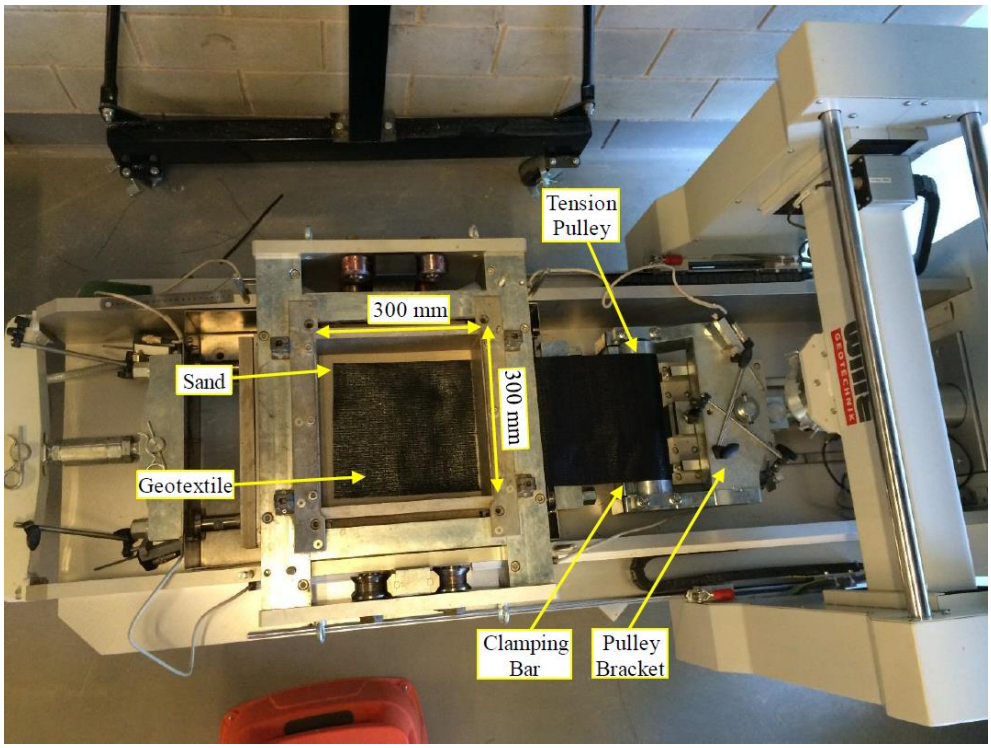

(a)

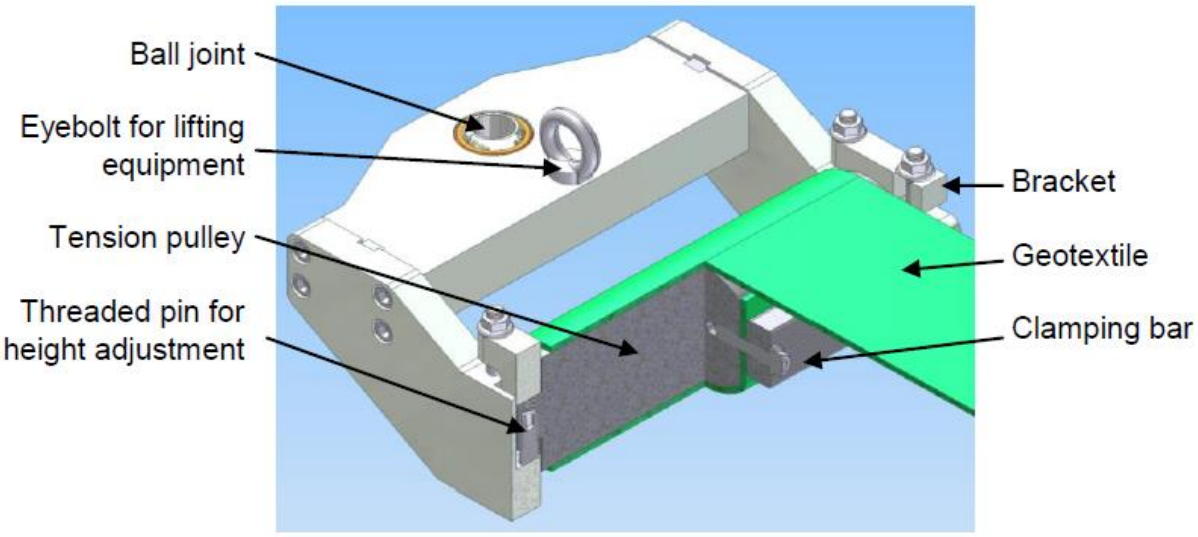

(b)

Figure 1 Pull-out equipment: (a) ADS-300 large-frame shear device; (b) roller clamp

A Wille Geotechnik ADS-300 large-frame shear device was utilised in this study (Figure 1), which is capable of performing both direct shear and pull-out tests. The shear box (or pull-

out box) has dimensions of 300 mm by 300 mm by 200 mm. A floating upper box is designed to create a gap between the upper and lower boxes by means of two compression springs. As shown in Figure 1 in a pull-out test, the geotextile is embedded in the sand with 20 mm clearance on each side to reduce the boundary effect and then pass through the gap between the upper and lower boxes. The end of the geotextile is fixed around a roller clamp. The roller clamp together with a pulling rod is connected to a load cell, which is used to measure the pull-out force mobilised along the soil-geotextile interface. The machine can accommodate a maximum pull-out displacement of 100 mm. During the pull-out testing process, the vertical displacement of the soil specimen, the pull-out displacement of the geotextile and the pull-out force mobilised along the geotextile-soil interface are measured and recorded at desired time intervals.

4 Testing Program

4.1 Shear box tests

First, large-scale (300 mm by 300 mm) and small-scale (100 mm by 100 mm) direct shear box tests were carried out on the sand specimens under applied normal stresses of 25 kPa, 50 kPa, 75 kPa or 100 kPa at a displacement rate of 1 mm/min to determine the basic shear strength parameters of the sand. Large-scale interface shear tests were also carried out on the sand-geotextile interface to determine the interface parameters at the same normal stress levels and displacement rate. It should be noted that all the specimens were sheared to a shear strain of 10% for both the large-scale (sheared 30 mm) and small-scale (sheared 10 mm) direct shear box tests to avoid excessive distortion of the top cap and possible erroneous results.

4.2 Pull-out tests

Pull-out tests were then carried out on the geotextile that was simply laid out and embedded in the sand with 20 mm clearance on each side (simple run-out anchorage), as shown in Figure 1a. The pull-out tests were carried out under applied normal stresses of 25 kPa, 50 kPa, 75 kPa or 100 kPa at a displacement rate of 1 mm/min to determine the pull-out resistance of the geotextile simple run-out anchorage.

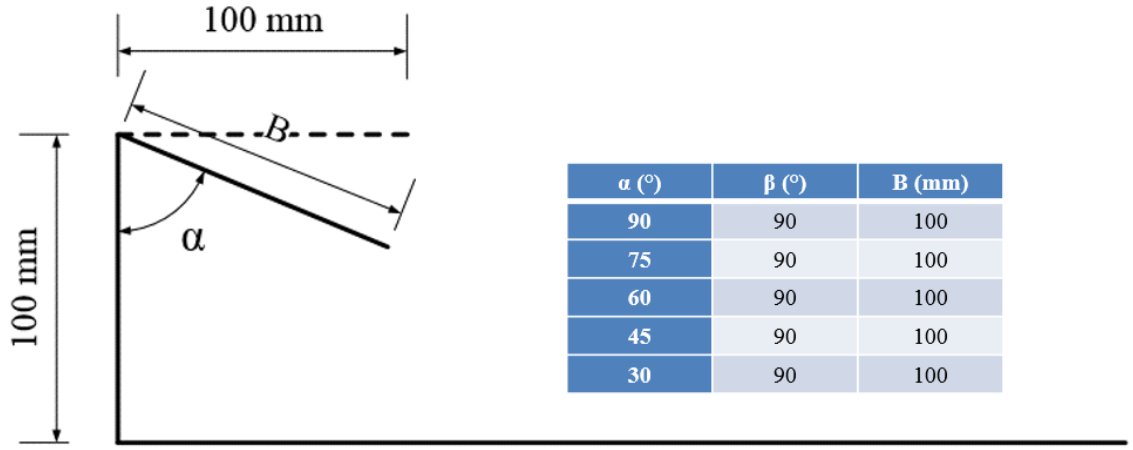

α (°)	β (°)	B (mm)
90	90	100
75	90	100
60	90	100
45	90	100
30	90	100

(a)

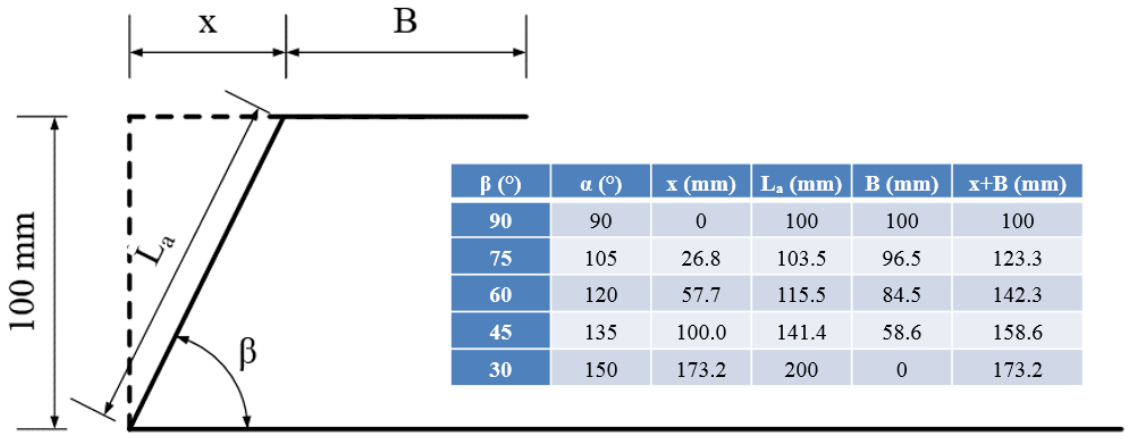

β (°)	α (°)	x (mm)	L_a (mm)	B (mm)	x+B (mm)
90	90	0	100	100	100
75	105	26.8	103.5	96.5	123.3
60	120	57.7	115.5	84.5	142.3
45	135	100.0	141.4	58.6	158.6
30	150	173.2	200	0	173.2

(b)

Figure 2 Two geometric control variables: (a) top angle *α*; (b) bottom angle *β*

Finally, in order to study the influence of anchorage angles on pull-out resistance of the geotextile wrap around anchorage, pull-out tests were also carried out on the geotextile that was configured at varying anchorage angles (wrap around anchorage). This group of pull-out tests were carried out under the same normal stress of 25 kPa at a displacement rate of 1 mm/min. Two geometric control variables (anchorage angles), top angle *α* and bottom angle *β*, were introduced and investigated (see Figure 2). As shown in Figure 2, five anchorage angles (90°, 75°, 60°, 45° and 30°) were investigated for both the top and bottom anchorage angles. The total length of the geotextile wrap around anchorage was kept constant in order to ensure the comparability of the test results. Also shown in Figure 2 are the geometric parameters for each wrap around anchorage configuration. The vertically wrap around anchorage represents *α*=90° and *β*=90°; therefore, total nine wrap

around anchorage configurations with varying anchorage angles were investigated through a series of pull-out tests.

5 Anchorage Angle Preparation

5.1 Bottom angle *β*

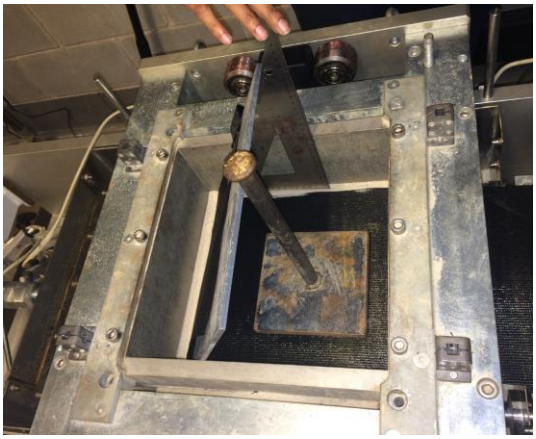

(a)

(b)

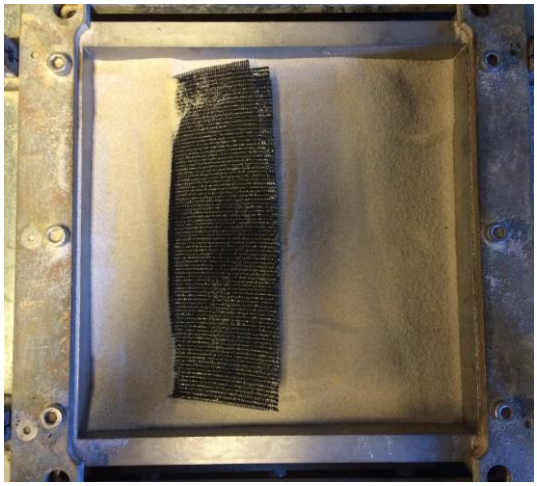

(c)

Figure 3 Preparation of bottom angle *β*: (a) control bottom angle by a fixing board and a set square; (b) fill sand to maintain bottom angle; (c) fold top section horizontally

Since the bottom angle *β* needs to be configured at the sample preparation stage, the anchorage angle preparation method for varying bottom angles is introduced first herein.

The length of the wrap around part of the geotextile was pre-calculated and marked before installation (L_a and B, see Figure 2b). Figure 3 briefly shows the procedures of the bottom angle preparation. As shown in Figure 3a, the wrap around part of the geotextile was clamped to a fixing board, and a set square was utilised to control the desired bottom angles of 90°, 75° (combining the two triangular pieces by placing the hypotenuses together will yield a 75° angle), 60°, 45°, 30°. A temporary support was used to maintain the inclination angle of the fixing board before pouring the sand. The sand was evenly filled into the pull-out box to maintain the bottom angle of the anchor, and then the fixing board and temporary support were gently removed (Figure 3b). More sand was needed to compensate for the loss of the volume of the board and the temporary support until the desired height (the fold mark) reached. Then, the top section of the geotextile was folded horizontally (Figure 3c). Finally, more sand was placed in the box to cover the geotextile until the final target height was reached.

5.2 Top angle α

Before configuring the top angle α, the bottom angle β was first controlled vertically at 90° by using a fixing board and a set square (Figure 4a). The vertical bottom angle was maintained after pouring sand into the pull-out box. Next, the slope of sand in the anchorage area was trimmed to achieve the desired top angles. The top section of the geotextile was then folded and attached to the slope (Figure 4c). Finally, more sand was placed in the box to maintain the top angle and cover the geotextile anchorage until the final target height was reached. The general procedures of the top angle preparation are shown in Figure 4. It should be noted that for preparing a top angle of 45° or 30°, the top section of geotextile needs further support to maintain the underlying sand having a slope of 45° or 60°, which is greater than the natural angle of repose of the sand. It is believed that it would be difficult for cohesionless materials in the field. Therefore, in terms of construction practice, it would be more appropriate for in-situ cohesive soils. However, for research interest, these two angles were still attempted to be configured in the sand in this study in order to compare a broader range of anchorage angles. Future study will be carried out on in-situ cohesive soils to validate and extend this research.

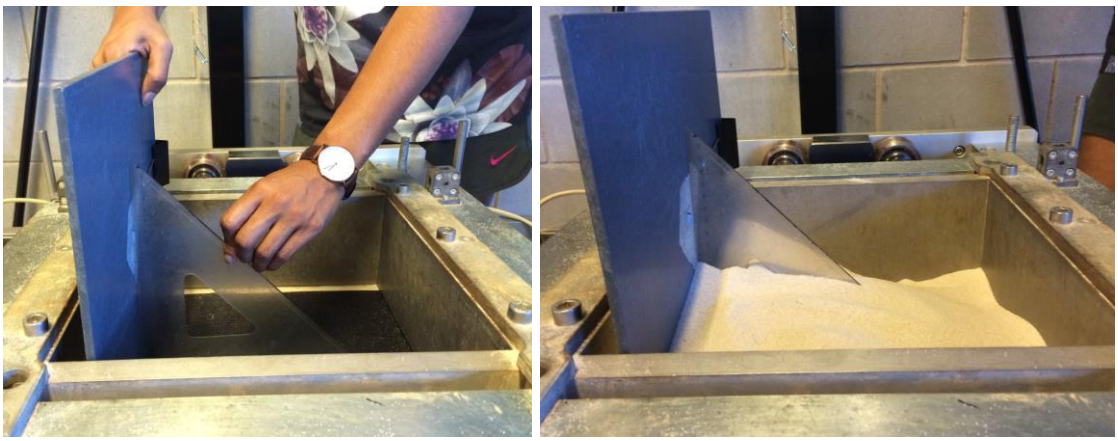

(a) (b)

(c)

Figure 4 Preparation of top angle *α*: (a) control bottom angle *β* at 90°; (b) fill sand to maintain bottom angle; (c) fold top section to form a target top angle *α*

6 Experimental Results

6.1 Direct and interface shear test

Figure 5 presents the shear test results for the sand and sand-geotextile interface under nominal applied normal stresses of 25 kPa, 50 kPa, 75 kPa or 100 kPa. Figure 5a compares the raw shear stress curves obtained during shearing, indicating that the interface shear stress mobilised along the sand-geotextile interface is slightly lower than the internal shear stress of the sand alone. The obtained interface friction angle of sand-geotextile interface is very close the internal friction angle of the sand, which was found to be 31°. A possible explanation for this might be that the shear surface of sand-geotextile interface may still occur in the sand layer, which lies slightly above the geotextile after

applying the normal stresses. The geotextile may still have a slight influence on the interface shear because it is close to the shear surface, which can be reflected on the plots shear stress versus shear displacement, as shown in Figure 5a. That is, the interface stress curves are slightly lower than the internal shear stress curves of sand.

It is evident that the shear stress increased with shear displacement to an ultimate shear strength and then levelled out, without an apparent peak for the large shear box tests. However, the shear stress peaked at 2% - 3% shear strain for the small shear box tests, with a clear drop-off to an ultimate shear strength at large strain. The applied normal stresses and measured shear stresses were corrected for area reduction and plotted to provide the shear strength envelopes, as shown in Figure 5b and Table 2. The shear strength and interface parameters were obtained from the Mohr-Coulomb shear strength criterion:

$$\tau_s = c + \sigma_n \tan\phi \quad (1)$$

where τ_s is the internal shear strength of the sand, c is the apparent cohesion, ϕ is the internal friction angle, σ_n is the applied normal stress.

$$\tau_{ds} = c_a + \sigma_n \tan\delta \quad (2)$$

where τ_{ds} is the interface shear strength of the sand-geotextile interface, c_a is the apparent adhesion, δ is the interface friction angle.

As the large shear box can accommodate more shear displacement (shear 30 mm) than the small shear box (shear 10 mm), the corrected normal stresses and shear stresses at failure for area reduction were slightly higher than the results from the small shear box tests (see Table 2). Overall, it was found that the shear strength parameters of the sand obtained from both the large and small shear box tests matched closely. The interface shear strength between the sand and the geotextile under each applied normal stress was slightly lower that the internal shear strength of the sand alone.

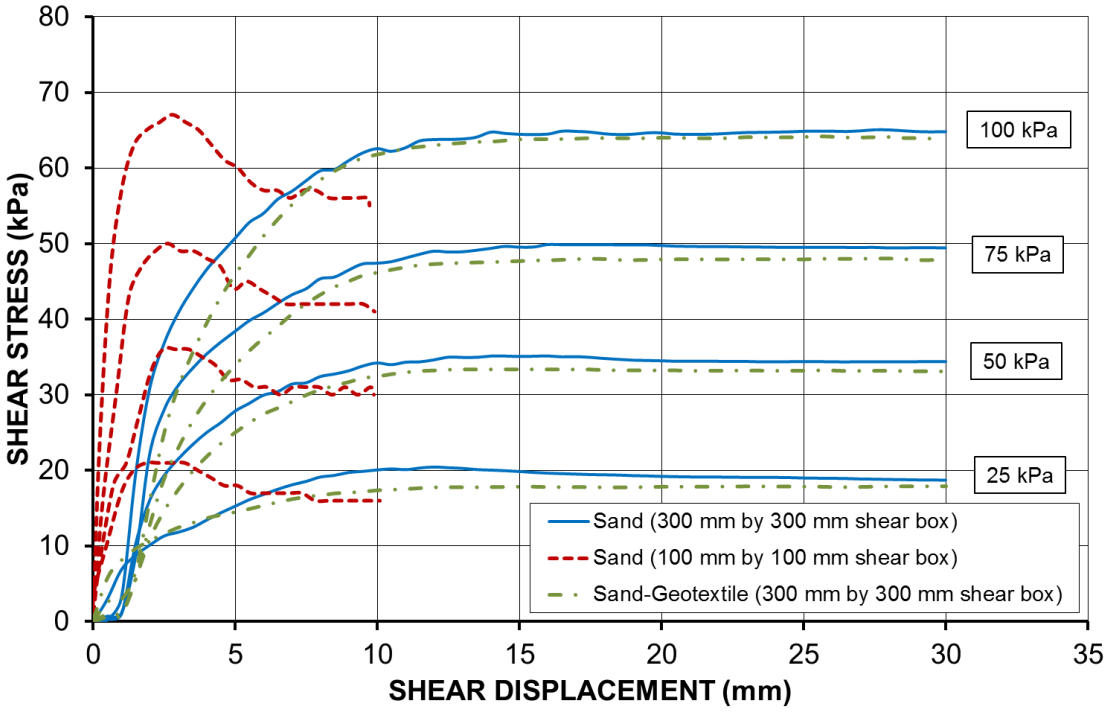

(a)

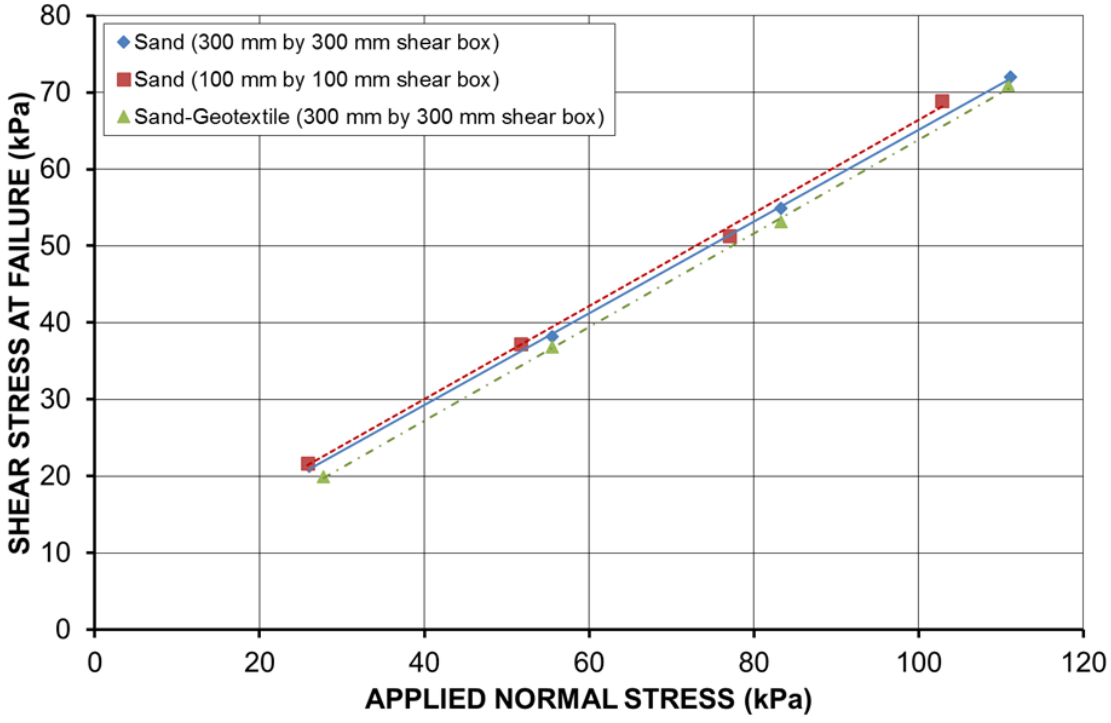

(b)

Figure 5 Shear strength of sand and sand-geotextile interface: (a) shear stress curves; (b) failure envelops

Table 2 Corrected normal and shear stresses in small and large shear box tests

Small shear box test (Sand)		Large shear box test (Sand)		Large interface shear test (Sand-Geotextile)	
σ_n (kPa)	τ (kPa)	σ_n (kPa)	τ (kPa)	σ_n (kPa)	τ (kPa)
25.8	21.7	26.0	21.3	27.8	19.9
51.7	37.3	55.6	38.2	55.6	36.8
77.0	51.3	83.3	54.9	83.3	53.1
102.8	68.9	111.1	72.0	110.9	70.9
c (kPa)	φ (°)	c (kPa)	φ (°)	c_a (kPa)	δ (°)
5.7	31	5.4	31	2.8	31

6.2 Simple run-out anchorage

Figure 6 presents the pull-out test results for the geotextile simple run-out anchorage under nominal applied normal stresses of 25 kPa, 50 kPa, 75 kPa or 100 kPa. According to the ASTM D6706 standard (ASTM D6706-13), the pull-out resistance is calculated by the following equation:

$$P_R = \frac{F_p}{W_g} \tag{3}$$

where P_R is the pull-out resistance, F_p is the pull-out force, W_g is the width of the geotextile.

Figure 6a shows the pull-out resistance versus pull-out displacement during the pulling process. The higher the applied normal stress, the higher the maximum pull-out resistance tended to achieve at a larger pull-out displacement.

The pull-out shear stress mobilised along the soil-geotextile interface in the pull-out test can be calculated by the following equation (ASTM D6706-13):

$$\tau_p = \frac{\mathrm{P}_R}{2L_R} \tag{4}$$

where τ_p is the pull-out shear stress mobilised along the soil-geotextile interface in the pull-out test and L_R is the effective reinforcement length embedded in the sand.

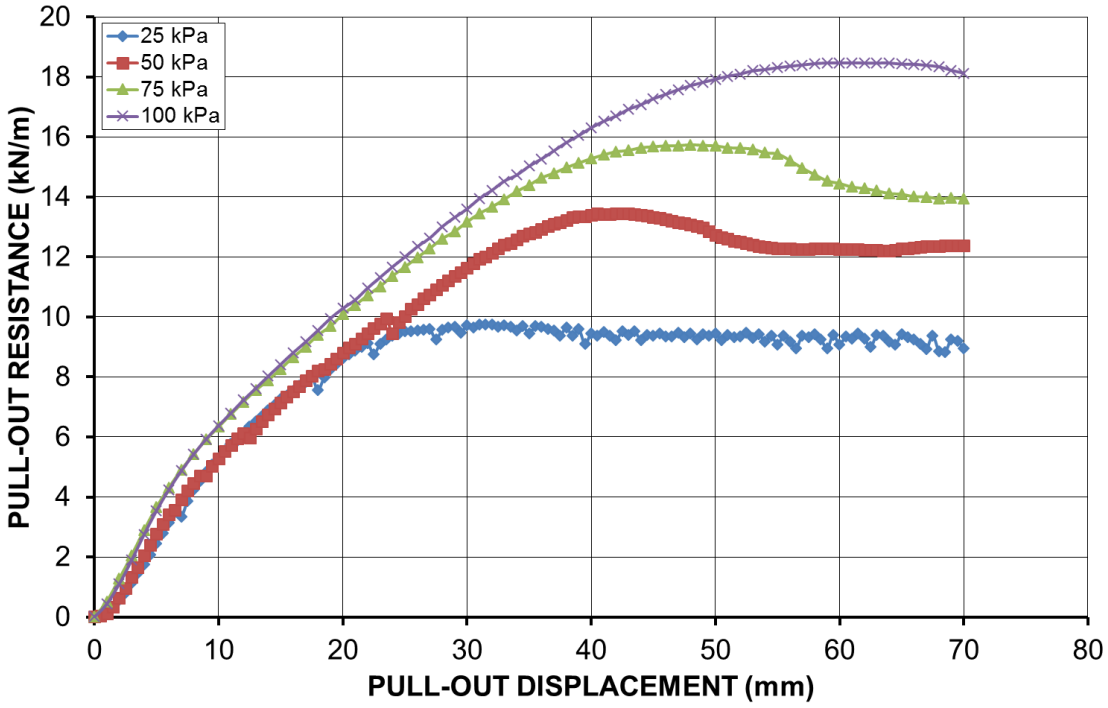

(a)

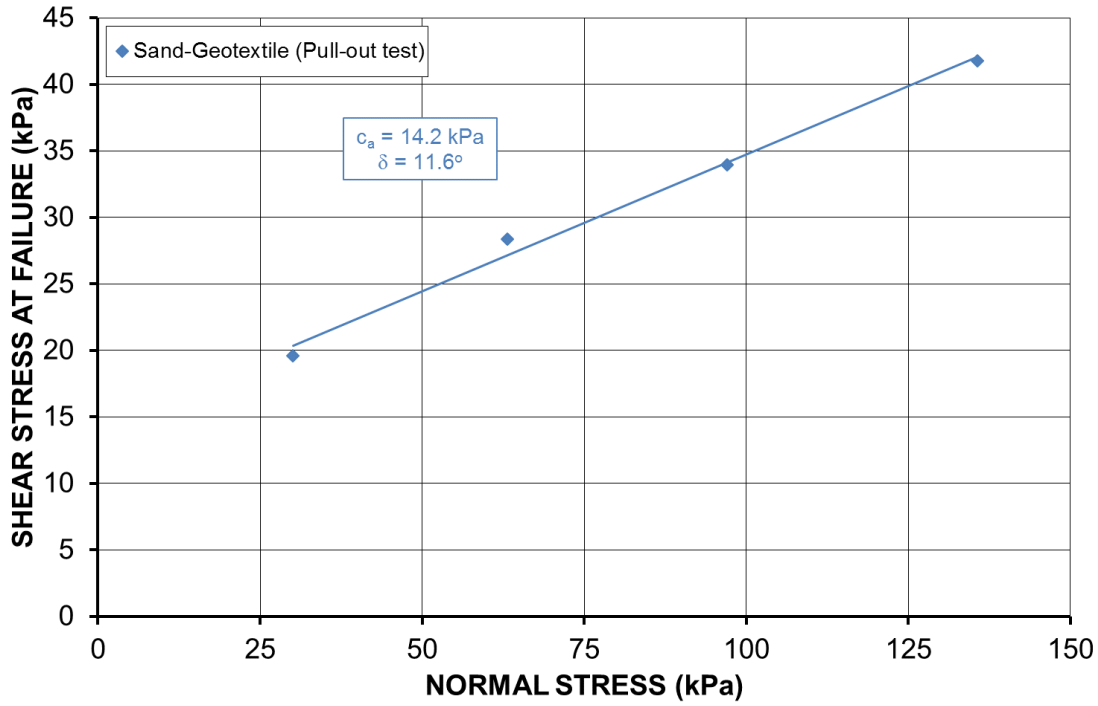

(b)

Figure 6 Pull-out test results of sand-geotextile interface: (a) pull-out resistance curves; (b) failure envelop

Therefore, the pull-out shear stress can be calculated by pull-out resistance using Eq. (4), and the pull-out shear stress at failure versus normal stress is then plotted in Figure 6b. As shown in Figure 6b The relationship between the pull-out shear strength and applied normal stress is also interpreted by Mohr-Coulomb shear strength criterion using Eq. (2). Both the normal and shear stresses at failure were corrected for the contact area reduction between the sand and the geotextile during pulling. It was found that the pull-out shear stress mobilised in the pull-out test increased much slower than the interface shear stress mobilised in the interface shear test for the same applied normal stress. Furthermore, the pull-out shear strengths achieved in the pull-out tests were much lower than the interface shear strengths achieved in the interface shear tests. Therefore, the pull-out testing resulted in lower interface parameters than the interface shear testing.

6.3 Wrap around anchorage: bottom angle *β*

Figure 7 compares the influence of the bottom angle *β* on the pull-out resistance of the geotextile wrap around anchorage embedded in the sand. At the initial stage (Stage 1 - pull-out displacement from 0 to 40 mm) a smaller bottom angle *β* tended to provide a slightly higher initial pull-out resistance, as shown in Figure 7a. For example, it is evident that the initial pull-out resistance curve of the geotextile wrap around anchorage with a bottom angle of 30° was higher than that of a bottom angle of 90° in Stage 1. For Stage 1, the pull-out resistance is mainly contributed by the bottom angle *β* and the bottom layer of the geotextile at the initial pull-out stage. A smaller bottom angle tended to provide a higher resistance at the initial stage. Following the first stage, the pull-out resistance remained approximately constant or increased slightly (Stage 2 - pull-out displacement from 40 mm to 60 mm), most noticeable for *β*=75°, 60° and 45°. Stage 2 demonstrates the movement of the vertical segment of the geotextile between the top angle *α* and bottom angle *β*. In the final stage, the pull-out resistance started increasing again at a faster rate until the maximum pull-out displacement was reached (Stage 3 - pull-out displacement from 60 mm to the maximum). Stage 3 reflects that the top angle *α* and the top layer of the geotextile start to further contribute to the overall anchorage resistance at large displacement. It was found that the maximum (ultimate) pull-out resistance closely matched at the end of Stage 3 for *β*=90°, 75°and 60°. However, the pull-out resistance of the geotextile wrap around anchorage with *β*=45° and 30° tended to increase at a slower rate in Stage 3, resulting in a slightly lower final pull-out resistance. This is mainly because

a larger obtuse top angle and a shorter top layer length *B* tended to make a smaller contribution to the further development of the final pull-out resistance during Stage 3 (geometric parameters can be found in Figure 2b). In addition, it was found that a larger bottom angle tended to result in a more significant tilting of the top cap, especially for β=90°, as shown in Figure 7b. This is because the sand wrapped around in the anchor was pushed to the right during pulling, leading to sinking of the top sand on the left and rising of the top sand on the right.

6.4 Wrap around anchorage: top angle α

Figure 8 compares the influence of the top angle α on the pull-out resistance of the geotextile wrap around anchorage embedded in the sand. In the initial stage (Stage 1), it is evident that the pull-out resistance curves matched closely because the bottom angle was initially set up 90° for each test. This confirms that the initial pull-out resistance is mainly mobilised by the movement of the bottom angle and the bottom layer of the geotextile. During the first stage, the bottom angle was changing during the pulling process, together with the movement of the lower part of the vertical segment. After Stage 1, the pull-out resistance continued increasing at a slower rate, and the smaller the top angle α, the lower the final pull-out resistance achieved, as shown in Figure 8a. There is no clear boundary between Stage 2 and Stage 3 for this group of tests with varying top angles. This is probably because the upper part of the vertical segment and the top angle were changing both together during pulling. In general, the pull-out resistance curves tended to gradually decrease and flatten out with a decreasing of the top angle after Stage 1. Therefore, the wrap around anchorage with a top angle of 90° provided the highest final (ultimate) pull-out resistance at the end of the pull-out test. In addition, it was also noticed that the tilting of the top cap was obvious after the pull-out test because the geotextile wrap around anchorage pushed the sand from the left to right during the pulling process. The larger the top angle in the wrap around anchorage, the more obvious tilting noticed (Figure 8b).

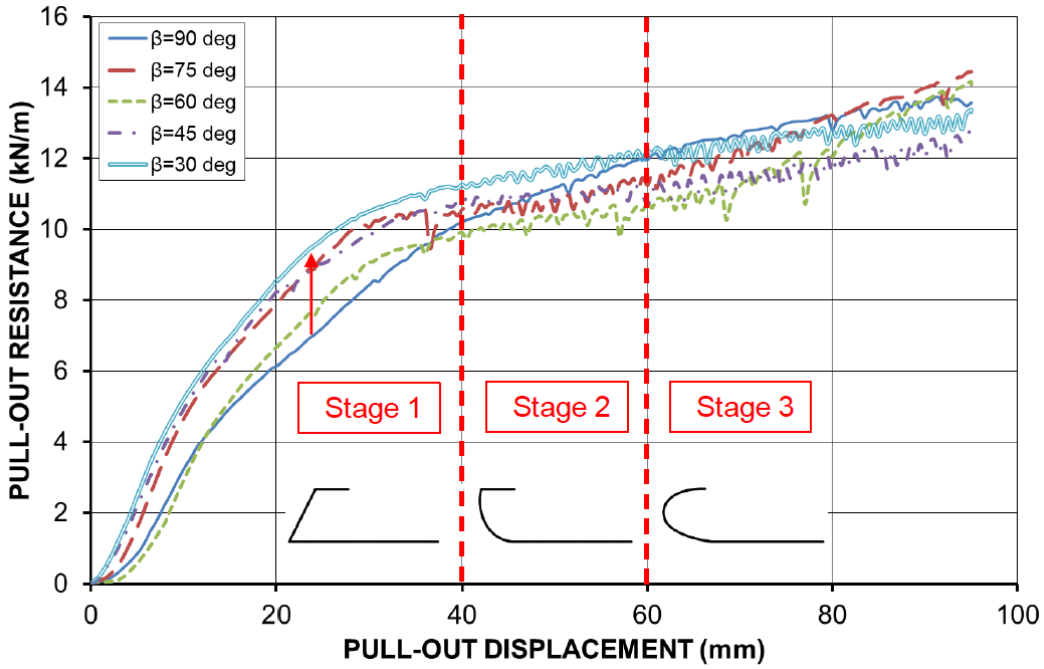

(a)

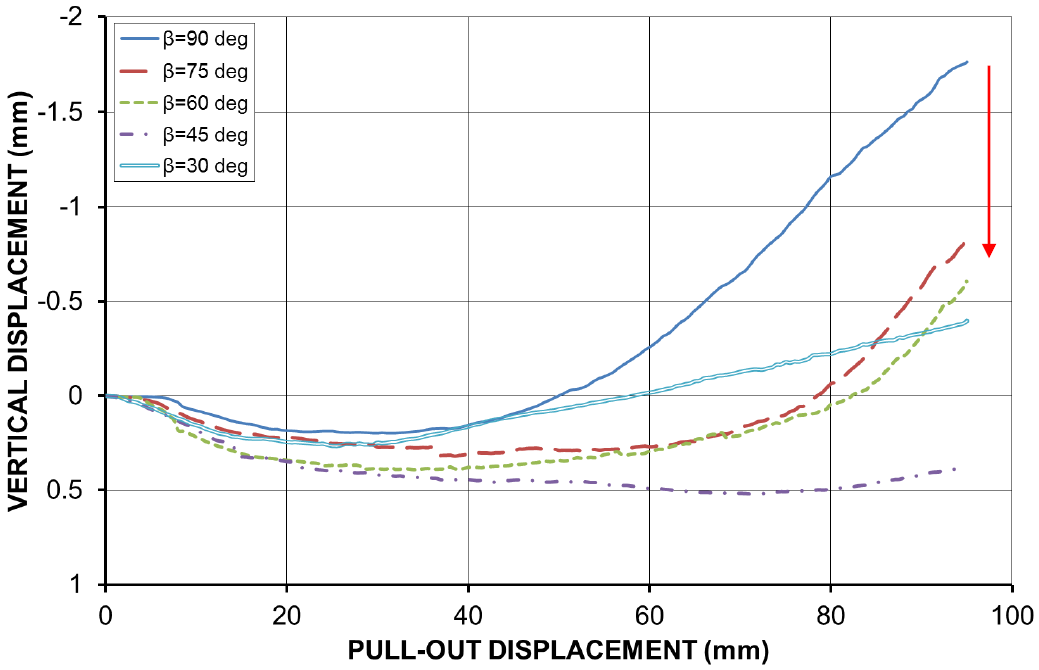

(b)

Figure 7 Influence of bottom angle *β* on pull-out performance: (a) pull-out resistance versus pull-out displacement; (b) vertical displacement versus pull-out displacement

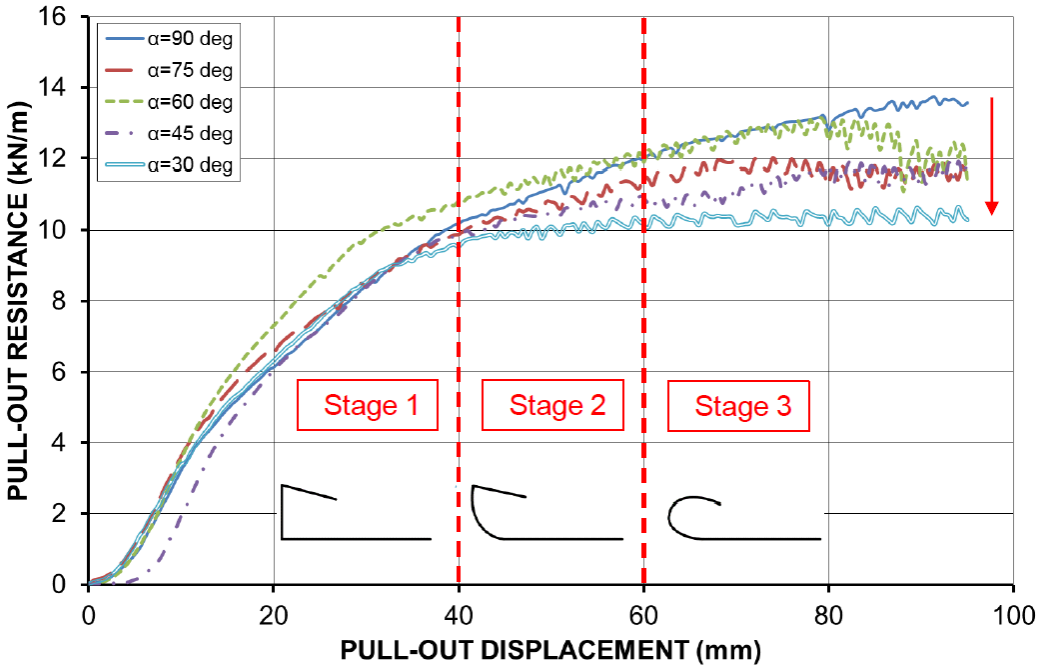

(a)

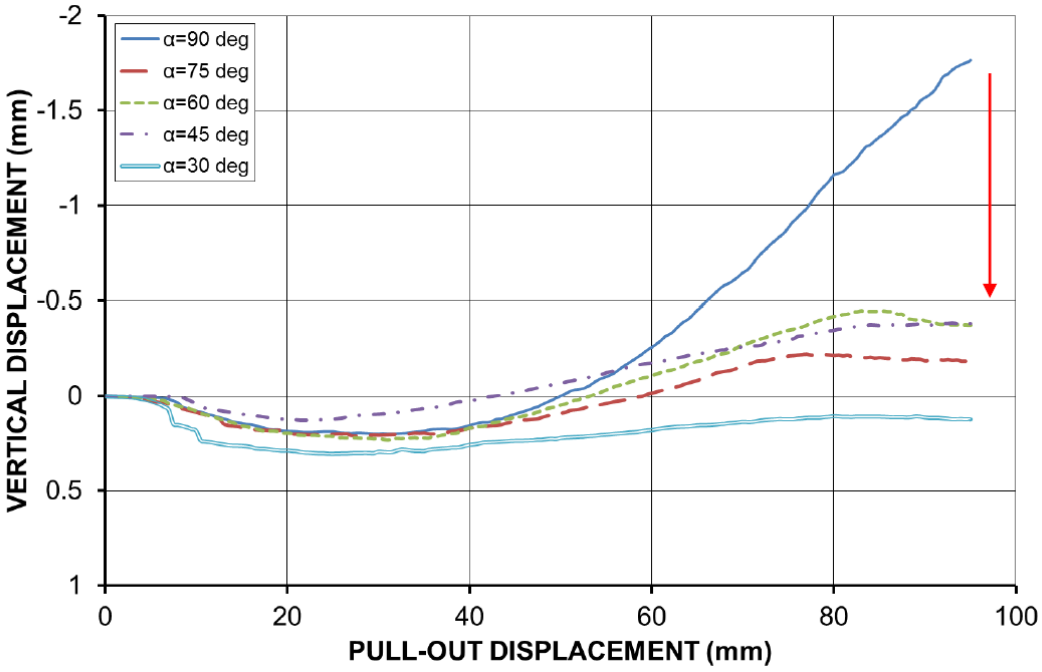

(b)

Figure 8 Influence of top angle *α* on pull-out performance: (a) pull-out resistance versus pull-out displacement; (b) vertical displacement versus pull-out displacement

7 Discussion

7.1 Three stages

For the pull-out testing of the geotextile wrap around anchorage with varying anchorage angles, the pull-out resistance increased gradually with the pull-out displacement to the maximum (ultimate) shear strength without an apparent peak or drop-off. Three stages were summarised to interpret the mobilisation of the pull-out resistance of the geotextile wrap around anchorage during the pulling process. The bottom angle and the bottom layer of the geotextile started functioning first to provide initial pull-out resistance; then the movement of the vertical segment of the geotextile slightly increased the pull-out resistance; finally the top angle and the top layer of the geotextile further contributed more pull-out resistance. The initial and final geometry of the wrap around anchorage after pull-out testing at a larger displacement is depicted in Figure 9.

(a)

(b)

(c)

Figure 9 Initial (black dashed line) and final (red solid line) shape of wrap around anchorage in pull-out test: (a) bottom angle *β*; (b) top angle *α*; (c) *α*=*β*=90°

7.2 Pull-out resistance at different pull-out displacements

As there was no peak occurring in the pull-out testing of the geotextile wrap around anchorage, the maximum pull-out resistance recommended for the design and analysis is highly depended on the acceptable horizontal pull-out displacement. Figure 10 compares the pull-out resistance achieved at a pull-out displacement of 20 mm, 40 mm, 60 mm and 80 mm for different wrap around anchorage angles. Also highlighted in Figure 10 is the maximum (peak) pull-out resistance achieved at a pull-out displacement of 30 mm for the geotextile simple run-out anchorage (red dashed line). It was found that the initial pull-out resistances achieved at a pull-out displacement of 20 mm for all the geotextile wrap around anchorages with different anchorage angles were lower than that achieved for the simple run-out anchorage. This is probably because the wrap around anchorage is more flexible and adjustable than the simple run-out anchorage in the initial pulling stage, and the sand wrapped around in the anchor may experience more adjustment and movement after applying the pull-out displacement. Therefore, it may reduce the interaction efficiency between the geotextile and the sand, so the maximum frictional resistance might not have been fully developed. However, after the pull-out displacement reached 40 mm, the pull-out resistance of the wrap around anchorages went beyond the pull-out resistance of the simple run-out anchorage and continued increasing steadily with the pull-out displacement due to the further contribution of the anchor. The pull-out resistance of the simple run-out anchorage dropped after peaking at a pull-out displacement of 30 mm. As such, the

maximum (ultimate) pull-out resistances of the wrap around anchorages achieved at the end of the pull-out tests were much higher than that of the simple run-out anchorage.

As shown in Figure 10a, it has been proven again that the smaller the bottom angle, the higher the initial pull-out resistance achieved for Stage 1, i.e., before a pull-out displacement of 40 mm. However, the pull-out resistance achieved at a larger pull-out displacement (60 mm or 80 mm) did not follow this trend, because the bottom angle β had been completely destroyed for Stage 2 and Stage 3, as mentioned earlier. In terms of the top angle α, it is evident that the smaller the top angle, the lower the final pull-out resistance achieved at end of the pull-out test (also see Figure 8a and Figure 10b).

7.3 Pull-out resistance versus anchorage angle

Figure 11 shows the pull-out resistance versus anchorage angle at different pull-out displacements, which does not see a consistent trend. However, for a pull-out displacement less than 60 mm, a bottom angle of β=30° provides the highest pull-out resistance, proving again that the bottom angle is dominant in the early stage. The contribution of the top angle and the top layer of the geotextile in the later stage is much more complex because varying the bottom angle changed the top angle α and the top layer length B (constant total length), as also shown in Figure 2b. In terms of the influence of the top angle α, a top angle of α=30° provides the lowest final pull-out resistance at the end of the pull-out test, and a larger top angle tends to provide a higher pull-out resistance in the later stage. Overall, it was found that the maximum pull-out resistances achieved in the wrap around anchorages with different anchorage angles were higher than that achieved in the simple run-out anchorage (P_{Rmax}=9.75 kN/m), indicating that wrap around anchorage can provide higher pull-out resistance. The pull-out resistances obtained for different bottom angles tended to be slightly higher than those for different top angles.

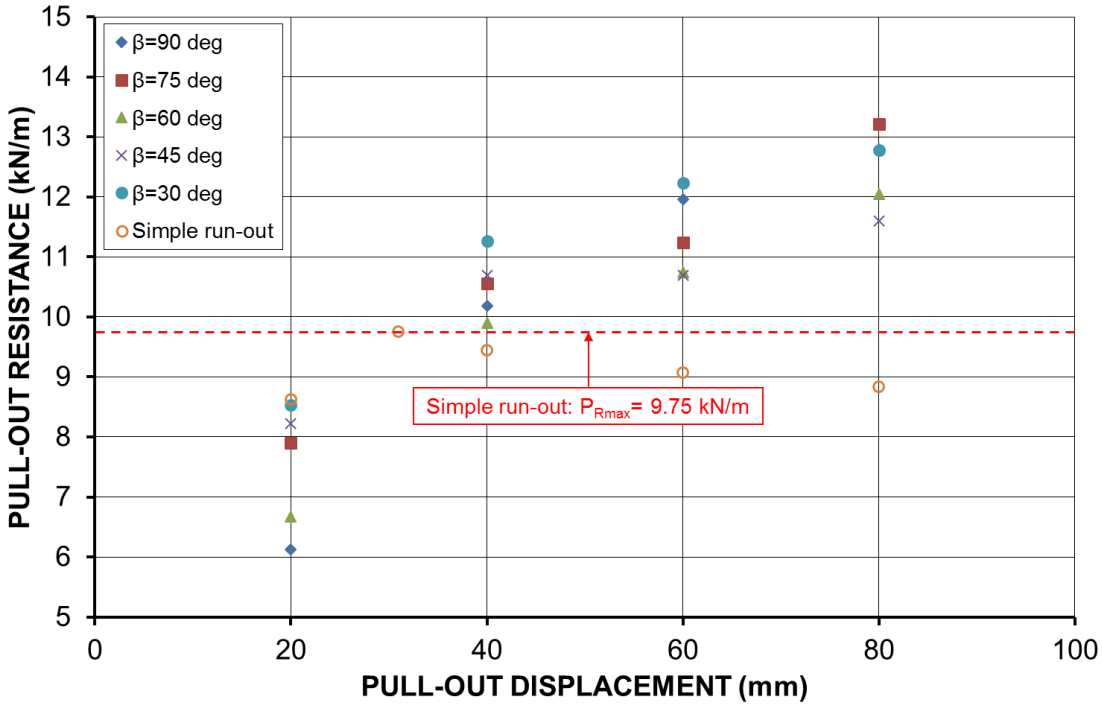

(a)

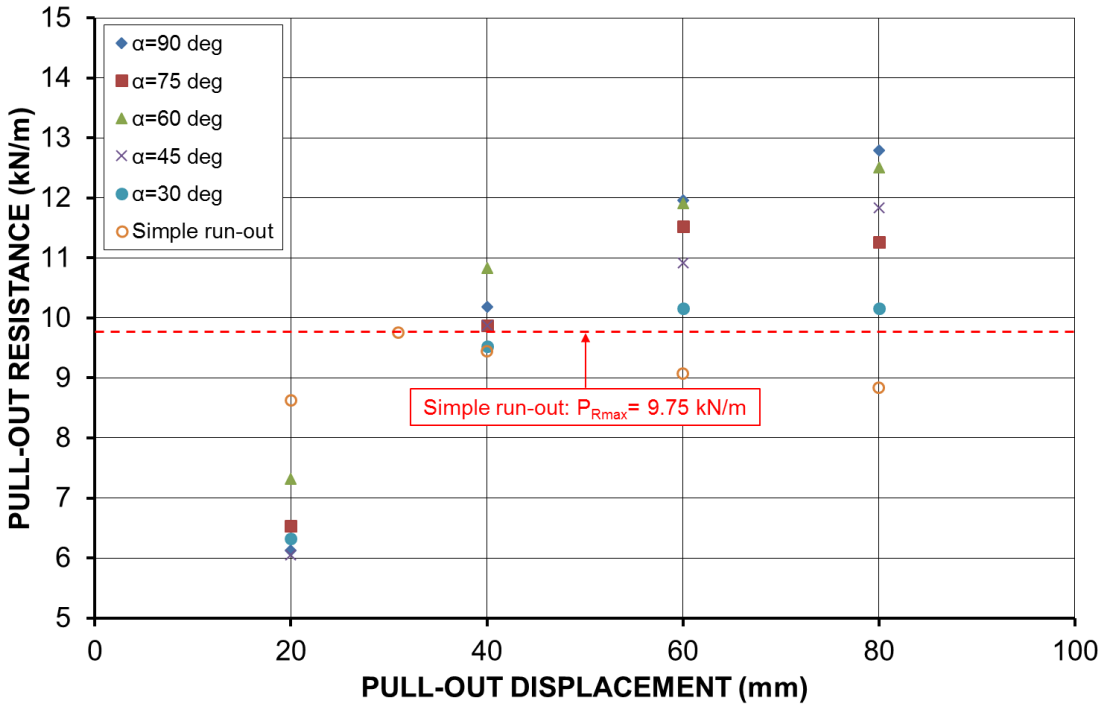

(b)

Figure 10 Pull-out resistance achieved at different pull-out displacements: (a) bottom angle *β*; (b) top angle *α*

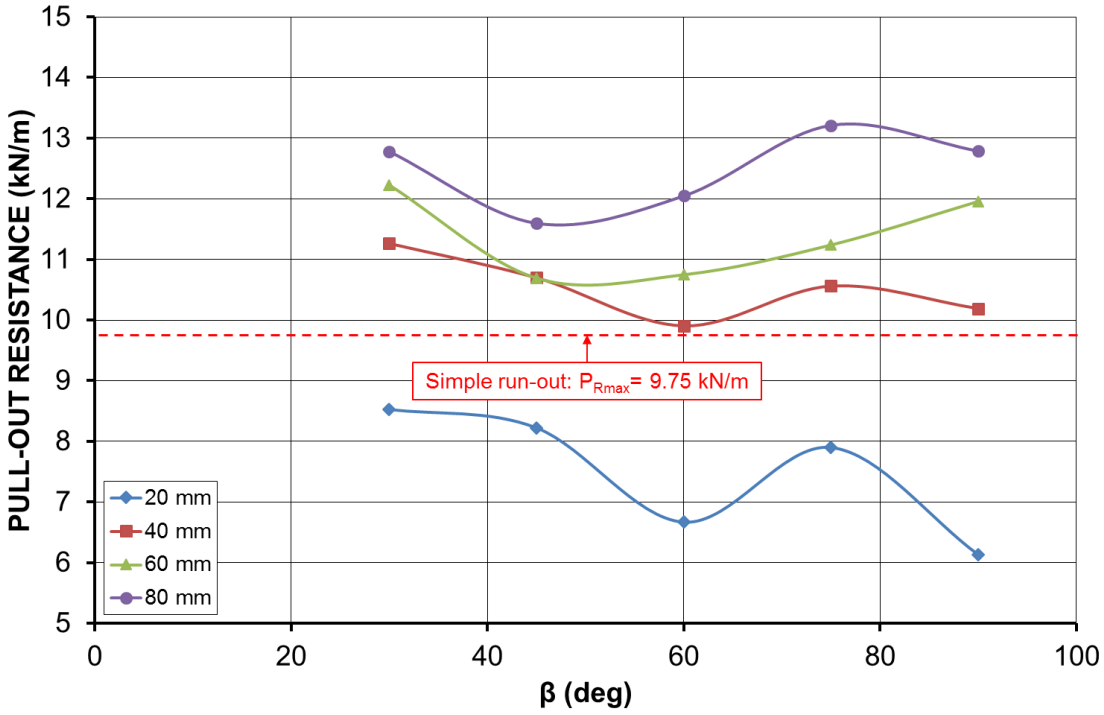

(a)

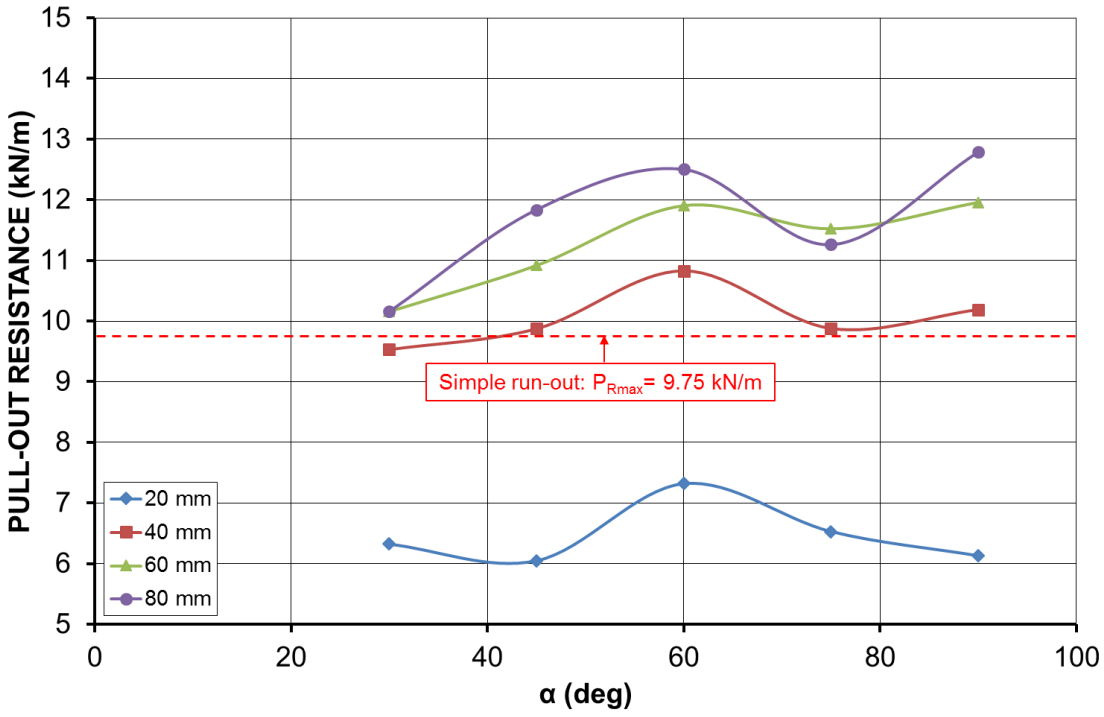

(b)

Figure 11 Pull-out resistance versus anchorage angle at different pull-out displacements: (a) bottom angle *β*; (b) top angle *α*

8 Theoretical Interpretation

Theoretical expressions were derived for the pull-out resistance of the geotextile wrap around anchorage (or called anchorage capacity) as a function of the sand-geotextile interface friction angle δ and the geometric parameters of the anchor, i.e., the length of the bottom layer L, the bottom angle β, the height of the anchor D, the top angle α, and the length of the top layer B. Figure 12 shows the static equilibrium of the wrap around anchorage characterised by varying the bottom angle β and the top angle α. The total pull-out resistance of the geotextile wrap around anchorage is the sum of the individual frictional resistance of each segment that is calculated independently by the Mohr-Coulomb interface friction law. In this study, because the total height of the sand above the geotextile is only 120 mm, it is reasonable to neglect the change of normal stress on the geotextile due to the weight of overburden sand. Based on the previous studies (Villard and Chareyre 2004), a weighting coefficient K was introduced to calculate the tensile stress (force) of the geotextile near a change of angle:

$$T_1 = K_1 T_1' \tag{5}$$

$$K_1 = \mathrm{e}^{\beta \tan \delta} \tag{6}$$

$$K_1 = \min\left[\mathrm{e}^{\beta \tan \delta}, \cos\beta + \sin\beta \tan\phi \right] \tag{7}$$

where T_1 is the tension after a change of angle, T_1' is the initial tension before a change of angle and K_1 is the weighting coefficient. Eq. (6) is used for the rigid soil mass (cohesive soil), Eq. (7) is used for the soil mass failure (frictional soil). It should be noted that T_1/T_1' must be theoretically greater than or equal to1 (i.e., $K_1 \geq 1$). When the calculated K_1 is less than 1 for some values of β and ϕ, it is assumed that the soil is very unstable near the bend and does not provide any additional resistance, so a weighting coefficient of 1 is assumed in these situations (Villard and Chareyre 2004).

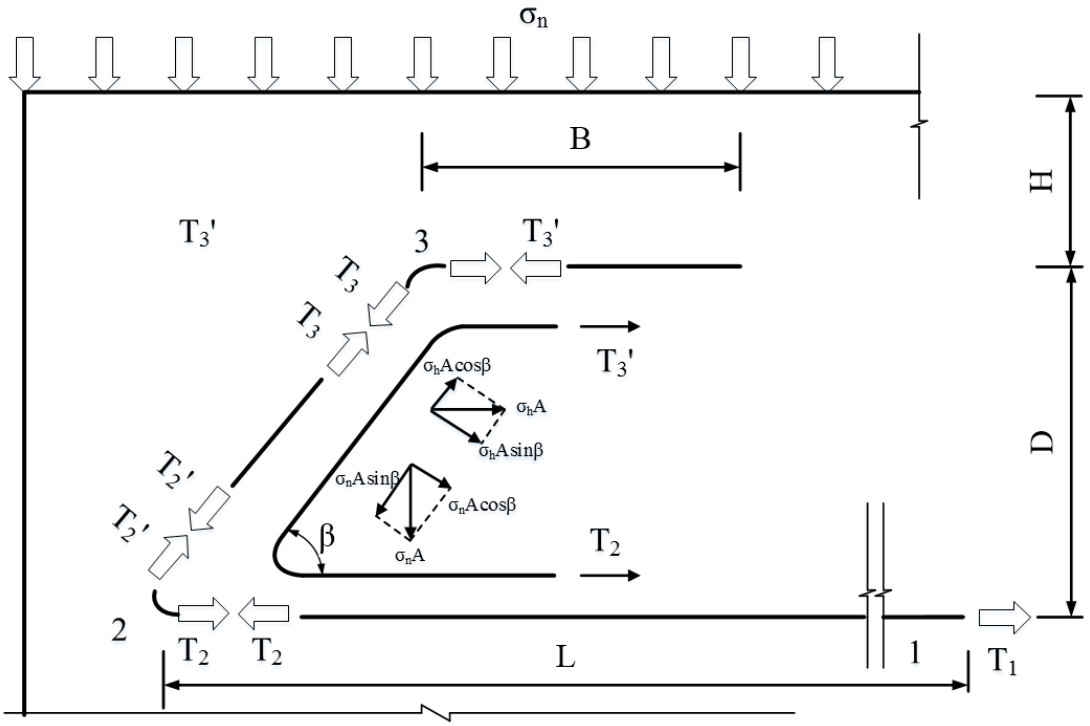

(a)

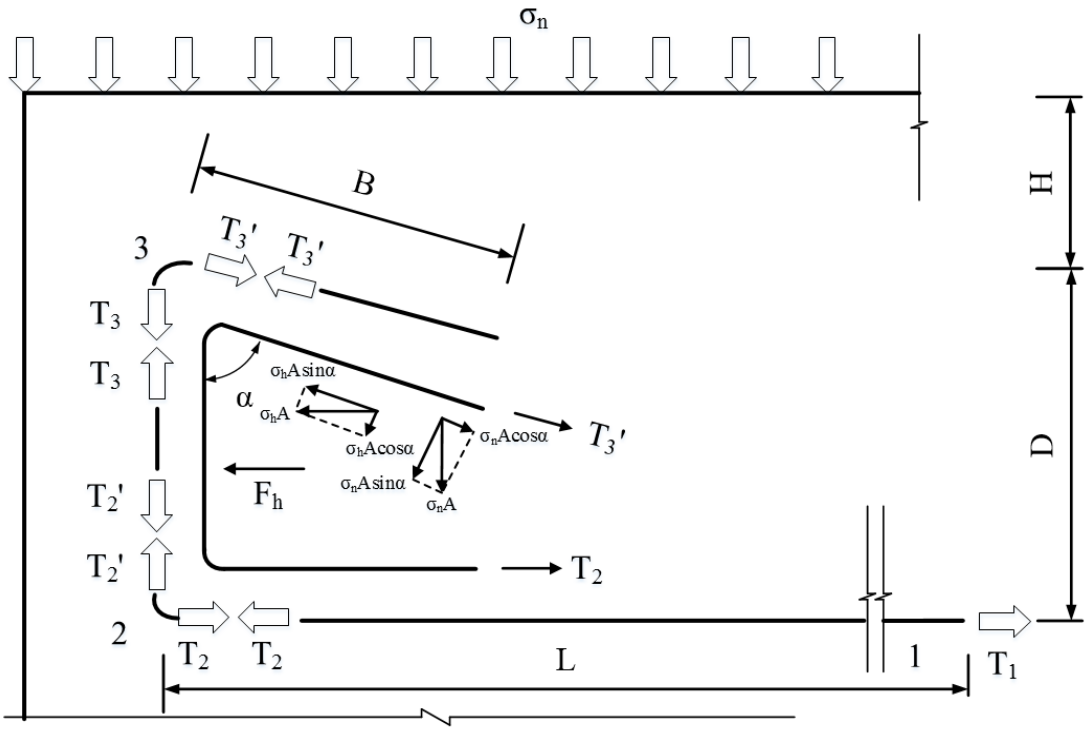

(b)

Figure 12 Static equilibrium of geotextile wrap around anchorage: (a) bottom angle *β*; (b) top angle *α*

8.1 Bottom angle β

Figure 12a shows the static equilibrium of a geotextile anchor with a bottom angle β in the wrap around anchorage configuration. The total pull-out resistance T_1 that can be mobilised is determined by static equilibrium analysis of each segment of the geotextile. The static derivation of the pull-out resistance is shown as follows:

Segment 3:

$$T_3' = 2\sigma_n B \tan\delta \tag{8}$$

$$T_3 = K_3 T_3' \tag{9}$$

$$T_3 = 2K_3\sigma_n B \tan\delta \tag{10}$$

where T_3' is the frictional resistance mobilised along the top layer of the geotextile (Segment 3), σ_n is the applied normal stress, B is the length of the top layer of the geotextile, δ is the sand-geotextile interface friction angle, K_3 is the weighting coefficient at bend 3 and T_3 is the frictional resistance mobilised after a change of angle (bend 3).

Segment 2:

$$T_2' = T_3 + 2(\sigma_n \cos\beta + K_0\sigma_n \sin\beta)\frac{D}{\sin\beta}\tan\delta = T_3 + 2\sigma_n(\cot\beta + K_0)D\tan\delta \tag{11}$$

$$T_2 = K_2 T_2' \tag{12}$$

$$T_2' = 2K_3\sigma_n B\tan\delta + 2\sigma_n(\cot\beta + K_0)D\tan\delta \tag{13}$$

$$T_2 = 2K_2\sigma_n \tan\delta\left[K_3 B + (\cot\beta + K_0)D\right] \tag{14}$$

where D is the height of the anchor, T_2' is the frictional resistance mobilised along the vertical part of the geotextile (Segment 2), K_0 is the coefficient of lateral earth pressure at rest, which can be calculated by K_0=1-sinϕ for the sand, β is the bottom angle of the anchor, K_2 is the weighting coefficient at bend 2 and T_2 is the frictional resistance mobilised after a change of angle (bend 2).

Segment 1:

$$T_1 = T_2 + 2\sigma_n L \tan\delta \tag{15}$$

$$T_1 = 2K_2\sigma_n \tan\delta\left[K_3 B + (\cot\beta + K_0)D\right] + 2\sigma_n L \tan\delta \tag{16}$$

$$T_1 = 2\sigma_n \tan\delta\left\{K_2\left[K_3 B + (\cot\beta + K_0)D\right] + L\right\} \tag{17}$$

where T_1 is the frictional resistance mobilised along the bottom layer of the geotextile (Segment 1) and L is the length of the bottom layer of the geotextile.

8.2 Top angle α

Figure 12b shows the static equilibrium of a geotextile anchor with a top angle α in the wrap around anchorage configuration. The total pull-out resistance T_1 that can be mobilised is determined by static equilibrium analysis of each segment of the geotextile. The static derivation of the pull-out resistance is shown as follows:

Segment 3:

$$T_3' = 2(K_0\cos\alpha + \sin\alpha)\sigma_n B \tan\delta \tag{18}$$

$$T_3 = K_3 T_3' \tag{19}$$

$$T_3 = 2K_3(K_0\cos\alpha + \sin\alpha)\sigma_n B \tan\delta \tag{20}$$

where T_3' is the frictional resistance mobilised along the top layer of the geotextile (Segment 3), α is the top angle of the anchor, σ_n is the applied normal stress, B is the length of the top layer of the geotextile, δ is the sand-geotextile interface friction angle, K_3 is the weighting coefficient at bend 3 and T_3 is the frictional resistance mobilised after a change of angle (bend 3).

Segment 2:

$$T_2' = T_3 + 2K_0\sigma_n D \tan\delta \tag{21}$$

$$T_2 = K_2 T_2' \tag{22}$$

$$T_2' = 2\sigma_n \tan\delta\left[K_3(K_0\cos\alpha + \sin\alpha)B + K_0 D\right] \tag{23}$$

$$T_2 = 2K_2\sigma_n \tan\delta\left[K_3(K_0\cos\alpha + \sin\alpha)B + K_0 D\right] \tag{24}$$

where D is the height of anchor, T_2' is the frictional resistance mobilised along the vertical part of the geotextile (Segment 2), K_0 is the coefficient of lateral earth pressure at rest, which can be calculated by K_0=1-sinϕ for the sand, K_2 is the weighting coefficient at bend 2 and T_2 is the frictional resistance mobilised after a change of angle (bend 2).

Segment 1:

$$T_1 = T_2 + 2\sigma_n L\tan\delta \tag{25}$$

$$T_1 = 2K_2\sigma_n \tan\delta\left[K_3(K_0\cos\alpha + \sin\alpha)B + K_0 D\right] + 2\sigma_n L\tan\delta \tag{26}$$

$$T_1 = 2\sigma_n \tan\delta\left\{K_2\left[K_3(K_0\cos\alpha + \sin\alpha)B + K_0 D\right] + L\right\} \tag{27}$$

where T_1 is the frictional resistance mobilised along the bottom layer of the geotextile (Segment 1) and L is the length of the bottom layer of the geotextile.

8.3 Comparison between theoretical and experimental results

In this study, Eq. (7) is used to calculate K_2 and K_3 for the frictional sand (soil mass failure) in the pull-out tests, and it is found that the calculated weighting coefficients are very close to 1 for different anchorage angles, as shown in Table 3. Therefore, the frictional pulley effect is not significant for cohesionless soils (soil mass failure scenario). Therefore, K_2 and K_3 were taken as 1 for simplicity herein, and Eq. (17) and Eq. (27) can be simplified as the following equations to calculate the pull-out resistance with different anchorage angles:

$$T_1 = 2\sigma_n \tan\delta\left[B + (\cot\beta + K_0)D + L\right] \tag{28}$$

$$T_1 = 2\sigma_n \tan\delta\left[(K_0\cos\alpha + \sin\alpha)B + K_0 D + L\right] \tag{29}$$

It is evident that the pull-out resistance is a function of applied normal stress σ_n, interface friction angle δ and geometric parameters of the anchor (B, D, L, β, α). Eq. (28) shows that the pull-out resistance is also a function of cotβ, indicating that it increases as the bottom angle β decreases. Mathematically, the domain of definition for the variable β in the

function cotβ is ($0<\beta\leq 90°$) for this specific engineering problem. However, it can't be equal to 0°. This finding is basically consistent with the experimental observation for the early stage (see Figure 7a and Figure 11a). Furthermore, Eq. (29) shows that there exists an optimum top angle α to maximize the pull-out resistance, as illustrated in the following equations:

$$f(\alpha) = K_0 \cos\alpha + \sin\alpha = \sqrt{1+K_0^2}\,\sin(\psi+\alpha) \tag{30}$$

$$\sin\psi = \frac{K_0}{\sqrt{1+K_0^2}} \tag{31}$$

In this study, K_0=1-sin31°=0.485, leading to ψ=25.9°. When α=90°-ψ=64.1°, $f(\alpha)$ reaches its maximum value. This finding could also be verified by the experimental results. It was found that the pull-out resistance of the wrap around anchorage with a top angle of 60° was highest in Stage 1 and Stage 2 from the experimental results (Figure 8a). A repeated test on 60° was also conducted to further verify the finding, and the two curves obtained from the two repeated tests almost coincide for a displacement less than 70 mm.

Overall, the theoretical and experimental results produced consistent findings of the influence of the anchorage angles on the initial pull-out resistance in Stage 1 and Stage 2. The maximum pull-out resistances of the geotextile wrap around anchorage with varying anchorage angles obtained from the experimental and theoretical studies are compared in Figure 13. Also, by comparing Figure 11 with Figure 13, it is also found that the theoretical trends are basically consistent with the experimental results in early and middle stage. However, in terms of the maximum pull-out resistance achieved at the final largest displacement, the experimental results do not show a consistent relationship, as shown in Figure 13. There are several possible reasons for this. For example, sometimes, the tension pulley may skew at large displacement, causing experimental errors. However, through this study, it is believed that the theoretical and experimental results have proven the influencing trends of anchorage angles on pull-out resistance during the pulling process. Future study has been proposed to carry out the pull-out test on geotextile anchorage embedded in clay with different anchorage configurations to validate and extend the conclusion of this research, and it is expected that for rigid soil mass (cohesive soil), the influence of angle angles on pull-out resistance would be more significant due to the frictional pulley effect (Villard and Chareyre 2004; Gourc et al. 2005). Moreover, scale

effects on the experimental tests should also be noted, and the future study would be increased to a larger scale or field condition in order to optimise the anchorage configurations.

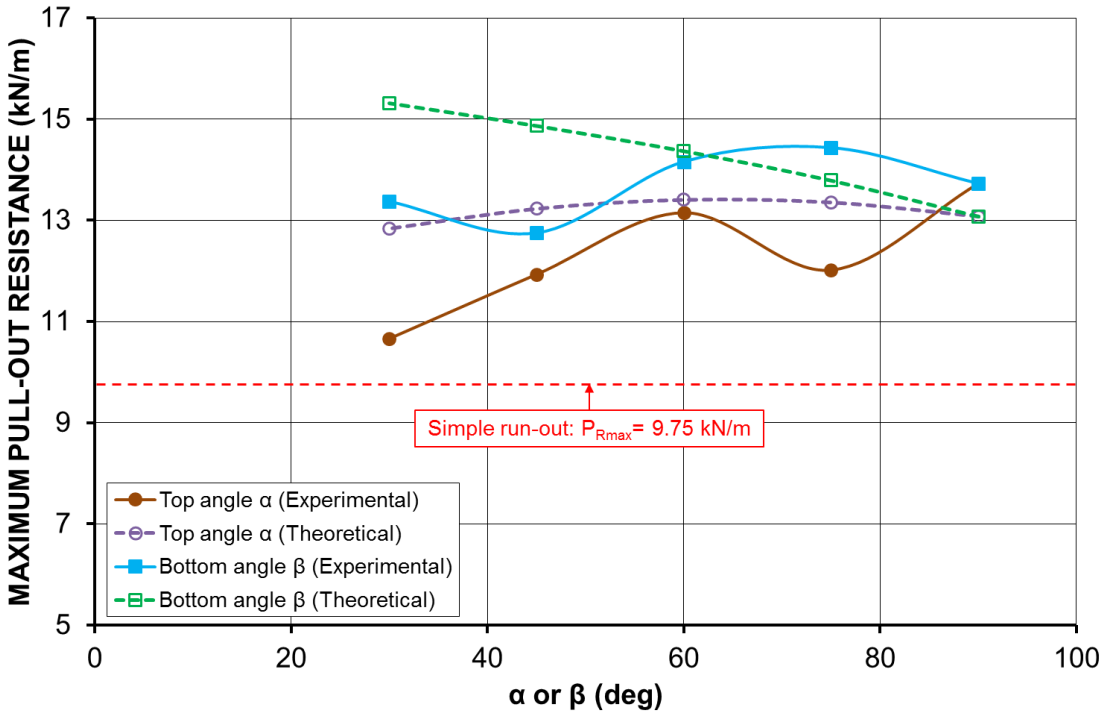

Figure 13 Comparison of maximum pull-out resistances from experimental and theoretical results

Table 3 Calculated value of weighting coefficients

β (°)	$K_3 \geq 1$ ($\beta=\beta$)			$K_2 \geq 1$ ($\beta=\pi-\beta$)		
	$\exp(\beta\tan\delta)$	$\cos\beta+\sin\beta\tan\delta$	K_3	$\exp(\beta\tan\delta)$	$\cos\beta+\sin\beta\tan\delta$	K_2
90	2.61	0.61	1	2.61	0.61	1
75	2.22	0.85	1	3.06	0.33	1
60	1.89	1.03	1.03	3.59	0.03	1
45	1.62	1.14	1.14	4.21	-0.28	1
30	1.38	1.17	1.17	4.94	-0.56	1
α (°)	$K_3 \geq 1$ ($\beta=\pi-\alpha$)			$K_2 \geq 1$ ($\beta=\pi/2$)		
	$\exp(\beta\tan\delta)$	$\cos\beta+\sin\beta\tan\delta$	K_3	$\exp(\beta\tan\delta)$	$\cos\beta+\sin\beta\tan\delta$	K_2
90	2.61	0.61	1	2.61	0.61	1
75	3.06	0.33	1	3.06	0.33	1
60	3.59	0.03	1	3.59	0.03	1
45	4.21	-0.28	1	4.21	-0.28	1
30	4.94	-0.56	1	4.94	-0.56	1

9 Conclusions

A series of pull-out tests were carried out on the geotextile with different anchorage configurations embedded in sand, including simple run-out and wrap around anchorages with varying anchorage angles. The influence of the anchorage angles on pull-out resistance of the geotextile wrap around anchorage was investigated experimentally and theoretically. The main conclusions obtained in this paper are drawn as follows:

(1) The wrap around anchorage can provide a higher anchorage capacity than the simple run-out anchorage in the pull-out tests.

(2) Three stages were summarised to interpret the mobilisation of the pull-out resistance of the geotextile wrap around anchorage during the pulling process.

(3) The smaller the bottom angle, the higher the initial pull-out resistance achieved in early and middle stages, while the larger the top angle, the higher the final pull-out resistance achieved in final stage.

(4) The theoretical expressions of the pull-out resistance of the geotextile wrap around anchorage with varying anchorage angles were derived based on static equilibrium analysis, and the theoretical trends are basically consistent with the experimental findings in early and middle stage.

References

ASTM D6706-13. (2013) Standard Test Method for Measuring Geosynthetic Pullout Resistance in Soil. ASTM International, West Conshohocken, Pennsylvania, USA.

Abdelouhab, A., Dias, D., and Freitag, N., (2010). Physical and analytical modelling of geosynthetic strip pull-out behaviour. Geotextiles and Geomembranes, 28(1), 44-53.

Alfaro, M., Miura, N., and Bergado, D., (1995). Soil-Geogrid Reinforcement Interaction by Pullout and Direct Shear Tests. Geotechnical Testing Journal, 18(2), 157-167.

Bakeer, R. M., Sayed, S. M., Cates, P., and Subramanian, R., (1998). Pullout and shear tests on geogrid reinforced lightweight aggregate. Geotextiles and Geomembranes, 16(2), 119-133.

Briançon, L., Girard, H., and Villard, P., (2008). Geosynthetics Anchorage: Experimental and Numerical Studies. Proceedings of the 4th European Geosynthetic Congress, Edinburgh, UK.

Chareyre, B., Briançon, L., and Villard, P., (2002). Theoretical Versus Experimental Modeling of the Anchorage Capacity of Geotextiles in Trenches. Geosynthetics International, 9(2), 97-123.

Chareyre, B., and Villard, P., (2005). Dynamic Spar Elements and Discrete Element Methods in Two Dimensions for the Modeling of Soil-Inclusion Problems. Journal of Engineering Mechanics, 131(7), 689-698.

Chen, R. -H., Chi, P. -C., and Fon, K. -Y., (2012). Model tests for anchored geosynthetic slope systems under dry and seepage conditions. Geosynthetics International, 19(4), 306-318.

De, A., and Vellone, D. A., (2005). Experimental and Numerical Modeling of Geosynthetic Anchor Trench. Proceedings of the Geo-Frontiers 2005 Congress, Austin, TX, USA.

Fannin, R. J., and Raju, D. M., (1993). On the pullout resistance of geosynthetics. Canadian Geotechnical Journal, 30(3), 409-417.

Farrag, K., Acar, Y. B., and Juran, I., (1993). Pull-out resistance of geogrid reinforcements. Geotextiles and Geomembranes, 12(2), 133-159.

Ferreira, F. B., Vieira, C. S., Lopes, M. L., and Carlos, D. M., (2016). Experimental investigation on the pullout behaviour of geosynthetics embedded in a granite residual soil. European Journal of Environmental and Civil Engineering, 20(9), 1147-1180.

Ghiassian, H., Jalili, M., and Kasemi, D., (2009). Model study of sandy slopes under uniform seepage and reinforced with anchored geosynthetics. Geosynthetics International, 16(6), 452-467.

Girard, H., Briançon, L., and Rey, E., (2006). Experimental tests for geosynthetic anchorage trenches. In Proceedings of the Eighth International Conference on Geosynthetics, 8th ICG, Japan, 18–22 September 2006, pp. 211-216.

Gourc, J. P., Reyes-Ramirez, R., and Villard, P., (2005) Geosynthetic reinforcement in landfills design: European perspectives. Proceedings Geo-Frontiers 2005, Geotechnical Special Publication 141 (CD-ROM), ASCE, Reston, VA.

Gurung, N., (2000). A Theoretical Model for Anchored Geosynthetics in Pull-Out Tests. Geosynthetics International, 7(3), 269-284.

Hullings, D. E., and Sansone, L. J., (1997). Design concerns and performance of geomembrane anchor trenches. Geotextiles and Geomembranes, 15(4), 403-417.

Lajevardi, S. H., Briançon, L., and Dias, D., (2014). Experimental studies of the geosynthetic anchorage – Effect of geometric parameters and efficiency of anchorages. Geotextiles and Geomembranes, 42(5), 505-514.

Lajevardi, S. H., Dias, D., and Briançon, L., (2015a). Experimental studies of the behaviour of geosynthetic wrap around anchorage. Geosynthetics International, 22(3), 249-256.

Lajevardi, S. H., Silvani, C., Dias, D., Briançon, L., and Villard, P., (2015b). Geosynthetics anchorage with wrap around: experimental and numerical studies. Geosynthetics International, 22(4), 273-287.

Moraci, N., and Recalcati, P., (2006). Factors affecting the pullout behaviour of extruded geogrids embedded in a compacted granular soil. Geotextiles and Geomembranes, 24(4), 220-242.

Mosallanezhad, M., Hataf, N., and Sadat Taghavi, S. H., (2016). Experimental and large-scale field tests of grid-anchor system performance in increasing the ultimate bearing capacity of granular soils. Canadian Geotechnical Journal, 53(7), 1047-1058.

Rajabian, A., and Viswanadham, B. V. S., (2016). Behaviour of anchored geosynthetic-reinforced slopes subjected to seepage in a geotechnical centrifuge. Geosynthetics International, 23(1), 36-47.

Raviteja, K. V. N. S., and Munwar Basha, B., (2018). Optimal reliability based design of v-shaped anchor trenches for MSW landfills. Geosynthetics International, 1-46.

Sieira, A. C. C. F., Gerscovich, D. M. S., and Sayão, A. S. F. J., (2009). Displacement and load transfer mechanisms of geogrids under pullout condition. Geotextiles and Geomembranes, 27(4), 241-253.

Villard, P. and Chareyre, B., (2004). Design methods for geosynthetic anchor trenches on the basis of true scale experiments and discrete element modelling. Canadian Geotechnical Journal, 41(6), 1193-1205.

Yasuhara, K., and Recio-Molina, J., (2007). Geosynthetic-wrap around revetments for shore protection. Geotextiles and Geomembranes, 25(4), 221-232.

Zornberg, J. G., (2005). Geosynthetic reinforcement in landfill design: US perspectives. Proceedings Geo-Frontiers 2005, Geotechnical Special Publication 141 (CD-ROM), ASCE, Reston, VA.

Attached Paper V

Paper V: Triaxial Testing of Clay with Geotextile Encased Sand Column

Xu, Y., Wu, S., Williams, D. J., Serati, M., 2018. Triaxial testing of clay with geotextile encased sand column. (submitted) – incorporated as **Paper V**.

Triaxial Testing of Clay with Geotextile Encased Sand Column

Youwei Xu[a,], Shengshen Wu[b], David J. Williams[c], Mehdi Serati[d]*

[a] PhD candidate, School of Civil Engineering, The University of Queensland, Brisbane, QLD 4072, Australia. Email: youwei.xu@uq.edu.au

[b] PhD candidate, School of Engineering, RMIT University, Melbourne, VIC 3001, Australia. E-mail: s3479492@student.rmit.edu.au

[c] Professor, School of Civil Engineering, The University of Queensland, Brisbane, QLD 4072, Australia. Email: d.williams@uq.edu.au

[d] Postdoctoral Research Fellow, School of Civil Engineering, The University of Queensland, Brisbane, QLD 4072, Australia. Email: m.serati@uq.edu.au

Abstract

Reinforcing soft soil with granular columns is an effective and economic ground improvement technique. With the additional inclusion of geosynthetic encasement to provide extra confinement for granular columns, the reinforcing performance could be further improved. Some researchers have carried out triaxial tests on cylindrical composite soil specimens with different granular column reinforcing configurations, mainly focusing on the investigations of the improved load capacity. However, there has been little discussion about the effects of the granular column or geosynthetic encasement on pore water pressure dissipation during the consolidation stage, induced pore water pressure change during the shearing stage, total and effective stress Mohr circles, and total and effective stress paths, etc. Therefore, isotropically consolidated undrained (CU) triaxial tests with pore pressure measurement were carried out on the Kaolin, Kaolin with ordinary sand column (OSC) and Kaolin with geotextile encased sand column (GESC) to further study the shear strength and pore water pressure behaviour of the composite materials. The effects of OSC and GESC on pore water pressure, shear strength, Mohr circle, failure envelope and stress path

were discussed and interpreted, from both total stress and effective stress perspectives. Given that the excavation process in the field would make the normally consolidated clay change to an overconsolidated state as a result of overburden unloading, the effects of different OCRs (i.e., 1, 2, 4 and 8) on pore water pressure, shear strength, Mohr circle and stress path in the CU triaxial tests were also investigated and interpreted. These investigations will enhance the understanding of the triaxial behaviour of clay with the inclusion of OSC and GESC.

Keywords: sand column; geotextile encased sand column; Mohr circles; over consolidation ratio; shear strength; triaxial

1 Introduction

Soft soils have low bearing capacity, low shear strength and high compressibility, and hence, they need to be treated prior to the construction of overlying structures. Reinforcing soft soil with granular columns is an effective and economic ground improvement technique, which has been widely used in many applications, such as embankments, foundations, pavements, etc. The inclusion of granular columns can not only improve the bearing capacity and reduce the settlement of soft soils, but also accelerate the consolidation process as they act as vertical drains (Black et al. 2006; Black et al. 2007; Black et al. 2011; Andreou et al. 2008; Murugesan and Rajagopal 2007, 2009, 2010; Mohapatra et al. 2016, 2017; Najjar et al. 2010; Najjar 2013; Najjar and Skeini 2015; Castro 2017).

However, for extremely soft soils, the reinforcing performance of the granular columns is not satisfying due to the insufficient lateral confinement of the surrounding soft soil, which commonly leads to a bulging failure (excessive radial expansion) of the granular columns. One of the most effective solutions to address this issue is to encase the granular columns with geosynthetics. The geosynthetic encasement is able to provide extra confinement for granular columns; hence, the effectiveness of the ground treatment can be significantly improved. A large number of laboratory model tests have been carried out on different types of soils with the inclusion of encased or non-encased granular columns under vertical loading in the model tanks, to study the reinforcing performance and effectiveness of the different

granular column reinforcing configurations (Muir Wood et al. 2000; Ayadat and Hanna 2005; Gniel and Bouazza 2009, 2010; Murugesan and Rajagopal 2007; 2009; 2010; Najjar et al. 2010; Ali et al. 2012, 2014; Hong et al. 2016; Miranda and Da Costa 2016; Mohapatra et al. 2016, 2017). These studies mainly focused on the load-settlement behaviour and bearing capacities of the reinforced soil composite.

Review of the literature has revealed that most of the laboratory model tests failed to control the drainage condition in the soil and did not allow for the measurement of pore pressure change during the loading and consolidation processes. Triaxial testing method is able to control the stress state, drainage condition, loading rate and lateral pressure, and is also able to measure the induced pore pressure and volume change. Therefore, some researchers had carried out triaxial tests on the reinforced soil composite, such as the geosynthetic-encased or non-encased granular columns (Rajagopal et al. 1999; Wu and Hong 2009; Miranda and Da Costa 2016; Kadhim 2016), and clay with geosynthetic-encased or non-encased granular columns (Juran and Guermazi 1988; Sivakumar et al. 2004, 2011; Black et al. 2006; Black et al. 2007; Black et al. 2011; Kim et al. 2007; Andreou et al. 2008; Najjar et al. 2010; Frikha et al. 2015). Najjar and Skeini (2015) reviewed and analysed 114 triaxial test results of clays with encased or non-encased granular columns from 11 previously-published papers, focusing on the effects of loading rate and drainage condition on bearing capacity of the composite reinforced soils. It has been found that the load capacity obtained by triaxial testing of the clay composite with a single (or multiple) granular column (or groups) is closely related to the undrained shear strength of the clay, friction angle of the granular material, encased or non-encased conditions, the diameter of the granular column, length of the granular column (partially or fully penetrating), number of the columns, area replacement ratio, length to diameter ratio and the spacing of the column groups (Juran and Guermazi 1988; Muir Wood et al. 2000; Sivakumar et al. 2004, 2011; Andreou et al. 2008; Black et al. 2006, 2007, 2011; Najjar 2010, 2013, 2015; Frikha et al. 2015). The performance of clay reinforced with OSC or GESC subjected to lateral loading has also been experimentally modelled by direct shear box tests (Murugesan and Rajagopal 2009; Mohapatra et al. 2016; Xu et al. 2018).

However, most previous studies tend to focus only on the load capacity of the clay composite with different reinforcing configurations, as mentioned above, lacking the discussion about effects of the granular column or geosynthetic encasement on pore water pressure dissipation during the consolidation stage, induced pore water pressure change during the shearing stage, total and effective stress Mohr circles, and total and effective stress paths, etc. Therefore, to further investigate the shear strength and pore water pressure behaviour of clay reinforced with geosynthetic-encased and non-encased granular columns, isotropically consolidated undrained (CU) triaxial tests with pore pressure measurement were carried out on the Kaolin, Kaolin with ordinary sand column (OSC) and Kaolin with geotextile encased sand column (GESC), under effective confining pressures of 100 kPa, 200 kPa and 400 kPa, at a strain rate of 2.4 %/h (i.e., 0.04 mm/min).

In addition, overconsolidated soils would be commonly encountered in excavations in the field as a result of overburden unloading, and thus, the stress-dependent behaviour of soils has also attracted some researchers' interest through K_o-consolidated or isotropically consolidated triaxial tests (Zhu and Yin 2000; Abdulhadi et al. 2012; Gu et al. 2016; Wu et al. 2017). Therefore, the effects of over consolidation ratio (OCR) on undrained shear strength, pore pressure change, Mohr circle and stress path were also investigated and interpreted in this study through the CU triaxial tests with pore pressure measurement.

2 Materials

A Kaolin clay was used in this study. The Kaolin has a high liquid limit (LL) of 90% and a plastic limit (PL) of 35%, resulting in a plasticity index (PI) of 55%. A poorly graded (SP) fine sand, with the grain size ranging between 0.3 mm and 0.6 mm, was used to construct the sand column in the middle of the cylindrical Kaolin specimen. The air-dry sand was found to have a friction angle of 30.1° determined by direct shear testing. A woven polypropylene geotextile, Tencate Mirafi HP340, was used as the encasement material, which has an ultimate tensile strength of 40 kN/m and a nominal thickness of 0.6 mm. The properties of the materials used in this study are summarised in Table 1. It is worthwhile mentioning the limimation of the scale effects in the small-scale tests. That is, a prototype-scale geotextile has been combined with

a small-scale model, so the small-model maybe over-reinforced. The improvement in triaxial behaviour is expected to be less if an appropriately-scaled geotextile had been used, i.e., a model inclusion with much lower strength and stiffness. Therefore, large-scale triaxial tests were recommended in the future study.

Table 1 Properties of materials used

Kaolin	Property or Value	Sand	Property or Value	Geotextile	Property or Value
LL (%)	90	ϕ (°)	30.1	Brand	Tencate HP340
PL (%)	35	c (kPa)	12.9	Polymer	Polypropylene
PI (%)	55	ρ_{dmax} (t/m^3)	1.734	Texture	Woven
w (%)	55 ± 1	ρ_{dmin} (t/m^3)	1.582	Tensile strength (kN/m)	40
G_s	2.615	G_s	2.644	Nominal thickness (mm)	0.6
USCS	CH	USCS	SP	Strain at maximum load (%)	15

3 Triaxial testing program

3.1 Sample preparation

A uniform Kaolin slurry was prepared using a mechanical mixer at an initial water content of 135%, which is close to 1.5 times liquid limit (LL=90%). The Kaolin slurry was then poured into a slurry consolidometer and consolidated under a vertical pressure of 100 kPa to prepare the clay specimens for triaxial testing. Double drainage was allowed in the slurry consolidation process to ensure the uniformity of the clay specimens. The slurry consolidometer has a diameter of 150 mm and a height of 400 mm (Shokouhi et al. 2017). After the induced pore pressure had fully dissipated and the settlement became stable, the cylindrical triaxial Kaolin specimens were extruded from the slurry consolidometer using a sampling mould. The inner and outer diameters of the sampling mould are 48 mm and 50 mm (a wall thickness of 1 mm), respectively. Thus, all the prepared triaxial specimens were controlled to have a diameter of 48 mm and a height of 100 mm. The sample

preparation procedures are shown in Figure 1. It was found that the total height of the sample remained in the consolidometer was higher than 220 mm after the slurry consolidation test finished. Eight intact triaxial specimens could therefore be prepared from each slurry consolidation test (Figure 2). The average moisture content of the reconstituted Kaolin specimen was found to be 55% after the slurry consolidation test under the applied vertical pressure of 100 kPa.

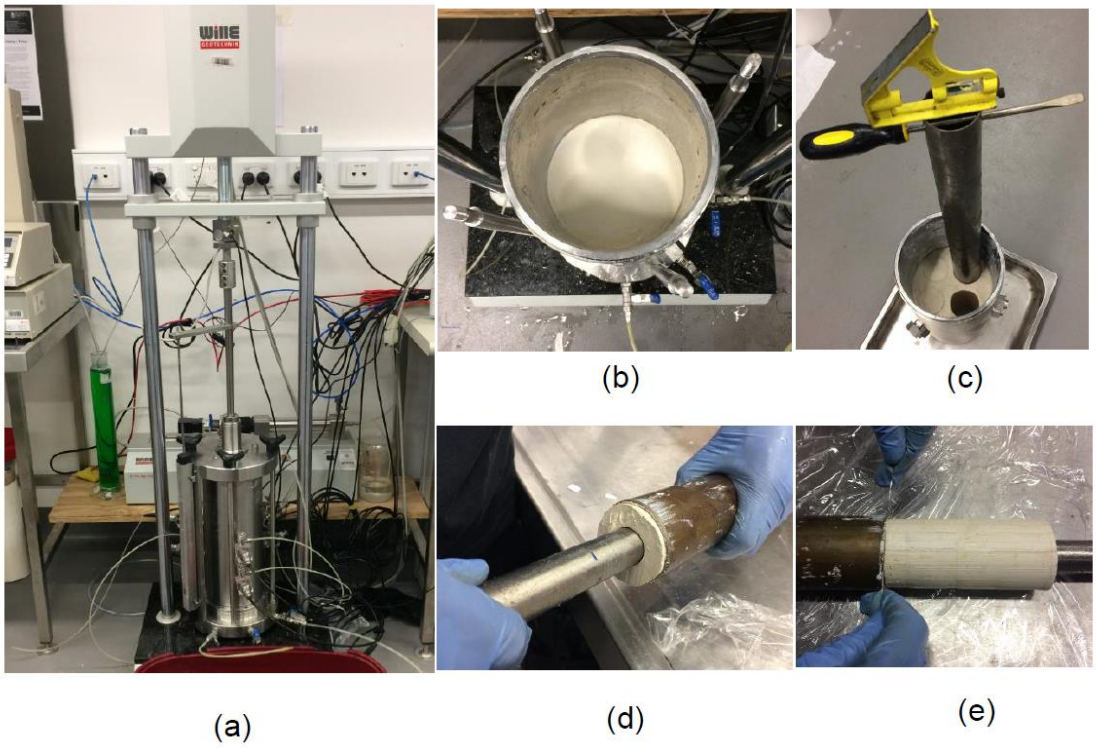

Figure 1 Sample preparation: (a) slurry consolidometer; (b) Kaolin after slurry consolidation; (c) sampling mould; (d) thin-walled tube; (e) triaxial specimen cutting

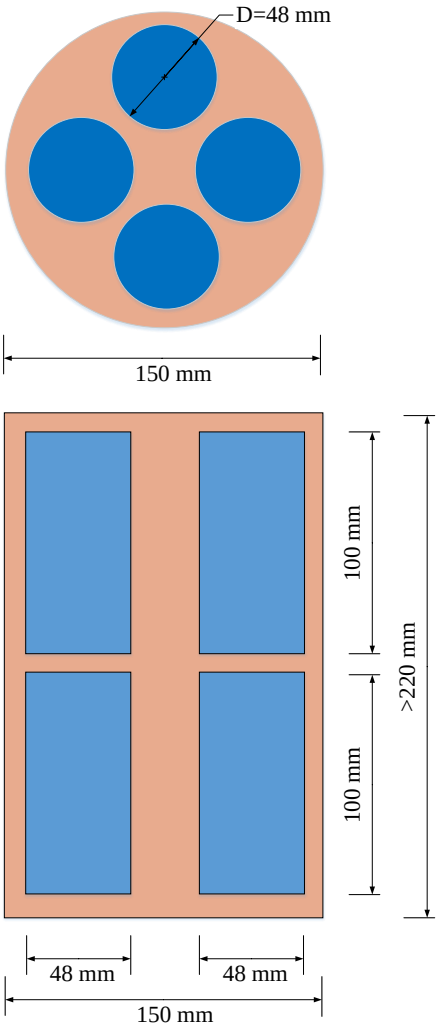

Figure 2 Eight triaxial specimens obtained from slurry consolidometer

3.2 OSC and GESC installation

Since the size of the cylindrical specimen (48 mm in diameter and 100 mm in height) is quite small, only a single sand column (22 mm in diameter) was installed in the middle of the clay specimen, resulting in an area replacement ratio of 21% and a column length to diameter ratio of 4.5. It is believed that installing triangular or square column groups (3 or 4 sand columns) in such a small specimen is not realistic and appropriate. This is because the column diameter to length ratio, the spacing and the scale effect would be great issues for the small-scale laboratory model tests.

Sivakumar et al. (2004) had found that columns with a length to diameter larger than five did not show further increase in the load-carrying capacity. Black et al. (2011) also reported that the optimum area replacement ratio was between 30–40% for the control of settlement, and there was no significant improvement when the length to diameter ratio was higher than 8%-10%. Therefore, a granular column with a very high length to diameter ratio (> 10) is obviously not practical and representative in the field. However, it was still found that a wide range of area replacement ratios (from 4% to 64%) and column length to diameter ratios (from 2.4 to 22.2) had been investigated in the literature (Najjar and Skeini 2015).

In this study, a single sand column was installed in the middle of the Kaolin specimen by the replacement method. That is, a smaller cylinder (22 mm in diameter) in the middle of the triaxial specimen (48 mm in diameter) was removed and replaced with the same volume of sand using a thin-walled tube, having an outer diameter of 22 mm (Figure 1d). The thin-wall tube was vertically inserted into the Kaolin specimen, extruding out the Kaolin in the middle. Thus, a hollow cylindrical specimen was formed, and the hole was then filled with air-dry sand using a funnel to construct the sand column (Figure 3). After that, the formed sand column was saturated by injecting water using a syringe. More sand might be needed to compensate for the reduction in height caused by saturation. Finally, the composite specimen (Kaolin with OSC) was covered with fully-saturated filter papers on the top and bottom to hold the sand. For the Kaolin with GESC, a prefabricated geotextile sleeve was first inserted into the hole before filling with sand. The general OSC and GESC installation procedures are shown in Figure 3.

(a)

(b)

Figure 3 Sand column installation in cylindrical Kaolin specimen: (a) OSC installation; (b) GESC installation

This sand column installation method is believed to be superior to the frozen sand column method adopted by some researchers (Sivakumar et al. 2004; Black et al. 2007; Kim et al. 2007; Najjar et al. 2010). This is because the diameter of the frozen sand column needs to be slightly smaller than the diameter of the predrilled hole so that the sand column could be inserted into it (see the photos in Najjar et al. (2010)). Furthermore, after the frozen sand column defrosts, it is expected that the final height of the sand column might be lower than the height of the surrounding clay because the defrosted sand column will deform and fill in the gap between the sand and the clay. In addition, being able to use an auger to predrill a hole in the cylindrical clay specimen means that the prepared clay specimen was not soft enough to represent the in-situ soft condition. Therefore, the clay specimen prepared in the laboratory should be soft enough to better represent the field condition that requires ground improvement. On the other hand, the clay specimen should not be too soft because it might fail to stand up in a triaxial test. A good balance between these two conflicting factors needs to be made with caution to achieve success in sample preparation. Andreou et al. (2008) prepared the triaxial specimens by preconsolidating the slurry in a special mould with a central thin tube (20 mm in diameter) in the middle where a granular column was installed later. The pre-remained hole was then filled with the compacted granular materials layer by layer. The main disadvantage of compaction is that it might have caused the expansion of the hole, resulting in variations in the initial specimens. The replacement method

used in this study by filling air-dry sand can ensure that the sand and clay are closely in contact at the interface, which also represents the loose dumping in the field. This procedure was found to be able to successfully produce uniform and repeatable triaxial clay specimens with OSC or GESC installed in the middle.

3.3 Testing procedure

The prepared triaxial specimen was placed in the triaxial cell, and was first saturated by vacuum saturation technique by applying a vacuum pressure of 75 kPa (< 100 kPa). The applied vacuum pressure was less than 100 kPa to ensure the specimen was still in a normally consolidated condition before triaxial testing. The vacuum saturation normally lasted for 2-3 hours for the Kaolin specimens until the outflow and inflow of the water were almost equal. For the Kaolin with OSC or GESC, vacuum saturation would be much faster due to the presence of the permeable sand column in the middle. To ensure the degree of saturation, the back pressure saturation technique was then applied to the specimen with a back pressure of 200 kPa. Because the clay specimens were formed from the initial slurry state, a target “B” value greater than 95% was easily achieved for all the specimens after applying these two saturation produces. After the saturation stage, the specimens were then isotropically consolidated under effective confining pressures of 100 kPa, 200 kPa and 400 kPa until the induced excess pore water pressure had been fully dissipated and drainage had completely ceased. It is believed that the excess pore water pressure dissipation would stop first, but the drainage might still be ongoing, resulting in continuous deformation of the specimen. Therefore, the consolidation stage was controlled to run for a duration of approximately 24 hours for all the tests in this study. Finally, shearing was carried out in an undrained condition at a slow strain rate of 2.4 %/h (i.e., 0.04 mm/min) to accurately measure the induced pore water pressure change during shearing.

For the triaxial testing of the Kaolin specimens with various OCRs (i.e., 1, 2, 4, or 8), the specimens were first isotropically consolidated under an effective confining pressure of 400 kPa, and then were unloaded to 200 kPa, 100 kPa and 50 kPa respectively, to achieve the target OCRs of 2, 4 and 8. Unloading caused a significant decrease in the pore water pressure, which was lower than the applied

back pressure. It was found that at least half a day was needed to allow for a new pore water pressure equilibrium when it was equal to the applied back pressure again. Finally, shearing was carried out at the same strain rate of 2.4 %/h after the new equilibrium state has reached.

3.4 Testing program

Nine isotropically consolidated undrained (CU) triaxial tests with pore water pressure measurement were carried out on the Kaolin, Kaolin with OSC and Kaolin with GESC under effective confining pressures of 100 kPa, 200 kPa and 400 kPa. Another three CU tests with pore water pressure measurement were carried out on the overconsolidated Kaolin specimens with the OCRs of 2, 4 and 8, which were achieved by unloading, as previously described. In summary, a total of twelve CU triaxial tests were carried out to further investigate the effects of OSC, GESC and OCR on the triaxial behaviour of the specimens, such as deviator stress, pore pressure change, Skempton's pore water pressure parameter A_f, undrained strength ratio, Mohr circle, stress path, principal stress, failure envelope, K_f line, shear strength parameter, etc.

4 Results and discussion

The CU test results were discussed and interpreted in detail in this section, highlighting the pore pressure dissipation during the consolidation stage, stress-strain behaviour and pore pressure change during the shearing stage, the obtained failure envelopes, inferred shear strength parameters, Mohr circles, stress paths and the effects of OSC, GESC and OCR, from both total stress and effective stress perspectives. A summary of all the CU test results obtained is also included in Table 2.

4.1 PWP dissipation versus time during consolidation stage

Figure 4 compares the pore water pressure dissipation versus time during the consolidation stage for the triaxial testing of the Kaolin, Kaolin with OSC and Kaolin with GESC under effective confining pressures of 100 kPa, 200 kPa and 400 kPa. The consolidation process lasted for about 24 hours for each test to ensure

consistency. It can readily be seen that for the Kaolin with the inclusion of OSC or GESC, the induced pore water pressure could only increase by approximate 30 kPa after applying the effective confining pressure of 400 kPa, and it also dissipated very quickly. It was found that the excess pore water pressure had been fully dissipated within 1000 seconds (Figures 4b-c). However, it is believed that the deformation (or consolidation) of the surrounding clay was still continuing for a very long time. This could be proven by noticing the increasing water volume in the burette after the excess pore water pressure had been fully dissipated, indicating that the water was still slowly draining out from the specimen. However, for the Kaolin specimen, the excess pore water pressure could increase by up to 380 kPa after increasing the effective confining pressure to 400 kPa, and the induced excess pore water pressure (380 kPa) took over 16 hours to fully dissipate (Figure 4a). Thus, it has been proven that the OSC and GESC could dramatically speed up the rate of consolidation process of the clay, and the sand column is already very effective in drainage, regardless of the permeable geotextile encasement.

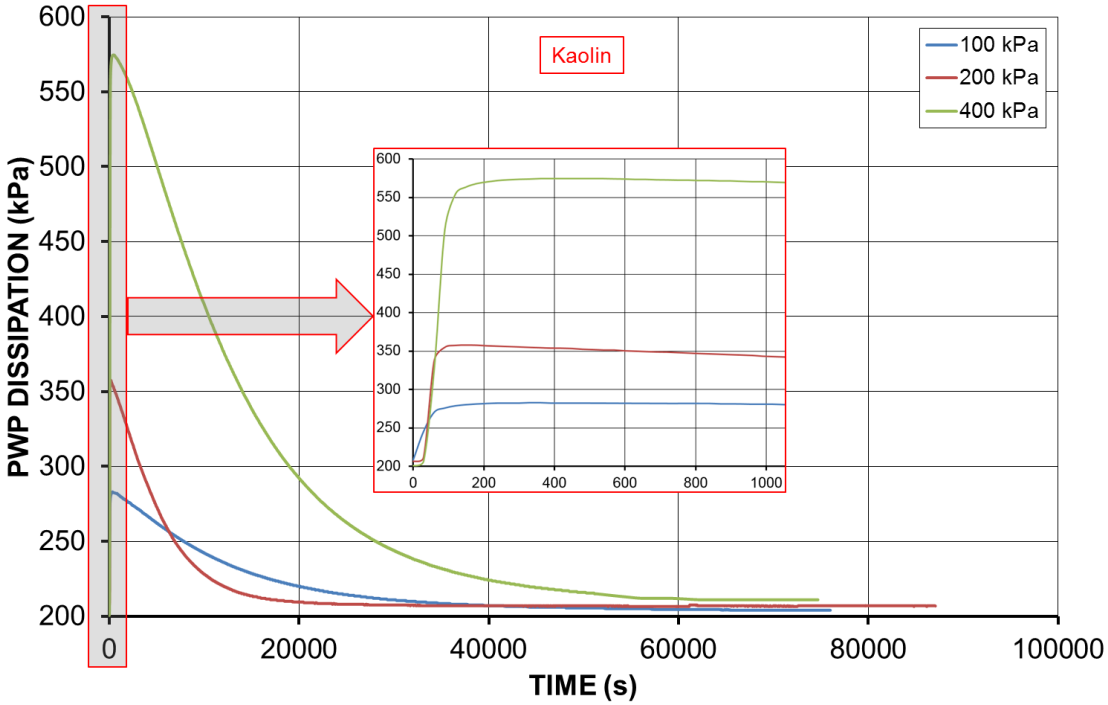

(a)

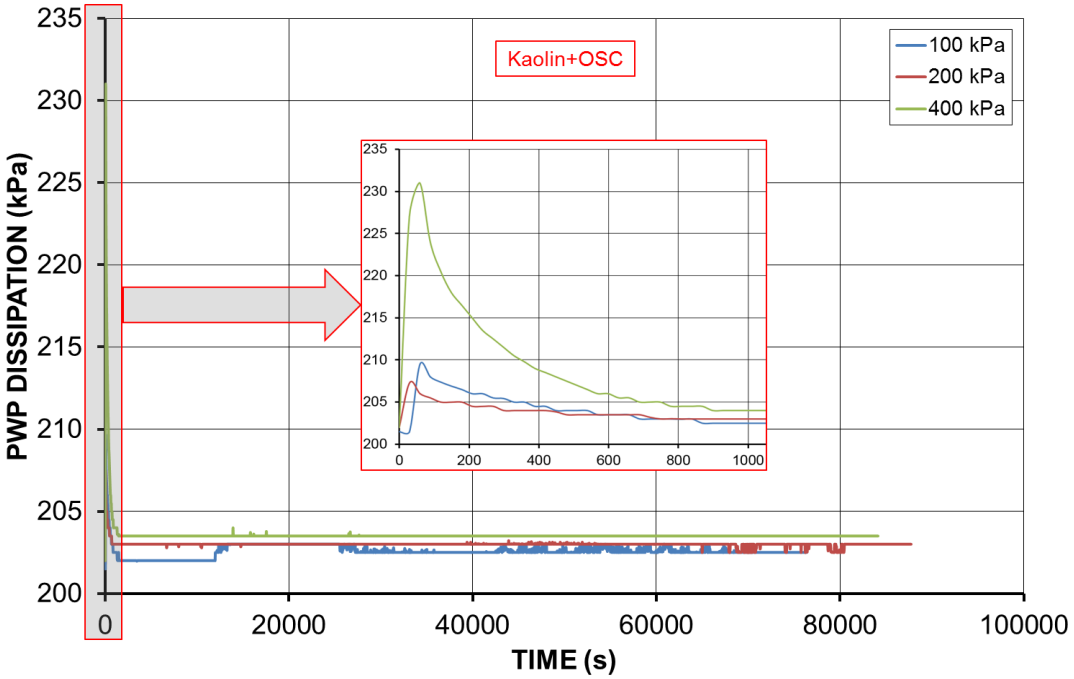

(b)

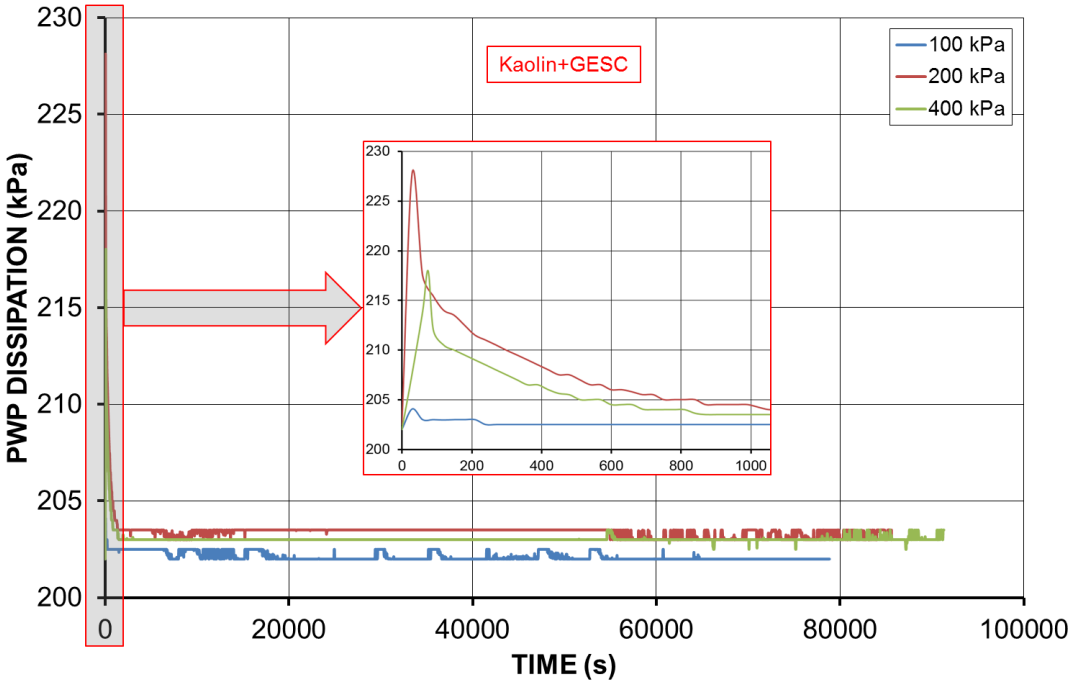

(c)

Figure 4 Pore water pressure (PWP) dissipation during consolidation stage: (a) Kaolin; (b) Kaolin with OSC; (c) Kaolin with GESC

Table 2 CU triaxial test results

Specimens	σ_{3c}' (kPa)	$\Delta\sigma_{df}$ (kPa)	Δu_f (kPa)	σ_{1f} (kPa)	σ_{3f} (kPa)	σ_{1f}' (kPa)	σ_{3f}' (kPa)	$\Delta\sigma_{df}'$ (kPa)	p_f (kPa)	p_f' (kPa)	q_f (kPa)	A_f
Kaolin	100	48	53	348	300	83	35	48	324	59	24	1.11
	200	92	110	492	400	172	79	92	446	126	46	1.19
	400	164	207	764	600	329	164	164	682	247	82	1.26
Kaolin+OSC	100	104	32	404	300	165	61	104	352	113	52	0.31
	200	203	68	603	400	330	127	203	501	229	101	0.33
	400	376	133	976	600	636	260	376	788	448	188	0.35
Kaolin+GESC	100	194	36	494	300	254	60	194	397	157	97	0.19
	200	287	85	687	400	392	105	287	543	249	143	0.30
	400	442	166	1042	600	669	227	442	821	448	221	0.38
OCR=1	400	164	207	764	600	329	164	164	682	247	82	1.26
OCR=2	200	106	58	506	400	245	138	106	453	192	53	0.54
OCR=4	100	78	14	378	300	157	79	78	339	118	39	0.18
OCR=8	50	56	5	306	250	99	42	56	278	70	28	0.09

4.2 Deviator stress and PWP change versus axial strain

The plots of deviator stress and pore water pressure change versus axial strain are shown in Figure 5 for the Kaolin, Kaolin with OSC and Kaolin with GESC under effective confining pressures of 100 kPa, 200 kPa and 400 kPa. The higher the effective confining pressure, the higher the deviator stress and the induced pore water pressure achieved for each group of CU tests. It can clearly be noticed that for the Kaolin with OSC or GESC, the induced pore water pressure during shearing had reduced to some extent. For example, under the effective confining pressure of 400 kPa, the maximum induced pore water pressure had reduced from 210 kPa to 130 kPa or 170 kPa for the Kaolin with OSC and GESC respectively. Similar reduction trends in the induced pore water pressure during shearing were also found for the other tests carried out under the effective confining pressures of 100 kPa and 200 kPa. This is likely because the presence of the sand column could reduce the induced pore water pressure during shearing. The maximum deviator stress achieved for the Kaolin with OSC had increased dramatically due to the reinforcement of the sand column. Moreover, the additional inclusion of geotextile encasement further increased the deviator stress achieved for the Kaolin with GESC. Therefore, the gaps between the deviator stress and pore water pressure developed in the CU tests are getting larger for the Kaolin with OSC and GESC, as shown in Figure 5. The deviator stress steadily increased with the axial strain until peaking at a certain axial strain (7%~12%), followed by a slight drop-off at a larger strain. Furthermore, the induced pore pressure kept increasing steadily with the axial strain and then reached a stable stage. It was noticed that there were two peaks occurring on the deviator stress-strain curves for the Kaolin with GESC. This is likely due to the distortion of the geotextile encasement during triaxial compression loading.

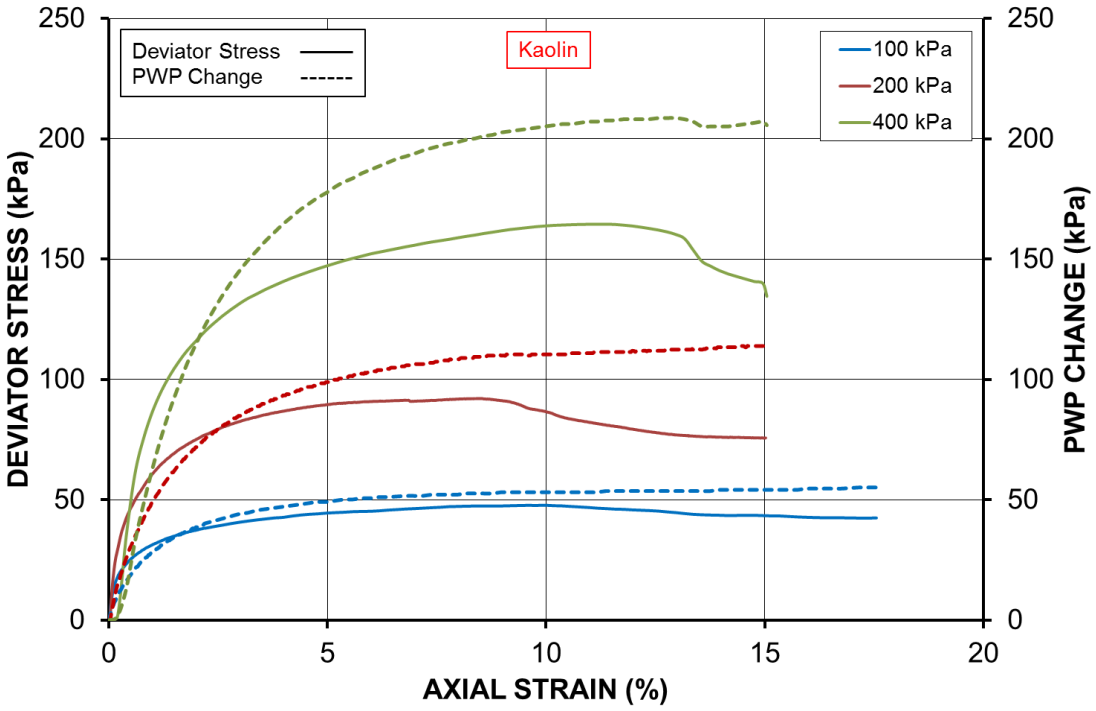
Deviator Stress
PWP Change
Kaolin
100 kPa
200 kPa
400 kPa
DEVIATOR STRESS (kPa)
PWP CHANGE (kPa)
AXIAL STRAIN (%)
0
50
100
150
200
250
0
5
10
15
20

(a)

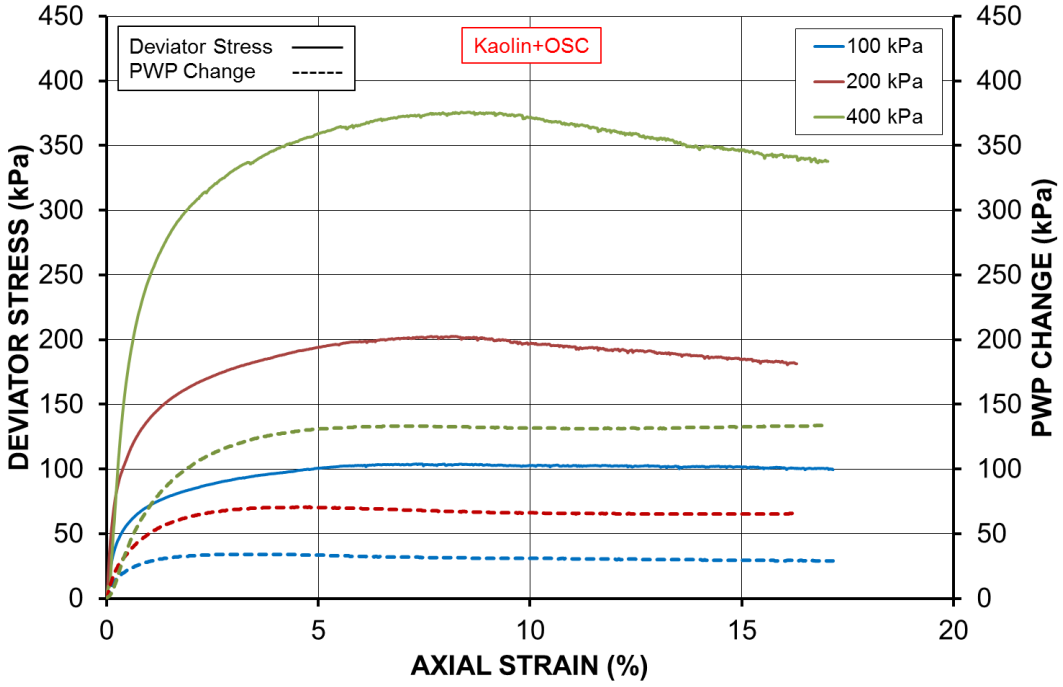
Deviator Stress
PWP Change
Kaolin+OSC
100 kPa
200 kPa
400 kPa
DEVIATOR STRESS (kPa)
PWP CHANGE (kPa)
AXIAL STRAIN (%)
0
50
100
150
200
250
300
350
400
450
0
5
10
15
20

(b)

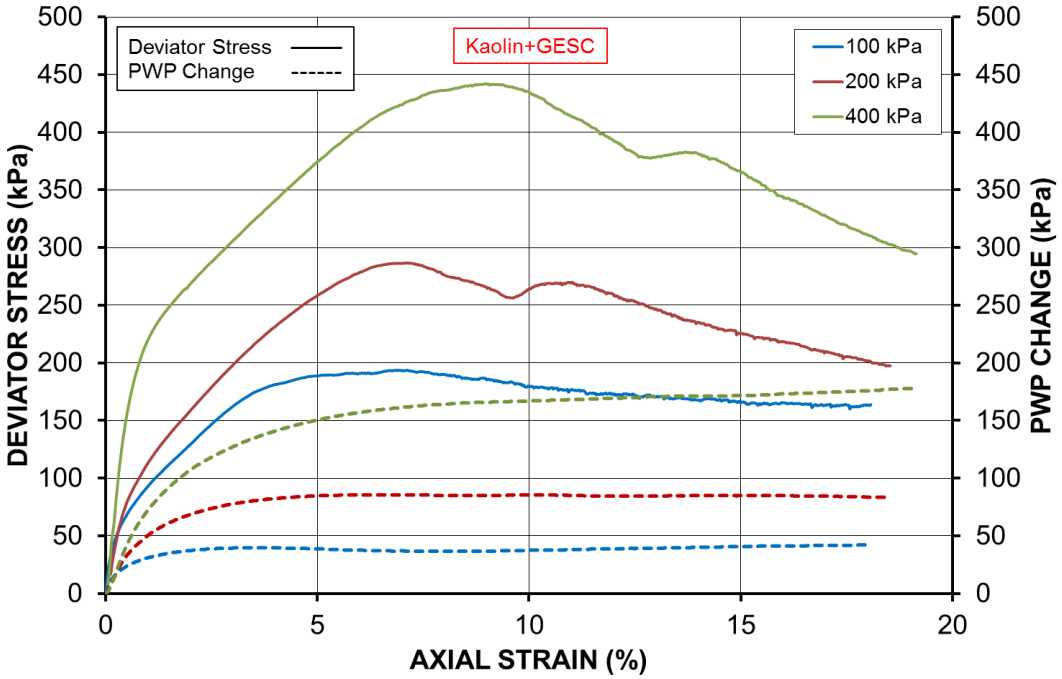

(c)

Figure 5 Stress-strain behaviour and PWP change during shearing stage: (a) Kaolin; (b) Kaolin with OSC; (c) Kaolin with GESC

4.3 Mohr circles and effective shear strength parameters

Figure 6 shows the total stress (TS, solid line) and effective stress (ES, dash line) Mohr circles for the Kaolin, Kaolin with OSC and Kaolin with GESC under effective confining pressures of 100 kPa, 200 kPa and 400 kPa. Because a back pressure of 200 kPa was maintained throughout the CU tests, the corresponding total minor principal stresses were 300 kPa, 400 kPa and 600 kPa. Also shown in Figure 6 are the K_f lines, the effective stress failure envelopes and the inferred effective shear strength parameters. The total and effective minor principal stresses at failure (σ_{3f} and σ_{3f}'), the total and effective major principal stresses at failure (σ_{1f} and σ_{1f}') and the maximum deviator stress at failure ($\Delta\sigma_{df}$ and $\Delta\sigma_{df}'$) under the effective confining pressure of 400 kPa (the biggest Mohr circle) are also highlighted in Figure 6. It was found that the effective stress Mohr circles were displaced to the left from the total stress Mohr circles, towards the origin. This is because the specimens developed positive pore water pressure during shearing. Both the total and effective stress

Mohr circles have the same diameter as the maximum deviator stresses remained unchanged (undrained). The inferred effective shear strength parameters and the best-fit Mohr-Coulomb effective stress failure envelope are deduced from the K_f line, as shown in Figure 6.

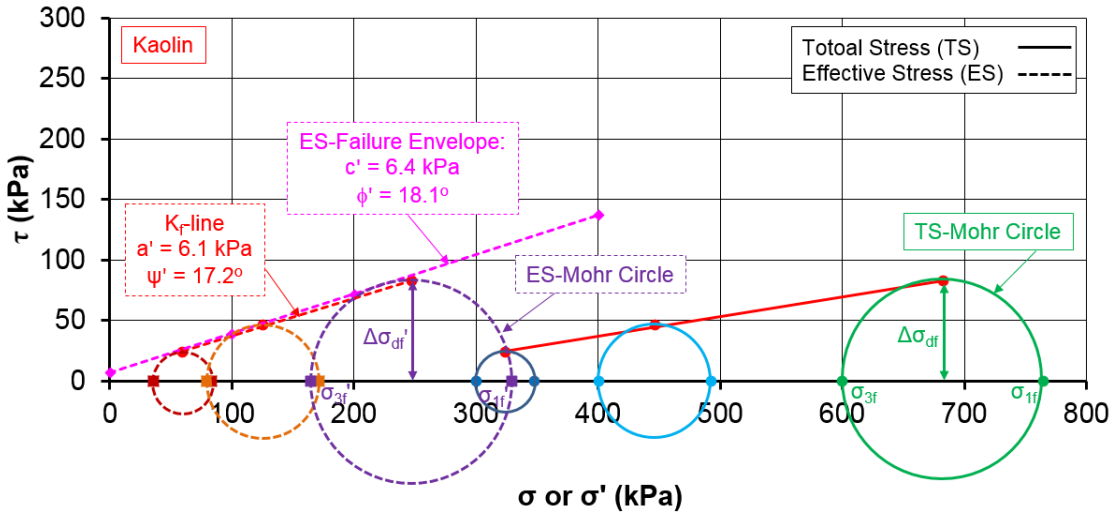

(a)

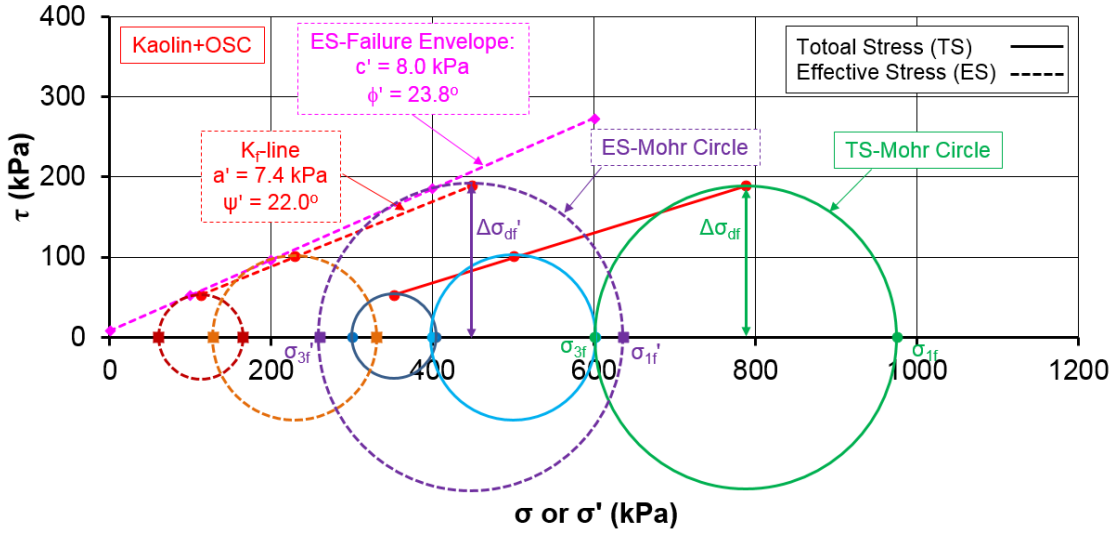

(b)

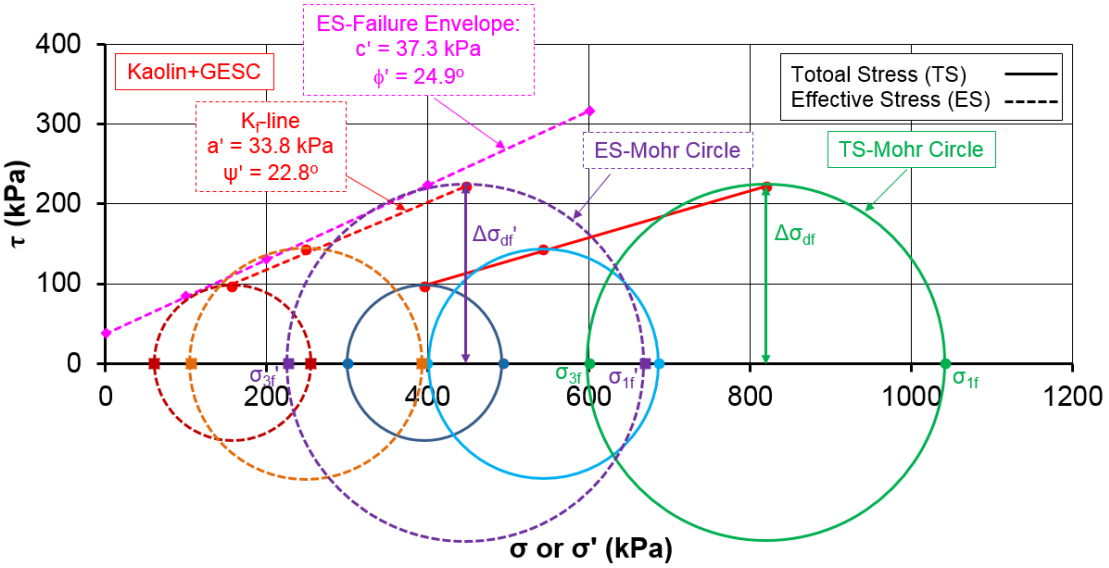

(c)

Figure 6 Total and effective stress Mohr circles: (a) Kaolin; (b) Kaolin with OSC; (c) Kaolin with GESC

It can be seen that the effective shear strength parameters of the composite clay specimens have been improved significantly after including the OSC or GESC. The effective friction angle was increased from 18.1° to 23.8° or 24.9° for the Kaolin with OSC and GESC respectively. Furthermore, the further improvement in the shear strength caused by the geotextile encasement was mainly accounted for the increase in the apparent cohesion (increasing from 8.0 kPa to 37.3 kPa), due to the further confinement provided by the geotextile encasement. In comparsion with the recent study outcomes on direct shear strengths of clay with OSC and GESC (Xu et al. 2018), it also has been found that OSC and GESC can significantly improve the direct shear strength of clay when subjected to lateral loading in the direct shear tests, resulting in a significant increase in friction angles. However, the impact on the inferred apparent cohesions was found to be minor, which is different from the finding from this study. A possible explanation for this may be due to the different mechanisms of triaxial and direct shear tests on the clay with OSC and GESC compsite specimens.

4.4 Stress paths

Figure 7 shows the MIT *p*-*q* diagrams, highlighting the total stress path (TSP), effective stress path (ESP), total-initial pore pressure stress path ((T-u_0)SP), K_f line, effective stress failure envelope and the inferred effective shear strength parameters. Based on the ESP and (T-u_0)SP, the induced pore water pressure at failure Δu_f is also highlighted in Figure 7. The stress paths indicate the locus of the stress points, which have the coordinates $p=(\sigma_1+\sigma_3)/2$ and $q=(\sigma_1-\sigma_3)/2$, representing the states of stress of the soil during triaxial compression loading. Because the MIT *p*-*q* coordinate system was selected to interpret the CU triaxial test results obtained, it is evident that the TSPs and (T-u_0)SPs result in straight lines inclined at 45° from the horizontal (a slope of 1), rather than a slope of 3 if using the Cambridge *p*-*q* coordinate system. Moreover, the q_f achieved was the same for all the three stress paths because the failure is defined at the maximum deviator stress. The axial compression loading on the normally consolidated specimens induced positive pore water pressure; therefore, the ESP bends to the left of the (T-u_0)SP, as shown in Figure 7. After touching the failure point, the ESP drops dramatically due to the decrease in deviator stress. Because the OSC and GESC reduced the induced pore water pressure during shearing, the ESPs of the composite specimens became much steeper than that of the clay alone. Also can readily be found in Figures 7a-c is a significant reduction in induced pore pressure at failure Δu_f in the composite specimens with the inclusion of OSC and GESC.

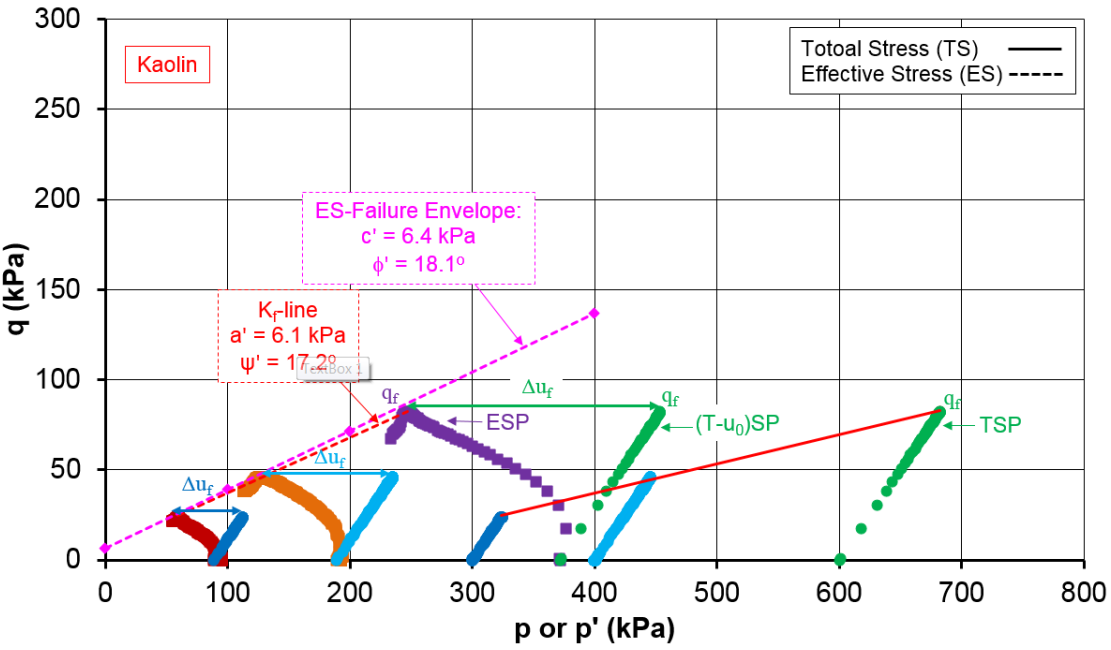
Kaolin
Totoal Stress (TS)
Effective Stress (ES)
ES-Failure Envelope:
c' = 6.4 kPa
ϕ' = 18.1°
Kf-line
a' = 6.1 kPa
ψ' = 17.2°
ESP
(T-u0)SP
TSP
Δuf
qf
q (kPa)
p or p' (kPa)
0
50
100
150
200
250
300
0
100
200
300
400
500
600
700
800

(a)

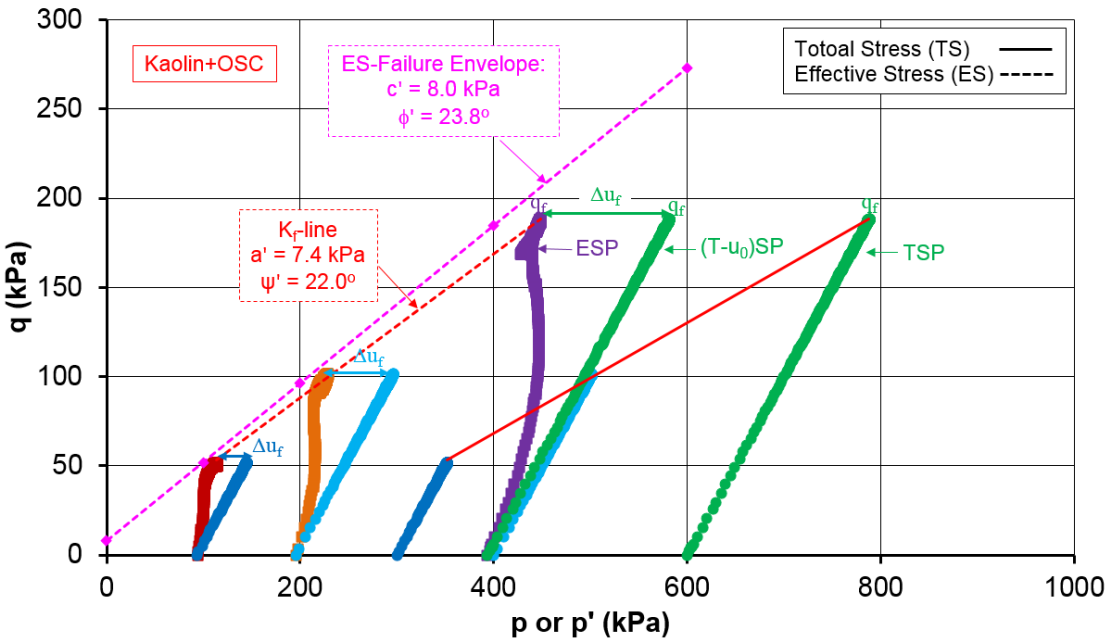
Kaolin+OSC
Totoal Stress (TS)
Effective Stress (ES)
ES-Failure Envelope:
c' = 8.0 kPa
ϕ' = 23.8°
Kf-line
a' = 7.4 kPa
ψ' = 22.0°
ESP
(T-u0)SP
TSP
Δuf
qf
q (kPa)
p or p' (kPa)
0
50
100
150
200
250
300
0
200
400
600
800
1000

(b)

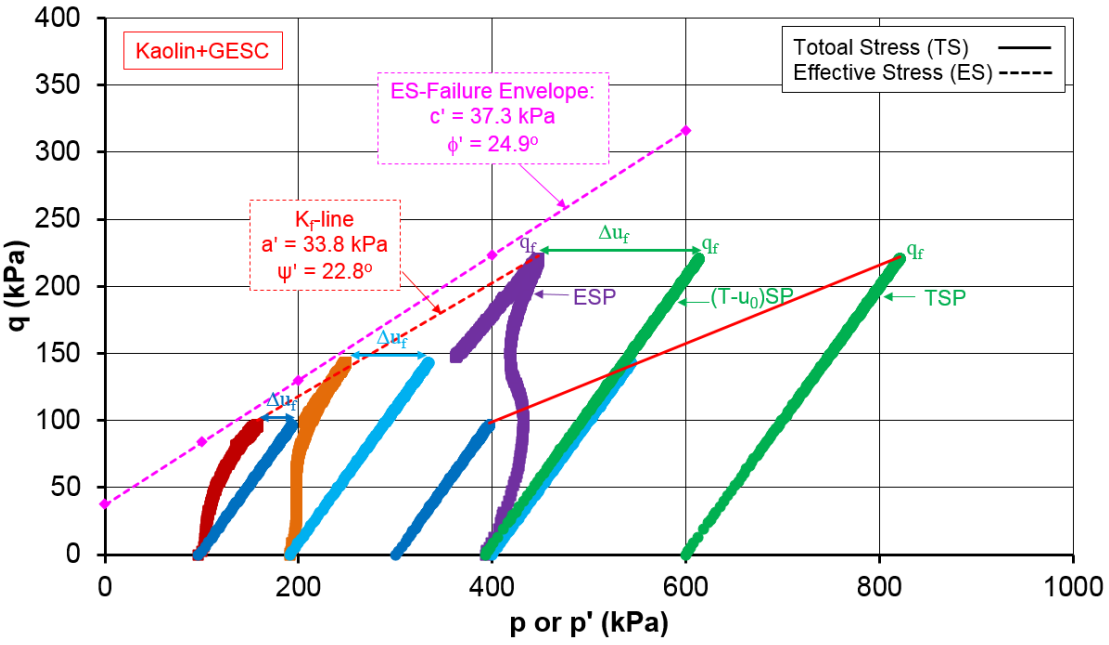

(c)

Figure 7 Total and effective stress paths: (a) Kaolin; (b) Kaolin with OSC; (c) Kaolin with GESC

4.5 Effects of OSC and GESC

The effects of OSC and GESC on the total stress and effective stress Mohr circles and stress paths are shown in Figures 8a-c, corresponding to the effective confining pressures of 100 kPa, 200 kPa and 400 kPa, respectively. It can readily be seen that with the inclusions of OSC and GESC, the Mohr circles are getting bigger. The total stress and effective stress Mohr circles have the same size for each specimen due to the undrained shearing. The TSPs of the Kaolin, Kaolin with OSC and Kaolin with GESC overlapped and inclined at 45° for the same effective confining pressure (Figure 8). The ESPs bend to the left for the Kaolin specimens, while the ESPs bend to the right after including OSC and GESC, towards a much higher maximum deviator stress. In addition, because the OSC and GESC reduced the induced pore water pressure during shearing, the effective stress and total stress Mohr circles are getting closer, as shown in Figure 8. This tendency is more evident for a higher effective confining pressure.

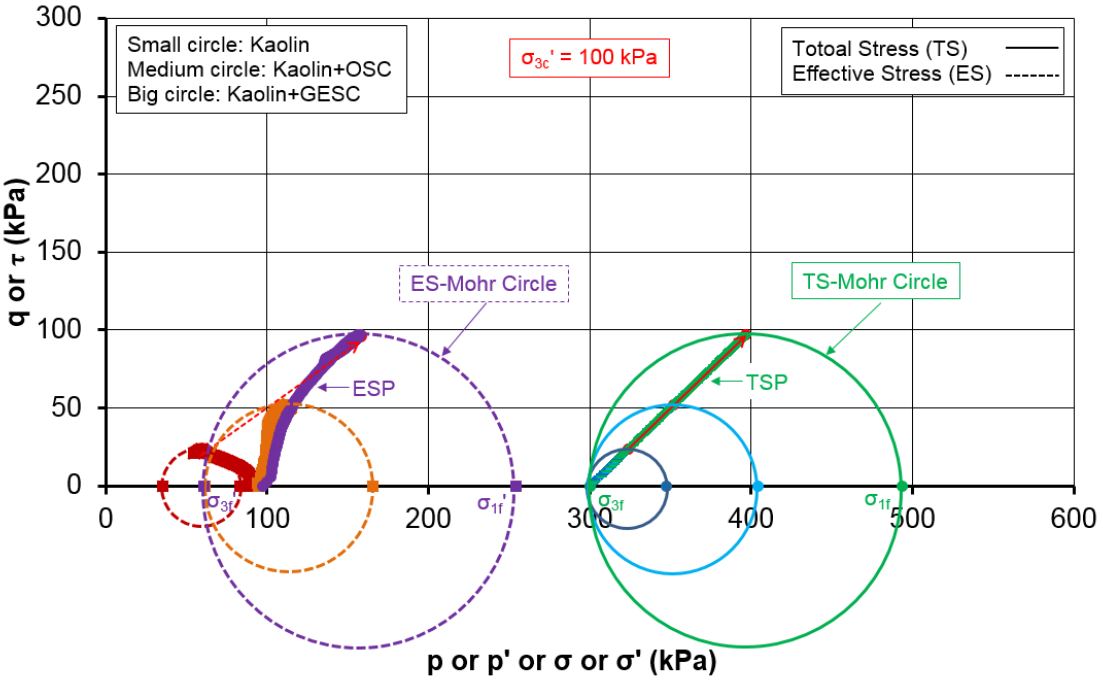
Small circle: Kaolin
Medium circle: Kaolin+OSC
Big circle: Kaolin+GESC
σ3c' = 100 kPa
Totoal Stress (TS)
Effective Stress (ES)
ES-Mohr Circle
TS-Mohr Circle
ESP
TSP
q or τ (kPa)
p or p' or σ or σ' (kPa)

(a)

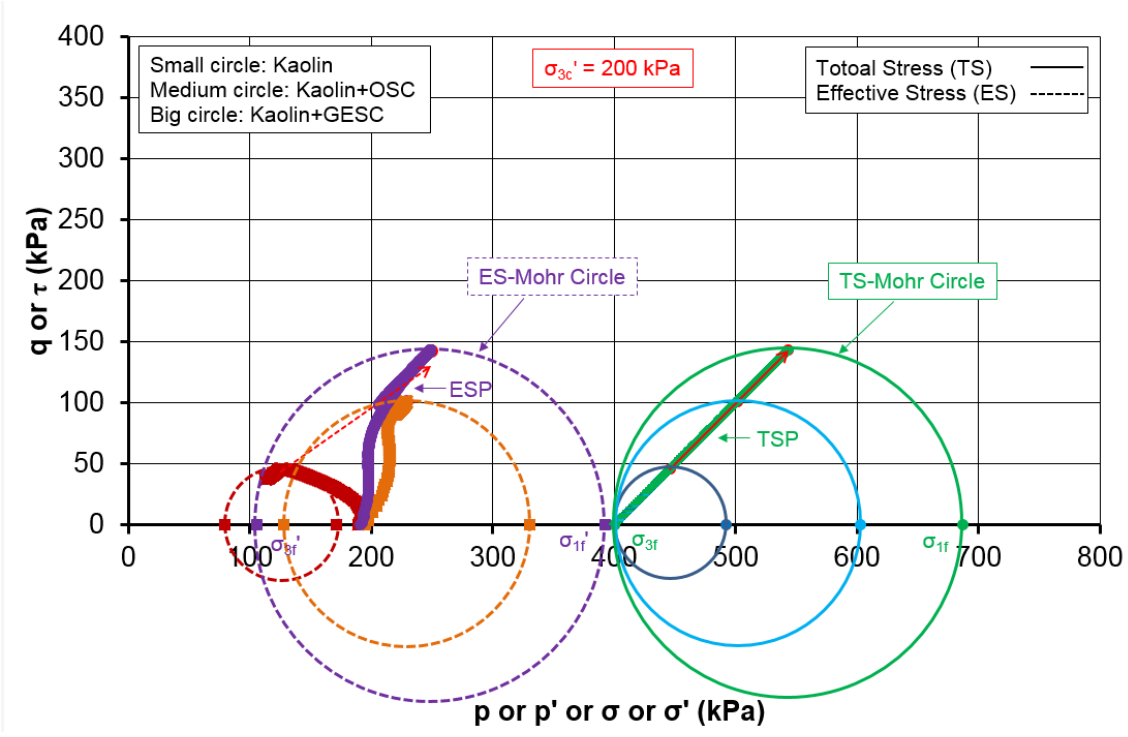
Small circle: Kaolin
Medium circle: Kaolin+OSC
Big circle: Kaolin+GESC
σ3c' = 200 kPa
Totoal Stress (TS)
Effective Stress (ES)
ES-Mohr Circle
TS-Mohr Circle
ESP
TSP
q or τ (kPa)
p or p' or σ or σ' (kPa)

(b)

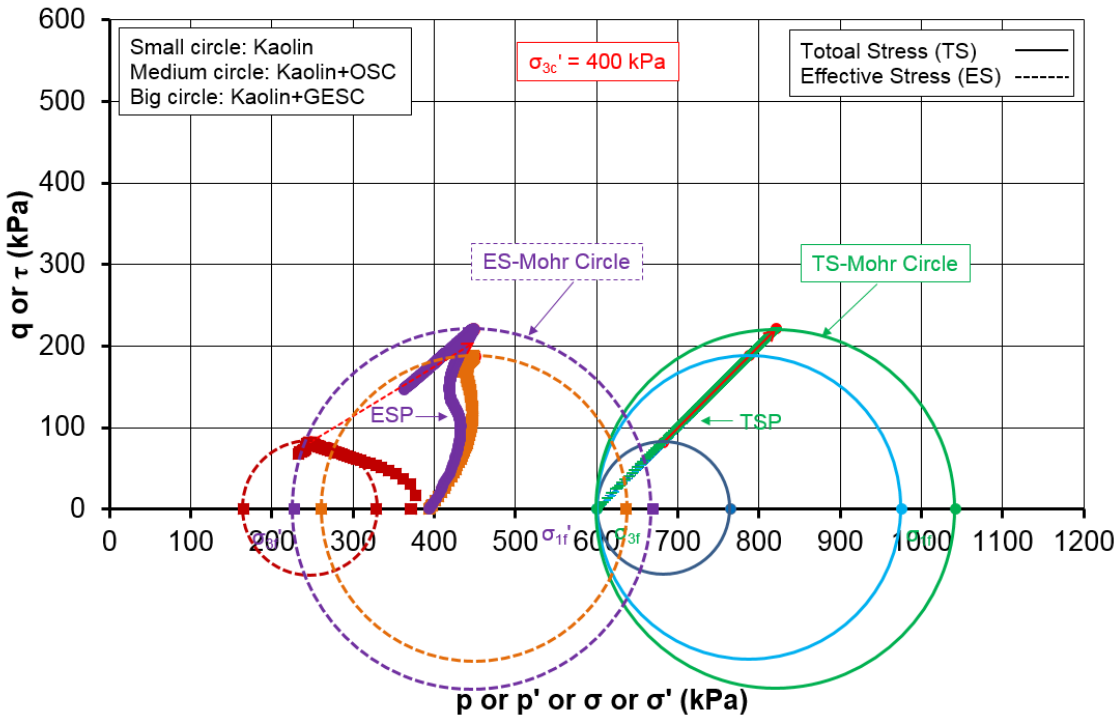

(c)

Figure 8 Comparisons of Mohr circles and stress paths of Kaolin, Kaolin with OSC and Kaolin with GESC under effective confining pressures of: (a) 100 kPa; (b) 200 kPa; (c) 400 kPa

It is believed that the reinforcing performance of the sand column is dependent on the confinement. The higher the effective confining pressure, the higher the confinement, and the higher the stiffness of the surrounding clay would achieve after the consolidation stage. Therefore, a stiffer surrounding clay would provide a higher confinement for the sand column inside, leading to a higher shear strength of the composite soil specimen. Bergado and Lam (1987) had found from the full-scale load tests that the ultimate bearing capacity recorded was three to four times greater than that of the untreated ground. Black et al. (2007) found that the shear strength of the clay with a single sand column, with an area replacement ratio of 10%, had been increased by 33% over that of the clay without columns. Andreou et al. (2008) reported the undrained shear strength of the reinforced clay with a single small sand column (a very small area replacement ratio of 4%) was about twice higher than that for the unreinforced clay in their CU triaxial tests. In this study, it was found that for

an area replacement ratio of 21%, the maximum deviator stress achieved for the reinforced clay with a single OSC (or GESC) was average 2.2 times (or 3.3 times) greater than that of the Kaolin without reinforcement. Figure 9 shows the photos of the Kaolin, Kaolin with OSC and Kaolin with GESC before and after the CU triaxial tests. The inclined shear plane after shear failure could clearly be noticed in the Kaolin and Kaolin with OSC specimens. However, for the Kaolin with GESC specimens, with the inclusion of geotextile encasement, it was a bulging failure that occurred in the upper part of the specimen (Figure 9).

4.6 Effects of OCR

Figure 10a shows the plots of the deviator stress and pore water pressure change versus axial strain during triaxial compression loading for the Kaolin specimen with different OCRs of 1, 2, 4 and 8. It can readily be seen that the peak of the deviator stress-strain curve tends to occur much earlier for the overconsolidated specimens (OCR>1), compared to the normally consolidated specimen (OCR=1). The normally consolidated specimen (OCR=1) steadily developed positive pore water pressure, resulting in the ESP bending to the left. However, in the overconsolidated specimens (OCR>1), after an initial increase in the pore water pressure, a drop-off was then noticed, which then gradually became stable as the axial strain increased, finally resulting in the ESP bending to the right. This is most noticeable for the specimen (OCR=8), as shown in Figures 10a-b. For OCR=8, it was noticed that the pore water pressure started out slightly positive, and then became negative (negative with respect to the back pressure u_0) after an axial strain of 8%, and finally stabilised until the test stopped. The decrease in induced pore water pressure with increasing axial strain is because the overconsolidated specimen tends to expand or swell during shearing. Therefore, the ESP bends slightly to the left of the (T-u_0)SP at first, and then as the pore water pressure decreases increasingly, the ESP starts bending to the right until the maximum deviator stress is reached for the overconsolidated specimens. The higher the OCR, the smaller the Mohr circles, and the lower the maximum deviator stress achieved due to unloading (Figure 10b). Moreover, the higher the OCR, the lower the induced pore water pressure during shearing, even leading to negative pore water pressure. This result may be explained by the fact

that the higher the OCR after unloading, the lower the reduced effective confining pressure or confinement, so the specimens tend to expand during shearing, resulting in negative pore water pressure. Therefore, the calculated Skempton's pore water pressure parameter A_f decreased with the OCR dramatically from 1.26 to 0.09, as shown in Figure 10c and Table 2. Also shown in Figure 10c is the plot of undrained strength ratio versus OCR. It was evident that the undrained strength ratio increases with OCR, and it could be best fitted using SHANSEP equation (Ladd and Foott 1974). This finding agrees with the previously published results (Zhu and Yin 2000; Abdulhadi et al. 2012; Gu et al. 2016; Wu et al. 2017). In addition, after the CU triaxial test, the final water content of the specimen was also measured, and it was found that the higher the OCR, the higher the final water content tends to be. A possible explanation for this might be due to the absorption of water during new pore water pressure equilibrium after unloading, as mentioned before, in order to achieve different OCRs. The additional evidence to prove this is by noticing a decrease in the water level in the back pressure burette and an increase in the water level in the cell pressure burette during the new pore water pressure equilibrium process, indicating that the specimen might swell slightly after unloading.

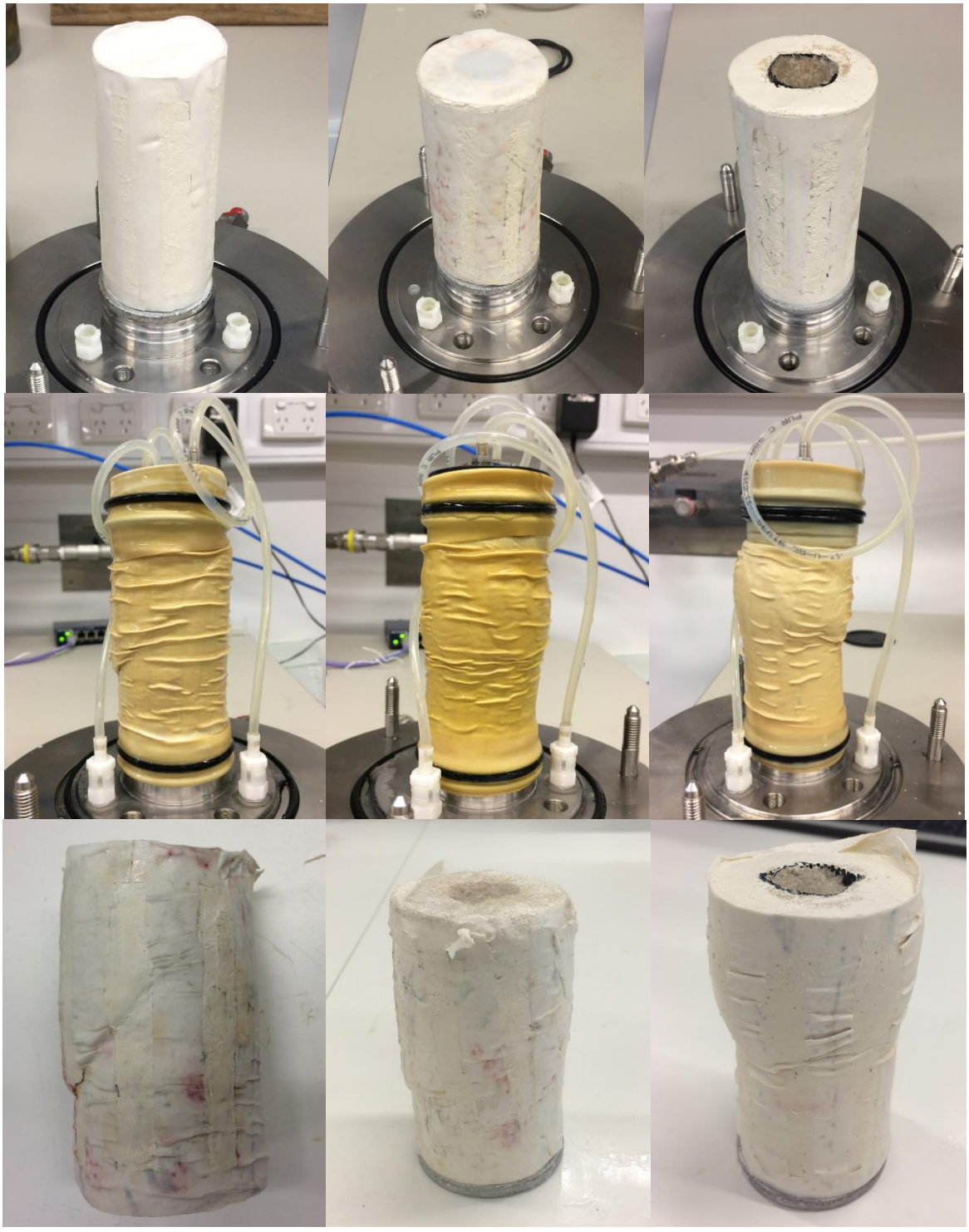

Figure 9 Photos of Kaolin, Kaolin with OSC and Kaolin with GESC specimens in CU trixial tests before and after failure

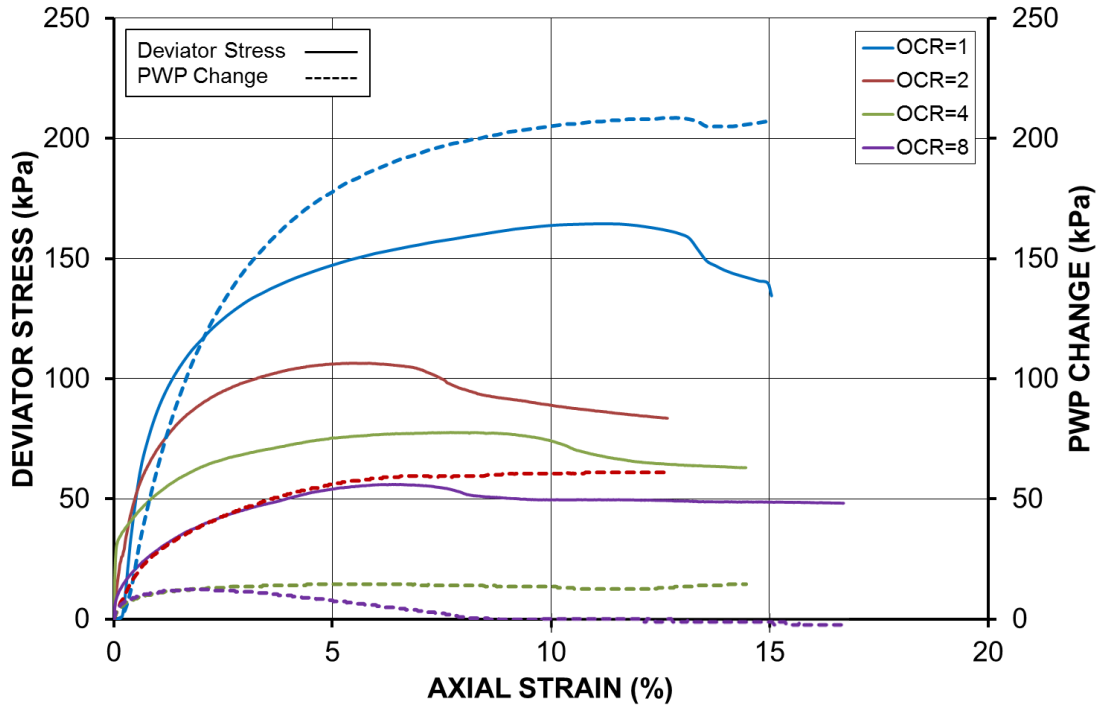
Deviator Stress
PWP Change
OCR=1
OCR=2
OCR=4
OCR=8
DEVIATOR STRESS (kPa)
PWP CHANGE (kPa)
AXIAL STRAIN (%)
0
50
100
150
200
250
0
5
10
15
20

(a)

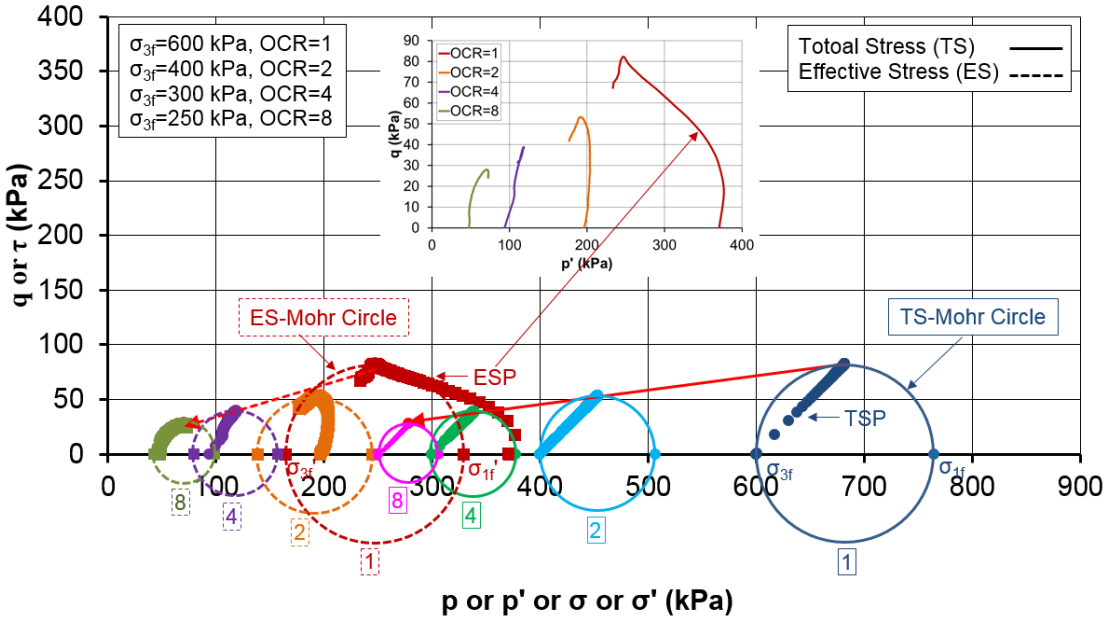
σ3f=600 kPa, OCR=1
σ3f=400 kPa, OCR=2
σ3f=300 kPa, OCR=4
σ3f=250 kPa, OCR=8
Totoal Stress (TS)
Effective Stress (ES)
OCR=1
OCR=2
OCR=4
OCR=8
q (kPa)
p' (kPa)
ES-Mohr Circle
TS-Mohr Circle
ESP
TSP
σ3f
σ1f'
σ1f
q or τ (kPa)
p or p' or σ or σ' (kPa)

(b)

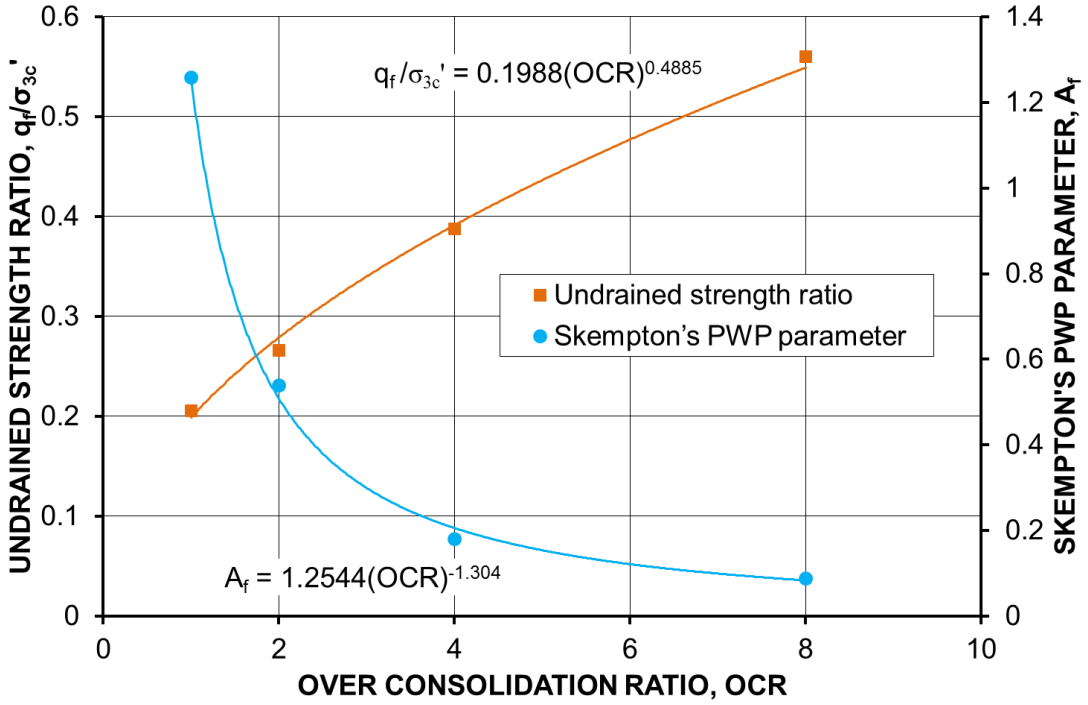

(c)

Figure 10 Effects of OCR on: (a) deviator stress and PWP change; (b) Mohr circle and stress path; (c) undrained strength ratio and Skempton's PWP parameter A_f

5 Conclusions

This study has further investigated the shear strength and pore pressure behaviour of clay reinforced with OSC and GESC by carrying out CU triaxial tests with pore pressure measurement. Based on the experimental results obtained and their interpretations, the main findings are drawn as follows:

(1) During the consolidation stage, the OSC and GESC could dramatically speed up the rate of consolidation process of the clay, and the sand column is already very effective in drainage, regardless of the permeable geotextile encasement.

(2) During the shearing stage, the OSC and GESC could significantly decrease the induced pore water pressure and increase the shear strength, resulting in

bigger Mohr circles. The presence of the sand column mainly increases the friction angle, and the geotextile encasement could further improve the apparent cohesion due to the additional confinement provided.

(3) The ESPs of the Kaolin with OSC or GESC become much steeper than that of the clay alone because the OSC and GESC could reduce the induced pore water pressure during shearing. Furthermore, the effective stress and total stress Mohr circles obtained for the Kaolin with OSC or GESC are getting closer, compared to the Mohr circles of the Kaolin. This tendency is more evident for a higher effective confining pressure.

(4) The normally consolidated specimen (OCR=1) steadily developed positive pore water pressure, resulting in the ESP bending to the left. However, in the overconsolidated specimens (OCR>1), after an initial increase in the pore water pressure, a drop-off was then noticed, which then gradually became stable as the axial strain increased, resulting in the ESPs bending to the right.

Acknowledgement

The first author would like to thank Ms. Jayamini Methiwala for her kind help with the trial-and-error composite clay sample preparation for triaxial testing, and also thank her for proofreading and reviewing this paper.

References

Abdulhadi, N. O., Germaine, J. T., and Whittle, A. J., (2012). Stress-dependent behavior of saturated clay. Canadian Geotechnical Journal **49**(8): 907-916. doi: 10.1139/t2012-057.

Ali, K., Shahu, J. T., and Sharma, K. G., (2012). Model tests on geosynthetic-reinforced stone columns: a comparative study. Geosynthetics International, 19(4), 292-305. doi: 10.1680/gein.12.00016.

Ali, K., Shahu, J. T., and Sharma, K. G., (2014). Model tests on single and groups of stone columns with different geosynthetic reinforcement arrangement. Geosynthetics International, 21(2), 103-118. doi: 10.1680/gein.14.00002.

Andreou, P., Frikha, W., Frank, R., Canou, J., Papadopoulos, V., and Dupla, J. C., (2008). Experimental study on sand and gravel columns in clay. Proceedings of the Institution of Civil Engineers - Ground Improvement, 161(4), 189-198. doi: 10.1680/grim.2008.161.4.189.

Ayadat, T., and Hanna, A. M., (2005). Encapsulated stone columns as a soil improvement technique for collapsible soil. Proceedings of the Institution of Civil Engineers - Ground Improvement, 9(4), 137-147. doi: 10.1680/grim.2005.9.4.137.

Bergado, D. T., and Lam, F. L., (1987). Full scale load test of granular piles with different densities and different proportions of gravel and sand on soft bangkok clay. Soils and Foundations, 27(1), 86-93. doi: 10.3208/sandf1972.27.86.

Black, J. A, Sivakumar, V., Madhav, M. R., and McCabe, B., (2006). An improved experimental test set-up to study the performance of granular columns. Geotechnical Testing Journal, 29(3), 193-199.

Black, J. A., Sivakumar, V., and Bell, A., (2011). The settlement performance of stone column foundations. Géotechnique, 61(11), 909-922. doi: 10.1680/geot.9.P.014.

Black, J. A., Sivakumar, V., Madhav, M. R., and Hamill, G. A., (2007). Reinforced stone columns in weak deposits: laboratory model study. Journal of Geotechnical and Geoenvironmental Engineering, 133(9), 1154-1161. doi: 10.1061/(ASCE)1090-0241(2007)133:9(1154).

Castro, J., (2017). Modeling stone columns. Materials, 10(7), 782. doi: 10.3390/ma10070782.

Frikha, W., Tounekti, F., Kaffel, W., and Bouassida, M., (2015). Experimental study for the mechanical characterization of Tunis soft soil reinforced by a group of sand columns. Soils and Foundations, 55(1), 181-191. doi: https://doi.org/10.1016/j.sandf.2014.12.014.

Gniel, J., and Bouazza, A., (2009). Improvement of soft soils using geogrid encased stone columns. Geotextiles and Geomembranes, 27(3), 167-175. doi: https://doi.org/10.1016/j.geotexmem.2008.11.001.

Gniel, J., and Bouazza, A., (2010). Construction of geogrid encased stone columns: A new proposal based on laboratory testing. Geotextiles and Geomembranes, 28(1), 108-118. doi: https://doi.org/10.1016/j.geotexmem.2009.12.012.

Gu, C., Wang, J., Cai, Y., Sun, L., Wang, P., and Dong, Q., (2016). Deformation characteristics of overconsolidated clay sheared under constant and variable confining pressure. Soils and Foundations, 56(3), 427-439. doi: https://doi.org/10.1016/j.sandf.2016.04.009.

Hong, Y. -S., Wu, C. -S., and Yu, Y. -S., (2016). Model tests on geotextile-encased granular columns under 1-g and undrained conditions. Geotextiles and Geomembranes, 44(1), 13-27. doi: https://doi.org/10.1016/j.geotexmem.2015.06.006.

Juran, I., and Guermazi, A., (1988). Settlement response of soft soils reinforced by compacted sand columns. Journal of Geotechnical Engineering, 114(8), 930-943. doi: 10.1061/(ASCE)0733-9410(1988)114:8(930).

Kadhim, S.T., (2016). Stability analysis of geotextile encased sand columns. PhD dissertation, The University of Kansas, USA.

Kim, S. S., Han, S. J., Jung, S. Y., and Shin, H. Y., (2007). Drained triaxial behavior of scp-reinforced composite ground with low area replacement ratio. International Society of Offshore and Polar Engineers, 17(2), 152-158.

Ladd, C. C., and Foott, R., (1974). New design procedure for stability of soft clays. Journal of the Geotechnical Engineering Division, 100(7), 763–786.

Miranda, M., and Da Costa, A., (2016). Laboratory analysis of encased stone columns. Geotextiles and Geomembranes, 44(3), 269-277. doi: https://doi.org/10.1016/j.geotexmem.2015.12.001.

Mohapatra, S. R., Rajagopal, K., and Sharma, J., (2016). Direct shear tests on geosynthetic-encased granular columns. Geotextiles and Geomembranes, 44(3), 396-405. doi: https://doi.org/10.1016/j.geotexmem.2016.01.002.

Mohapatra, S. R., Rajagopal, K., and Sharma, J., (2017). 3-Dimensional numerical modeling of geosynthetic-encased granular columns. Geotextiles and Geomembranes, 45(3), 131-141. doi: https://doi.org/10.1016/j.geotexmem.2017.01.004.

Muir Wood, D., Hu, W., and Nash, D. F. T., (2000). Group effects in stone column foundations: model tests. Géotechnique, 50(6), 689-698. doi: 10.1680/geot.2000.50.6.689.

Murugesan, S., and Rajagopal, K., (2007). Model tests on geosynthetic-encased stone columns. Geosynthetics International, 14(6), 346-354. doi: 10.1680/gein.2007.14.6.346.

Murugesan, S., and Rajagopal, K., (2009). Shear load tests on stone columns with and without geosynthetic encasement. Geotechnical Testing Journal, 32(1), 35-44.

Murugesan, S., and Rajagopal, K., (2010). Studies on the behavior of single and group of geosynthetic encased stone columns. Journal of Geotechnical and Geoenvironmental Engineering, 136(1), 129-139. doi: 10.1061/(ASCE)GT.1943-5606.0000187.

Najjar S. S., Sadek, S., and Maakaroun, T., (2010). Effect of sand columns on the undrained load response of soft clays. Journal of Geotechnical and Geoenvironmental Engineering, 136(9), 1263-1277. doi: 10.1061/(ASCE)GT.1943-5606.0000328.

Najjar, S. S., (2013). A state-of-the-art review of stone/sand-column reinforced clay systems. Geotechnical and Geological Engineering, 31(2), 355-386. doi: 10.1007/s10706-012-9603-5.

Najjar, S. S., and Skeini, H., (2015). Triaxial response of clays reinforced with granular columns. Proceedings of the Institution of Civil Engineers - Ground Improvement, 168(4), 265-281. doi: 10.1680/grim.13.00049.

Rajagopal, K., Krishnaswamy, N. R., and Madhavi Latha, G., (1999). Behaviour of sand confined with single and multiple geocells. Geotextiles and Geomembranes, 17(3), 171-184. doi: https://doi.org/10.1016/S0266-1144(98)00034-X.

Shokouhi, A., Zhang, C., and Williams, D. J., (2017). Settling, consolidation and desiccation behaviour of coal tailings slurry. Mining Technology, 1-11. doi: 10.1080/14749009.2017.1308691.

Sivakumar, V., Jeludine, D. K. N. M., Bell, A., Glynn, D. T., and Mackinnon, P., (2011). The pressure distribution along stone columns in soft clay under consolidation and foundation loading. Géotechnique, 61(7), 613-620. doi: 10.1680/geot.9.P.086.

Sivakumar, V., McKelvey, D., Graham, J., and Hughes, D., (2004). Triaxial tests on model sand columns in clay. Canadian Geotechnical Journal, 41(2), 299-312. doi: 10.1139/t03-097.

Wu, C. -S., and Hong, Y. -S., (2009). Laboratory tests on geosynthetic-encapsulated sand columns. Geotextiles and Geomembranes, 27(2), 107-120. doi: https://doi.org/10.1016/j.geotexmem.2008.09.003.

Wu, S., Lok, T., and Zhou, A., (2017). Undrained Behavior of Macau Marine Clay with Various Strain Rates and Different Stress Histories. In Congrès International de Géotechnique–Ouvrages–Structures. Springer. pp. 816-826.

Xu, Y., Methiwala, J., Williams, D. J., Serati, M., 2018. Strength and consolidation characteristics of clay with geotextile encased sand column. Proceedings of the Institution of Civil Engineers - Ground Improvement. 1-10. https://doi.org/10.1680/jgrim.17.00070

Zhu, J. -G., and Yin, J. -H., (2000). Strain-rate-dependent stress-strain behavior of overconsolidated Hong Kong marine clay. Canadian Geotechnical Journal, 37(6), 1272-1282. doi: 10.1139/t00-054.

Attached Paper VI

Paper VI: Strength and Consolidation Characteristics of Clay Reinforced with Geotextile Encased Sand Column

Xu, Y., Methiwala, J., Williams, D. J., Serati, M., 2018. Strength and consolidation characteristics of clay with geotextile-encased sand column. Proceedings of the Institution of Civil Engineers - Ground Improvement. 171 (3) 125-134. https://doi.org/10.1680/jgrim.17.00070 – incorporated as **Paper VI**.

Strength and Consolidation Characteristics of Clay Reinforced with Geotextile Encased Sand Column

Youwei Xu[a,], Jayamini Methiwala[b], David J. Williams[c], Mehdi Serati[d]*

[a] PhD candidate, School of Civil Engineering, The University of Queensland, Brisbane, QLD 4072, Australia. Email: youwei.xu@uq.edu.au

[b] Graduate Engineer, GHD, Brisbane, QLD 4000, Australia. E-mail: jayamini.methiwala@uq.net.au

[c] Professor, School of Civil Engineering, The University of Queensland, Brisbane, QLD 4072, Australia. Email: d.williams@uq.edu.au

[d] Postdoctoral Research Fellow, School of Civil Engineering, The University of Queensland, Brisbane, QLD 4072, Australia. Email: m.serati@uq.edu.au

Abstract

Installing sand columns in clays is one of the common ground improvement techniques used to treat soft soils, and the inclusion of geotextile to encase the sand column can further improve the performance of the reinforced clay composite. Most studies in clay reinforced with sand column have only focused on the vertical loading condition. In this paper, the shear strength and consolidation characteristics of clay, clay with ordinary sand column (OSC), and clay with geotextile encased sand column (GESC) were investigated by carrying out laboratory direct shear and oedometer tests to study the response of the reinforced clay composite under both lateral and vertical loading conditions. It was found that OSC and GESC significantly increased the shear strength of the clay, mainly by improving the friction angle, with little impact on the apparent cohesion. Furthermore, OSC and GESC reduced the compression index, swell index, and recompression index of the clay to some extent. The calculated secondary compression indexes and coefficients of consolidation fluctuate wildly over the effective consolidation stress for both loading and reloading stages. However, some consistent trends could still be found. The secondary compression indexes obtained from the reloading stage are lower than those from the

initial loading stage, indicating that over consolidated clay have lower secondary compression index than normally consolidated clay. The coefficients of consolidation show an upward trend as the effective consolidation stress increases. In addition, the compressibility and hydraulic conductivity tend to decrease with increasing effective consolidation stress. These findings enhance our understanding of the shear strength and consolidation characteristics of clay with OSC and GESC under both lateral and vertical loading conditions.

Keywords: compression index; compressibility; consolidation; failure envelope; geotextile encased sand column; shear strength

1 Introduction

Soft clay brings up a lot of safety concerns for geotechnical engineers, such as the low bearing capacity, high compressibility, low permeability, slow rate of consolidation, creep, etc. The estimated settlement, shear strength and permeability always turn out to be inaccurate as time goes by in the long term. One effective ground improvement technique is installing ordinary sand columns (OSC) or geotextile encased sand columns (GESC) in clay. The clay, sand columns and geotextile encasements work as a composite foundation to carry the load transferred to them. Typical applications of OSC or GESC improvement technique could be found in embankments and storage tanks constructed on soft clay soils. Because geotextile encasements can provide additional lateral confinement to the sand column, a further increase in bearing capacity and reduction in deformation of the composite foundation can be achieved (Alexiew et al. 2005; Black et al. 2007; Murugesan and Rajagopal 2009; Castro and Sagaseta 2011; Sivakumar et al. 2011; Najjar and Skeini 2014). The OSC and GESC also act as vertical drains in the clay due to the higher permeability of the sand column, so the consolidation process of the clay can be accelerated (Murugesan and Rajagopal 2009, 2010; Mohapatra et al. 2016, 2017). Furthermore, GESC has been found to have a better performance than OSC because the geotextile encasement can stop the lateral spreading of the granular materials into the surrounding soft clay (bulging phenomenon) (Ayadat and Hanna 2005; Murugesan and Rajagopal 2007; Andreou et al. 2008; Ali et al. 2012, 2014). Apart from the reinforcement function of a geotextile encasement, it also works as a filter and separation layer and

prevents clogging of the granular materials to guarantee that the drainage path is unblocked (Murugesan and Rajagopal 2009, Castro and Sagaseta 2011).

A large number of laboratory model tests on clay, clay with the OSC or GESC had been studied by many researchers during the past decades, which have mainly focused on the vertical loading condition (Alexiew et al. 2005; Malarvizhi and Ilamparuthi 2007; Murugesan and Rajagopal 2007; Gniel and Bouazza 2009, 2010; Ali et al. 2012, 2014; Dash and Bora 2013; Almeida et al. 2015; Hong et al. 2016). However, the model tests usually fail to control the drainage condition in the soil and did not allow for the measurement of pore pressure change during the loading and consolidation processes. Laboratory triaxial testing of clay with OSC or GESC by applying vertical compression therefore had also been studied by some researchers (Sivakumar et al. 2004, 2011; Ayadat and Hanna 2005; Black et al. 2007, 2011; Andreou et al. 2008; Najjar et al. 2010; Najjar and Skeini 2014). This is because triaxial compression testing is able to control the stress state, drainage condition, loading rate and lateral pressure, and is also able to measure the induced pore pressure and volume change. Sivakumar et al. (2004) and Black et al. (2007) used the medium-sized traixial machine having a diameter of 100 mm and a height of 200 mm to test the composite clay reinforced with the fine sand column. Until the year 2011, Black et al. (2011) and Sivakumar et al. (2011) started using the large-scale traixial machine having a diameter of 300 mm and a height of 400 mm to test the composite clay reinforced with the stone column (crushed basalt), which could better represent the field condition. However, in terms of the lateral loading on the OSC or GESC, very limited references could be found in the literature. It is believed that the sand columns below the toe of the embankment are primarily subjected to lateral loading or shear movement (Murugesan and Rajagopal 2009; Mohapatra et al. 2017), which may fail due to the inadequate confinement provided by the surrounding soft clay. The failure of supporting columns may cause unwanted excessive deformation of the embankment, promoting geotechnical instability. The performance of clay reinforced with OSC or GESC subjected to lateral loading could be experimentally modelled by direct shear box testing (Murugesan and Rajagopal 2009; Mohapatra et al. 2016). The performance of encased stone columns installed in clay under the lateral loading was first investigated by Murugesan and Rajagopal (2009) by carrying out large-scale direct shear box tests (300 mm by 300 mm). In addition, they designed a shear test in a large tank in which soft clay was reinforced with stone columns. By applying a surface load to the adjacent clay,

the stone columns were then subjected to lateral soil movement. After that, Mohapatra et al. (2016) recently carried out the large-scale direct shear box (305 mm by 305 mm) testing of a poorly-graded fine sand reinforced with granular columns and geosynthetic-encased granular columns. The effects of the size of column (50 mm or 100 mm), the group pattern (triangular or square), and the stiffness of geosynthetic encasement on the shear resistance were reported and discussed in their study. In their study, using a large-scale shear box can reduce the scale effect to some extent; however, using gravel columns to reinforce the sand is not representative of the actual field conditions where soft soils are present and ground improvement is therefore needed. Hence, clay should be used as the surrounding soil in their experiments rather than sand.

In this study, a series of conventional direct shear and 1-D consolidation tests were carried out on the Kaolin, Kaolin with OSC, and Kaolin with GESC, to study the shear strength and consolidation characteristics of clay with OSC and GESC under both lateral and vertical loading conditions. It should be mentioned that the scale effect of the present small-scale laboratory testing was the main problem to reflect the field condition, but it was still worth trying to study the impacts of the OSC and GESC on the shear strength and consolidation parameters of the reinforced clay composites.

2 Sample preparation

2.1 Materials used

Kaolin was used as the soft clay in this study. The Liquid and Plastic Limits of the Kaolin were found to be 90% and 35%, respectively, giving a Plasticity Index of 55%. A poorly graded (SP) fine sand with grain size ranging between 0.3 mm and 0.6 mm was used for the sand column. The sand has an average particle size D_{50} of 0.48 mm, and a uniformity coefficient C_u of 1.56. The air-dried sand has a friction angle of 30.1° determined by direct shear box testing. Hydrometer test on the Kaolin and sieving analysis on the sand were carried out, and the obtained particle size distribution curves are shown in Figure 1. A woven polypropylene geotextile, Tencate Mirafi HP340, was used as the encasement, which has an ultimate tensile strength of 40 kN/m and a nominal thickness of 0.6 mm. The basic properties of the materials used in this study are summarised in Table 1.

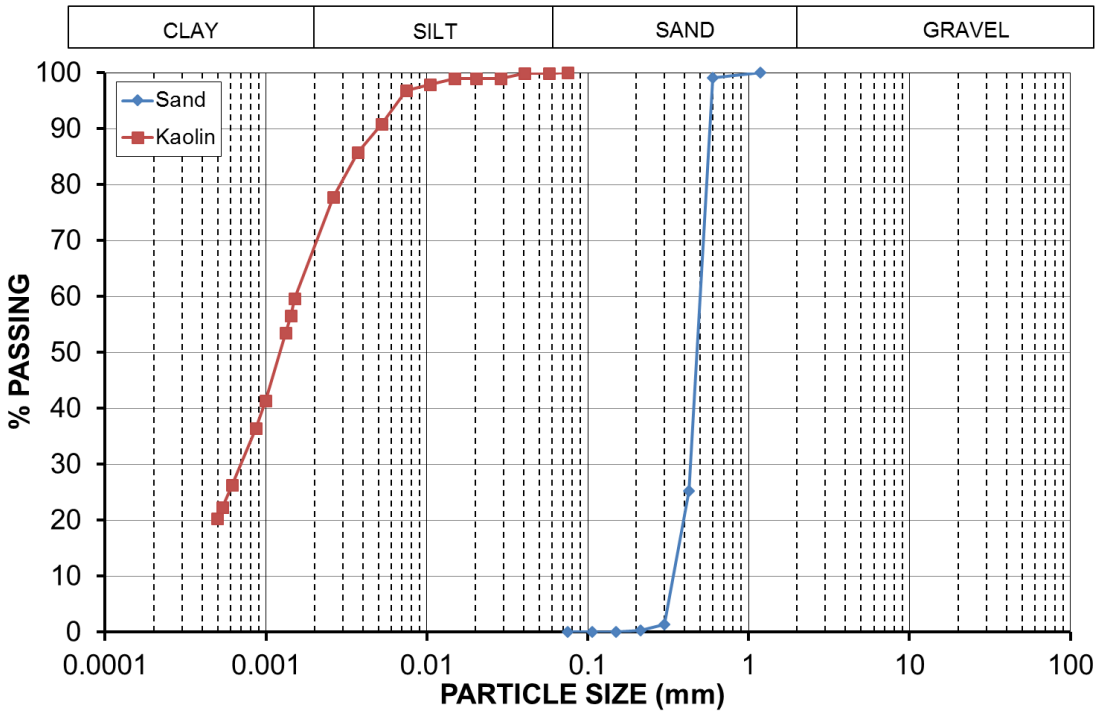

Figure 1 particle size distribution curves of sand and clay used

Table 1 Properties of materials used

Kaolin	Property or Value	Sand	Property or Value	Geotextile	Property or Value
LL (%)	90	ϕ (°)	30.1	Brand	Tencate HP340
PL (%)	35	c (kPa)	12.9	Polymer	Polypropylene
PI (%)	55	ρ_{dmax} (g/cm^3)	1.734	Texture	Woven
w (%)	55 ± 1	ρ_{dmax} (g/cm^3)	1.582	Opening size (mm)	0.3
G_s	2.615	G_s	2.644	Tensile strength (kN/m)	40
D_{50} (mm)	0.0012	D_{50} (mm)	0.48	Nominal thickness (mm)	0.6
F_{200} (%)	69	C_u	1.56	Strain at maximum load (%)	15
USCS	CH	USCS	SP	CBR Puncture (kN)	5

2.2 Sample preparation

The Kaolin specimen was mixed with water and prepared at an average moisture content of 55%. Three square (60 mm by 60 mm by 20 mm) and circular (75 mm in diameter and 20 mm in height) cutting rings were used as sample moulds to prepare specimens for

direct shear and oedometer testing (Figure 2). Due to the limitation of the small-scale model tests, only one single sand column was installed in the middle of the clay specimen by the replacement method. It is believed that installing triangular or square column groups (3 or 4 sand columns) in such a small specimen is not realistic and appropriate. A thin-walled tube, having an outer diameter of 22 mm, was used to form a hollow column in the middle of the Kaolin specimen. The hole was filled with the air-dried sand using a funnel to form an OSC, and then the sand column was fully saturated using a syringe (Figure 2a). More sand might be needed to compensate for the reduction in height caused by saturation. The total mass of the air-dried sand needed for the sand column installation was measured and used for the calculation in the later section. This sand column installation method also represents the actual loose dumping of sand in the field, and it is believed to be superior to the compaction method because compacting the sand would cause the expansion of the hole, resulting in variations in the initial specimens. For GESC, a geotextile encasement was prefabricated to have the same diameter of 22 mm and a height of 20 mm, and then was inserted and attached to the hole prior to filling the sand (Figure 2a). Finally, the composite specimens were covered with fully-saturated filter papers on the top and bottom to hold the sand column. In brief, this sample preparation method was found to be able to successfully produce uniform and repeatable clay specimens with OSC or GESC installed in the middle.

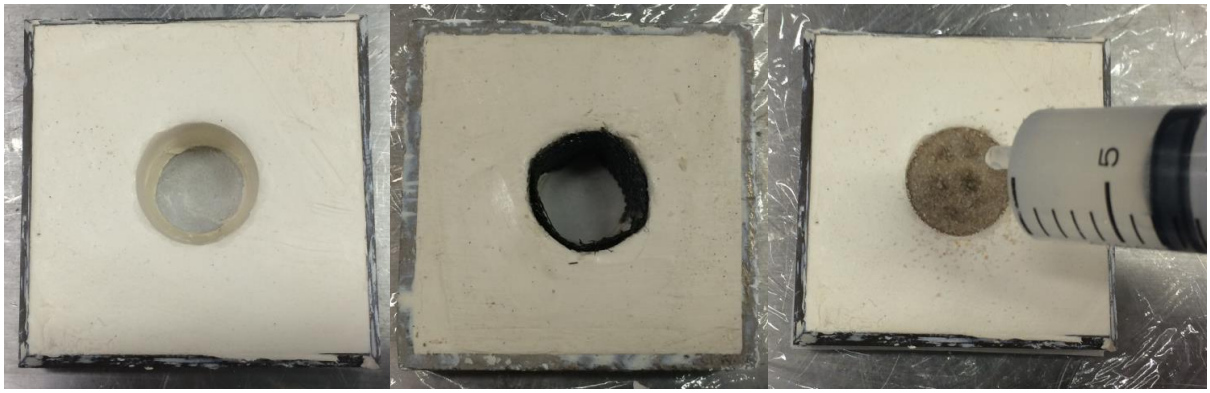

(a)

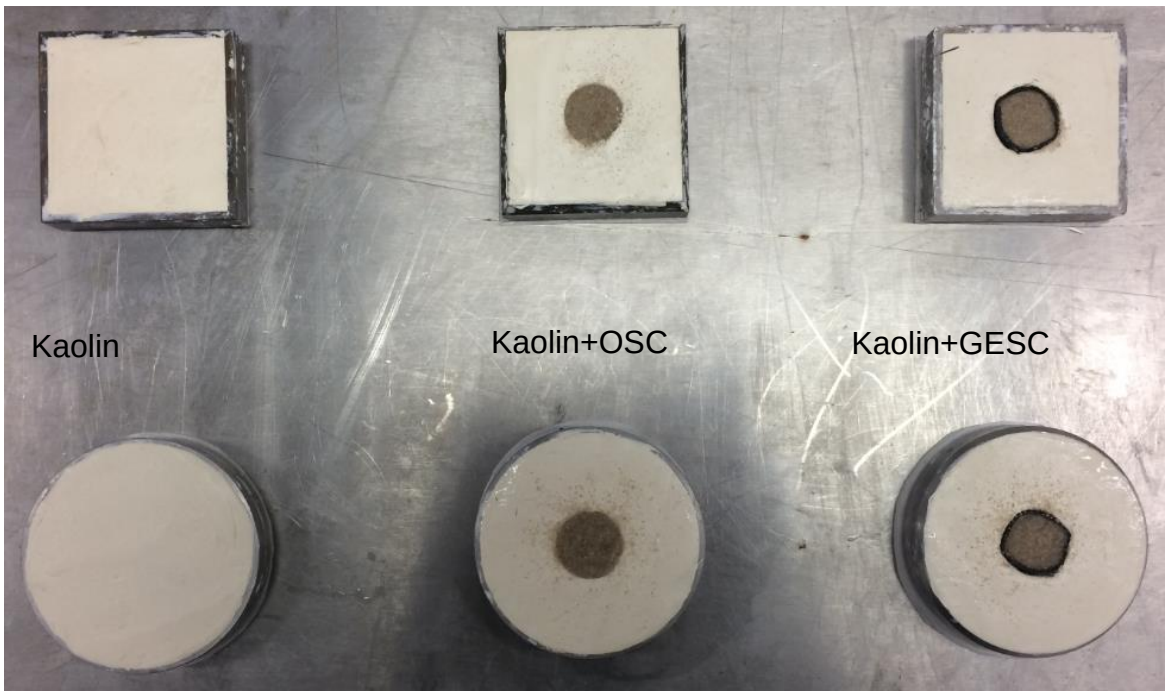

(b)

Figure 2 Sample preparation for direct shear and 1-D consolidation tests: (a) sample preparation process; (b) prepared specimens

3 Testing program

3.1 Direct shear test

Figure 3 Kaolin with sand column in shear box

The prepared specimen in the cutting ring was carefully pushed into the shear box prior to starting the direct shear testing (Figure 3). Conventional direct shear box tests were carried out on the Kaolin, Kaolin with OSC, and Kaolin with GESC specimens sitting in a

water bath under applied normal stresses of 54.5 kPa, 109 kPa, or 218 kPa to determine the failure envelopes and shear strength parameters. A slow shearing rate of 0.02 mm/min was selected to ensure a drained condition during shearing.

3.2 1-D consolidation test

Conventional oedometer tests were carried out on the Kaolin, Kaolin with OSC, and Kaolin with GESC specimens. The test consisted of three stages, namely, loading, unloading and reloading. The loading stage started from 25 kPa; the load on the specimen was doubled every day for each stage until 800 kPa was reached. For the unloading stages, the load was removed reversely until the load was reduced to 25 kPa. Finally, for the reloading stages, the loads were increased step by step up to 1600 kPa. Each load was kept for 24 hours, and thus the 1-D consolidation testing program lasted for 17 days in total (Table 2). The prepared specimens in the cutting rings (Figure 2) were placed in the consolidometers and were always kept under sufficient water throughout the duration of the test.

Table 2 1-D consolidation testing program

Loading stage (day)	1	2	3	4	5	6
Stress (kPa)	25	50	100	200	400	800
Unloading stage (day)	7	8	9	10	11	
Stress (kPa)	400	200	100	50	25	
Reloading stage (day)	12	13	14	15	16	17
Stress (kPa)	50	100	200	400	800	1600

4 Results and discussion

4.1 Direct shear test results and discussion

The selected direct shear test results under the applied normal stress of 218 kPa are presented to highlight the impact of OSC and GESC on the shear strength, as shown in Figure 4. An obvious peak was observed for the Kaolin specimen at a shear displacement of 3 mm, with a slight drop-off until reaching a residual state, while for the Kaolin with OSC and GESC specimens, there was no obvious peak reached. It is evident that Kaolin with sand column can mobilise more shear resistance when subjected to the lateral loading. For the Kaolin with OSC specimen, the sand is free to move and spread into the

surrounding clay, so the shear strength contributed by the frictional sand particles may not be maximally developed. A possible explanation for the sudden drop on the shear stress curves at a shear displacement of 3 mm for the Kaolin with OSC might be that some sand particles at the clay interface started penetrating into the clay, resulting a sudden decrease in the shear stress. When the smear zone has been formed, the shear stress started increasing again. For the Kaolin with GESC specimen, the geotextile separated the sand from the clay, so a further increase in shear strength was expected to see due to the distortion of the geotextile encasement during shearing. However, this expected further improvement by the GESC seems not very significant compared to the Kaolin with OSC specimen (Figure 4a). A general contraction was found during shearing for the three different specimens. Surprisingly, the compression of the Kaolin with GESC specimen was the largest during shearing, followed by the Kaolin with OSC, and finally the Kaolin (Figure 4b). This phenomenon could be attributed to the distortion of OSC and GESC, which caused more total compressions during shearing. The obtained shear strength envelopes and inferred shear strength parameters are presented and compared in Figure 5, which were best-fitted using the Mohr-Coulomb straight-line failure criterion. Both the applied normal stresses and the measured shear stresses were corrected for reducing shear area during the course of the tests. It was found that the Kaolin specimen had a very low direct shear strength, resulting in a low friction angle of 9.5° and an apparent cohesion of 6.0 kPa. For the Kaolin with OSC and GESC specimens, the frictional angle was improved dramatically to 18.0° and 21.1°, respectively, while the inferred apparent cohesion was still very low. It can readily be noticed that the friction angle has almost been doubled after including OSC. However, the additional inclusion of geotextile encasement for GESC only resulted in a slight increase in friction angle and a slight decrease in the apparent cohesion. This is because a lower shear strength value was obtained under the lowest normal stress of 54.5 kPa, indicating that the further improvement in shear strength provided by the geotextile encasement is not effective under a lower normal stress. The effectiveness tends to increase with the applied normal stress.

The theoretical shear resistance of the clay with the sand columns can be estimated by the following equation (Christoulas et al. 1997):

$$F = A_c\tau_c + A_s\tau_s \tag{1}$$

where A_c and A_s are the plane areas of the sand columns and intervening clay; τ_c and τ_s are the shear strengths of the clay and sand respectively; F is the shear resistance.

For the direct shear testing of clay with the sand column, the shear resistance in Eq. (1) divided by total area of the shear plane produces the shear strength mobilised along the shear surface as follows:

$$\tau = \frac{F}{A} = \frac{A_c}{A}\tau_c + \frac{A_s}{A}\tau_s = \alpha_c\tau_c + \alpha_s\tau_s \quad (2)$$

where τ is the direct shear strength, A is the total plane area of the shear plane, α_c and α_s are the proportions of the surface area of the clay and sand column to the total plane area of the shear plane. The shear strengths of Kaolin with OSC obtained by the experimental direct shear tests and also by the theoretical Eq. (2) are compared in Figure 6 and Table 3. It should be noted that both α_c and α_s used in the calculation of the predicted shear strength at failure were calculated considering the reduction in the contact area of the clay after shearing. It was observed that the measured shear strengths from the experimental direct shear tests are much higher than those obtained from the theoretical prediction by superposition, which is opposite to the findings from Murugesan and Rajagopal (2008). In their study, granular stone columns were installed in a 300 mm by 300 mm large shear box, and hence they believed that the stone columns may have not fully developed their shear strength, due to the inadequate confinement when shearing the clay soil mass in the direct shear box. However, for the fine sand column (particle size ranging from 0.3 to 0.6 mm) in a small shear box in our study, it was believed that the friction of the sand had been fully developed. Furthermore, because of the small-scale testing, the friction resistance contributed by the sand column could be much more significant than it was expected by simple superposition calculated using the proportion of surface area of the sand column. A significant increase in friction angle caused by including OSC also indicates that the frictional resistance provided by the sand column is a dominant factor contributing to the overall improvement in the shear strength of the composite. The theoretical interpretation of the shear strength of clay with sand column in direct shear testing deserves future research to quantify the contribution of each component. The shear strength contributed by the geotextile encasement is believed to be more complicated.

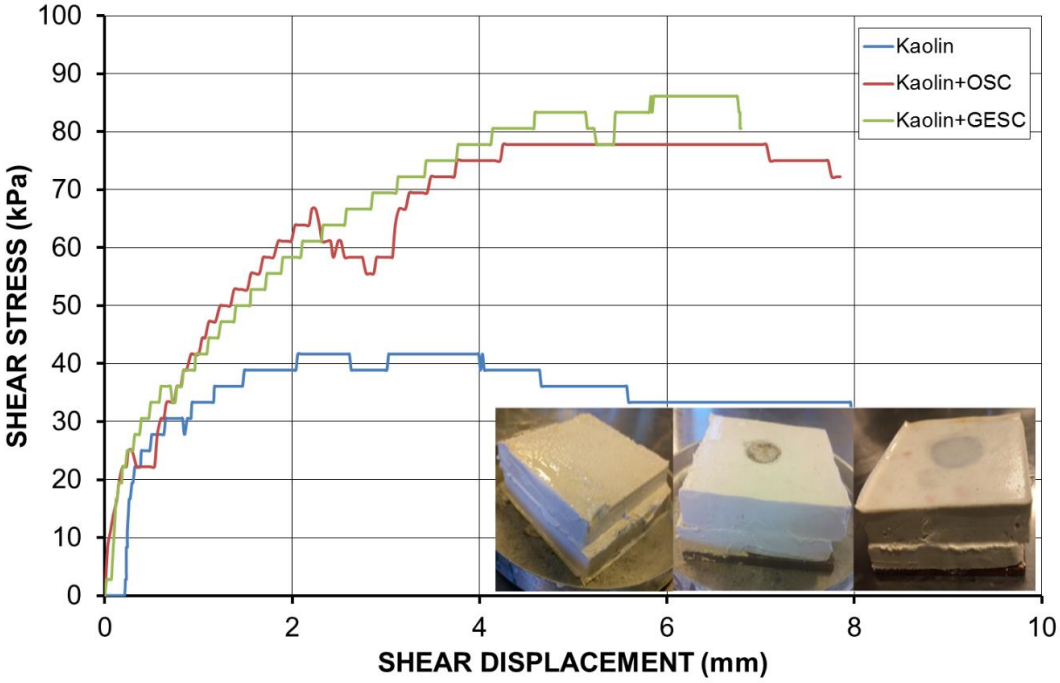

(a)

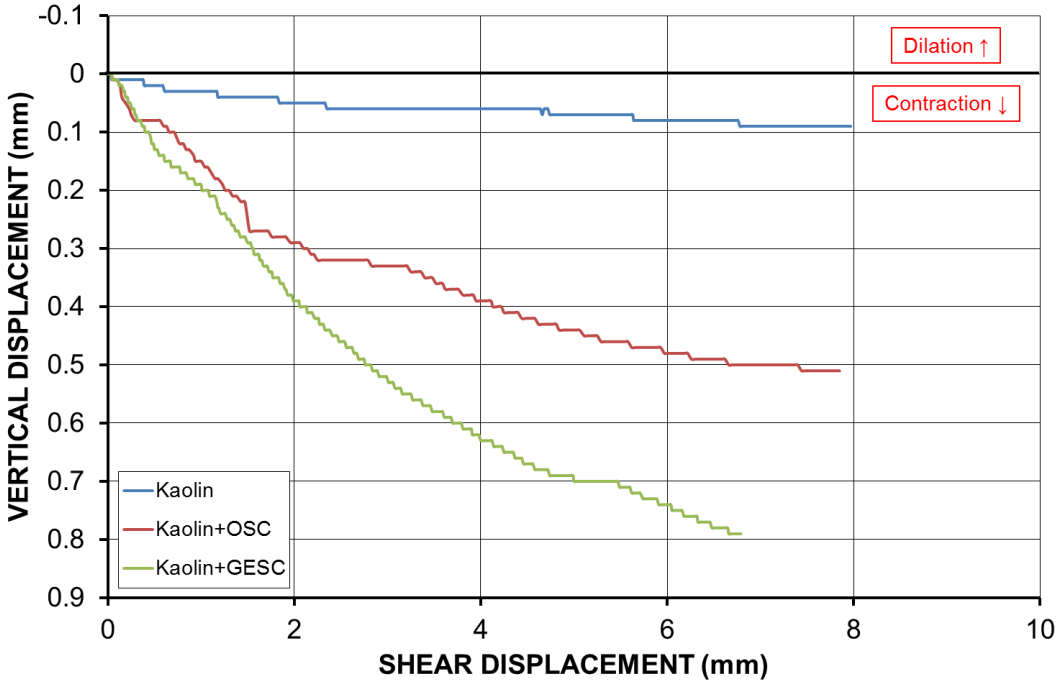

(b)

Figure 4 Single-stage direct shear test results under applied normal stress of 218 kPa: (a) shear stress versus shear displacement; (b) vertical displacement versus shear displacement

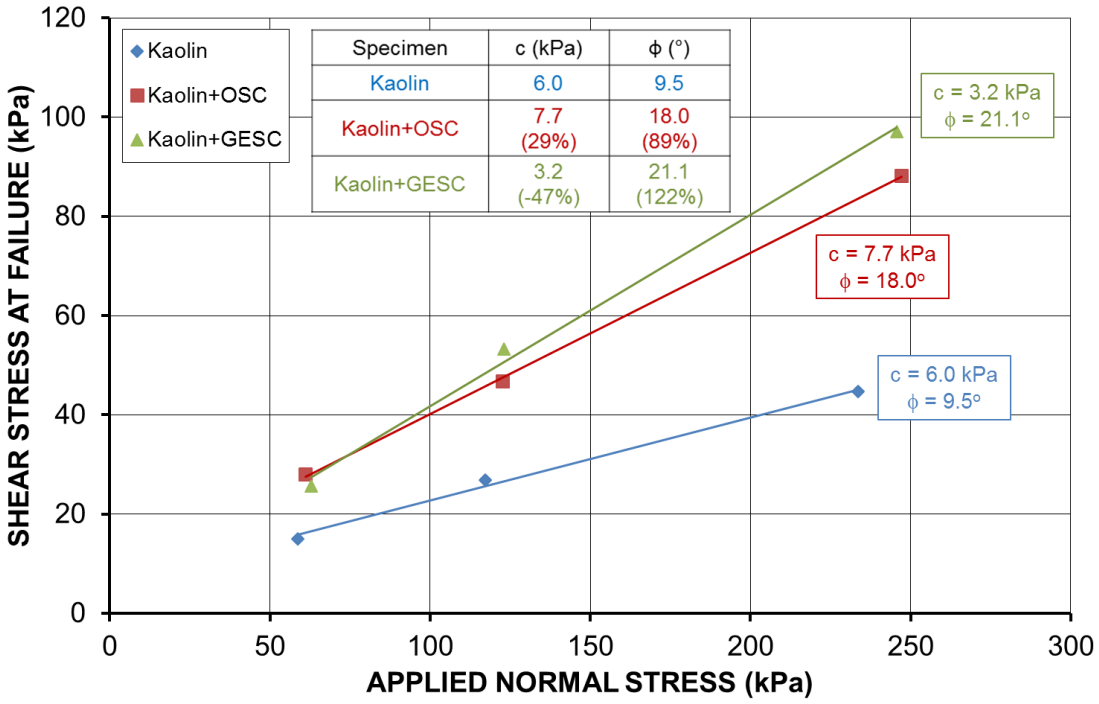

Figure 5 Shear strength envelopes of Kaolin, Kaolin with OSC, and Kaolin with GESC

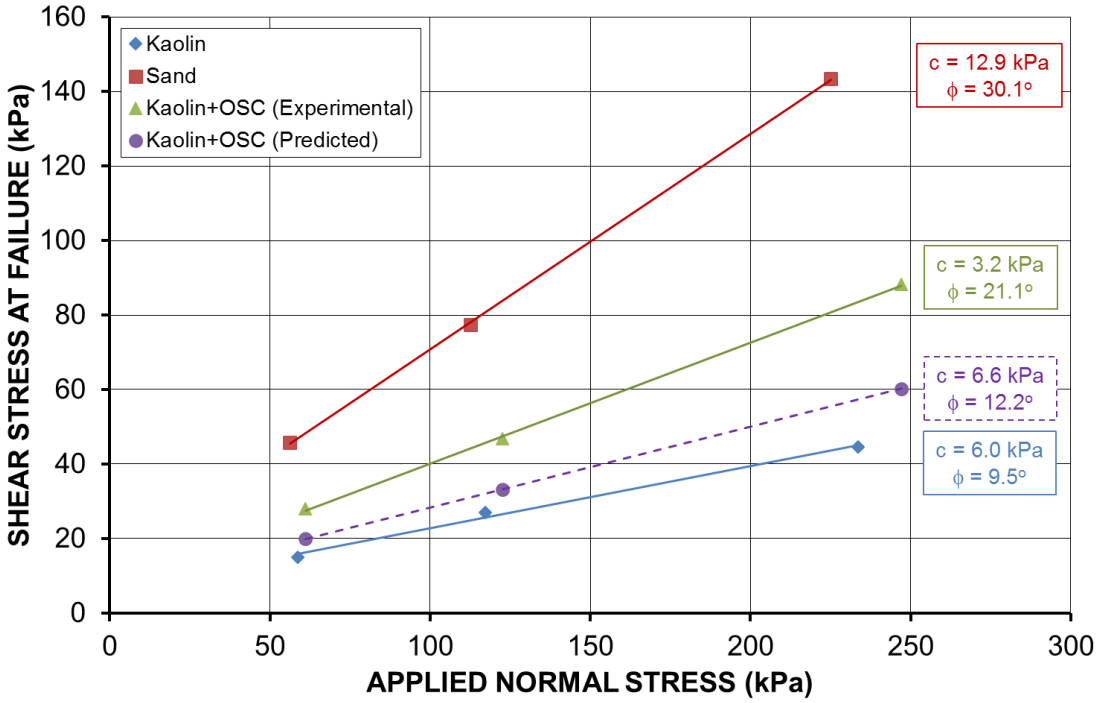

Figure 6 Comparison of the experimental and theoretically predicted shear strength of Kaolin with sand column

Table 3 Comparison of experimental and predicted shear strengths of Kaolin with OSC specimens

σ_{nf} (kPa)	D_f (mm)	A_t (mm^2)	A_s (mm^2)	A_c (mm^2)	α_c	α_s	$\tau_{f,exp}$ (kPa)	% increase	$\tau_{f,pred}$ (kPa)
61	6.45	3213	380.13	2832.87	0.8817	0.1183	28	87	20
123	6.65	3201	380.13	2820.87	0.8812	0.1188	47	74	33
247	7.06	3176	380.13	2796.27	0.8803	0.1197	88	97	60

Note: σ_{nf} is corrected normal stress at failure; D_f is the shear displacement at failure

4.2 1-D consolidation test results and discussion

1-D Consolidation tests on clay reinforced with OSC and GESC have not been investigated in the past. As mentioned before, scale effect of the conventional laboratory test is still the biggest shortcoming to reflect the field conditions, but it is still worth to know the impact of OSC and GESC on the consolidation characteristics of clay, including the compression index C_c, swell index C_s, recompression index C_r, secondary compression index C_α, coefficient of consolidation c_v, coefficient of compressibility a_v, coefficient of volume compressibility m_v, modulus of compressibility E_s, and hydraulic conductivity k.

To determine the void ratios at the end of each loading stage for the Kaolin, Kaolin with OSC, and Kaolin with GESC specimens, it is necessary to determine the mass of solids in the specimen, the height of solids, and the initial void ratio of the specimens. The specific gravity of the specimen is required for the calculations mentioned above. However, it is difficult to determine the specific gravity of the Kaolin with OSC and GESC composite specimens due to the existence of the two types of solids. In this study, the specific gravity of the composite was calculated by superposition using the following equation:

$$G_{s,comp} = G_{s,c} \times \frac{m_c}{m_t} + G_{s,s} \times \frac{m_s}{m_t} \tag{3}$$

where $G_{s,comp}$ is the specific gravity of the composite specimen; $G_{s,c}$ is the specific gravity of the clay; $G_{s,s}$ is the specific gravity of the sand,; m_c is the dry mass of the clay; m_s is the dry mass of the sand; m_t is the total mass of the composite specimen.

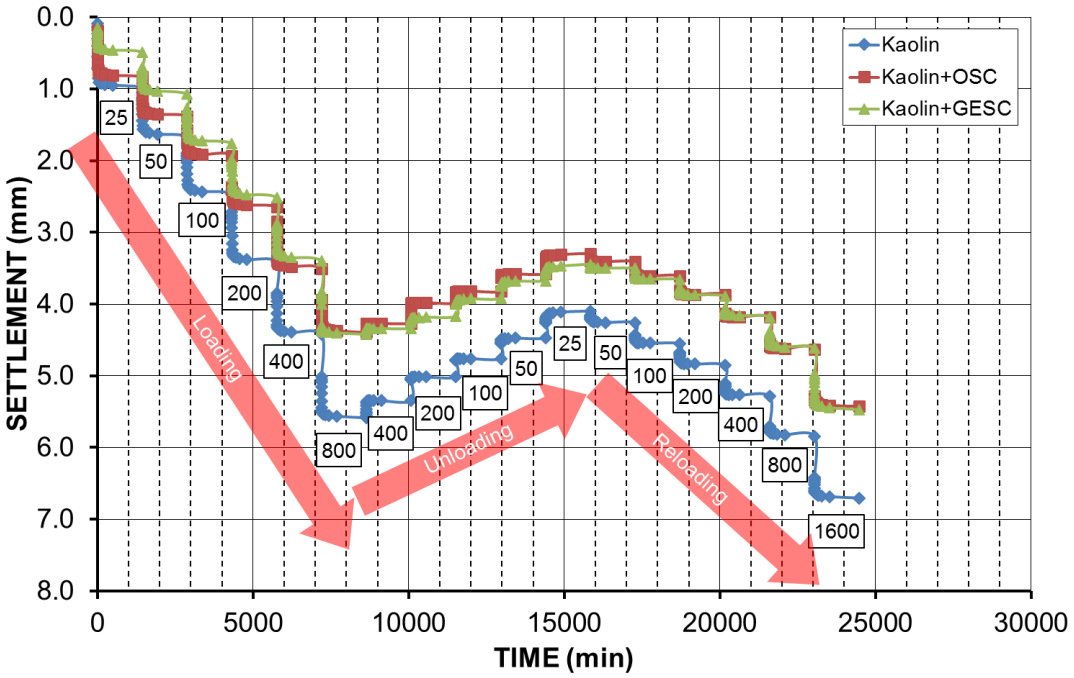

(a)

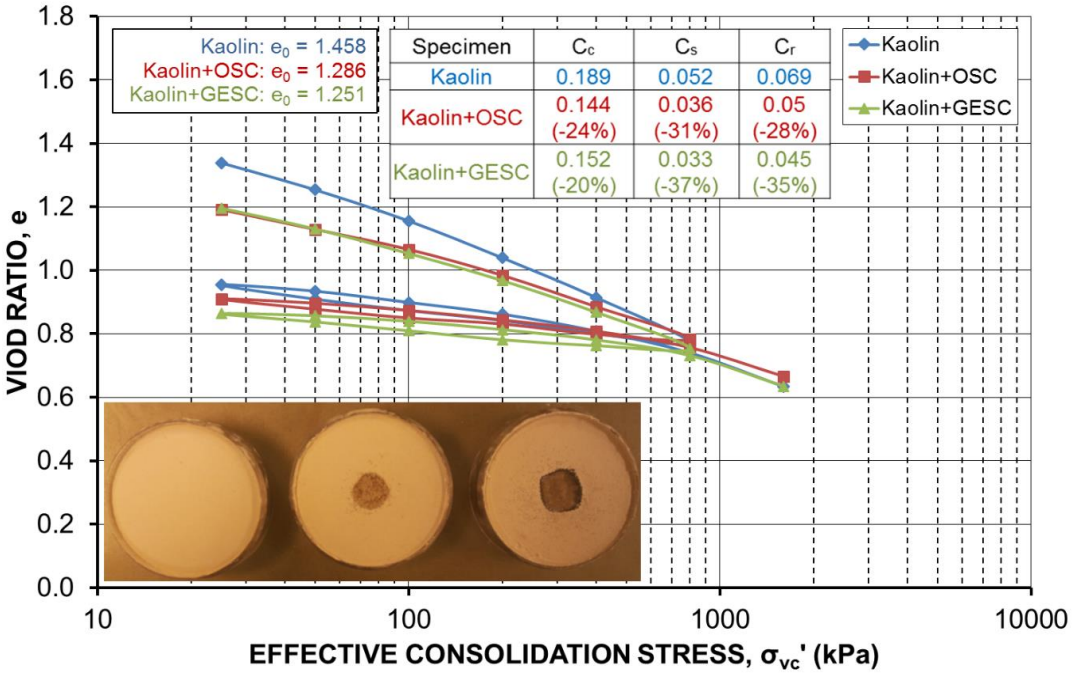

(b)

Figure 7 Consolidation characteristics of Kaolin, Kaolin with OSC, and Kaolin with GESC: (a) settlement versus time; (b) void ratio versus effective consolidation stress

The specific gravities of Kaolin and sand are 2.644 and 2.615 respectively determined by the pycnometer tests. The superimposed specific gravities calculated using Eq. (3) for the Kaolin with OSC and GESC specimens are 2.619 and 2.618 respectively, which are quite close to the specific gravity of Kaolin, because the mass of the sand column is much less than the total mass of the composite specimen.

The plots of settlement versus time for the loading, unloading and reloading stages for the Kaolin, Kaolin with OSC, and Kaolin with GESC specimens are shown in Figure 7a. The derived e-log σ_{vc}' curves and the photos of the consolidated specimens obtained from the oedometer tests are shown in Figure 7b. Also shown in Figure 7b are the initial void ratios and the corresponding C_c, C_s, and C_r calculated from the plotted e-log σ_{vc}' curves. It is evident that after the Kaolin was reinforced with the OSC or GESC, C_c, C_s and C_r had decreased by 20%-37%, indicating that OSC or GESC would reduce the settlement (loading or reloading) and rebound (unloading). However, the further impact of geotextile encasement seems insignificant when comparing the results of OSC with GESC. The obtained C_c of the Kaolin with GESC specimen was slightly higher than that of the Kaolin with OSC, but the obtained C_s and C_r were the opposite, as shown in Figure 7b. However, these parameters are still very close in value. The plots of C_α versus σ_{vc}' and c_v versus σ_{vc}' for the loading and reloading stages are shown in Figure 8. Loading and reloading stages represent that the specimens were in the normally consolidated (NC) and over consolidated (OC) conditions, respectively. Except for the last load 1600 kPa, the specimens had returned back to the normally consolidated condition. Wavy curves were obtained for the three specimens without consistent relationships in terms of the effective consolidation stress. Also, the influence of OSC or GESC on the C_α and c_v for the composite specimen is uncertain, compared to the Kaolin specimen. However, some consistent trends could still be found. It is evident that the secondary compression indexes C_α obtained from the reloading stages (from 50 kPa to 800 kPa) are lower than those obtained from the loading stages, indicating that the normally consolidated clay has a higher secondary compression index than the over consolidated clay. After the effective consolidation stress goes beyond 800 kPa (reloading up to 1600 kPa), C_α suddenly increases to the normal value range obtained from the initial loading stage because the past stress experience had been completely overcome and the specimen had returned back to the normal consolidated condition (Figure 8a). Both Casagrande's logarithm of time fitting method and Taylor's square root of time fitting method were attempted, and the

plots of coefficients of consolidation versus effective consolidation stress show wavy patterns. It was found that Taylor's method produces slightly higher coefficients of consolidation, which agrees with the findings from Robinson and Allam (1996) and Das (2006). However, there is a general upward trend observed from the calculated coefficients of consolidation as the effective consolidation stress increases. Based on the understanding of the definition of the coefficient of consolidation, the higher the coefficient of consolidation, the less time is required to achieve a specific degree of consolidation (50% for the log t method or 90% for the square root t method). That is, the consolidation rate seems faster under a higher effective consolidation stress. This finding could be explained by the fact that a higher effective consolidation stress would result in a lower sample height due to settlement, which means a shorter drainage path. As it is already known in Terzaghi consolidation theory, if the drainage path reduces by 1/2, the time required to achieve a certain degree of consolidation would reduce by 1/4 (t is inversely proportional to H^2). Therefore, the induced excess pore water pressure would dissipate faster under a higher effective normal stress, resulting in a faster consolidation rate. Therefore, the overconsolidated clay tends to have a higher c_v than the normally-consolidated clay (see the dash line). Figure 8b highlights the c_v results obtained from the log t method, which were used for the calculation of the hydraulic conductivity.

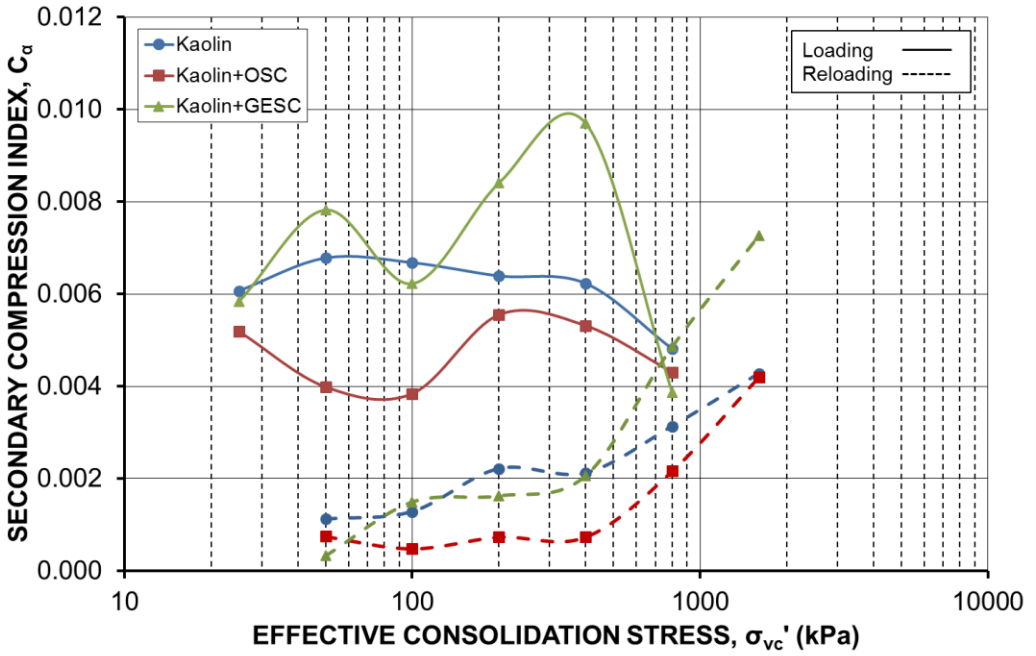

(a)

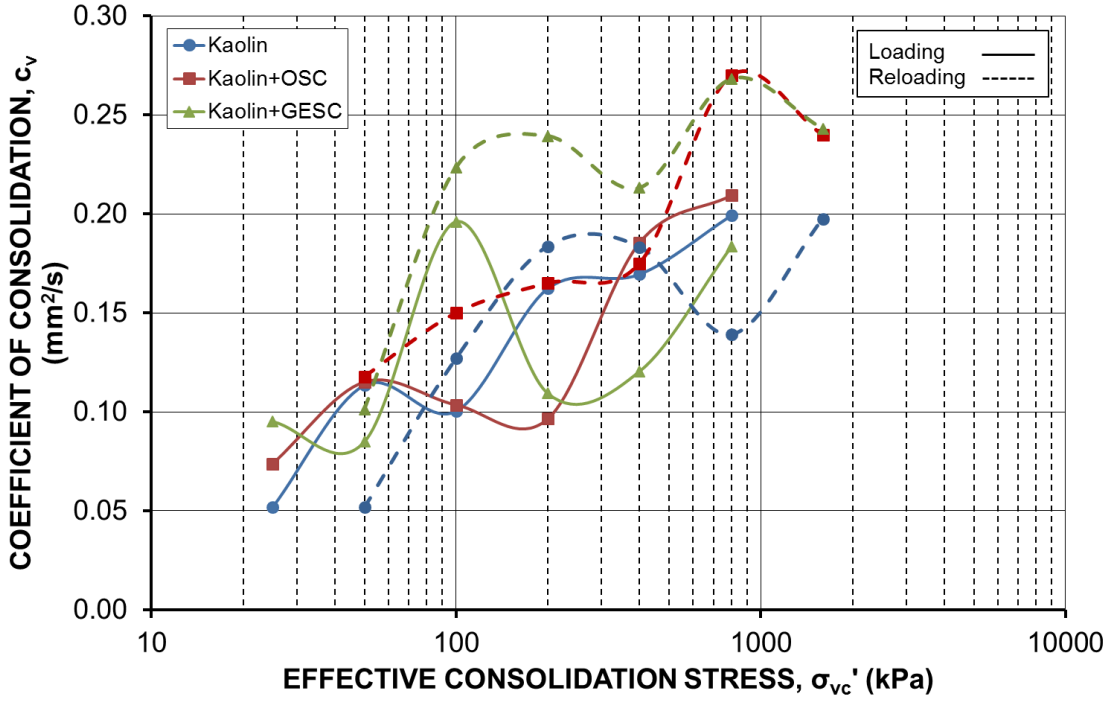

(b)

Figure 8 (a) secondary compression index; (b) coefficient of consolidation (log t method)

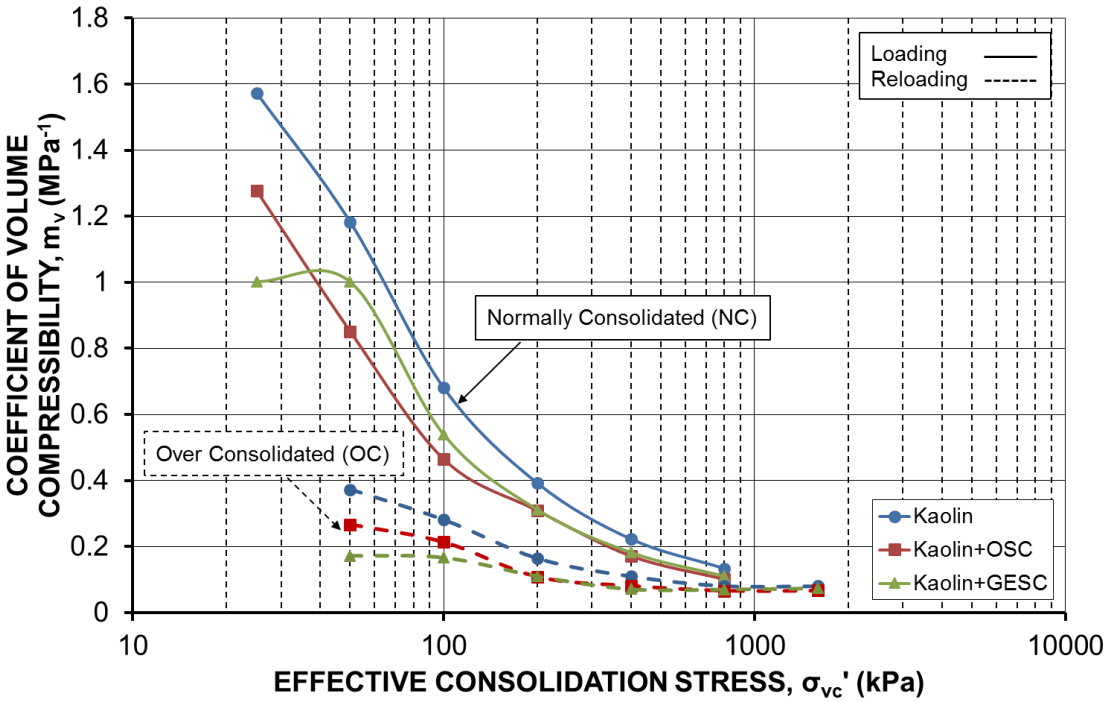

(a)

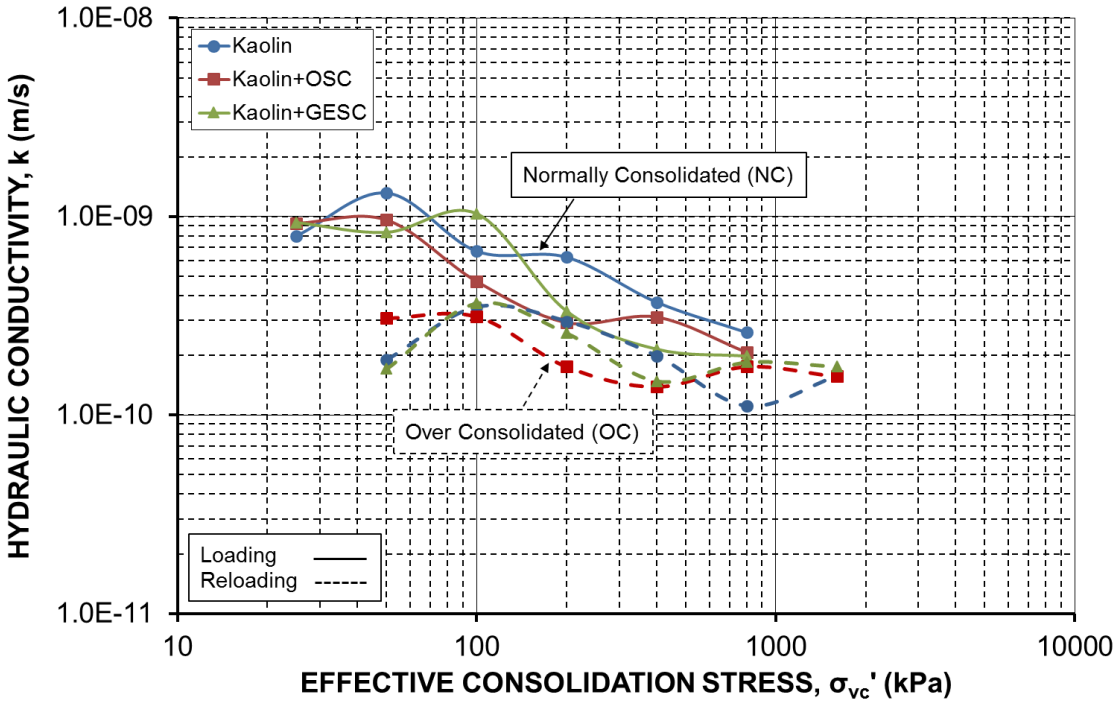

(b)

Figure 9 (a) coefficient of volume compressibility; (b) hydraulic conductivity

The coefficient of compressibility a_v, coefficient of volume compressibility m_v, modulus of compressibility E_s, and hydraulic conductivity k for both the loading (normally consolidated clay) and reloading stages (over consolidated clay) were also calculated and interpreted in this paper (Holtz and Kovacs 1981; Das 2006). The plots of m_v versus σ_{vc}' and k versus σ_{vc}' are highlighted and presented in Figure 9. It is evident that the compressibility of the specimens decreases as the effective vertical stress increases. This is particularly obvious for the loading stage from 25 kPa to 800 kPa. Furthermore, a slow downward trend in compressibility can be also observed for the reloading stage from 50 kPa to 1600 kPa. The higher the effective consolidation stress, the lower the compressibility tends to obtain, as shown in Figure 9a. In terms of the calculated hydraulic conductivity, it is governed by the coefficient of consolidation c_v and the coefficient of volume compressibility m_v. It has been found that m_v decreases with σ_{vc}', but c_v tends to increase with σ_{vc}' (although only upward wavy curves obtained). The final calculated hydraulic conductivity shows that k tends to decrease with σ_{vc}'. This indicates that hydraulic conductivity is mainly governed by the change of the coefficient of volume compressibility. However, there is a lack of data in the literature to prove the relationship between the coefficient of consolidation and the

effective consolidation stress, which also deserves further research. From the physical consolidation process point of view, consolidation densifies the soil and reduces the void ratio. Therefore, the reductions in a_v, m_v, and k with the increasing σ_{vc}' can theoretically be explained by the reduction in the void ratio (denser) caused by the increasing effective consolidation stress.

By contrast, it is evident that the inclusion of OSC and GESC reduced the compressibility of Kaolin based on the calculated a_v, m_v and E_s. It was expected that the hydraulic conductivity of the Kaolin with OSC and GESC specimens would be higher than the Kaolin specimen because of the existence of sand and geotextile. However, the calculated hydraulic conductivity does not show a significant difference between the Kaolin, Kaolin with OSC, and Kaolin with GESC specimens, which almost remains within the same order of magnitude (10^{-10} m/s). It means that for the soft clay with very low hydraulic conductivity, OSC and GESC does not significantly accelerate the consolidation process in the small-scale oedometer tests. Therefore, a further study has been proposed to study the consolidation characteristics of the clay reinforced with OSC and GESC by using a special designed large-scale slurry consolidometer (150 mm in diameter and 400 mm in height; Shokouhi et al. 2017) at the University of Queensland. This slurry consolidometer machine is able to overcome the small-scale effect to some extent and accommodate grouped columns testing. Six pore pressure transducers are installed along the height of the consolidometer, which is also able to measure the pore pressure dissipation of clay with and without OSC or GESC. Moreover, a load cell installed at the base is able to measure the friction loss and the load transferred from the top.

In summary, the average C_α, c_v, a_v, m_v, E_s, and k of the Kaolin, Kaolin with OSC, and Kaolin with GESC specimens under normally consolidated (NC) and over consolidated (OC) conditions, corresponding to the loading and reloading stages in the oedometer tests, are included in Table 4. Also shown in Table 4 are the percentage increases or decreases for each parameters of the Kaolin with OSC or GESC compared to the Kaolin. For the normally consolidated specimens, the inclusion of OSC or GESC reduced the secondary compression indexes C_α by average of 20% and reduced the coefficient of compressibility a_v and coefficient of volume compressibility m_v by about 25%. It was also found that the coefficient of consolidation c_v increased by only 3% or 4% for the loading stage; however, it increased by 28% or 47% for the reloading stage. This has proven again that for an

overconsolidated specimen, because the drainage path had decreased to some extent due to the settlement, the consolidation rate increased significantly, as explained before.

Table 4 Average parameters obtained from oedometer tests

Specimen	Condition	C_α	c_v (mm^2/s)	a_v (MPa^{-1})	m_v (MPa^{-1})	E_s (MPa)	K (m/s)
Kaolin	NC	0.0059	0.142	1.344	0.610	4.867	6.0×10^{-10}
	OC	0.0020	0.137	0.380	0.202	7.372	2.3×10^{-10}
Kaolin+OSC	NC	0.0046 (-21%)	0.146 (+3%)	0.972 (-28%)	0.463 (-24%)	5.446 (+12%)	4.8×10^{-10} (-20%)
	OC	0.0010 (-51%)	0.176 (+28%)	0.274 (-28%)	0.147 (-27%)	9.007 (+22%)	2.2×10^{-10} (-4%)
Kaolin+GESC	NC	0.0070 (+19%)	0.147 (+4%)	0.958 (-29%)	0.46 (-25%)	5.022 (+3%)	5.3×10^{-10} (-12%)
	OC	0.0021 (-65%)	0.209 (+47%)	0.215 (-84%)	0.118 (-81%)	9.832 (+102%)	2.3×10^{-10} (0)

Note: Numbers in parentheses are percentage increases or decreases compared to Kaolin

5 Conclusions

Shear strength and consolidation characteristics of the Kaolin, Kaolin with OSC, and Kaolin with GESC specimens were investigated by carrying out laboratory direct shear and oedometer tests. The obtained experimental results were compared and interpreted in this paper to study the behaviour of the OSC and GESC reinforced clay composites subjected to lateral loading in the direct shear tests and vertical loading in the oedometer tests. The main findings are summarised as follows:

(1) OSC and GESC can significantly improve the shear strength of clay when subjected to lateral loading in the direct shear tests, resulting in a significant increase in friction angle. However, the impact on the inferred apparent cohesion was found to be minor.

(2) OSC and GESC can reduce the compressibility of clay when subjected to vertical loading in the oedometer tests, resulting in a reduction in compression index C_c, swell index C_s, recompression index C_r, the coefficient of compressibility a_v, and coefficient of volume compressibility m_v. However, the further impact of the

geotextile encasement on the consolidation parameters seems insignificant by comparing the results between GESC and OSC.

(3) An over consolidated specimen tends to have a lower secondary compression index C_α, lower compressibility mv and lower hydraulic conductivity k than a normally consolidated specimen.

(4) The coefficient of consolidation cv tends to increase with the effective consolidation stress in this study, while coefficient of compressibility a_v, coefficient of volume compressibility m_v, and hydraulic conductivity k tend to decrease with the effective consolidation stress.

References

Alexiew D., Brokemper D., and Lothspeich S., (2005). Geotextile Encased Columns (GEC): Load Capacity, Geotextile Selection and Pre-Design Graphs. Proceedings of GeoFrontiers 2005, Austin, Texas, United States, pp. 497-510.

Ali K., Shahu J. T., and Sharma K. G., (2012). Model tests on geosynthetic-reinforced stone columns: a comparative study. Geosynthetics International, 19(4), 292-305.

Ali K., Shahu J. T., and Sharma K. G., (2014). Model tests on single and groups of stone columns with different geosynthetic reinforcement arrangement. Geosynthetics International, 21(2), 103-118.

Almeida M. S. S., Hosseinpour I., Riccio M., and Alexiew D., (2015). Behavior of Geotextile-Encased Granular Columns Supporting Test Embankment on Soft Deposit. Journal of Geotechnical and Geoenvironmental Engineering, 141(3), 04014116.

Andreou P., Frikha W., Frank R., Canou J., Papadopoulos V., and Dupla J. C., (2008). Experimental study on sand and gravel columns in clay. Proceedings of the Institution of Civil Engineers - Ground Improvement, 161(4), 189-198.

Ayadat T., and Hanna A. M., (2005). Encapsulated stone columns as a soil improvement technique for collapsible soil. Proceedings of the Institution of Civil Engineers - Ground Improvement, 9(4), 137-147.

Black J. A., Sivakumar V., and Bell A., (2011). The settlement performance of stone column foundations. Géotechnique, 61(11), 909-922.

Black J. A., Sivakumar V., Madhav M. R., and Hamill G. A., (2007). Reinforced Stone Columns in Weak Deposits: Laboratory Model Study. Journal of Geotechnical and Geoenvironmental Engineering, 133(9), 1154-1161.

Castro J., and Sagaseta C., (2011). Deformation and consolidation around encased stone columns. Geotextiles and Geomembranes, 29(3), 268-276.

Christoulas S., Giannaros C., and Tsiambaos G., (1997). Stabilization of embankment foundations by using stone columns. Geotechnical & Geological Engineering, 15(3), 247-258.

Das B. M., (2009). Principles of Geotechnical Engineering. Cengage Learning, Stamfort, Sixth Edition.

Dash S. K., and Bora M. C., (2013). Influence of geosynthetic encasement on the performance of stone columns floating in soft clay. Canadian Geotechnical Journal, 50(7), 754-765.

Gniel J., and Bouazza A., (2009). Improvement of soft soils using geogrid encased stone columns. Geotextiles and Geomembranes, 27(3), 167-175.

Gniel J., and Bouazza A., (2010). Construction of geogrid encased stone columns: A new proposal based on laboratory testing. Geotextiles and Geomembranes, 28(1), 108-118.

Holtz R. D., and Kovacs W. D., (1981). An Introduction to Geotechnical Engineering. Prentice-Hall.

Hong Y., Wu C., and Yu Y., (2016). Model tests on geotextile-encased granular columns under 1-g and undrained conditions. Geotextiles and Geomembranes, 44(1), 13-27.

Malarvizhi S. N., and Ilamparuthi K., (2007). Comparative study on the behavior of encased stone column and conventional stone column. Soils and Foundations, 47(5), 873-885.

Mohapatra S. R., Rajagopal K., and Sharma J., (2016). Direct shear tests on geosynthetic-encased granular columns. Geotextiles and Geomembranes, 44(3), 396-405.

Mohapatra S. R., Rajagopal K., and Sharma J., (2017). 3-Dimensional numerical modeling of geosynthetic-encased granular columns. Geotextiles and Geomembranes, 45(3), 131-141.

Murugesan S., and Rajagopal K., (2007). Model tests on geosynthetic-encased stone columns. Geosynthetics International, 14(6), 346-354.

Murugesan S., and Rajagopal K., (2009). Shear load tests on stone columns with and without geosynthetic encasement. Geotechnical Testing Journal, 32(1), 35-44.

Murugesan S., and Rajagopal K., (2010). Studies on the behavior of single and group of geosynthetic encased stone columns. Journal of Geotechnical and Geoenvironmental Engineering, 136(1), 129-139.

Najjar S. S., Sadek S., and Maakaroun T., (2010). Effect of sand columns on the undrained load response of soft clays. Journal of Geotechnical and Geoenvironmental Engineering, 136(9), 1263-1277.

Najjar S. S., and Skeini H., (2015). Triaxial response of clays reinforced with granular columns. Proceedings of the Institution of Civil Engineers - Ground Improvement, 168(4), 265-281.

Robinson R., and Allam M., (1996). Determination of Coefficient of Consolidation from Early Stage of Logt Plot. Geotechnical Testing Journal, 19(3), 316-320.

Shokouhi A., Zhang C., and Williams D. J., (2017). Settling, consolidation and desiccation behaviour of coal tailings slurry. Mining Technology,1-11.

Sivakumar V., Jeludine D. K. N. M., Bell A., Glynn D. T., and Mackinnon P., (2011). The pressure distribution along stone columns in soft clay under consolidation and foundation loading. Géotechnique, 61(7), 613-620.

Sivakumar V., Mckelvey D., Graham J., and Hughes D., (2004). Triaxial tests on model sand columns in clay. Canadian geotechnical journal, 41(2), 299-312.

APPENDIX B - PRACTICAL IMPLICATIONS FOR INDUSTRY

The knowledge, skills and experience gained from this research have been applied to several industry consulting projects in Australia during the PhD candidature, in particular for large-scale direct shear testing. The contribution of the research on multi-stage testing method has already got a number of practical implications for industry clients. This is mainly attributed to the established multi-stage testing procedures, and the multi-stage testing procedures have been programmed in the software GEOsys of the Wille machine at UQ, which makes the multi-stage testing much easier, faster and more user friendly. Multi-stage testing is found to have its superiority over single-stage testing in large-scale direct shear tests for some specific projects where the sampling was difficult and expensive, or the supplied sample showed significant variability, for example, Yarwun Fissure Clay and Lower Lacustrine Soil Foundation Samples. Table 1 shows a summary of all the industry consulting projects carried out during the PhD candidature. This table will contribute to providing valuable guidance on the future commercial direct shear testing, for the selection of testing method, sample size, dry or wet testing, stress range, shearing rate, timeline, etc. Some typical experimental photos of different industry consulting projects are also shown in Figure 1. In summary, apart from the six journal papers included in this thesis, the PhD candidate has also published another journal paper in Engineering Geology, and three conference papers based on the practical implications for industry, as shown in the previous section - publications during candidature.

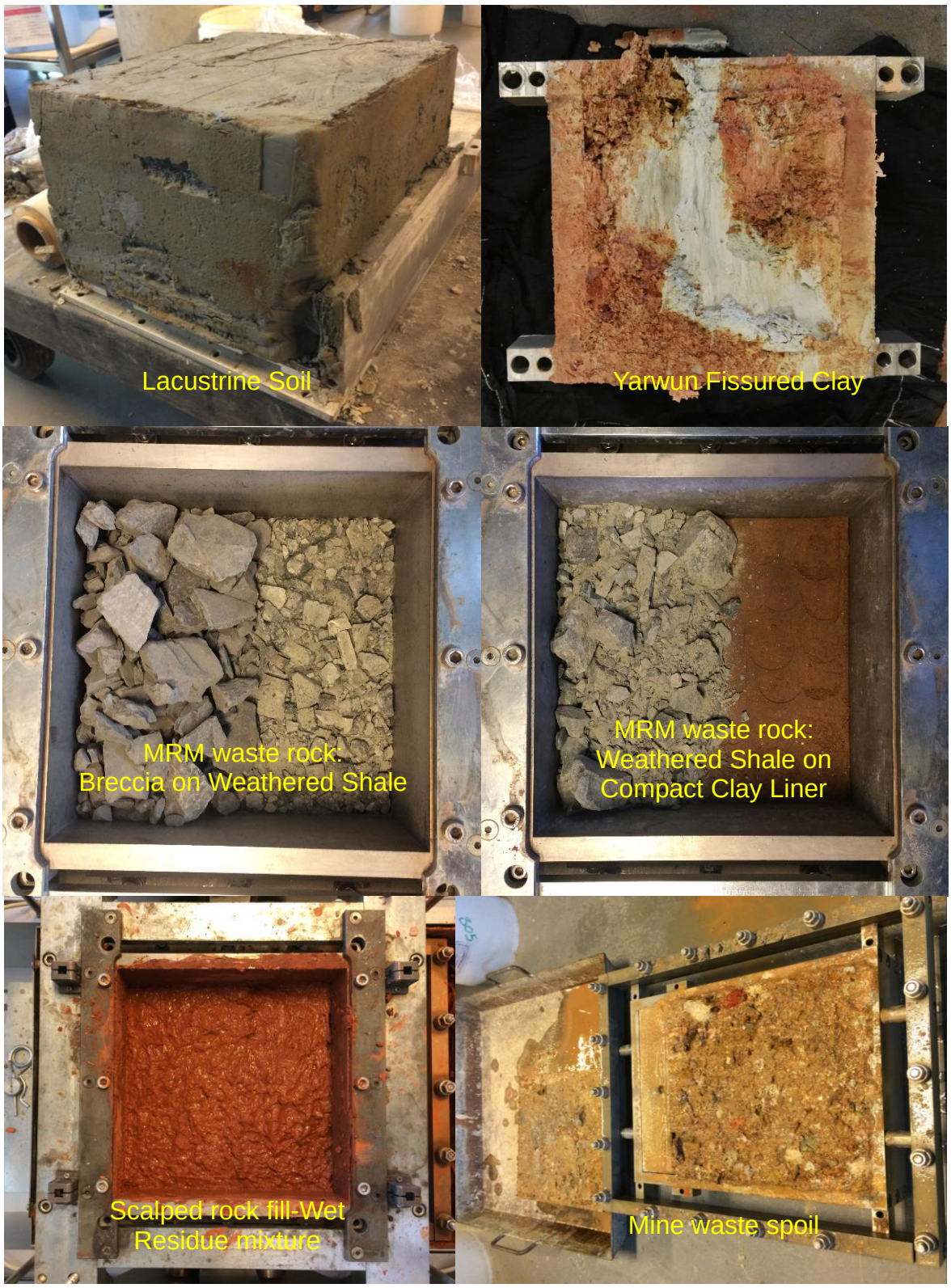

Figure 1 Experimental photos for industry consulting projects

Table 1 Summary of industry consulting projects carried out during the PhD candidature

Industry clients	Sample	Testing method	Specimen size (mm)	Normal stress (kPa)	Shearing rate (mm/min)	Duration
Edwards Exmin Service Pty Ltd: Downer Ramp	Mine waste spoil, top soil	Single-stage LDS	300 by 300 and 100 by 100	150, 250, 500	0.1	Jul-Sep, 2015
McArthur River Mine (MRM) Pty Ltd	Mine waste rock: Breccia (B), Weathered shale (WS), B on WS, WS on compacted clay (dry and wet)	Single-stage LDS	300 by 300	250, 500, 1000	0.1	Oct-Nov, 2015
McArthur River Mine (MRM) Pty Ltd	Mine waste rock: Breccia, Weathered shale	Dry and wet PSD, Slake durability test	-	-	-	Feb-Mar, 2015
Edwards Exmin Service Pty Ltd	Mine waste spoil (dry and wet)	Single-stage LDS	300 by 300	250, 500, 1000	0.1	July-Sep, 2016
McArthur River Mine (MRM) Pty Ltd	MRM compacted clay liner (dry and wet)	single-stage, multi-stage reverse SDS, UU, CU triaxial, UC	100 by 100 50 in diameter, 100 in height	50, 100, 200	0.01, 0.1, 1 (DS); 0.04 (TX)	May-Jun, 2017
Rio Tinto Alcan	Scalped rock fill-Wet Residue mixture (1.5:1 and 2.4:1)	Single-stage & Multi-stage LDS	300 by 300	50, 100, 200	0.1	Sep, 2017
EDG Consulting	Yarwun Fissured Clay (in a bath)	Multi-stage MDS & SDS	150 by 150 and 60 by 60	250, 500, 1000	0.02	Oct-Nov, 2017
GHD & Bluestone Mines Tasmania JV Pty Ltd	Lower Lacustrine Soil foundation samples (in a bath)	Multi-stage LDS	300 by 300 and 150 by 150	150, 300, 600	0.01, 0.05	Dec, 2017- Jan, 2018